THE DEVELOPMENT AND TESTING OF PULSED DETONATION ENGINE GROUND DEMONSTRATORS

by

PHILIP KOSHY PANICKER

Presented to the Faculty of the Graduate School of

The University of Texas at Arlington in Partial Fulfillment

of the Requirements

for the Degree of

DOCTOR OF PHILOSOPHY

THE UNIVERSITY OF TEXAS AT ARLINGTON

August 2008

Copyright © by Philip K. Panicker

All Rights Reserved

Psalm 53:1 (Please do not be one.)

2 Peter 3: 2-9 (Sign of the times.)

Psalm 127:1 Except the LORD build the house, they labor in vain that build it: except the LORD keep the city, the watchman waketh but in vain.

Mark 8:36, 37 For what shall it profit a man, if he shall gain the whole world, and lose his own soul? Or what shall a man give in exchange for his soul?

Psalm 103:2-5 Bless the LORD, O my soul, and forget not all his benefits: Who forgiveth all thine iniquities; who healeth all thy diseases; Who redeemeth thy life from destruction; who crowneth thee with loving kindness and tender mercies; Who satisfieth thy mouth with good things; so that thy youth is renewed like the eagle's.

Romans 10:13 For whosoever shall call upon the name of the Lord shall be saved.

The Holy Bible, Authorized KJV

ACKNOWLEDGEMENTS

I would first like to thank Dr. Frank Lu for his long and continual support and encouragement throughout this educational endeavor. I am grateful for the freedom to pursue research in my own direction, mostly, and for the opportunity to work at the ARC. I also am thankful for the pep talks, the apt refocusing of my attention during wavering moments and for all the help with research. I am extremely indebted to Dr. Lu for his diligent editing and proofreading of my dissertation manuscript. I wish to thank Dr. Don Wilson, who helped me with my scholarships and assistantships and other aid during my study here. I am grateful to him for making it possible for me to travel to Canberra, Australia and Reno, NV, for the AIAA conferences. I am also very thankful for his advice on the research subjects and for reading and editing my dissertation.

I want to thank Dr. George Emanuel for his advice and instructions during the brief time that he was on my committee. I would like to thank my committee members, Dr. Brian Dennis, Dr. Kamesh Subbarao and Dr. Albert Tong for their advice and feedback. I would like to thank Dr. J. Craig Dutton, who during his time here, encouraged me in my research work. I am also grateful to Dr. Wen S. Chan, who as graduate advisor, arranged for my teaching assistantships. In addition, I am obliged to Dr. S.M. You for granting me the opportunity to teach the MAE2381 class for two semesters.

I would like to thank the administrative staff of the MAE department, including Louella Carpenter, Janet Gober, Sally Thompson, Barbara Sanderson and Donna Woodhead, for their timely management of all bureaucratic procedures and for all their help in maintaining the smooth flow of operations without a hitch. Connie Niece will always be remembered for her friendly words and for her help with travel arrangements. I would like to thank Rodney Duke, Engineering

Technician at the ARC, who converted all the articles within my drawings and without into tangible material and for all other help in setting up our research apparatus.

I wish to thank Jiun-Ming (Jimmy) Li, who was my research partner during his one-year stint here at UTA and ARC, during which time we drew up designs, performed experiments and wrote papers together. I want to thank Dr. Daniel T.S. New, who got me started on the research on PDEs and also took on the bigger role in writing papers of our research. I am also grateful to Kin Fong Chui and Kim Seng Lim, who joined us here for research on PDEs. I want to thank Naveen Kumar Reddy and Harsha Shivashankar, who were co-researchers on the early PDEs.

I want to thank Rafaela Bellini, for her love, friendship and support for which I am truly indebted. I am grateful to her for wielding her great skills with MS Word for the formatting and typesetting of this manuscript and all other help she extended to me during my days writing this work.

I am very grateful to Albert Ortiz, my colleague and co-researcher, for all his invaluable help and partnership in performing the experiments and setting up equipment and instruments, and analyzing data; and as co-GTA of MAE2381. I want to thank my other colleagues here at ARC, Eric Braun, Richard Mitchell, Adam Pierce and Prashaanth Ravindran, who helped with research work and in running the PDEs. Along with the other inhabitants of the ARC, they made life here interesting and fun.

I want to thank my father P. Koshy Panicker, my mother Deenamma for their love, prayers and continued support for all my education. I also want to thank my brother, John, who supported me financially and spiritually in my education. I want to thank my sister, Anu Koshy and brother-in-law Binu John, for their love. I want to thank the Kuruvilla family for all their love, help and prayers during my life here in DFW.

I want to thank all who helped me along the way and could not be included by name here in this short list.

Above all, I want to thank my Lord and Savior Jesus Christ, who gave me life and blessed my life abundantly. May all glory be to God.

July 23, 2008

ABSTRACT

THE DEVELOPMENT AND TESTING OF PULSED DETONATION ENGINE GROUND DEMONSTRATORS

Philip K. Panicker, PhD.

The University of Texas at Arlington, 2008

Supervising Professor: Frank K. Lu

The successful implementation of a PDE running on fuel and air mixtures will require fast-acting fuel-air injection and mixing techniques, detonation initiation techniques such as DDT enhancing devices or a pre-detonator, an effective ignition system that can sustain repeated firing at high rates and a fast and capable, closed-loop control system. The control system requires high-speed transducers for real-time monitoring of the PDE and the detection of the detonation wave speed. It is widely accepted that the detonation properties predicted by C-J detonation relations are fairly accurate in comparison to experimental values. The post-detonation flow properties can also be expressed as a function of wave speed or Mach number. Therefore, the PDE control system can use C-J relations to predict the post-detonation flow properties based on measured initial conditions and compare the values with those obtained from using the wave speed. The controller can then vary the initial conditions within the

combustor for the subsequent cycle, by modulating the frequency and duty cycle of the valves, to obtain optimum air and fuel flow rates, as well as modulate the energy and timing of the ignition to achieve the required detonation properties. Five different PDE ground demonstrators were designed, built and tested to study a number of the required sub-systems. This work presents a review of all the systems that were tested, along with suggestions for their improvement. The PDE setups, ranged from a compact PDE with a 19 mm (3/4 in.) i.d., to two 25 mm (1 in.) i.d. setups, to a 101 mm (4 in.) i.d. dual-stage PDE setup with a pre-detonator. Propane-oxygen mixtures were used in the smaller PDEs. In the dual-stage PDE, propane-oxygen was used in the pre-detonator, while propane-air mixtures were used in the main combustor. Both rotary valves and solenoid valve injectors were studied. The rotary valves setups were tested at 10 Hz, while the solenoid valves were tested at up to 30 Hz on a 25 mm i.d. PDE. The dual-stage PDE was run at both 1 Hz and 10 Hz using solenoid valves. The two types of valves have their drawbacks and advantages which are discussed, along with ways to enhance their functionality. Rotary valves with stepper motor drives are recommended to be used for air flow control, while an array of solenoid injectors may be used for liquid or gaseous fuel injection. Various DDT enhancing devices were tested, including Shchelkin spirals (with varying thicknesses, lengths and pitches), grooved sleeves and converging-diverging nozzles. The Shchelkin spirals are found to be the most effective of all, at blockage ratios in the region of 50 to 55 %. To improve the durability of Shchelkin spirals, it is recommended that they be grooved into the inside of tubes or inserted as replaceable sleeves. Orifice plates with high blockage ratios, in the region of 50 to 80 %, are also recommended due to their simple and rugged design. All these devices along with the PDE combustor will require a strong cooling system to prevent damage from the extreme detonation temperatures. High energy (HE) and low energy (LE) ignition systems were tested and compared along with various designs of igniters and automotive spark plugs. It is concluded that while HE ignition may help unsensitized fuel-air mixtures to achieve detonations faster than LE systems, the former have severe drawbacks. The HE igniters get damaged quickly, and require large and heavy power

supplies. While the HE ignition is able to reduce ignition delay in a propane-oxygen pre-detonator, it did not show a significant improvement in bringing about DDT in the main combustor using propane-air mixtures. The compact pre-detonator design with a gradual area change transitioning to a larger combustor is found to be effective for detonation initiation, but the pre-detonator concept is recommended for high-speed applications only, since higher speeds requires more sensitive, easily detonable fuels that have short ignition delays and DDT run-up distances. Dynamic pressure transducers, ion detectors and photo-detectors were compared for the diagnostics of the detonation wave. The ion detector is found to be a safe, cheap and effective choice for obtaining detonation or flame velocities, and better than the optical detector, which is not practical for long-duration PDE operations. The piezoelectric dynamic pressure transducer has problems with heating and requires an effective cooling system to enable it to function in a PDE. Other diagnostics studied include thrust measurement and mass flow rate measurement techniques. Additionally, fuel sensitizing techniques, such as hydrogen blending, along with the DDT devices can ensure that detonations are produced successfully.

TABLE OF CONTENTS

LIST OF ILLUSTRATIONS

LIST OF TABLES

NOMENCLATURE

a	speed of sound
A	area, area of each detonation chamber
A	ampere, (unit of current)
a_0	speed of sound at inlet
ac	alternating current
atm	atmosphere, (unit of pressure)
b	bit
B	magnetic field, Wb/m^2 or T
B, kB, MB	byte, kilobyte, megabyte
BR	blockage ratio
c_d	discharge coefficient of valve/nozzle meter
CDWE	continuous detonation wave engine
C-J	Chapman-Jouguet
c_p	specific heat capacity at constant pressure
CRDI	common-rail diesel injector
c_v	specific heat capacity at constant volume
D	internal diameter of detonation tube
DAQ	data acquisition system
dB	decibel
d_c	critical diameter of detonation tube
dc	direct current
D_{CJ}	detonation velocity
DDT	deflagration -to-detonation transition
E	electro-motive force (emf), voltage (unit is Volts)
E	electric field intensity, V/m
EMI	electro-magnetic interference
F	uninstalled thrust
f	frequency of individual combustor
f_a	fuel-to-air ratio (by mass)
f_c	characteristic frequency for a transducer, Hz
f_n	natural frequency of a transducer/actuator, Hz
g	acceleration due to gravity (9.81 m/s2)
G	gain of amplifier
h, h_1, h_2	specific enthalpy, 1 is before wave, 2 is behind wave
H	Magnetic field intensity, A/m
HE	high energy (ignition system)
hp	Horse power (unit of power, 1 hp = 745 W)

h_{PR}	heat of reaction of fuel, kJ/kg
h_T	thermal efficiency (of engine)
HVLE	high voltage low energy (ignition system)
I	current, A
i.d.	internal diameter
in.	inch
I_{SP}	specific impulse
J, mJ	joules, milli-joules (unit of energy)
kmph	kilometers per hour
l	length of core of a solenoid
L/D	lenth-to-diameter ratio of detonation tube
LE	low energy (ignition system)
m	mass of fuel-air mixture in the combustor per cycle
$\dot{m}$	mass flow rate, kg/s
$\dot{m}_a$	mass flow rate of air, kg/s
$\dot{m}_f$	mass flow rate of fuel, kg/s
M_0, M_9	Mach numbers at inlet and exhaust nozzle exit respectively
M_E	mutual inductance of a transformer
N	number of detonation chambers
N_1, N_2	number of turns on a transformer/solenoid coil
NI	National Instruments
o.d.	outer diameter
p	static pressure (at given station)
p_a	ambient pressure
PDE	pulsed detonation engine
PDRE	pulsed detonation rocket engine
p_e	exhaust or exit pressure
P_E	power rating/consumption (electrical) W
ppm	parts per million
PWM	pulse width modulation
q	heat of combustion per unit mass of reactants
Q	volumetric flow rate
R	resistance, Ohm
R	universal gas constant,8.314472 kJ/K/kmol
R_{air}	gas constant of air, 286.9 J/K/kg
R-H	Rankine-Hugoniot
RMS	root mean square
rpm	revolutions per minute
s	seconds
S	specific fuel consumption
S	microphone sensitivity V/Pa
S/s, kS/s, MS/s	samples per second, kilo-samples per second, mega-samples per second
SMD	Sauter mean diameter
SPL	Sound pressure level
STP	Standard temperature (273.15 K) and pressure (1 atm)
T	temperature (at given station)
t	time, s

t	thickness of wire of Shchelkin spiral
t_b	blowdown time
t_c	combustion time
T_d	time delay, s
t_f	fill time
TOF	time-of-flight
t_p	purge time
TTL	transistor-transistor-logic (0-5 V)
u	specific internal energy
u_1, u_2	velocity of flow, 1 is before wave, 2 is behind wave
u_D	detonation wave velocity
u_e	exit velocity
V, mV, kV	volt, milli-volt, kilo-volt (unit of electric potential)
V_0, V_9	velocity of air at inlet and exhaust nozzle exit respectively
W, kW, MW	watt, kilo-watt, mega-watt (unit of power)
X_{DDT}	DDT run-up distance
ZND	Zeldovich-von Neumann-Doering

Greek symbols

τ	time period of each cycle
γ	ratio of specific heat
ϕ	equivalence ratio
Φ_m	magnetic flux, Wb
λ	detonation cell width
Ω	Ohm (unit of resistance)
ρ	density
μ	magnetic permeability, H/m
η_p	propulsive efficiency

CHAPTER 1

INTRODUCTION

1.1 Brief Look at Various Propulsion Systems

The first powered flight was performed by the Wright brothers in 1903, on an aircraft driven by a propeller and powered by a reciprocating internal combustion engine. The IC propeller engine was the only propulsion system available for flight until the first turbojet powered aircraft, the HE178, was flown by the German Heinkel company in 1939. Since then, the gas turbine engine has become the workhorse of the industry in powering aircraft, ships, tanks and electric power plants. The piston engine and the rotary engine are still in use today in smaller propellered aircraft. However, larger propellered aircraft and helicopters are powered by turboprop or turboshaft engines, which are limited to the low to mid subsonic regimes, because the propellers get extremely noisy and lose propulsive efficiency significantly over 550 kmph[1]. Gas turbine engines have a wide Mach number range; between 0 and 3.5 for turbojets[2]; making them very versatile. However, the ideal jet engine is less efficient at less than 700 kmph and modern aircraft engines are designed to operate at mid to upper subsonic speeds by combining the propeller and the gas turbine engine concepts in the form of turbofan engines[1]. Beyond Mach 3.5, the ramjet is more effective until it reaches an upper limit of about Mach 6, above which the temperature of the decelerated air entering the combustor is high enough to cause the reactants to dissociate and the resulting expansion is not enough to provide the exhaust velocity needed to sustain ramjet operation[3]. Therefore, at high supersonic flight speeds, it is not useful to decelerate the air flow to subsonic speeds, but rather to opt for a small amount of compression and deceleration using oblique shockwaves and to carry out the combustion at supersonic speeds, as in a scramjet[4]. Unfortunately, ramjets and scramjets have a high starting

velocity, which is about Mach 0.8 for ramjets and about Mach 5 to 6 for scramjets. The only other engine system in use, with a wider range than the jet turbine, is the rocket, which can operate at all speed regimes, provided enough fuel and oxidizer are carried on board. Because of the need for the onboard storage of oxidizer, rockets have very low specific impulse. Rockets cannot be easily reused and are therefore limited to very specific applications such as in missiles and for space travel.

Since the advent of the gas turbine engine more than six decades ago, there has not been a major revolution in engine technology, that can replace the gas turbine engine, while delivering better performance in terms of thrust, fuel efficiency, costs and range of Mach number of operation. Only the pulsed detonation engine (PDE) has the capability to offer all the above and more. The PDE is an internal combustion reaction engine that works in a pulsed cyclic fashion utilizing a constant volume combustion process[5]. In that sense, it is similar to the pulsejet which uses deflagrative combustion and has traditionally only been applied for subsonic applications. PDEs, on the other hand, use periodic detonation waves and can theoretically operate up to about Mach 5, when the total temperature at the inlet becomes higher than the auto-ignition point of most fuels. However, with proper design and control techniques, PDEs can be operated up to about Mach 8, although at hypersonic velocities, the continuous detonation wave engines are more effective[4]. A comparison of specific impulse vs. Mach number regimes of various propulsion systems are illustrated in Figure 1.1, clearly demonstrating the broad range of application of the PDE[6].

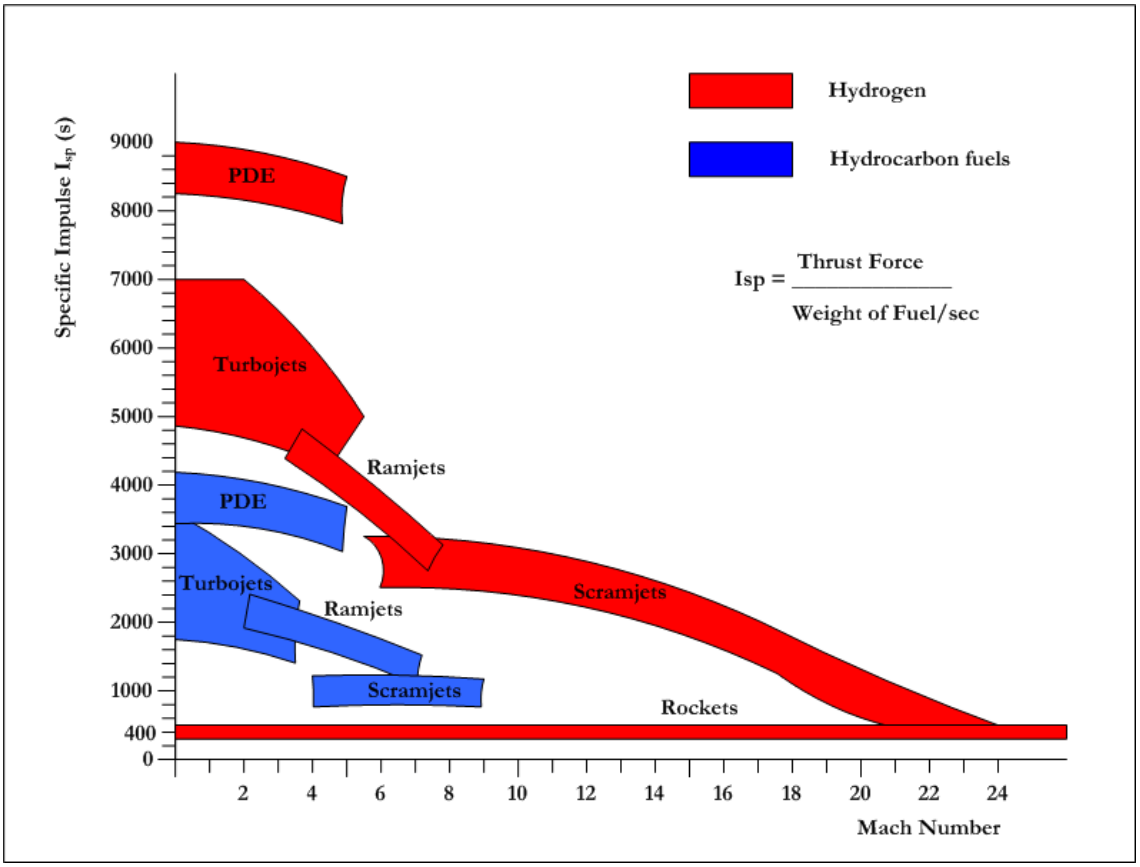

Figure 1.1 Specific impulse vs. Mach number regime of various propulsion systems[6].

1.2 The Pulsejet Engine

The invention of pulsejets is ascribed to many pioneers, including Charles de Louvrier, a Frenchman, and Martin Wiberg, a Swede, both in the late nineteenth century. However, fully functional pulse jets were first built by the German engineer, Paul Schmidt, in 1930. The Nazi German Luftwaffe, during World War 2, were the first to exploit the advantages of pulsejets, namely their simplicity of design and low costs of manufacturing and operation, by mass producing the pulse jet engine for their V-1 (Vergeltungswaffe-1) cruise missiles that were used to attack Britain between 1944 and 1945. Towards the end of WW2, the Germans were developing a VTOL aircraft known as the Focke-Wulf Fw Triebflugel, which had rotating wings powered by pulse jets at their tips. This vehicle never made it to the production line. A similar

application of the pulse jet was in the experimental helicopters built by American Helicopter, called the XA-5 Top Sergeant, which also featured pulse jet engines at the blade tips. Although prototypes were tested between 1946 and 1949, they never went into production.

Small pulsejets can reach as high as 250 cycles/s, while the larger ones are much slower owing to the longer fill times required. The V-1 missile engine could operate at about 45 cycles/s. The disadvantages of pulsejets are loud noise, heavy vibrations and low fuel efficiency. The last point is due to the absence of any internal compression mechanism. All the available working pressure is developed through the combustion of fuel in a constant volume process. Thus, pulsejets have poor pressure recovery and high specific fuel consumption (SFC) compared to gas turbine engines. As a result, in recent times, pulse jets have been relegated mainly to model aircraft, drone target aircraft and recreational vehicular propulsion, such as pulsejet-powered carts for example. Nevertheless, pulse jets are cheap to build, operate and maintain, and have been recommended for powering low cost UAVs[7].

Pulse jets can be classified into two types: those with mechanical valves and those with aerodynamic valves, also known as valveless pulsejets. In the former, the filling of air and fuel is controlled by means of valves and the ignition is timed carefully to fire when the valves are closed. Some valved designs employ one-way flapper or reed type valves that are closed by the buildup of pressure inside the combustion chamber after the combustion has been initiated. In the valveless designs, the intake of air and fuel are controlled aerodynamically by the pressure inside the combustion chamber. When the hot gases are vented after the combustion, the vacuum created induces fresh air and fuel to be drawn in, which ignites automatically from the heat left over from the previous combustion. Such an engine operates in a resonant mode, similar to that of a Helmholtz resonator[8]. Consequently, pulsejets with aerodynamic valves cannot accelerate on demand and therefore cannot be used for applications which require constant maneuvering or changing of speed.

1.3 The Pulse Detonation Engine

The PDE is a big improvement over the pulsejet in that it makes use of detonation waves to compress and combust the fuel-oxidizer mixture, whereby the temperatures and pressures released and the available power are much higher than pulsejets, gas turbine engines or rockets. Although the amount of energy released by deflagration and detonation is the same, because detonation is supersonic, the energy release occurs at a much faster rate; in other words, the power output is tremendously increased over deflagrative engines. Therefore, theoretically PDEs can be made smaller and faster than present day engine systems.

The operational frequency of PDEs can range from a few tens to a few hundred cycles per second[1]. The uninstalled thrust produced by the engine is a function of the number of detonation tubes, area of cross section of each tube, frequency of operation and exit velocity of the exhaust gases. The PDE has a simple geometry, consisting essentially of a tube which is filled with fuel and oxidizer, before the mixture is detonated. These benefits that PDEs can offer have spurred a growing worldwide interest in PDE research since the early 1990s, with the aim of realizing the next generation of propulsion systems to replace current gas turbines.

Detonation is a supersonic combustion process, which may be modeled as a shock wave followed immediately by a reaction flame front, together traveling through the mixture at several times the speed of sound of the unburnt gas mixture. On the other hand, deflagration is a subsonic combustion process, ranging in speeds from less than a few m/s to nearly 1000 m/s, well below the speed of sound.

1.3.1 Basic PDE

The basic PDE has a very simple structure, as seen in Figure 1.2, consisting essentially of a constant area tube, with valving to control the supply of fuel and oxidizer, an ignition system, and a nozzle for accelerating the flow if the engine is to be applied for propulsion. A practical PDE may also have one or more devices to bring about deflagration to detonation

transition (DDT), such as a Shchelkin spiral. The PDE cycle has four stages, namely fill, combustion, blow down (exhaust) and purge. The four stages are presented in Figure 1.3.

The PDE combustion chamber is filled with fuel and oxidizer during the fill stage. The time taken for the filling is denoted as t_f. When the fuel-oxidizer mixture is filled to the required volume, the combustion stage commences when a spark (arc or any other ignition initiator) is fired to start ignition. A detonation wave is soon created that moves through the mixture and causes the pressure and temperature behind it to rapidly shoot up. The time taken for the detonation wave to take shape and to move through to the end of the combustion chamber is denoted by t_c. The next stage is the blow down stage, when a series of rarefaction waves travel upstream into the combustion chamber and reflect off the end wall, causing the high pressure burnt gases to exit the combustion chamber at a high speed. The time taken for the blow down stage is denoted by t_b. This is then followed by the purge stage, when fresh air is blown through to clean and cool the tube before the fill stage starts again. The time taken for purging the tube with fresh air is denoted by t_p.

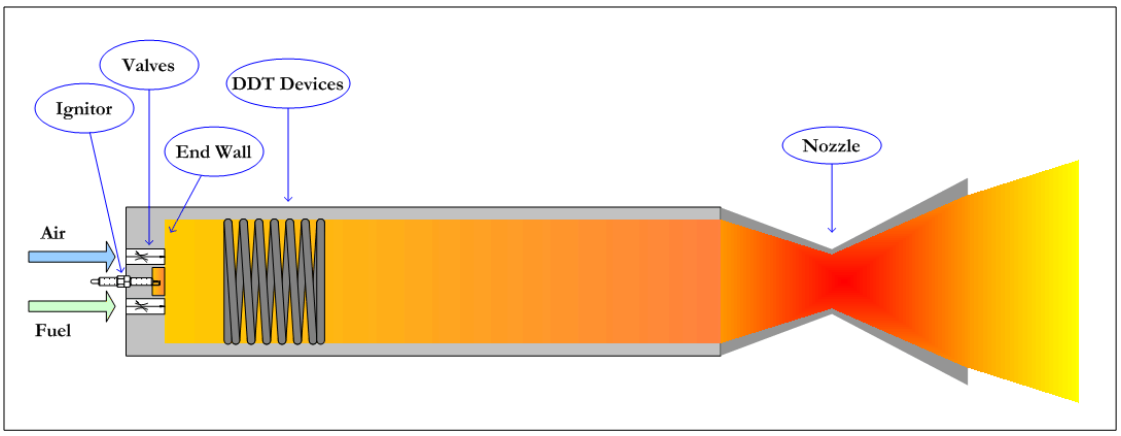

Figure 1.2 Schematic of a basic pulse detonation engine with valves at the inlet and a nozzle at the exhaust.

The purging process is very important as this cools the tube and prevents the fresh fuel-oxidizer mixture from igniting due to residual heat on entry into the combustion chamber. It also

protects the structure of the tube from heat buildup. The amount of time that the fuel-oxidizer mixture remains within the detonation tube is known as the residence time. At higher speeds, the residence time is very short, in the order of a few ms, and the combustion has to be initiated and advanced to detonation in as short as 1 to 5 ms.

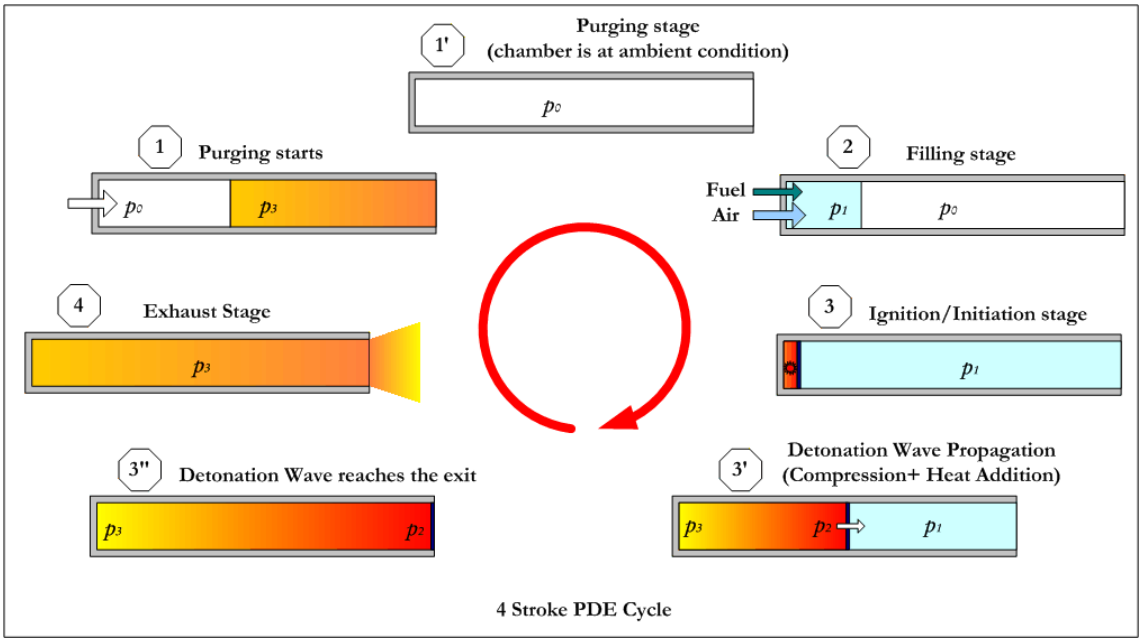

Figure 1.3 The four stages of a PDE cycle.

The total time period τ of one cycle is the sum of all the four stages, namely,

$$\tau = t_f + t_c + t_b + t_p \tag{1.1}$$

The frequency of operation f is the inverse of the time period, measured in Hz. Thus reducing the period increases the operational frequency. The filling and purging processes take a larger fraction of the time period. If the tube is long, filling and purging take longer amounts of time and only low frequencies are possible. However, the tubes cannot be shorter than the distance it takes for DDT to occur. The above processes hold true for an airbreathing PDE or one operating in a rocket mode, where the oxidizer and fuel are carried on board the aircraft. Such a configuration is known as a pulsed detonation rocket engine (PDRE).

1.3.2 Multi-Chambered PDE

In a multi-chambered PDE, two or more combustion chambers are joined to a common plenum chamber which conditions the flow before accelerating it through a common nozzle, as shown schematically in Figure 1.4, where a can-annular four chambered PDE is illustrated. With a multi-chambered design, each chamber can be at a different stage in the cycle, thus creating a smoother flow through the nozzle. The frequency of operation of the PDE can be effectively increased by increasing the number of chambers. Therefore, if the individual chamber frequency is f, the overall PDE frequency is proportional to f multiplied by the number of chambers. However, the flow into and out of each chamber does affect the flows in the other chambers, creating unsteady conditions at the inlets and outlets. It should be noted that the period for all four stages are not equal and more than one chamber may be in the same stage but off-phase from each other.

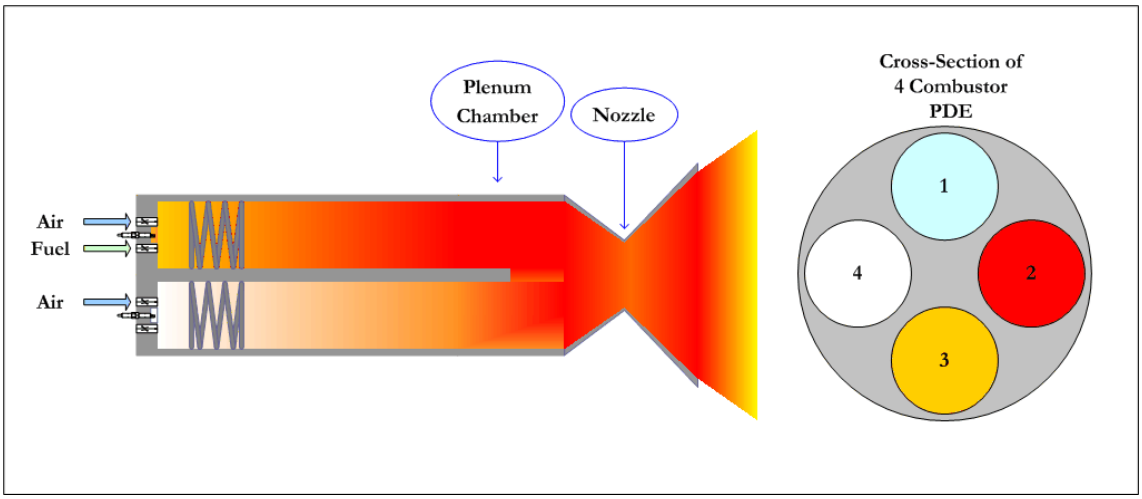

Figure 1.4 Schematic of a multi-chambered PDE, with each chamber in a different stage of the cycle.

The thrust of an ideal PDRE can be expressed similar to the thrust equation of a rocket[9] as

$$F \propto f\, N\left(\dot{\bar{m}} u_e + \left(p_e - p_a\right) A\right) \tag{1.2}$$

where f is the frequency of each detonation tube, N is the number of detonation tubes, $\bar{\dot{m}}$ is the average mass flow rate from each detonation tube per cycle, u_e is the exit velocity, p_e is the exit pressure, p_a is the ambient pressure and A is the exit area of the detonation tube.

1.3.3 Four-Stroke and Three-Stroke PDE

The four-stroke PDE was described earlier. In that system, the purging and filling stages are long and take up a significant portion of the total cycle time, during which time effectively no power is produced by the engine. Useful work is obtained in the combustion and blowdown stages only. In order to increase thrust, the engine has to be run at higher frequencies or be in a configuration of multiple chambers running in sequence. However, because the cycle period is long, high repetition rates are difficult to achieve unless larger valves or more valves are used. In a three-stroke PDE, the purging and filling stages are combined into one. After the blow-down stage, a fresh charge of cold air and fuel is introduced into the chamber which pushes the exhaust out. A large number of small fuel valves are needed for this operation, each one operating simultaneously or in a phased sequence. After the tube has been filled, the detonation wave is initiated. As the detonation wave exits the tube, the exhaust gases blow out in the blow-down stage. The three stages of the three-stroke PDE are displayed in Figure 1.5. Since the purging process is merged with the filling, there is a potential for auto-ignition as well as heat buildup and therefore, the tube has to be actively cooled to prevent overheating and meltdown. However, now that the cycle has been reduced, higher operational frequencies can be achieved.

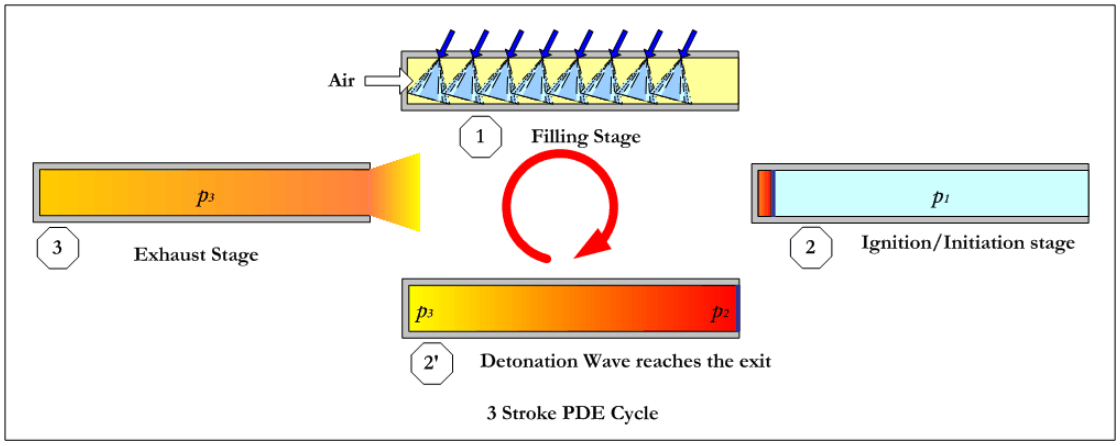

Figure 1.5 Schematic of a three stroke PDE cycle.

1.3.4 Ejector PDE

An ejector[10] in combination with an array of PDE or PDRE combustors, as shown schematically in Figure 1.6, has the potential to augment the thrust generated at all flight regimes. If the forebody of the PDE is aptly shaped and articulated, it may then be used to capture the shock system created at high Mach numbers. Another feature of the ejector design is that the detonation waves from the combustors can be used to initiate combustion in an afterburner thereby providing additional thrust enhancement. If the detonation is successfully transmitted to the afterburner, the afterburner may also operate in detonation mode.

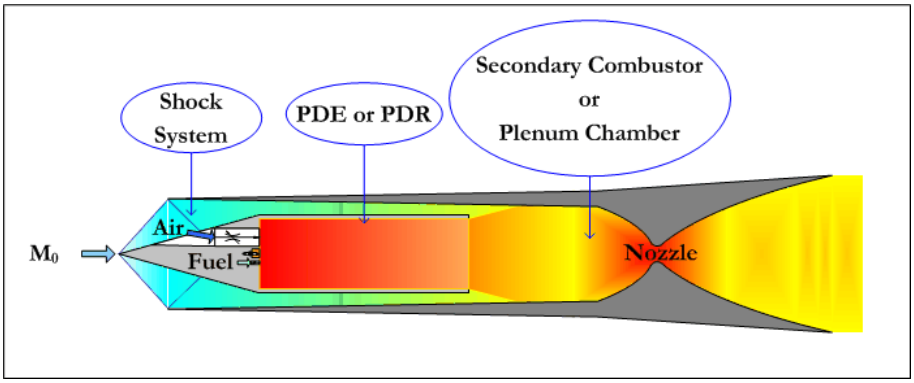

Figure 1.6 Schematic of an ejector-augmented PDE.

1.3.5 Hybrid Pulsed Detonation Gas Turbine Engine

In a hybrid pulsed detonation gas turbine engine, the combustor of a gas turbine engine is replaced with a bank of pulsed detonation combustors, as shown in Figure 1.7. This engine exploits the advantages of detonations, such as faster reaction speed, higher efficiency, pressure ratios, temperature ratios and power output, while integrating turbo-machinery to generate shaft-work. Since the detonation wave does the work of compressing the flow, the compressor will need fewer stages. However, pressurized air will be needed for purging, filling and for the operation of valves. The fan's bypass air augments the thrust of the core flow while the mixing cools the core flow and mitigates noise. Thus, the turbine also may be reduced in size, whereby the kinetic energy can be used for increased thrust. Hybrid PDE engines will prove to be very useful for electric power generation, where the available shaft work from the exhaust flow can be derived to drive generators. The exhaust can also be employed for co-generation or for combined cycle power generation, in which the hot exhaust is applied for the production of steam or to heat fluid that can be used for other processes.

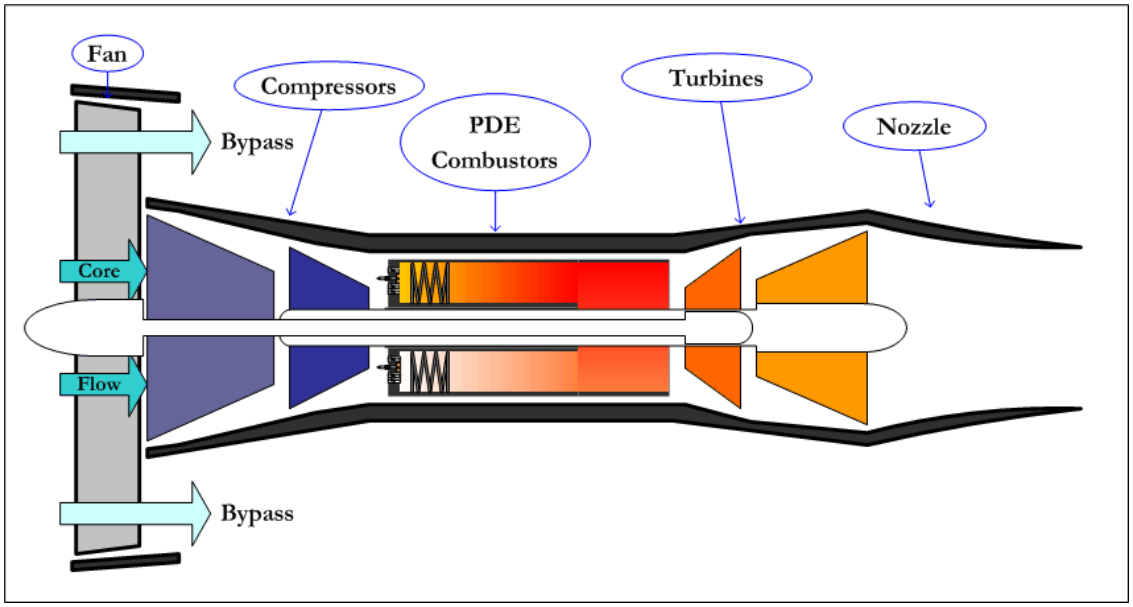

Figure 1.7 Schematic of a turbofan-PDE-hybrid.

1.3.6 PDE Turbine Integration

An integrated PDE-turbine architecture, as shown in Figure 1.8, has many uses, including electric power generation. For earth-based power generation, where high speeds or engine frequencies, are not required, detonation can be achieved naturally, which takes a longer distance and time. Therefore, the tube may be shaped in a helical form to make it more compact. The helical tube design is also known to improve the initiation of detonations[11].

There are two main issues that have to be taken into account when mating PDEs with turbines[12].

1. The constant barrage of detonation waves impacting the turbine blades can shorten the life of turbines, which are costly to maintain. Therefore, the detonation waves have to be attenuated before they hit the turbine blades.
2. In multi-chambered PDEs at low frequencies, the flow to the turbine will not be steady, which can cause unsteady motion in the turbine and also damage bearings and shafts.

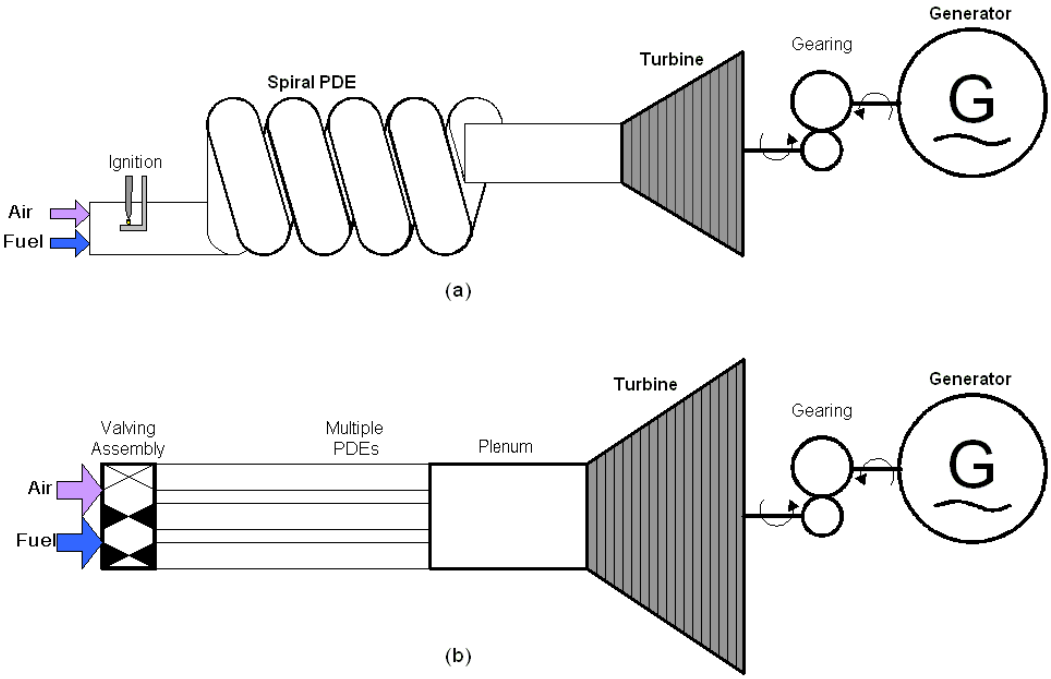

Figure 1.8 Schematic of hybrid PDE with turbine and generator for electric power production.

Detonations can be weakened by adding stator stages before the turbine. But the inlet temperature will still be very high. A plenum chamber can be added to condition the exhaust flow of the PDE combustors. If the detonation chamber does not meet the critical diameter criterion, i.e., if the detonation chambers internal diameter is less than 13λ, where λ is the detonation cell size, as explained in Section 2.4, the detonation will die out in the plenum chamber. Therefore, the length of the dimensions of the plenum chamber can be chosen so as to attenuate the detonations and to steady the flow.

In gas turbine engines, such as turbojets and turboprops, water is sometimes injected into the combustor to boost the thrust and to lower the turbine inlet temperature[1]. In some cases, an aqueous solution of methanol is injected into the compressor, to reduce the inlet air temperature and thus to increase density. The methanol also burns in the combustor for additional augmentation of thrust. This principle can be adopted for hybrid PDEs. Injecting water into the plenum chamber will add mass to the flow and cool the turbine inlet temperature and to dampen out any shocks. In addition to adding methanol in the compressor inlet, addition of methanol to the plenum chamber will dissipate the momentum of the detonation waves and cause them to die out, whilst the combustion of the methanol will provide extra momentum and mass flow to drive the turbines. In this case, the plenum chamber acts as a secondary combustion chamber. The above techniques are illustrated in Figure 1.9.

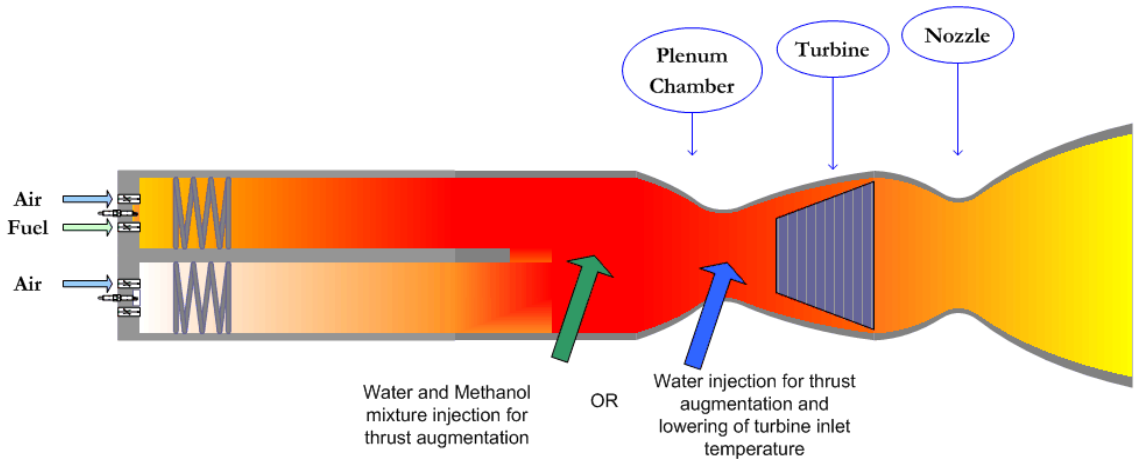

Figure 1.9 Schematic of the method of injecting water or a methanol solution into the PDE plenum chamber to augment thrust and to reduce the turbine inlet temperature.

1.3.7 Continuous Detonation Wave Engines

Continuous detonation wave engines (CDWE)[13] are used for high supersonic or hypersonic applications, where the Mach number of the incoming air in the combustion chamber is equal or greater than the CJ velocity of the fuel-air mixture, causing a stationary detonation wave to occur. One such engine is a scramjet with an oblique detonation wave at the inlet to the combustor, called the oblique detonation wave engine (ODWE)[4]. The fuel is injected and mixed with the flow stream behind the first oblique shock wave that forms between the leading edge of the body and the cowl of the engine inlet. The air entering through the oblique shock wave has been decelerated from the free stream Mach number and has undergone compression, before being mixed with the fuel. The fuel-air mixture is then passed through a standing oblique detonation wave into the engine chamber. Because combustion is partially performed externally, the length and consequently the drag and weight associated with the longer scramjet engine are reduced considerably.

1.4 History of the PDE

Although the early internal combustion engines all featured constant pressure deflagrative reactions, the benefits of constant volume detonations were well known to many pioneers in the propulsion arena. Several patents of the early twentieth century featured explosion or detonation combustion systems. A search of the U.S. patent database[14] reveals myriad applications for patents based on explosive-mode engine systems, dating as far back as 1899 for a rotary reaction explosive engine which produced shaft work. Many explosion engine concepts in the early 1900s produced shaft work and were designed to drive a variety of vehicles, including locomotives and ships, until the introduction of the jet engine in the 1930s. In 1941, H. Hoffman, in Germany, tested a pulsed detonation engine prototype, using acetylene/oxygen and benzene/oxygen mixtures. A few notable patent applications gleaned from the U.S.[15] and European[16] patent database are listed below.

1. In April 1942, Archibald G. Forsyth of Cheam, England, applied for a patent in Great Britain, for a "Periodically Actuated Jet Motor", which worked in the pulsed detonation mode, with the intention of powering aircraft. This patent [U.S. Pat. 2,427,845] was issued in September 1947.
2. In April 1945, Frank A. Hill, of Easton, Pennsylvania, filed for a patent for the "Explosion Gas Turbine Plant". This patent [U.S. Pat. 2,493,873] was approved in January 1950.
3. In November 1947, Albert Bodine, of Van Nuys, California, filed for a patent for a "Resonant Wave Pulse Engine and Process" which featured a standing Mach or shock wave to initiate detonation. This patent [U.S. Pat. 2,480,626] was issued in August of 1949.
4. In June 1950, F.E. Null of Dayton, Ohio, applied for a patent [U.S. Pat. 2,659,202] for an "Augmented Thrust Pulse Jet Pump or Motor" and the patent was received in November 1953. This design used a rotary compressor to pump premixed fuel-air mixture through a rotary valve into the combustion chamber, where a highly sensitive mixture is used to initiate detonation by means of a row of spark plugs. The inventor of this design proposed to

use it for aircraft or marine-craft propulsion and also for venting and conditioning the air within buildings by creating a venturi vacuum effect with the exhaust gases.

5. In September 1952, William Bollay of California, applied for a patent [U.S. Pat. 2,942,412] on a "Pulse Detonation Jet Propulsion" system and was granted the patent in June 1960. This design does not have compressors or turbines, but has multiple valves that enable the movement of a shock wave to trigger a detonation wave in the fuel-air mixture. It had a set of ignition plugs that were only used to start the ignition after which the engine kept operating until fuel was cut off.

Between 1952 and 1956, Nicholls[17] et al. at the University of Michigan, Ann Arbor, claiming to have independently come up with the idea of using intermittent detonations for propulsion, performed single-shot shock tube detonations and multi-cycle detonations using hydrogen and acetylene as fuels with oxygen or air as oxidizer. They then compared the test results with those of Hoffman. Nicholls, et al. in a report in 1955, proposed the PDE as a viable propulsion system and even enumerated the potential benefits, such as simplicity of design, thrust availability from static condition through to supersonic velocities, higher thrust levels and lower fuel consumption over pulsejets, thus bridging the gap between the pulsejet and the ramjet. Nicholls et al. noticed a significant DDT run-up time and distance. They suggested that smaller tubes be used in a flight engine at the cost of a lower thrust-to-weight ratio. They also suggested that one detonation tube be closed at both ends to allow a reflected detonation wave to be transferred to another chamber whereby no delay is experienced for detonation initiation in the second tube.

In June 1962, L.J. Krzycki[18], from the Naval Ordnance Test Station at China Lake, California, published a paper with his results of experimental studies of a propane-air pulsed detonation engine running at 25 and 50 Hz. He concluded that a major factor for the engine's low operating frequencies was due to the filling times, which further resulted in poor thrust production. Therefore, he deduced that PDEs did not appear to be promising due to the low frequency of operations achievable with detonative combustion.

Interest in PDEs waned for more than two decades following this, until D. Helman, S. Eidelman and their colleagues revived its study by performing experimental investigations starting in 1984 at the Science Applications International Corporation (SAIC) in McLean, VA. Their seminal paper[19] in 1986, which outlined the basic operational concepts and the benefits of the PDE, is considered to be responsible for the renewed surge in world-wide interest in PDEs. In Eidelman's original PDE design, the detonation igniter is located at the downstream end of the combustor tube. The detonation wave travels upstream into the combustor and then reflects off a thrust wall. CFD studies were also performed by Eidelman et al. into the late 1990s on PDREs and airbreathing PDEs. They forecasted that PDEs would be incorporated into space and atmospheric flight vehicles by the early 2000s. Following their publication, there has been massive involvement in research by contenders from the military, private and the university sector both in the US and abroad. This is verified by the huge number of patent applications related to PDEs in the 1990s and 2000s.

Starting in the early 1990s, experimental study of single and multi combustor PDEs were conducted by Bussing et al., at Adroit Systems, Inc., a company that was bought up by Pratt and Whitney in early 2001. Bussing et al.'s tests used a variety of fuels including ethylene and hydrogen. Soon interest picked up in other parts of the US and around the world; and experimental and computational studies were begun in many other countries, including France, Japan, Russia and lately China. Presently, work on PDEs continue in various parts of the US, including AFRL at WPAFB, NASA GRC, Pratt and Whitney, Boeing Phantom Works and GE, all of whom also collaborate with many universities.

Much of the current PDE studies are performed using CFD in order to comprehend and quantify the unsteady detonation phenomenon. There is also considerable experimental detonations research underway on a variety of platforms including single shot shock tubes, single shot and short duration multi-cycle testbeds that have single or multiple detonation chambers. Some of these studies have successfully demonstrated detonations in short duration tests of multi-cycle PDEs running on hydrocarbon fuel and air mixtures.

The first PDE powered flight took place on January 31st, 2008 at the Mojave Desert Air and Space Port in California. A light aircraft, called the Long-EZ, built by the Scaled Composites, Inc., took off using a turbojet engine and then cruised for about 10 s on PDE power at a speed of about 190 km/h at an altitude of about 20 to 30 m above the runway. The PDE, built at the AFRL by Fred Schauer et al., used the valving system of a four cylinder automotive engine retrofitted with four detonation tubes of 2 in i.d. and about 4 ft. in length. Each of the tubes fired at 20 Hz for a combined frequency of 80 Hz. A peak thrust of about 200 lbs was measured.

1.5 PDE Research at the University of Texas at Arlington

Since 1994, studies related to detonation physics have been pursued at the Aerodynamics Research Center focused toward the development of PDEs. Detonation experiments were performed with a detonation driven shock tube. This facility comprises of three sections, namely, a high pressure driver tube, a detonation driver and a driven section. The high pressure driver tube is 3 m and the detonation driver is 2.74 m long, both with an i.d. of 15.24 cm (6 in.). Additional driven tube sections with a total length of over 9 m and i.d. of 4.125 cm can be added[20].

In 1995, Stanley[21] undertook experimental study of PDEs by developing a test platform on which single shot tests were carried out using hydrogen, propane and methane as fuels with oxygen as oxidizer, all at stoichiometric conditions. The combustion chamber was 53.34 cm (21 in.) in length and had an internal diameter of 7.62 cm (3 in.) giving it a length to diameter (L/D) ratio of 7. It was found that detonation-like pressure profiles appeared towards the middle to the end of the tube for a clean tube configuration. When a Shchelkin spiral was introduced, DDT was observed. Higher initial pressures were found to yield over-driven detonation velocities with detonations occurring earlier, for hydrogen (2 atm), methane (3 atm) and for propane (1 and 2 atm). Propane was found to be a favorable fuel due to ease of detonability with oxygen at lower pressures. In later tests[22], a capacitor-storage high-energy arc discharge ignition system

capable of delivering about 20 J of energy was used and detonation pressure spikes were found to occur in the pressure history of the test runs, though CJ detonations were not observed. But it was conjectured that the high energy arcs produced a shock wave to occur, which could enable DDT to occur faster. Since hydrogen and most other fuels readily detonate in pure oxygen, the lack of detonation in the tests was attributed to improper mixing. Also the L/D ratio is too small for DDT. Longer tubes would be required for successful DDT with L/D ratios in the range of 10 to 20. Another systemic issue identified was the low sampling rates of the data acquisition system used, which was set at 100 kS/s, this being too low to be able to properly capture the detonation pressure spikes, and also introduces large sampling errors into the time-of-flight calculations.

In 1995, Burge[23] extended this study to fuel-air mixtures on the same test platform by adding a 30.48 cm (12 in.) fuel-air section to the end of the previous fuel-oxygen combustor. In this configuration, the fuel-oxygen section behaves as a pre-detonator, in which detonation is formed easily in the fuel-oxygen mixture and then transfers its energy to the fuel-air mixture, whereby the detonation should occur faster. The fuels tested were hydrogen and propane and the ignition was initiated by a capacitor bank arc discharge system that delivered about 20 J of energy into the fuel-oxygen mixture. The tests showed that detonation waves that originated in the fuel-oxygen section did not successfully transmit into the fuel-air zone. The detonation pressure profiles showed signs of decoupling followed by a galloping nature, of increasing and decreasing wave speeds, all the time remaining below C-J detonation velocity. Again, the reasons for failure were attributed to the improper mixing and short length. In the later part of the 1990s, Stuessy et al.[24] added a rotary injection system to deliver fuel, oxygen and air into the same test bed. Tests performed with hydrogen and oxygen stoichiometric mixtures at operating frequencies of 2 to 5 yielded repeated detonation like pressure profiles. However, the TOF velocities were found to be slightly below C-J velocity, although the velocity is seen to increase towards the end of the tube, where it reaches about 90% C-J velocity. This again points to the length of the tube being less than the DDT run up distance. The failure of this

system to attain DDT was due to improper fuel-oxygen mixing. The slow sampling rate also produced large errors in the data analysis. In 2000, Meyers[25] performed various tests on the same platform as that of Stuessy's with propane-oxygen mixtures to test the efficacy of Shchelkin spirals and high energy arcs to reduce DDT run-up distance. The motorized rotary valve allowed engine operating frequencies of up to 20 Hz. The capacitor-storage arc-discharge unit employed for this study was capable of delivering between 20 and 25 J per firing at frequencies below 20 Hz. The data was sampled on a 12-bit data acquisition system at a rate of 100 kS/s. At the lower speeds of 4.4 Hz and 6.9 Hz with Shchelkin spiral installed, rapid DDT was achieved and overdriven detonation velocities were observed. However, the detonation was seen to decouple and weaken towards the exit. At frequencies of 14.4 and 20 Hz, detonation pressure profiles were seen, but wave velocities were significantly below C-J values. Once again, the detonation front weakened as it approached the exit. For this and the previous tests, the rotary valve injection system was found to be severely lacking. The flow rates were measured using sonic nozzle critical flow meters, which were later found to be too small. Their small throats choke the flow through them. Consequently, at higher frequencies, the rotary valves cannot deliver the correct amounts of oxygen and propane into the detonation chamber and the large volume of the detonation chamber may not be fully filled. The concentration of fuel and oxygen closer to the exit of the tube would be diffused and causing the detonation waves to weaken and die away towards the exit. In addition, the drive belt of the rotary valve system caused slippage so that the different valves were not always properly phased. Low sampling rates also caused errors in the data analysis. It was proposed at the end of this study to use smaller diameter tubes for future studies along with solenoid valves for fuel and gas injection.

1.6 The PDE Cycle

The idealized PDE cycle is often represented by the Humphrey cycle, but a better representation would be the Fickett-Jacobs cycle[26, 27]. In Figure 1.10, the p-v and T-s diagrams of the ideal PDE cycle are superimposed on those of the ideal Brayton cycle representing the

gas turbine engine cycle and the Lenoir cycle[28, 29], which closely fits the ideal pulsejet engine cycle. The PDE cycle is numbered (0-3"-4"-10"-0), the Brayton cycle is numbered (0-3'-4'-10'-0) and the Lenoir cycle is numbered (0-4-10-0); with the numbers signifying the station numbers represented in the engine schematics, as shown in Figures A1.1 through A1.4. The area covered by the T-s diagram is the heat throughput of the engine, while the area of the p-v diagram represents the work throughput of the engine[30].

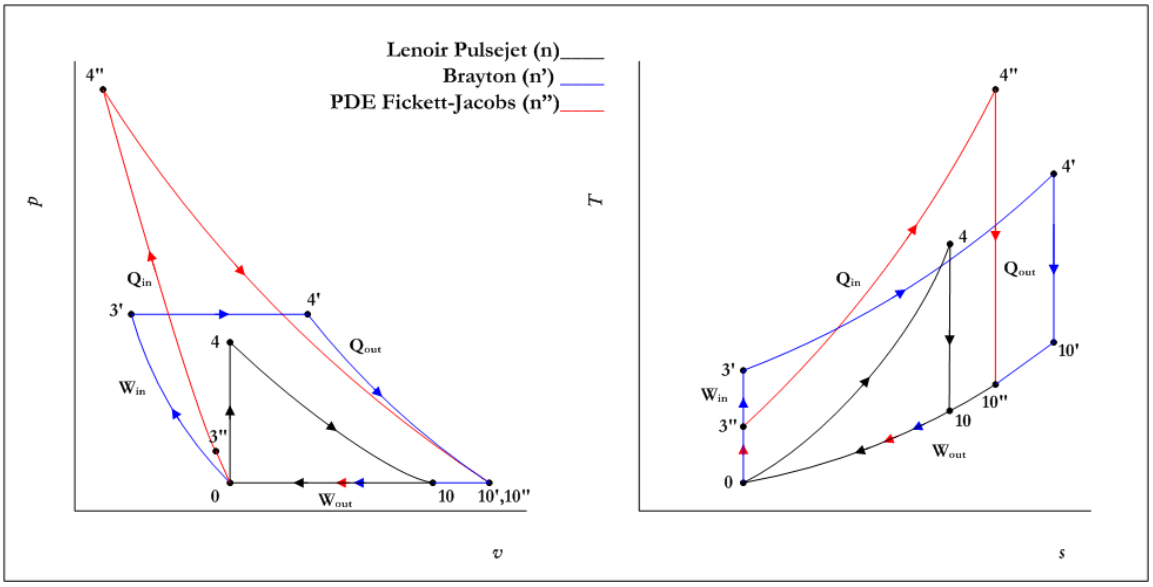

Figure 1.10 The T-s and p-v diagrams of the pulsejet, the Brayton and the PDE cycles respectively.

1.7 Scaling the PDE

A PDE can be scaled to meet the necessary thrust requirement in four ways.

1.7.1 Frequency Scaling

The thrust of a PDE is directly proportional to the frequency of operation of the engine, as shown in Equation (1.2). In the case of automotive engines where the speed of the vehicle is determined by the speed of the engine, to attain a higher vehicular speed, the engines speed is increased by increasing the air fill rates, which automatically adjusts the fuel fill rate through the

carburetor or fuel injection system. Similarly, an aircraft powered by PDEs can increase the frequency to attain higher thrust levels.

The slowest stages in the PDE cycle are the fuel-oxidizer filling stage and the purge stage. The detonation and blow down stages are very fast, together taking about 5% of the total time period. Therefore, to achieve higher frequencies, the filling and purging stages has to be sped up. This may be done with multiple inline valves rather than filling from the back end wall since the latter takes a much longer time for the fluid to fill up the entire length of the combustor.

1.7.2 Area Scaling

The thrust is proportional to the area of the detonation tube. However, the distance for detonation to develop within the combustor tube is a factor of the diameter[32-35]. Detonations are seen to occur in shorter distances in smaller tubes. The minimum tube diameter is limited by the detonation cell size. Larger tubes require longer detonation run-up distances. As a result, the engine may be limited from attaining high operating frequencies due to the increased detonation run-up times as well as the extended blowdown times associated with the longer combustor.

1.7.3 Length Scaling

When the length of the detonation tube is increased, the larger volume also provides for a larger mass flow per cycle, thereby increasing the thrust. However, longer tubes have larger frictional drag due to increases wetted area. Also, longer tubes take longer times to fill and purge and consequently reduces the operating frequency of the engine. Thus, the volume (area and length) have to be selected carefully depending on the type of fuel used, the Mach number range of operation and the other factors, such as weight, drag, etc.

1.7.4 Number of Detonation Chambers

As mentioned earlier, the frequency of the PDE can be effectively increased by operating several detonation chambers in sequence. The total thrust may be expressed as a product of the total number of detonation chambers and the frequency of each chamber. But the

increase in number of combustors also increases the complexity of the engine, requiring more complex ducting and valving mechanisms.

1.8 Motivation for PDE Research

1. No new engine concept has emerged into the market place since the advent of the gas turbine engine, which can meet or better the benefits and overcome the shortcomings. PDEs can help the aerospace sector develop better, faster aircraft, space vehicles, etc.
2. The PDE using detonations to derive the energy from its fuel is more efficient than deflagrative engines. In this day of increased fuel and operating costs for aircraft and dwindling profits for the airline industry, PDEs can provide considerable savings through improved fuel efficiency and lower engine initial and operating costs. Exergy analysis study[36] has shown that a PDE based power generation system is significantly more efficient compared to the gas turbine engine based power generation systems. Thermodynamic cycle analysis of PDEs[37] reveal that the ideal thermodynamic cycle efficiency of the PDE for common hydrocarbon fuels range from 0.4 to 0.8 with ideal specific impulses ranging from 3000 to 5000 s, outperforming the Brayton cycle in all aspects.
3. The PDE has the potential to enable smaller and faster engine systems because detonation releases the fuel energy much more rapidly as a result of which the power density is considerably higher than that of deflagrative engines.
4. The PDE is a versatile engine concept. The PDE can be applied for aircraft propulsion or power generation. PDE can be used in hybrid designs with turbine and compressors or as afterburner configuration. In addition, detonation in pulsed or continuous wave mode can be employed in ramjets, scramjets and rockets. Pulsed detonation rockets can be used for spaceship attitude control and for spacecraft propulsion. They can be made more efficient and compact than gas discharge or electric propulsion rockets.

5. The PDE has a wide Mach number range of 0 to about 5. At higher Mach numbers, the inlet static temperature of the air passing through one or more shocks in the inlet is high enough to auto-ignite the fuel-air mixture. At such velocities, it is advantageous to use the scramjet or the shramjet mode of combustion[9, 10, 13].

1.9 The Main Difficulties Impeding the Maturation of PDEs

Although the first recorded flight of a PDE powered aircraft took place in early 2008, some six decades since the concept of detonation engines began to be studied, there are still many aspects of the design and operation that have to be refined or considerably improved. Presently, single-shot and short-duration multi-cycle PDE experimental studies in the laboratory setting along with the associated computational research are continuing worldwide. Obtaining detonations in single-shot pre-mixed tubes filled with fuel-air or fuel-oxygen mixtures is not a very challenging task. Quiescent mixtures are easy to ignite and take only small amounts of energy. Mixtures of fuels with oxygen ignite and progress to detonation effortlessly. Premixed mixtures of fuel and air can be detonated easily if the right conditions are met, including proper equivalence ratio, minimum tube diameter and adequate tube length for deflagration to transition to detonation. However, achieving detonations in multi-cycle setups is much more difficult. Inadequate supply of fuel-oxidizer mixtures and improper mixing lead to detonation failure. Short duration oxygen-based and pre-mixed fuel-air based multi-cycle detonation combustors have been successfully tested. Some of the main issues that have to be worked out before PDEs can transition from the theoretical realm into real world applications are described below.

1.9.1 Achieving Successful and Consistent Detonations Repeatedly

The biggest hurdles to cross are to achieve detonations within the fuel-oxidizer mixture in as short a distance as possible and to attain detonations consistently. The detonations must also be fully controllable and the results repeatable at a very high rate in order to allow the

effective on-demand throttling of a PDE-based propulsion system. As explained before, a deflagration propagating within a constant area tube filled with a fuel-oxidizer mixture will naturally transition to a detonation wave if the tube is long enough, typically on the order of 1 to 10 m, depending on the sensitivity or energy content of the fuel-oxidizer mixture.

1.9.2 Sustaining Detonations Repeatedly

Even after detonation has been achieved, the unsteady nature of PDE operation can often lead to the deterioration and eventual extinction of the detonation wave. The main cause of this is improper mixing of fuel and oxidizer, so that some regions of lean or zero reactant concentration exist within the tube, while in some regions, the concentration may be fuel rich. As the detonation wave approaches the regions of low fuel concentrations, the detonation wave may weaken and decouple. Also, the cell size is very sensitive to fuel concentrations, being lowest at stoichiometric or slightly fuel rich condition. If the cell size increases due to change in the equivalence ratio away from unity and eventually becomes larger than the tube diameter, the detonation will fail.

1.9.3 Protection of Internal Structures and Components of the PDE

The highly unsteady and extremely severe combustion process of the PDE is not favorable for the long-term survival of critical engine parts, such as valves, ignition plugs, DDT devices, fittings, joints, etc. Short-duration multi-cycle tests have demonstrated the extent of the damage suffered by the combustion tube and various components[38]. In industrial fuel gas transmission tubes that experience detonations, a large bulge is seen at the location where deflagration-to-detonation transition (DDT) occurred[39]. Consequently the region of DDT has to be reinforced. Making the whole tube of uniform thickness and rigidity may not be a feasible option for saving weight and design costs in a practical engine. Therefore, the regions of high stress intensities have to be identified. The deflagration process causes more heat buildup in the tube, since it is slower and lingers longer in the tube. Once the detonation wave has been

created, it prefers a clean tube free from major barriers, which create drag and strip energy from the detonation wave. It has been noted from experiments that the location of the DDT device is where most of the heating takes place[38]. The DDT devices can be heavily damaged and expelled out of the tube by the high pressures. These and other factors will be discussed in more detail later.

1.9.4 Inlet and Nozzle Design

Unless the PDE is operated in a single chamber rocket mode, external flows heavily influence the dynamics of the engine. Moreover, the freestream airflow has to be diffused efficiently without raising the static temperature above the autoignition point of the fuel, and then correctly diverted to the combustion chamber with no dead zones in the path. At supersonic speeds, shockwaves will form within the inlets and if the valves are suddenly closed the inlet can unstart. Hybrid PDEs or PDE with bypass flows also result in complex designs to ensure a smooth flow of air through the engine as well as the proper filling and purging of the combustors. Nonetheless, inlet design is not a concern in this study.

1.9.5 Valving Design

The speed and consequently the thrust of a PDE can be effectively controlled with the help of valves. Thrust control is an essential requirement for an aircraft during takeoff, landing and for maneuvering. In a multi-combustor PDE, acoustic interactions of inlet and exhaust flows between the various chambers introduce added complexity to the system. Also, for high supersonic flight, valves and other flow control components pose a barrier that create drag or lead to the formation of shock waves. These are issues that will have to be dealt with in the design of a flight-weight PDE.

In addition, the mass flow rate of air in an air-breathing engine is tremendously higher than the flow rate of fuel. Therefore, the valves have to be designed and placed to allow effective filling of the combustors within the short time available at high speeds. The fuel valves

have to be designed to achieve thorough mixing of liquid fuels with air. Moreover, the electromechanical valves have to be cooled and meet the power and weight requirement of the aircraft. Some of these issues will be looked at in more detail later.

1.9.6 Ignition System

The initiation of detonation can be achieved by transferring a large amount of energy into the fuel-oxidizer mixture, such as from a laser ignition system or arc discharge ignition system. High voltage low energy ignition systems have been in use on automobiles and in aircraft engines for about a century. One of the concerns is that the igniter itself has to survive the harsh detonation environment of the PDE. The various ignition systems will be compared in detail later on.

1.9.7 Fuel Selection

PDEs, like gas turbine engines, can theoretically run on any type of conventional fuels, whether gaseous or liquid. In addition, coal particles, in the range of 10 μm, forms highly detonable mixtures with air and may be used for a ground-based PDE-power generation system. The fuel delivery systems will have to be developed for special fuels. The sizing of the engine is dependent on the cell size of the fuels. Various fuels will be analyzed in more detail later.

1.9.8 Minimization of harmful or undesirable exhaust products

Although detonations can ensure thorough burning of the fuels, preventing the formation of CO or soot, the higher temperatures can result in the formation of NOX. More research, possibly into the application of catalytic converters, need to be done to resolve the issue of adverse byproducts. This topic is not a subject of this study.

1.9.9 Vibration and Noise

Vibration and noise are two of the factors that need to be dealt with when combining a PDE with other onboard aircraft systems. But these can be solved with active noise suppression and damping. Noise can also be minimized by increasing bypass for subsonic engines. This topic is not a subject of this study.

1.9.10 Conformity with other onboard systems and suitability for mission

The PDE itself has to correctly mate with the existing systems onboard an aircraft for it to be chosen as a candidate engine for a particular flight application. For example, the vibration induced by the pulsing or the heat generated must not damage sensitive instruments. The electrical noise generated by the ignition system must be within the acceptable range of communication or radar systems. Also, the audible noise must not be too loud for critical missions where audio range noise is an issue. These factors, however, will not be dealt with in this study.

1.9.11 Control System, Diagnostics Instrumentation and Data Acquisition Systems

Detonation is a very unsteady process and is prone to fail if the conditions are not just right within the combustor. Therefore, the conditions have to be monitored and controlled using a closed-loop feedback system. Once the physical structure of the engine has been built and the overall geometry, including the DDT devices, has been set, the only control inputs to the combustor are the filling (which can be subdivided into mass flow rate, fuel-oxidizer ratio, mixing, timing of the valves, selection of the combustor, etc.) and the ignition (timing and ignition energy). But the status of the combustion and the location and speed of the detonation has to be determined. Therefore, sensors are required within the combustion chamber which can survive the severe temperatures and pressures caused by the detonations. The sensors allow the control system to regulate the valve timing and flow rates and the ignition settings so that the engine will produce the required thrust at the required speed. As detonation occurs at

supersonic speeds, the computer onboard has to be able to process data from the various sensors at very high speeds. Present day computer systems are very small and fast, making PDE control possible. The author believes that the reason PDEs were not a reality until now has been due to the lack of small and fast computerized control systems.

However, sensors are still not adequately developed to meet the requirements of the PDE. All transducers are affected by heat. When transducers are subjected to the extremely high temperatures and repeated shock pressure loading in a test PDE, they produce significant errors in their readings and may be destroyed after a few minutes of continuous exposure. In this study, various sensors and their applications, along with the data acquisition techniques are discussed in detail. The closed loop feedback system is not delved into any further than just a brief description of its potential application for a PDE based propulsion system.

1.10 Objectives of This Study

The main elements that are required for a successful PDE are techniques to initiate and sustain detonations, fuel-oxidizer injection systems and control and diagnostic systems. The primary objective of this study was to develop PDE setups that can achieve multi-cycle detonations for a short duration, on which the various sub-systems could be studied. With the help of the setups, detonations in a variety of fuels, with fuel-air or fuel-oxygen mixtures, may be tested. The size of the detonation tube depends on the fuel and choice of oxidizer, as explained in Section 2.7. The injection of the reactants in the right proportions and at the right times can be achieved with high-speed valves. The proper design and operation of valves are essential to PDE development and is a subject of this study. Repeated detonations in liquid fuel-air mixtures are more difficult to achieve because the fuel has to be vaporized and mixed with air effectively. The placement of the valves is also important for the proper mixing of the reactants. In addition, the design of the entry ports and conduits for the flow of fluid into the combustor has to be studied for the same reason.

The initiation of detonation, explained in Section 2.6, is another subject of study. Direct initiation, using a high energy ignition system or a predetonator system, has to be investigated for their efficacy in a multi-cycle detonation engine. Another method of detonation initiation is to cause a deflagration to transition to detonation by means of detonation enhancing devices, called DDT devices. Thus, a multi-cycle PDE platform would make it possible to study the effect of various DDT devices on repeated detonations. A PDE must have a proper ignition system that is able to ignite the mixture repeatedly at high frequencies for the entire duration of the engine's run time. Thus, it should be powerful enough to initiate combustion and impart enough energy to reduce ignition delay, while being durable enough to withstand the constant detonation environment. The PDE setups shall provide the ability to test various ignition systems and igniter designs.

It can be seen from C-J detonation theory, explained in Section 2.2, that all detonation properties can be expressed as a function of the wave speed. Thus, it is vital to measure wave speed along with the properties before and after the detonation, including pressure, temperature, fuel-oxidizer ratio, etc. One of the objectives of this study is to study the effectiveness of various transducers, such as dynamic pressure transducers, ion detectors and photo-detectors to detect the detonation waves. However, the transducers have to be made to withstand the harsh detonation environment and efforts have to be made to mitigate the effects of high temperature and shock loading. The protection of the sensors is a matter of vital interest in this study.

For a PDE ground demonstrator, an open-loop control system is sufficient since the test times are short and the variables, such as the initial fuel-oxidizer ratios, pressures and temperatures, as well as the operational frequency of the engine, are held constant during the test run. The control techniques developed in this study shall help in the future development of a fully functional flight model PDE. One of the objectives of this study is to enable the control of the operation of a PDE ground demonstrator using computerized control systems. Thus, the integration of the various sub-systems, including valving, ignition and data acquisition is critical.

The development of the data acquisition methodology and data analysis is also an important objective.

CHAPTER 2

THEORY OF DETONATION

2.1 Detonation vs. Deflagration

Detonation is a supersonic combustion process which is essentially a shock front driven by the energy release of the reaction zones in the flow right behind it. The shock wave is very thin, being only a few molecular mean-free-paths in width. The reaction zone may be much thicker and can be a few mm in width under normal conditions. The shock wave and the reaction zones are tightly coupled in a detonation wave and together move at supersonic speeds through the medium at a few thousand meters per second.

On the other hand, deflagration is a subsonic combustion process in which a flame front passes through the reactant mixture (or vice versa) with flame speeds from less than a few meters per second to a few hundred meters per second, releasing the heat of reaction at a much slower pace. In the case of scramjets, the flow may be moving at supersonic speeds, but the reaction is still termed as a deflagration process because of the lack of shock waves. Deflagration[39] can be premixed or non-premixed (diffusive). For propulsion applications the premixed reaction is preferred over improperly mixed or unmixed diffusion reactions.

Figure 2.1 shows a wave-centric representation of a detonation and a deflagration wave. Table 1 lists the properties of the flow for both cases. Even though the total energy is same for both waves, detonation is able to produce higher pressures, temperatures and densities at much higher speeds. It would indeed be very advantageous to exploit these benefits of detonations for propulsion applications.

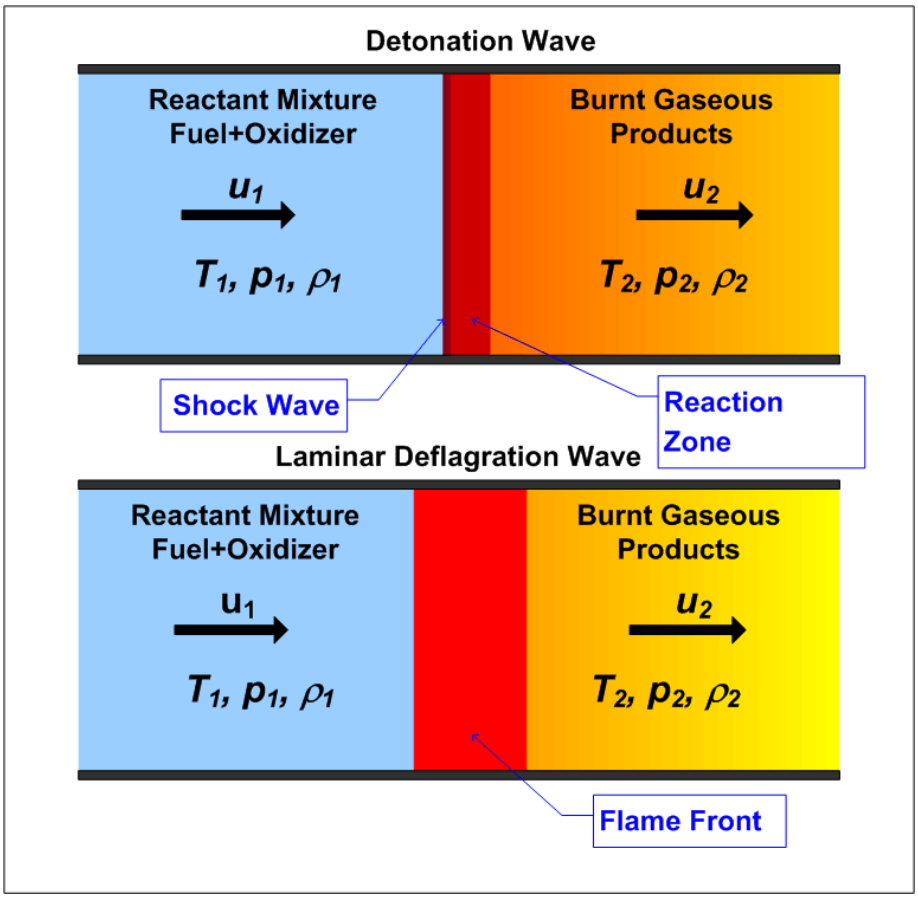

Figure 2.1 Wave-centric schematics of a detonation wave (top) and a deflagration wave (bottom) respectively, with the reactive flows passing through the stationary waves.

Table 2.1 Comparison of properties of detonation vs. deflagration[41].

Property	Detonation	Deflagration
u_1/c_1	5 - 10	0.0001 - 0.03
u_2/u_1	0.4 - 0.7 (deceleration)	4 - 6 (acceleration)
p_2/p_1	13 - 55 (compression)	≈ 0.98 (slight expansion)
T_2/T_1	8 - 21 (heat addition)	4 - 16 (heat addition)
ρ_2/ρ_1	1.7 - 2.6	0.06 - 0.25

At this point, it would be expedient to mention the color of the flames[41], so that one may understand the reaction from the flame observed at the exhaust of the PDE. For a fuel-lean mixture, the high concentrations of excited CH radicals in the flame give it a deep violet color. Fuel rich mixtures produce a green colored flame due to the large concentrations of C_2 molecules. When the reaction is complete, the flame burns with a blue color, the more energetic shorter wavelengths denoting the hottest part of the flame. Large concentrations of cooler CO_2 and H_2O produce a reddish colored (longer wavelength) glow in the exhaust gas. Fuel-rich mixtures cause carbon particles (soot) to form in the exhaust which glow brightly with a yellow color. Hydrogen in air burns with a pale blue to almost colorless flame.

Detonation[26,34,40,41] was studied in the last quarter of the 19th century by various scholars, including Berthelot, Vieille, Mallard and Le Chatelier. There are presently two well-known theories that are used to model detonation waves, namely the Chapman-Jouguet (C-J) theory and the Zeldovich-von Neumann-Doering (ZND) theory.

2.2 Chapman-Jouguet Theory

This is the simplest and the first theory proposed individually by Chapman (1899) and by Jouguet (1905)[26]. The theory treats the detonation wave as an infinitesimally thin one-dimensional reaction zone, which can be considered a shock wave with infinite chemical reaction rates, either moving through the gaseous medium or as stationary with the gas moving through it, as shown in Figure 2.1 (top). The three conservation laws, which are assumed to apply across the wave, as well as the perfect gas law are used to derive the Rankine-Hugoniot (or just Hugoniot) equation[41]. The detonation wave is assumed to propagate adiabatically at a steady speed with no heat loss to the surrounding tube wall. The conservation equations for steady one-dimensional flow, with no body forces, for the burned and unburned gases can be given by

$$\rho_1 u_1 = \rho_2 u_2 \tag{2.1}$$

$$p_1 + \rho_1 u_1^2 = p_2 + \rho_2 u_2^2 \tag{2.2}$$

$$h_1 + \frac{1}{2}u_1^2 = h_2 + \frac{1}{2}u_2^2 \tag{2.3}$$

where ρ, u, p and h denote density, velocity, pressure and enthalpy of the flow respectively. The velocities u_1 and u_2 are measured with respect to the detonation wave, with subscript 1 denoting the flow upstream of the wave (reactants) and subscript 2 denoting the flow downstream of the wave (products). The pressure behind the detonation wave is obtained as

$$p_2 = \rho_2 R_2 T_2 \tag{2.4}$$

where R is the specific gas constant. Combining Equations (2.1) and (2.2) to eliminate u_2, gives Equation (2.5), which is generally referred to as the Rayleigh-line relation.

$$\rho_1^2 u_1^2 = \rho_1^2 u_D^2 = \frac{p_2 - p_1}{1/\rho_1 - 1/\rho_2} \tag{2.5}$$

In the above equation, u_D is the detonation wave velocity. The above equations can be combined to obtain the Hugoniot relation

$$h_2 - h_1 = \frac{1}{2}(p_2 - p_1)\left(\frac{1}{\rho_1} + \frac{1}{\rho_2}\right) \tag{2.6}$$

The enthalpy can be expressed as $h_1 = c_{p_1} T_1 + h_1^\circ$ and $h_2 = c_{p_2} T_1 + h_2^\circ$, where h° is the enthalpy of formation at standard state, 298.15 K and 1 atm and c_p is the specific heat capacity at constant pressure. If the heat of combustion (heat release) is given by

$$q \equiv h_1^\circ - h_2^\circ \tag{2.7}$$

then, Equations (2.5) and (2.6) can be combined to obtain the Rankine-Hugoniot (R-H) relationship,

$$\left(\frac{\gamma_2}{\gamma_2 - 1}\right)\frac{p_2}{\rho_2} - \left(\frac{\gamma_1}{\gamma_1 - 1}\right)\frac{p_1}{\rho_1} - \frac{1}{2}(p_2 - p_1)\left(\frac{1}{\rho_1} + \frac{1}{\rho_2}\right) = q \tag{2.8}$$

where γ is the ratio of specific heats. For a polytropic gas, with constant specific heat, the R-H relationship can be expressed as

$$\frac{\gamma}{\gamma-1}\left(\frac{p_2}{\rho_2}-\frac{p_1}{\rho_1}\right)-\frac{1}{2}\left(p_2-p_1\right)\left(\frac{1}{\rho_1}+\frac{1}{\rho_2}\right)=q \tag{2.9}$$

The final states can then be obtained as follows:

$$\frac{p_2}{p_1}=\frac{1+\gamma M_1^2}{1+\gamma} \tag{2.10}$$

$$\frac{\rho_2}{\rho_1}=\frac{\left(1+\gamma\right)M_1^2}{1+\gamma M_1^2} \tag{2.11}$$

$$\frac{T_2}{T_1}=\frac{\left(1+\gamma M_1^2\right)^2}{M_1^2\left(1+\gamma\right)^2} \tag{2.12}$$

$$M_1=\sqrt{2\left(\gamma+1\right)\left(\frac{q}{\dot{m}c_pT_1}\right)} \tag{2.13}$$

In the above equations, M is the Mach number. From Equation (2.13), it is seen that pre-heating the reactants reduces the detonation Mach number (though not the velocity), whereas, increasing the initial pressure increases the detonation velocity.

The Rankine-Hugoniot curve (also known as the Hugoniot curve) is the locus of all possible solutions for the final state of a flow going through a shock or combustion wave. Equation (2.9) can be used to plot the R-H curve on a p vs. $1/\rho$ space for any given value of q, which yields rectangular hyperbolae, as shown in Figure 2.2. The Rayleigh line equation, given in Equation (2.5), can then be used to plot constant velocity lines on the same chart, originating on the shock R-H curve at a point A, denoting the initial pressure and density, as seen in Figure 2.3. The intersection of a Rayleigh line and the R-H curve of the particular value of q is the steady-state solution of the final state of a detonation or deflagration wave. Based on the flow velocity,

the R-H curve can thus be divided into five regions, each yielding a different solution of the final state, as shown in Figure 2.3.

At a certain minimum velocity, the Rayleigh line touches the R-H curve tangentially at the point U, called the upper Chapman-Jouguet (C-J) point. This is the minimum velocity solution for detonation of the particular mixture, at which the burnt products are travelling at Mach 1 with respect to the detonation wave. For higher velocities, the Rayleigh line cuts the R-H curve at two locations, denoted by W and S. W is the weak solution for detonation, at which point the velocity of the burnt products is supersonic ($(M_2 > 1)$ with respect to the detonation wave. As a result, a growing region of constant state is created between the reaction zone of the detonation wave and the head of the rarefaction wave[26]. The region between U and W1 (Region II in Figure 2.3) yields the weak detonation solution. The point S is called the strong point, representing a pressure higher than C-J pressure. The velocity of the burnt products in this solution is subsonic with respect to the detonation wave. As a result, the rarefaction wave may overtake the detonation wave and weaken it to a C-J detonation. Therefore, the strong, or over-driven, detonation is unstable. The portion of the R-H curve above U, called Region I in Figure 2.3, is called the strong detonation region, in which the final state of the flow is always a strong detonation.

In region III of the R-H curve, the slope of the Rayleigh line is positive and the wave velocity u_D is imaginary. Therefore, region III has no solutions and offers no state that is physically possible. If a tangential Rayleigh line is drawn to the lower side of the R-H curve from A, then it hits the curve at L, which is known as the Lower Chapman-Jouguet or CJ deflagration point. At this point, the velocity of the burnt gases with respect to the detonation wave is sonic. However, this condition is not experimentally verifiable. Regions IV and V on the R-H curve in Figure 2.3 are deflagration solutions, where the wave speeds are subsonic. However, region V corresponding to strong deflagration is physically impossible. Region IV offers stable weak deflagration solutions and as can be easily seen in Figure 2.3, the final state has a slight pressure drop.

The C-J detonation properties can be calculated from the initial conditions using Equations (2.10) through (2.13). It is seen that the calculated states are significantly close to the experimental observations, as seen in Table 2.2. Computer programs that compute thermodynamic and transport properties using equilibrium chemistry are widely available for calculating C-J detonation properties. One such program is the NASA Chemical Equilibrium with Applications (CEA) code[42]. Table 2.3 is a sample list of detonation properties obtained from the CEA code for a selection of common fuels.

The relations for case where specific heat ratio is not held constant, the following relations may be used[34].

$$p_2 \simeq 2q\rho_1(\gamma_2 - 1) \tag{2.14}$$

$$T_2 \simeq \frac{2q\gamma_2}{(\gamma_2 + 1)a_2} \tag{2.15}$$

$$u_2 = \sqrt{\frac{2q(\gamma_2 - 1)}{\gamma_2 + 1}} \tag{2.16}$$

$$u_D \simeq \sqrt{2q(\gamma_2^2 - 1)} \tag{2.17}$$

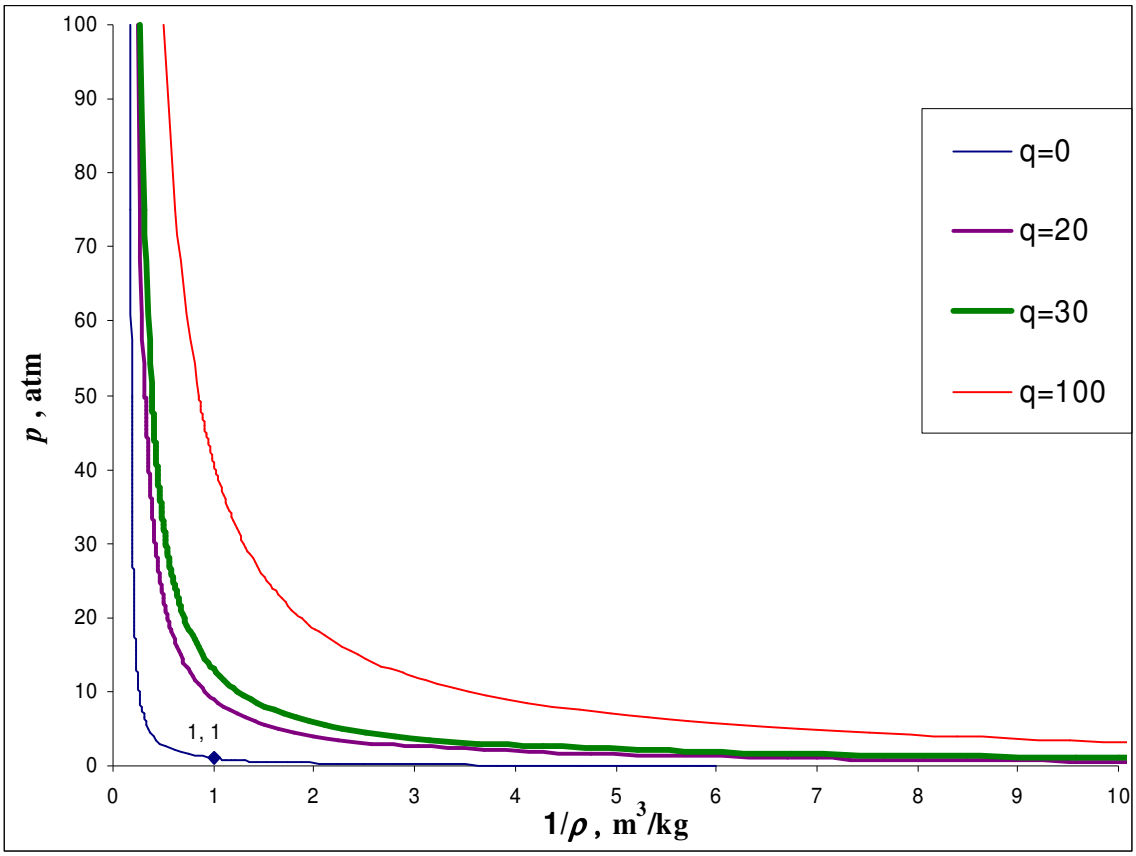

Figure 2.2 A family of rectangular hyperbolic Rankine-Hugoniot curves for a range of q values. The shock Hugoniot is labeled $q = 0$.

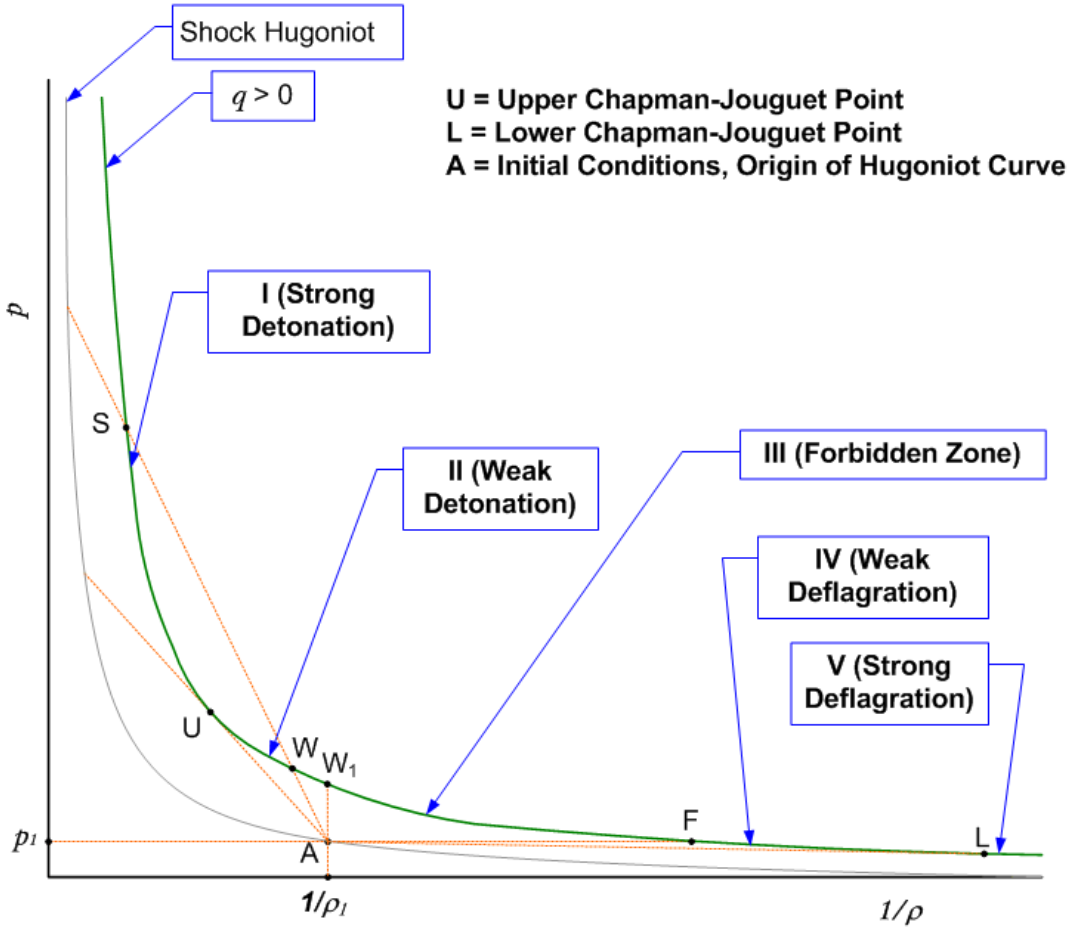

Figure 2.3 Schematic of Rankine-Hugoniot curve corresponding to the C-J theory of detonation. Rayleigh lines originating from point A hit the curve at U (Chapman-Jouguet detonation point) and L (Chapman-Jouguet deflagration point).

Table 2.2 Comparison of detonation velocities obtained by C-J theoretical calculations with experimental values[41].

Reactants (mixture) + Diluent	p_2 (atm)	T_2 (K)	$u_{1\text{-calc.}}$ (m/s)	$u_{1\text{-expt.}}$ (m/s)	Error[a] (%)
$(2H_2+O_2)$	18	3583	2806	2819	0.46
$(2H_2+O_2) + O_2$	17.4	3390	2302	2314	0.52
$(2H_2+O_2) + N_2$	17.4	3367	2378	2407	1.20
$(2H_2+O_2) + 5N_2$	14.4	2685	1850	1822	-1.54
$(2H_2+O_2) + 6H_2$	14.2	2650	3749	3532	-6.14
$(2H_2+O_2) + 5Ar$	16.3	3097	1762	1700	-3.65
$(2H_2+O_2) + 3Ar$	17.1	3265	1907	1800	-5.94
$(2H_2+O_2) + 1.5Ar$	17.6	3412	2117	1950	-8.56
$(2H_2+O_2) + 1.5He$	17.6	3412	3200	3010	-6.31
$(2H_2+O_2) + 3He$	17.1	3265	3432	3130	-9.65
$(2H_2+O_2) + 5He$	16.3	3097	3617	3160	-14.46

[a] $$\%\,\text{Error} = \frac{u_{1-\text{expt.}} - u_{1-calc.}}{u_{1-\text{expt.}}} \times 100$$

Table 2.3 Detonation properties calculated using the C-J model by the CEA code[42].

Fuel	Oxidizer	Mole Ratio	C-J Vel., m/s	C-J Mach No.	p/p_1	T/T_1	ρ/ρ_1	T_1, K	p_1, atm
Hydrogen	air	1:2.38	1966	4.8179	15.497	9.817	1.804	300	1
(H_2)	oxygen	1:0.5	2835.7	5.2562	18.657	12.253	1.8384	300	1
Methane	air	1:9.52	1800.8	5.0968	17.09	9.269	1.8057	300	1
(CH_4)	oxygen	1:2	2389.8	6.7058	29.136	12.403	1.8539	300	1
propane	air	1:23.8	1797.4	5.2919	18.148	9.409	1.8105	300	1
(C_3H_8)	oxygen	1:5	2356.6	7.6569	35.951	12.742	1.8571	300	1
Octane	air	1:59.5	1793.3	5.3762	18.548	9.442	1.8119	300	1
(C_8H_{18})	oxygen	1:12.5	2339.7	8.168	39.608	12.874	1.8583	300	1
Acetylene	air	1:11.9	1864.7	5.3904	19.029	10.386	1.8182	300	1
(C_2H_2)	oxygen	1:2.5	2425.2	7.3322	33.647	14.046	1.8416	300	1
Ethylene	air	1:14.28	1821.7	5.2731	18.257	9.755	1.8139	300	1
(C_2H_4)	oxygen	1:3	2373.5	7.2311	33.212	13.111	1.8516	300	1
Methanol	air	1:7.14	1799.3	5.2777	18.077	9.191	1.8129	300	1
(CH_3OH)	oxygen	1:1.5	2269.2	7.1079	31.557	11.814	1.86	300	1
Ethanol	air	1:14.28	1789.7	5.3322	18.316	9.273	1.8124	300	1
(C_2H_5OH)	oxygen	1:3	2285.3	7.6339	35.391	12.249	1.8604	300	1
Jet A	air	1:84.49	1786.8	5.389	18.544	9.454	1.8122	300	1
($C_{12}H_{23}$)	oxygen	1:17.75	2316.2	8.2606	39.945	12.933	1.8579	300	1
JP-10	air	1:66.64	1785.3	5.3432	18.504	9.517	1.8129	300	1
($C10H_{16}$)	oxygen	1:14	2299.8	8.0226	39.098	13.032	1.8564	300	1

2.3 ZND Theory

Developed independently by Zeldovich (1940), von Neumann (1942) and Doering (1943), the ZND theory of detonation is a one-dimensional detonation wave model which solves the hydrodynamic Euler equations coupled with finite rate chemical reactions. The detonation wave is modeled as a shock wave followed by an induction zone and a reaction zone, as shown in Figure 2.4, all of which travel together at the detonation velocity. The shock is considered to be a very thin region, only a few molecular mean-free-paths in width, so thin that not enough molecular collisions take place to cause reactions to occur. As the flow goes through the shock, it experiences a sudden rise in temperature, pressure and density, all of which remain relatively flat

over a short distance called the induction zone, the thickness of which depends on the shock strength, the post-shock velocity, the pre-shock conditions and the chemical kinetic rates of the reactants. After the induction zone, the reaction rate increases rapidly and the reaction continues till the thermodynamic properties reach C-J state, in a region known as the reaction zone. The thickness of the reaction zone is dependent on the rate of reaction. The reaction causes the temperature to shoot up, while the pressure falls due to the expansion of the products. A rarefaction is formed between the end of the reaction zone and the rear boundary wall of the test chamber. The thickness of the detonation wave is considered to be of the order of 1 cm.

Although, the ZND theory also predicts the same final state as the C-J theory, the former is able to predict the von Neumann spike. This can be clearly illustrated on an R-H curve as shown in Figure 2.5. The possible paths taken by the flow going through the detonation wave are shown as a, b, c and d in Figure 2.5. Path a would require a large amount of energy deposition to the flow to induce direct detonation initiation. Path b would require extremely fast chemical kinetics, whereas path c would require slow chemical kinetics. The most feasible path is d, starting with an adiabatic compression along the shock R-H curve, till it reaches a zenith, termed the von Neumann spike, and then the path diverts sharply downward along the Rayleigh line to complete the course at point U. The pressure at the von Neumann point rises is at a value that is 30 to 100 times higher than the initial pressure, lasting for a period of about 1 μs , which is similar to the vibrational relaxation times of gases[41]. Figure 2.6 shows the profile of an actual detonation wave captured by a piezoelectric pressure transducer at a sampling rate of 2 MS/s with the various zones identified. Another significant point about the ZND model is that it can also predict the properties of strong, also known as over-driven, detonation waves. Thus, a strong detonation travels up the shock R-H curve to reach a higher von Neumann pressure level before turning down on the Rayleigh line to finally reach point S, as seen from Figure 2.7. The larger slope of the Rayleigh line shows that the shock velocity of a strong detonation is higher than the C-J detonation velocity.

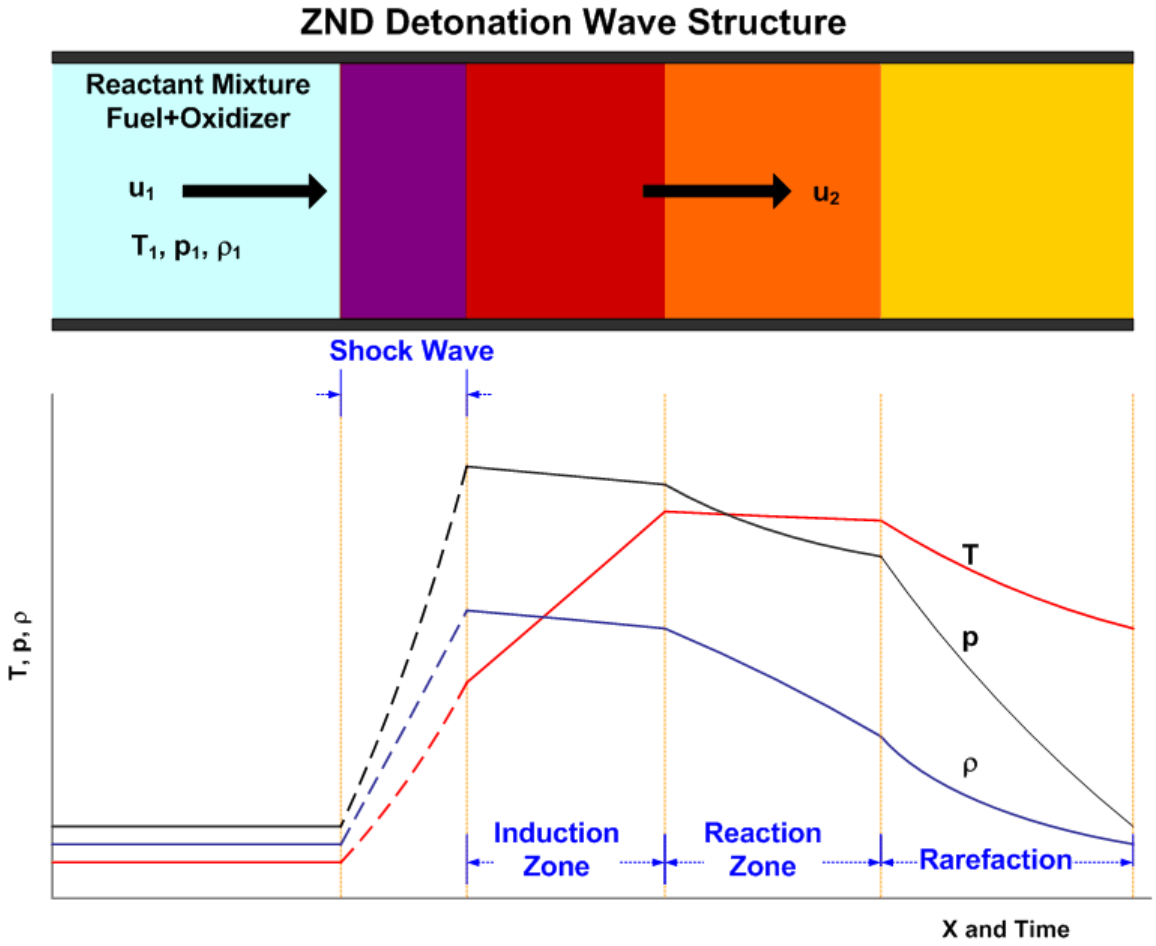

Figure 2.4 Schematic of the pressure, temperature and density profiles of a ZND detonation model.

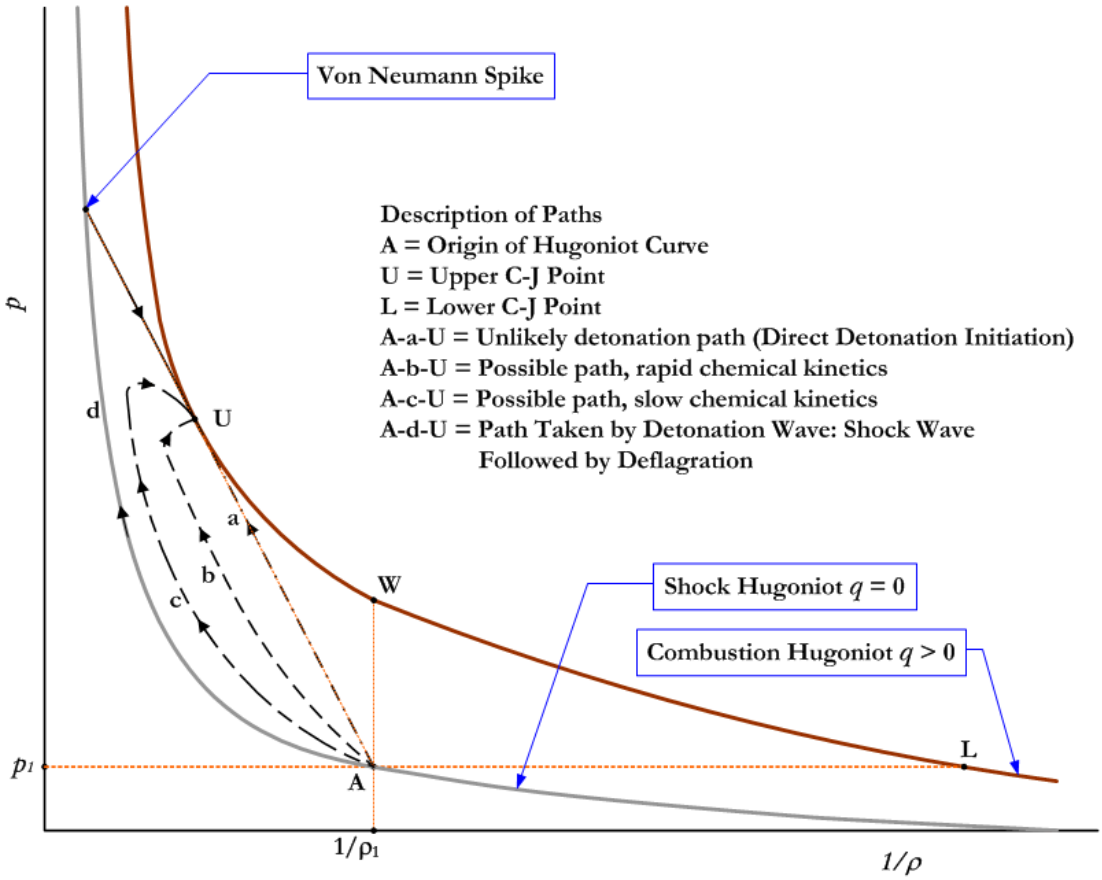

Figure 2.5 Schematic of the Rankine-Hugoniot plot corresponding to the ZND detonation theory showing the various possible paths that may be taken to the C-J detonation point. Path d is the one taken in the ZND model[41].

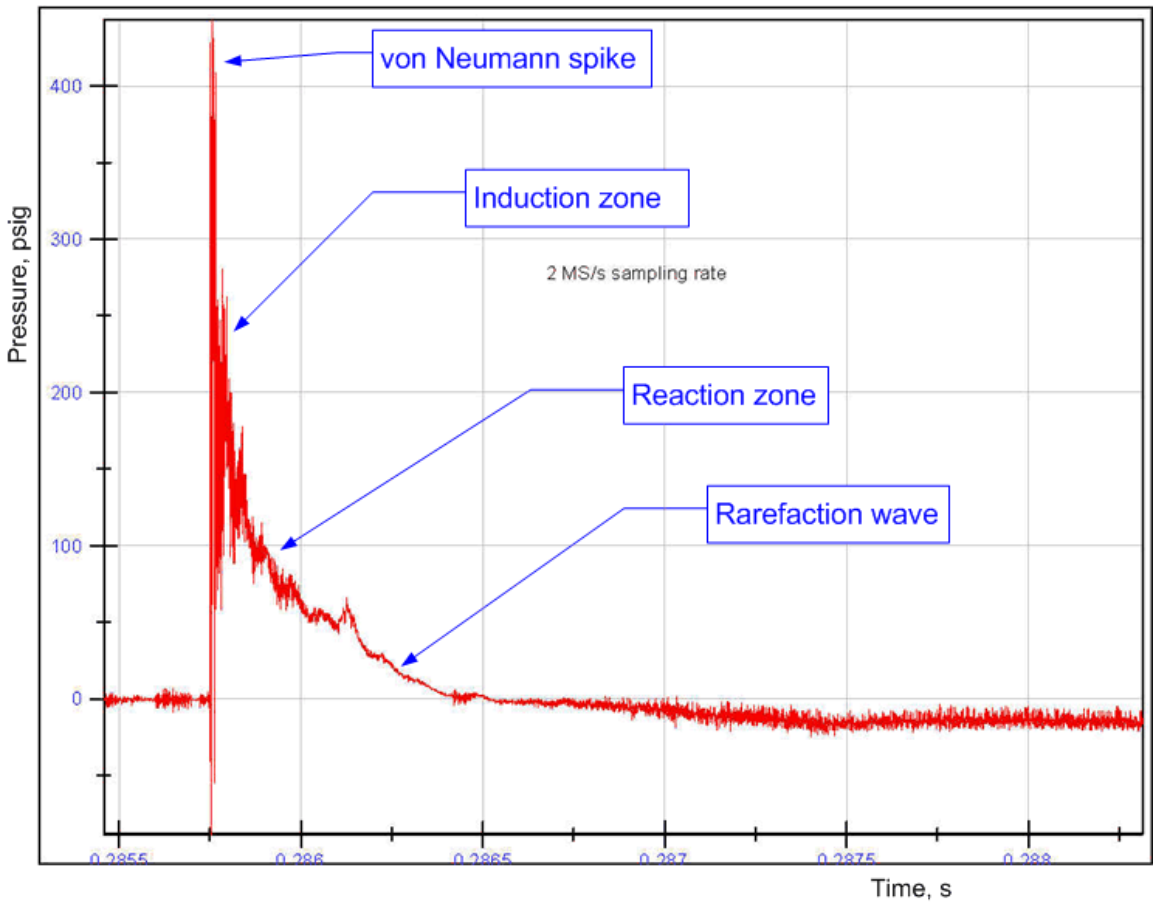

Figure 2.6 The pressure history of an actual detonation wave of a stoichiometric propane-oxygen mixture, sampled at 2 MS/s with a dynamic piezoelectric pressure transducer, with the von Neumann spike, the induction zone, the reaction zone and the rarefaction region marked up. Each division on the x-axis is 0.00025 s.

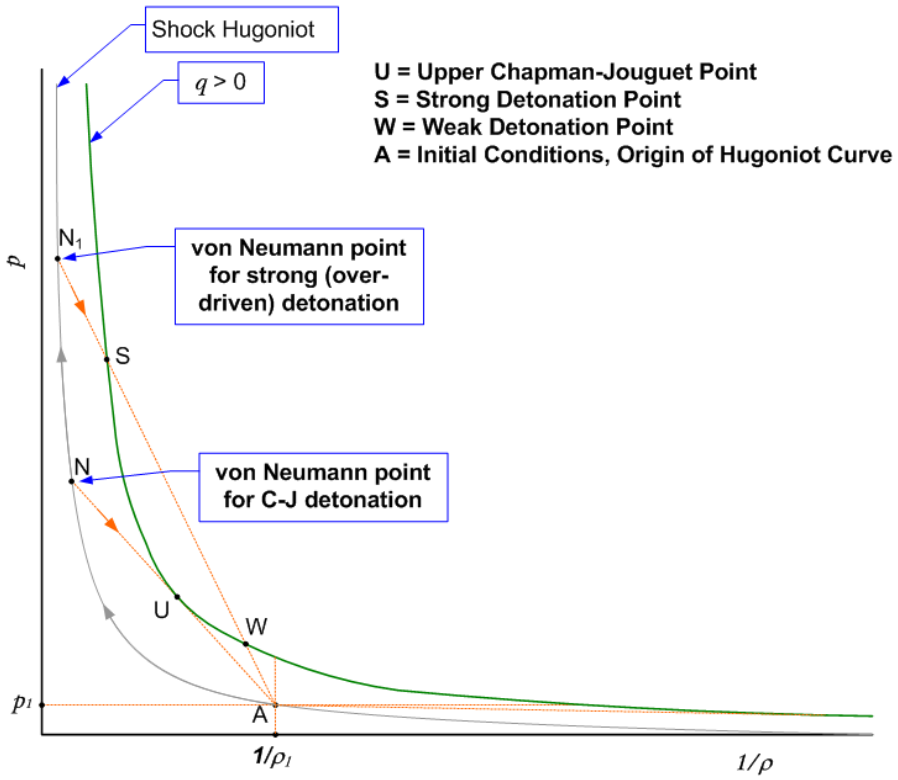

Figure 2.7 Schematic of the Rankine-Hugoniot curve showing the path taken for a C-J detonation as well as a strong detonation wave.

2.4 Three-Dimensional Structure of Detonation Waves and Cell Size

The detonation wave front is in reality not a flat region but rather a wrinkled three-dimensional unsteady structure that is caused by the dynamic interaction of the forward going wave with transverse reflected waves and Mach stems, which causes triple points to occur[26, 41]. The loci of the triple points form diamond shapes, which can be observed by the imprints left behind on soot-covered plates attached to the inner walls of detonation tubes, as depicted schematically in Figure 2.8. These diamond-shaped patterns are referred to as detonation cells. Figure 2.9 shows a more detailed schematic illustrating the formation of the diamond shapes as the detonation wave front moves towards the right of the page. Since the flow in the reaction front with respect to the detonation wave is subsonic, instabilities in the reaction front can catch up to

the detonation wave and weaken it, creating regions of decoupled shock and reaction fronts and transverse shocks that moves perpendicular to the direction of the detonation wave. The triple points are created by the intersection of the leading shocks or Mach stems, the incident shocks and the transverse shocks, as seen in Figure 2.9. The triple points approach each other in a direction perpendicular to the flow and collide, which is then followed by the decaying of the Mach stem and the leading shock into decoupled shocks and reaction zones. These collisions and reactions continue in a cyclical fashion, creating the diamond-shaped patterns.

The width of the cell, as depicted in Figure 2.8, is also known as the cell size and is denoted by λ. Table 2.4 shows a list of cell sizes for common fuel-air mixtures at stoichiometric condition. The cell size varies with the equivalence ratio of the mixture, with the minimum cell size seen at an equivalence ratio of between 1 and 1.1, and then increasing as the equivalence ratio moves away from 1 in either direction, forming a distinctive U-shaped curve, as seen in Figures 2.10 and 2.11. The cell size is directly related to the sensitivity of a mixture, with more sensitive reactants having smaller cell sizes. Therefore, fuel-oxygen mixtures have smaller cell sizes than fuel-air mixtures, as seen in the case of propane in Figure 2.12. Thus, a stoichiometric propane-oxygen mixture (50 kPa, 293 K) has a cell size of about 2.5 mm, whereas it is about 52 mm for a corresponding propane-air mixture (1 atm, 300 K). Increasing the percentage of diluents, such as nitrogen, argon, carbon dioxide, etc., increases the cell size, making the mixture less detonable. Experimental evidence has shown that cell sizes decrease with increasing initial temperature and pressure. This is clearly seen in the plots of cell size vs. initial pressure in Figures 2.12 – 2.14.

As seen from Table 1, propane-air mixtures have similar cell sizes as that of various liquid fuels such as jet fuel and kerosene. Therefore, propane-air mixtures are good surrogates of such liquid hydrocarbon-air mixtures in detonation studies where a gas may be easier to use. The cell size is used as a primary parameter to associate detonation properties, including detonability limits, ignition delay and the minimum and critical tube diameters.

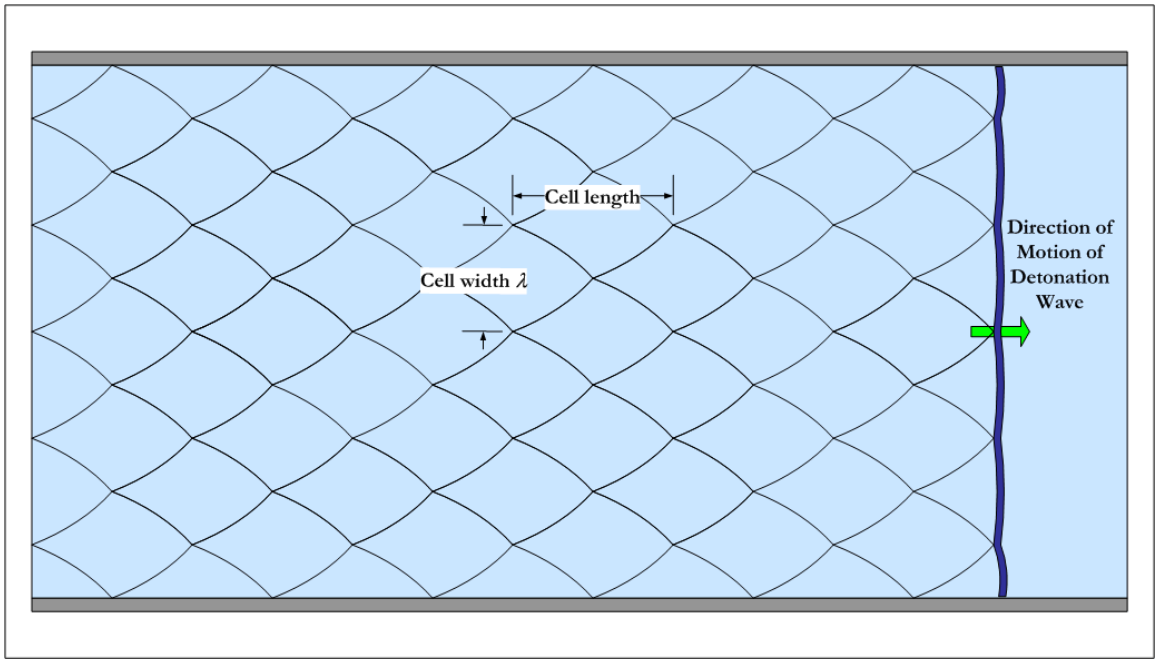

Figure 2.8 Schematic of detonation cells formed within a tube as the detonation wave travels down its length[41].

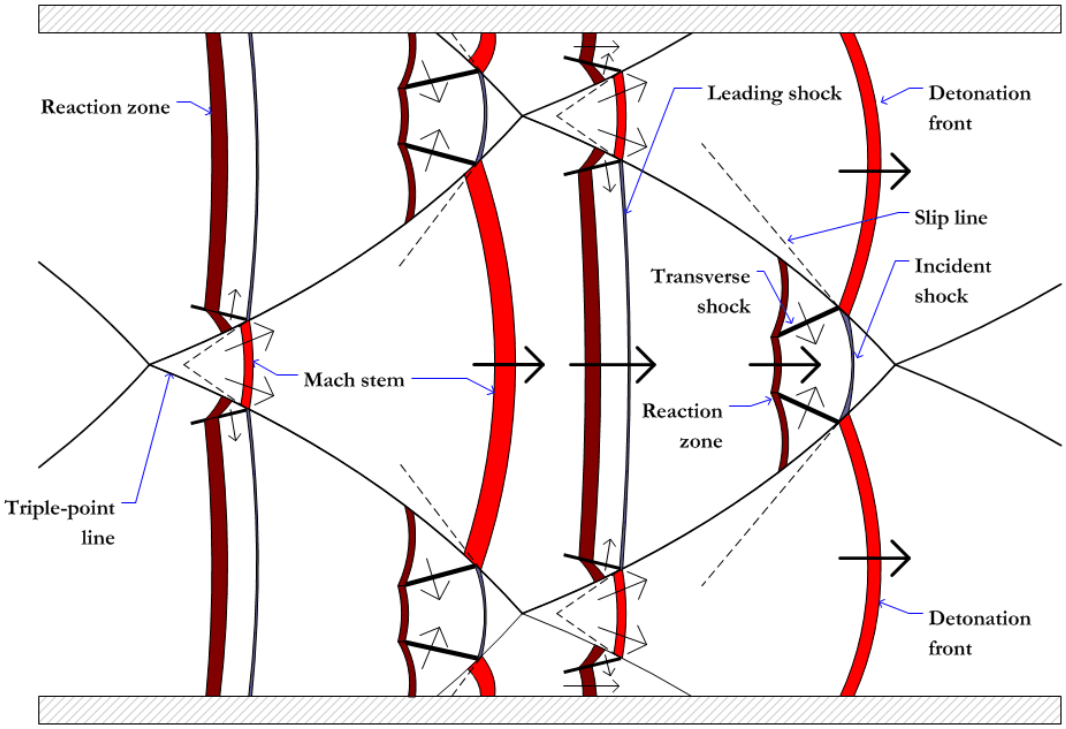

Figure 2.9 Detailed schematic illustrating the formation of the diamond pattern by the movement of the triple points[41].

Table 2.4 List of cell sizes for various fuel-air mixtures at stoichiometric condition[32, 43].

Fuel	Cell width (mm)	Pressure (Atm)	Temperature (˚C)
Hydrogen	10.9	1	22
Methane	280	1	22
Acetylene	9	1	22
Ethylene	22.8	1	22
Propane	51.3	1	22
Benzene	126	1	100
Hexane	51.1	1	22
Octane	42	1	100
JP-10	60.4	1	100
JP-10	47	1	135
JP-10	54.7	2	100
Decane	42	1	100
Jet-A	45	1	135
JP-4	45	1	100

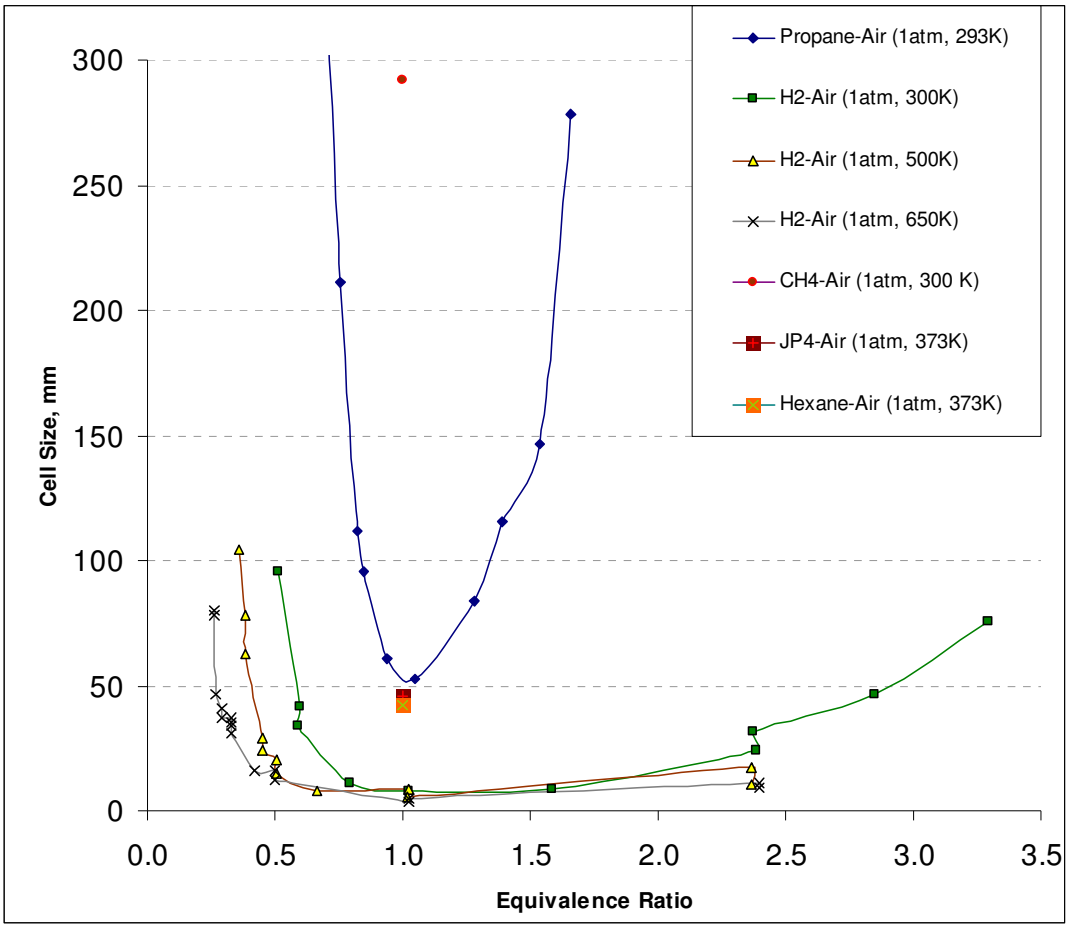

Figure 2.10 A plot of cell size vs. equivalence ratio for various mixtures. The U-shape in the variation of cell size with equivalence ratio is a common feature for most fuels[43].

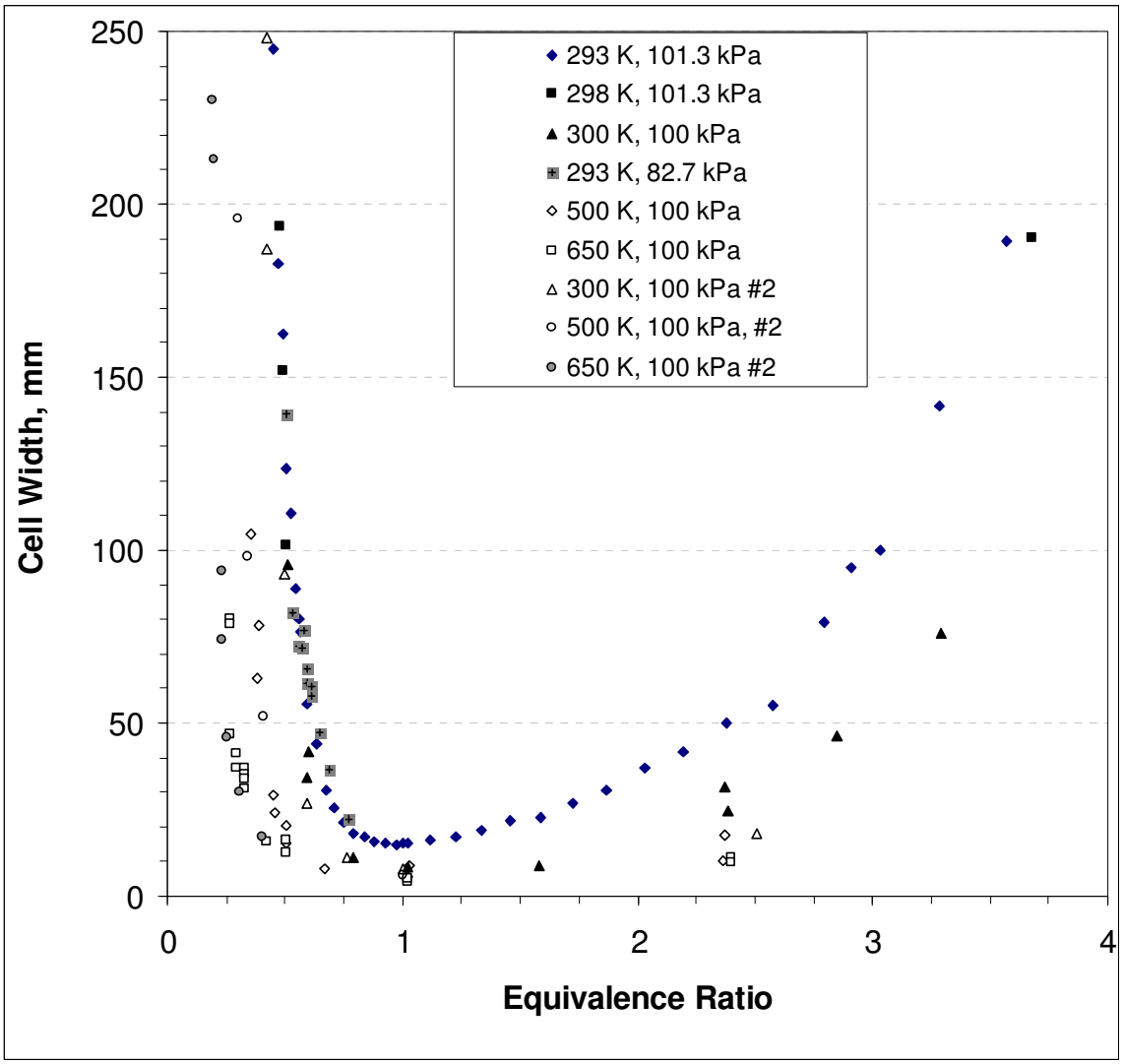

Figure 2.11 A plot of cell size vs. equivalence ratio for hydrogen-air mixtures[43]. The U-shaped curve with a minimum at an equivalence ratio of 1 is seen clearly.

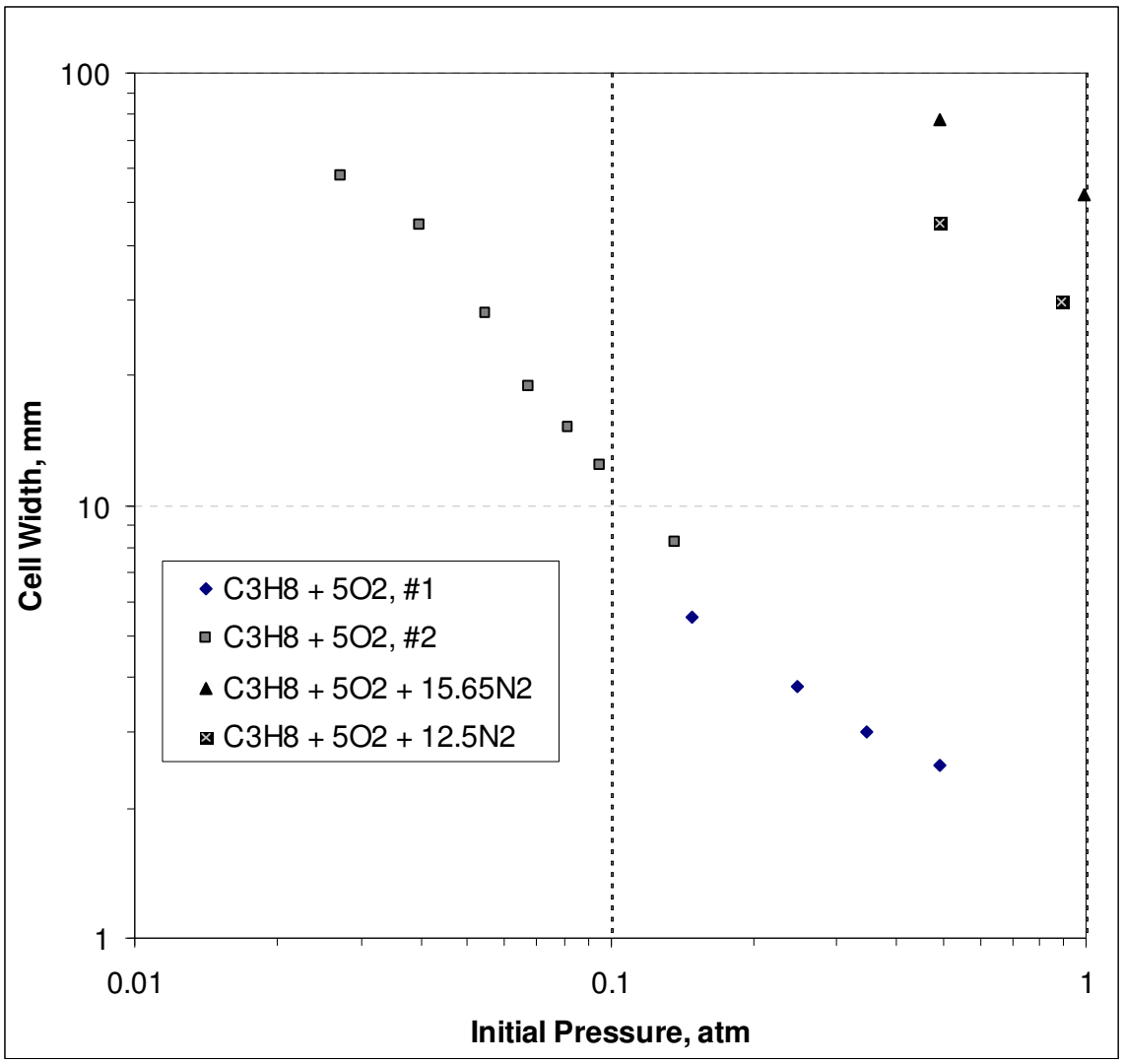

Figure 2.12 A plot of cell size vs. initial pressure for propane with oxygen with diluents[43]. The inverse relationship of cell size with initial pressure is evident. The initial temperature for the above cases is 293 K.

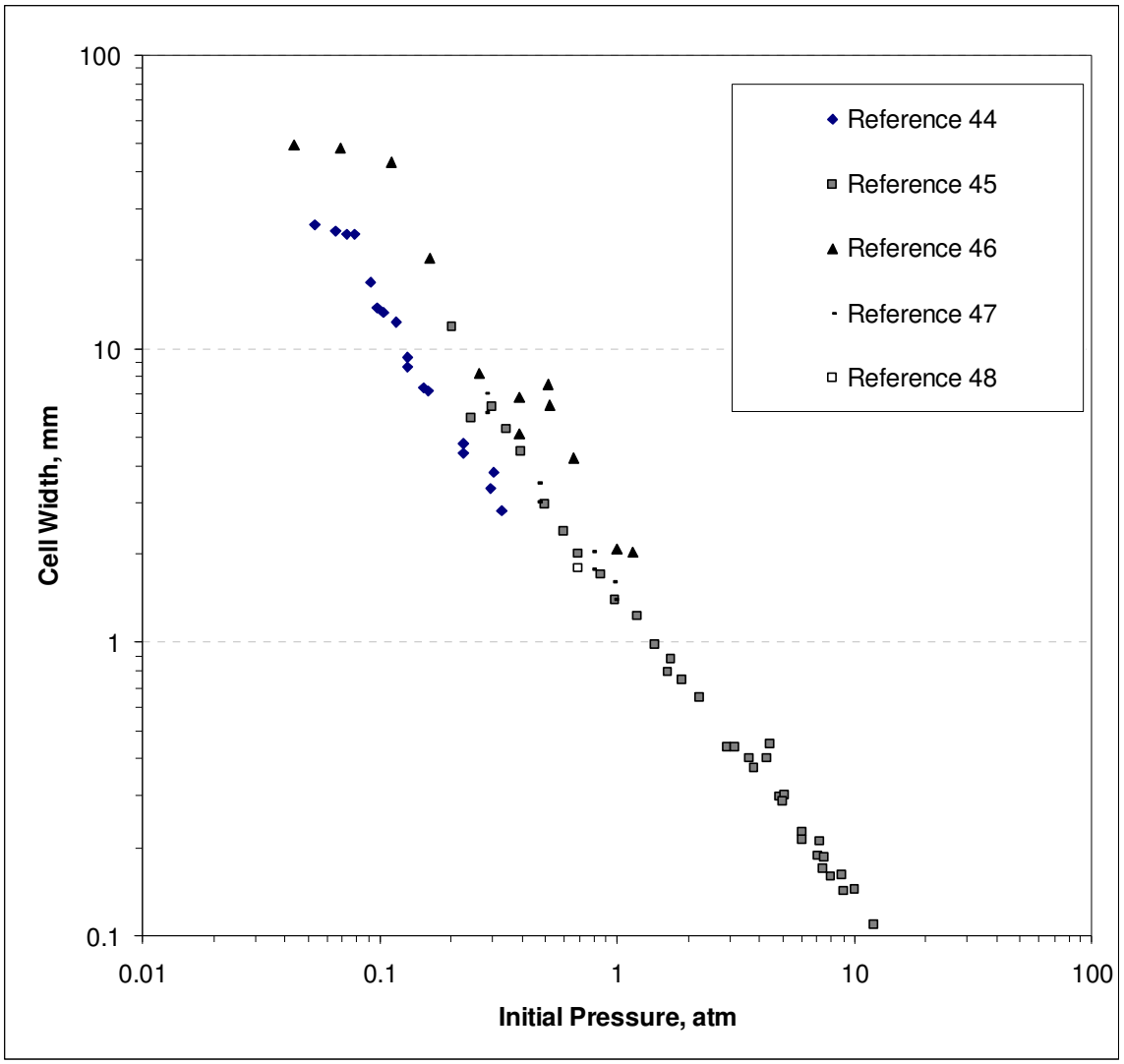

Figure 2.13 A plot of cell size vs. initial pressure for hydrogen, showing an inverse relationship of the cell width with initial pressure[43]. All the above cases are for an initial temperature of 293 K at an equivalence ratio of 1.

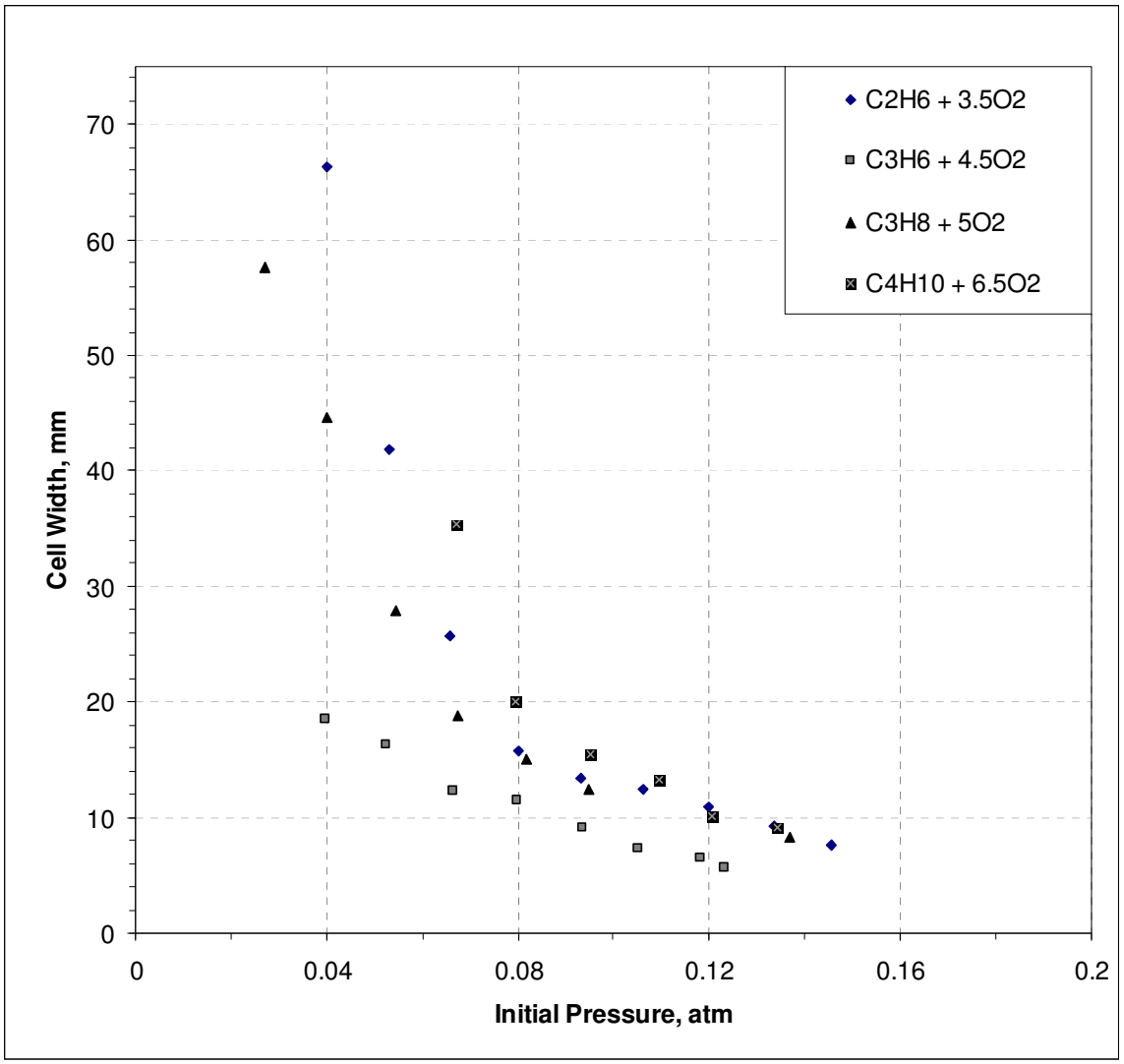

Figure 2.14 A plot of cell size vs. initial pressures for a handful of gaseous fuels at initial temperature of 293 K[43, 49].

2.5 Detonation Nomenclature

2.5.1 C-J Detonation

A C-J detonation condition is defined in the C-J theory according to which the detonation wave is a thin one-dimensional surface with an instantaneous chemical reaction. If the detonation wave is held static with the flow passing through it, the velocity of the products with respect to the detonation wave is considered to be sonic and, consequently, the velocity of the

reactants is supersonic with respect to the detonation wave front. Therefore, the wave is considered to choke the flow passing through it. The pressure and temperature of the products can now be calculated using the C-J relations presented earlier. On the Rankine-Hugoniot plot, the C-J detonation condition is denoted by U, as shown in Figure 2.3. The estimation based on the C-J relations is quite accurate and is widely used to predict detonation properties. The CEA code[42] is widely used to obtain the C-J detonation properties, including the detonation pressures and wave velocities, to compare with experimental results.

2.5.2 Over-Driven Detonation

When the detonation wave is accelerated by the buildup of pressure and temperature in the reaction zone, the wave may attain velocities in excess of C-J detonation velocity, causing it to become an over-driven detonation wave. Over-driven detonation waves are stronger than the C-J detonation wave, with the pressures having much higher values than the C-J value. Over-driven detonations are less stable than C-J detonations and are subject to weakening by the rarefaction waves behind it. As a result, over-driven detonations continuously decay until they reach the C-J state[32] or may weaken further to the quasi-detonation state if the detonability limits are reached.

2.5.3 Retonation

When a detonation wave is formed, a shock wave is created that travels back into the burnt gas. This shock is known as a retonation wave. It re-compresses the flow that has undergone deflagration before the detonation wave originated. If the burnt gas still has unburnt reactants, it will enhance the shockwave to form a detonation wave. In some cases, the retonation wave can reflect off the back wall and then travel back in the forward direction. As the sonic velocity in the burnt gas is higher, the retonation wave may even catch up with the original detonation wave and combine with it, making it stronger.

2.5.4 Spinning Detonation

In smooth circular tubes, if the diameter of the tube is near the detonability limits or if the concentration of the reactants is such that the cell size is near the detonability limit (see Section 3.1.4), the relatively planar one-dimensional detonation wave structure develops into a spinning three-dimensional formation, causing the wave front and the flow behind it to spin about the axis of the tube. This phenomenon was observed by the presence of helical marks left behind on the inside of tubes. Since the cell size λ is dependent on the fuel concentration (equivalence ratio), the appearance of spin can also be expressed in terms of λ and tube inner diameter d. Spinning detonation fronts are caused as the tube diameter nears the minimum diameter, which is generally accepted as λ/π for circular tubes and λ for ducts with a square or rectangular cross-section.

2.5.5 Galloping Detonation

Just like spin detonations, when the mixture of reactants within the detonation tube is near the detonability limits, the detonation wave is seen to accelerate and decelerate in a cyclical fashion. The over-driven detonation state can persist for extended tube lengths, of the order of 0.1 m, with velocities exceeding C-J velocity by as much as 35 %, with a similar increase in pressure[34]. Overdriven detonations are inherently unstable and are weakened by the rarefaction waves behind them, causing them to slowdown and decouple. The shock and deflagration wave system may be accelerated again to a detonation by the interaction with the boundary layer and the process may continue if the tube is long enough. The wave speed can vary as much as 50 % to 150 % of C-J velocity[39]. This phenomenon has been observed in experiments at the ARC in multi-cycle PDE setups using propane-oxygen mixtures.

2.5.6 Quasi-Detonation

A quasi-detonation is a shock wave followed at some short distance by a flame front. This phenomenon is observed right before the coupling of a shock wave and flame front into a detonation wave or just after a detonation wave has decoupled into the shock and flame fronts. Thus, it is a shock wave followed by a strong deflagration wave. A quasi-detonation will die out into a deflagration or can be accelerated into a detonation using obstacles, provided that enough tube length with a reactive mixture is present.

2.6 Initiation of Detonation

A detonation wave originates when a large amount of ignition energy is transferred to a reactive medium, causing rapid chemical reactions. As a result, the pressure and temperature levels swell causing a detonation wave to occur. There are many ways to trigger a detonation wave.

2.6.1 Direct Initiation

A detonation wave can be initiated in a reactive mixture by detonating a small explosive charge, firing a high powered laser into it or by discharging an arc whereby a significant quantity of energy is expelled into the mixture. While explosives are not practical for a propulsion device, lasers and arc discharge devices are also not very convenient as they are highly power consuming and require large on-board power supplies.

2.6.2 Shock Induced Detonation

When a shock wave enters a reactive medium, the resulting compression energizes the reaction rates behind the shock, creating a buildup of high pressure and temperature in the flow behind. As a result, the shock wave develops into a detonation wave. This technique is employed in detonation-driven shock tubes for producing high enthalpy flows. For example, the ARC's detonation-driven shock tube uses an air or helium driver to detonate mixtures of hydrogen and

oxygen diluted with helium, and produces high speed flows with total temperatures as high as 4200 K and total pressures of about 34 atm.

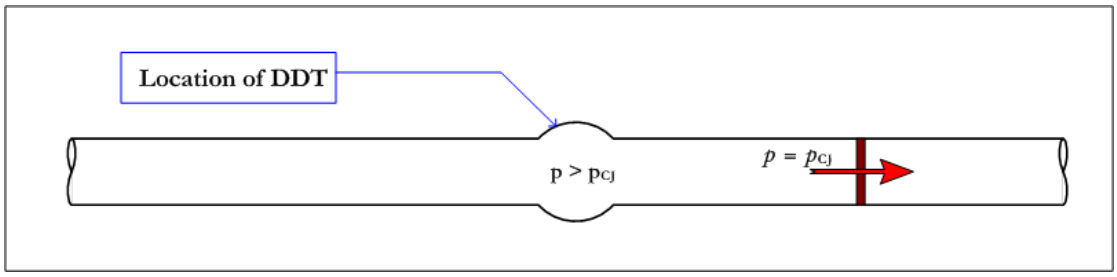

Figure 2.15 The location where DDT occurred in fuel lines is often seen by the presence of a bulge in fuel lines that have undergone a flashback or unwanted detonation[41].

2.6.3 Deflagration to Detonation Transition (DDT)

A deflagration within a confined reactive mixture can naturally transition to a detonation due to the buildup of pressure and temperature behind the flame front, provided that the tube length is sufficient. Typically tube lengths of the order of 1 to 2 m are needed for a deflagration flame front to form a shock wave and then to couple with it. Less energetic mixtures are known to take up to 10 m for DDT to occur[43]. DDT run up distance is often expressed in terms of length-to-diameter ratio (L/D). For less sensitive mixtures, natural DDT run up distances may require an L/D of 10-60, whereas sensitive mixtures, such as acetylene-air or fuel-oxygen mixtures, may require an L/D of 3-10[39]. However, DDT can be accelerated by means of increasing wall roughness and turbulence. This fact was discovered by Shchelkin, who used spiral wires of various thicknesses to simulate wall roughness. It was found that the spirals cause the flame front to accelerate due to the formation of hot spots and pressure pulses in the flow. A laminar flame front in a reactive mixture will interact with the surface obstacles and the boundary layer creating pockets of hot burning gases and compression waves. Eventually, the compression

waves preceding the flame front coalesce into a shock wave. The buildup of pressure behind the flame front accelerates it enough to cause it to couple with the shock, forming a self-sustaining C-J detonation. At the moment of the coupling, a retonation wave is also formed that travels back into the flow. There are various obstacles that may be placed in the flow path to bring about DDT, such as spiral fins, spiral grooves and orifice plates. However, the hot spots created by the obstacles also subject the obstacles to heavy shock and thermal loading, which can eventually destroy them. For application within a PDE, it is important to find an obstacle that is capable of withstanding repeated shocks and high temperatures without breaking down.

2.6.4 The Pre-detonator Method

Similar to the direct initiation and shock induced processes, a detonation wave can be created within a highly reactive mixture and then transmitted to a less reactive mixture. This method may also be referred to as detonation-initiated-detonation, because detonation in a highly sensitized fuel-oxidizer mixture is transmitted to a less sensitive mixture. In a propulsion system that works on this principle, a small tube containing an energetic mixture, such as propane, acetylene or hydrogen with oxygen, known as a pre-detonator, is connected to the main combustor of larger volume that uses a less energetic fuel-air mixture. Ignition is started in the pre-detonator in which a detonation wave is soon formed, and then passed on to the main combustor. This causes the less reactive fuel-air mixture to detonate. Thus, only a small quantity of oxygen and fuel charge is required to maintain detonations.

2.7 Detonation Parameters

2.7.1 Minimum Tube Diameter

It has been experimentally verified that the cell size of a reactive mixture may be used as a criterion to determine whether a detonation will successfully propagate in a tube filled with the mixture. For a tube, the diameter must be larger than $\lambda/3$, where λ is the cell size. At this

minimum diameter, one cell is wrapped around the circumference of the tube. For square and rectangular ducts, the height and width of the duct must be larger than λ. The minimum detonation tube diameter is always larger than the flame quench diameter, which is the smallest size of a tube that will support the propagation of a flame within it. It can be as small as a fraction of a cm. Thus, this factor can be used for deciding the minimum diameter of an engine based on the fuel it is intended to run on.

2.7.2 Critical Tube Diameter

For detonation to be passed successfully from a tube of smaller to one of larger diameter, the smaller tube must have a minimum diameter $d_c > 13\lambda$. For square or rectangular ducts, the critical dimension is $d_c > 10\lambda$. For tubes of smaller diameters, the detonation wave will die out as it exits the tube. However, the flame will continue to propagate if the reactants are present.

The minimum and critical diameters, as depicted in Figure 2.16, are important parameters for PDEs. Engine sizes have to match the minimum diameter criteria for the fuel-oxidizer mixture intended for use. Also, to prevent detonation waves from harming turbine blades or other components downstream of the detonation combustor, the detonation tube may be made smaller than the critical diameter.

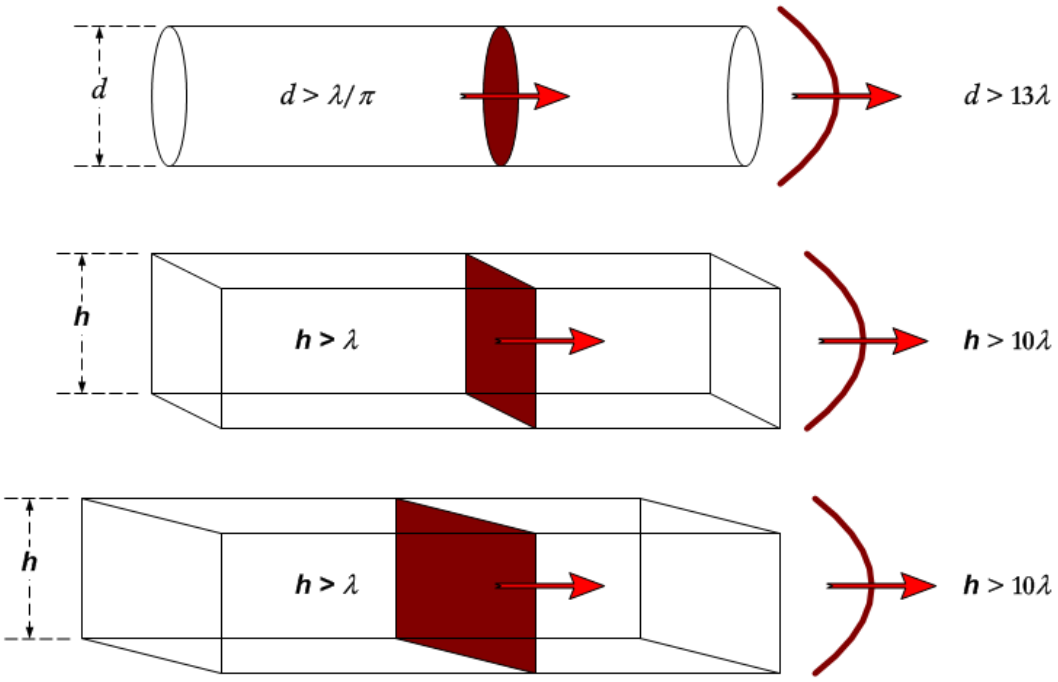

Figure 2.16 A schematic showing the minimum and critical diameters for tubes and ducts[39,41].

CHAPTER 3

A BRIEF REVIEW OF FUELS FOR PDE APPLICATION

3.1 Definitions

3.1.1 Flash point

The flash point of a liquid fuel is the lowest temperature at which the vapor pressure of the fuel is high enough to form a combustible mixture with air, which will burn if an ignition source is provided[50].

3.1.2 Auto-ignition temperature

The auto-ignition temperature[50] is the minimum temperature at which a fuel will spontaneously ignite without the introduction of a spark or flame. Gasoline has a low flash point (related to boiling point) which allows it to mix with the air inside the engine, but it has a high auto-ignition temperature so that it does not spontaneously ignite during the compression stroke of the engine, until the spark has been fired. Gas turbine fuels, which are derived mostly from kerosene, have relatively higher flash points and lower auto-ignition temperatures than those of gasoline.

3.1.3 Minimum Ignition Energy

The minimum ignition energy required to start a deflagration is in the order of 1 to 10 mJ for most fuel-air mixtures at rest. The energy requirements will increase to 100 mJ or higher with increasing flow velocity. If the velocity is too high, the spark may be quenched altogether. Thus, a flame holder will be required for PDE applications. However, flame holders are sources of drag and have to be resistant to the high shock and temperature environment within the PDE. Therefore, the pre-detonator method is a viable option for PDEs where flame holders are not

feasible. To lower the ignition energy, the initial temperature and total pressure may be increased. When deciding on igniter designs, it is vital to ensure that the igniter electrode separation is close to the quenching distance. In designing the ignition system, it is important to consider the fact that ignition energy is also the lowest at stoichiometric conditions. However, the energy release and temperature is highest at stoichiometric condition. Equivalence ratios of between 0.9 and 1.1 are safe zones as many parameters are close to that of the stoichiometric case, including cell size, minimum tube diameters, DDT run up distance and ignition energy. Ignition energy requirements are further discussed in Section 7.1 and a chart of ignition energy variation with temperature for jet fuels is shown in Figure 7.1. Table 3.1 presents a list of ignition temperatures for various fuels in air at 1 atm. It is more efficient to start a deflagration with minimal ignition energy and then to utilize DDT to obtain detonations within a PDE because high energy ignition systems will not be required.

3.1.4 Heat of Combustion and Heating Value

The heat of combustion[50, 51] (or enthalpy of reaction) is the magnitude of the enthalpy change when one mole of the substance is fully reacted with oxygen, i.e., in a stoichiometric reaction. The enthalpy of combustion is expressed as a negative quantity for exothermic reactions. The heat of combustion is determined in kJ/mol and then expressed in more convenient units of energy/mass of fuel or energy/volume of fuel. The heating value (or calorific value) of a fuel is the amount of heat released for a particular amount (specified in mass, volume or moles) of a fuel reacting in oxygen when all the products have been cooled down to the initial temperature. The higher heating value (HHV) is obtained when the water produced in the reaction is in liquid form. The lower heating value (LHV) is obtained when the water is in vapor form and is calculated by subtracting the latent heat of vaporization of the water vapor formed in the reaction from the HHV.

3.1.5 Explosion limit

The explosion limit[39,50] (also known as detonability limit) of a fuel, expressed as a percentage of the volume of the fuel to the volume of the mixture, is the concentration limit required for the mixture to ignite and explode in the presence of a spark or flame. Below the lower explosion limit (LEL), the mixture is too fuel lean to sustain the explosion; and above the upper explosion limit (UEL), there is not enough oxygen to sustain the explosion. The stoichiometric level will be somewhere in between the two limits. As the detonability limits are reached, the ignition energy increases exponentially[40]. The explosion limits are considered to be narrower than the flammability limits, which are the limits required to sustain deflagration, and both the above are dependent on temperature and pressure. However, in many fuels there is no such clear definition.

For detonations within a tube, the detonability limits may also be explained in terms of cell width[33]. If the diameter of the tube is larger than the cell width of the mixture, then DDT can occur within it and a self sustained detonation is possible. Since the cell width is dependent on the thermodynamic properties of the mixture, namely, the pressure and temperature, it can be shown that the detonability limits are also closely related to the initial pressure and temperature of the reactant mixture.

3.1.6 Isomers

Different compounds having the same molecular formula are known as isomers[50, 51]. For example hexane (C_6H_{14}) has five isomers, including two types of methylpentane and two types of dimethylbutane, all of which are colorless liquids at room temperature, but have differing physical and chemical properties. Similarly, ethanol (CH_3-CH_2-OH), a liquid, and dimethyl ether (CH_3-O-CH_3), a gas, are functional isomers with the chemical formula C_2H_6O.

3.1.7 Saturated and unsaturated hydrocarbons

A saturated hydrocarbon[50] is one in which no two carbon atoms have double or triple covalent bonds. In hydrocarbon molecules, the bond between two carbon atoms may be saturated single covalent bonds or unsaturated double or triple bonds. The greater the number of hydrogen atoms in a hydrocarbon molecule, the greater is the heat content per unit mass of the fuel.

3.1.8 Aromatic and aliphatic hydrocarbon compounds

Hydrocarbons can be generally classified as aromatic and aliphatic compounds[50,51,52]. Aromatic molecules have carbon rings with alternating unsaturated bonds, lone pairs or empty orbitals. This arrangement gives aromatic molecules high stability and makes them less reactive than straight chained molecules. Benzene is the most common aromatic compound, followed by toluene, which is a benzene molecule with one hydrogen atom replaced by a CH_3 group. Toluene and xylene (isomer of dimethyl benzene) are added to aviation fuel to prevent detonation[52]. Aromatics are denser than aliphatics because of the fewer number of hydrogen atoms and, as a result, an aromatic compound with the same number of carbon atoms as an aliphatic compound has lower heat content per unit mass, but higher heat content per unit volume. Aromatics are generally not desired in aviation fuels because they produce smoke and form coke deposits on combustor surfaces[52].

Aliphatic compounds may be straight chained, branched or carbon rings with saturated or unsaturated bonds, but contain no aromatic rings. The ringed aliphatic molecules are also known as alicyclic. All alkanes, alkenes and alkynes are aliphatic compounds.

3.1.9 Naphthalenes

Naphthalenes[51] are double ringed aromatic compounds commonly used in mothballs (C10H8) and in pyrotechnics to produce black smoke and for simulated explosions[53]. Mothballs were added to gasoline by auto-enthusiasts to increase the octane number, which prevents

knocking[54]. Thus, the presence of naphthalenes would retard the initiation and propagation of detonation. The concentration of naphthalenes in aviation fuels is limited due to their negative effects on combustion, including smoke production and formation of coke deposits on the inside surfaces of combustors[52].

3.1.10 Alkanes

Alkanes[51] are the simplest hydrocarbon molecules, having the general formula $C_nH_{2n+2,}$ e.g. methane (CH_4) and ethane (C_2H_6). Alkanes have the highest heat content per unit mass amongst all hydrocarbon fuels due to the higher hydrogen-to-carbon ratio[51]. However, that also makes them more stable and less reactive than the unsaturated hydrocarbons such as alkenes or alkynes, which means that they will have longer induction times. Straight chained alkanes are also known as paraffins, while those with branches are known as iso-alkanes or iso-paraffins. The straight chained alkanes have higher energy content because of the greater hydrogen-to-carbon ratio than iso-paraffins. The straight chained alkanes are known to be less resistant to knocking in piston and turbine engines than iso-paraffins. For detonation application, regular alkanes would be preferable. Iso-octane content is increased in aviation gasoline (for piston engines) to increase its octane number and reduce its detonability.

Alkanes with one or more rings are known as cycloalkanes, cycloparaffins or naphthenes and follows the chemical formula $C_nH_{(2n-r)}$ where r is the number of rings. The smallest naphthene ring will have three carbon atoms. Naphthenes are clean burning and have lower octane ratings, i.e., they are conducive to detonation.

3.1.11 Alkenes

Alkenes (also known as olefins[51]) are hydrocarbons with at least one carbon-to-carbon double bond and thus have a lower number of hydrogen atoms per molecule than alkanes. Ethylene (C_2H_4, also known as ethene) is the simplest alkene. Olefins are less stable than alkanes and therefore pose a problem for storage (in terms of shelf life) and safety at higher

temperatures. Thus, olefin content is kept low in turbine fuels. However, for detonation, a higher percentage of olefins would be beneficial especially to reduce the induction time.

3.1.12 Alkynes

Alkynes[51] (also known as the acetylene series) are those hydrocarbons that have at least one carbon-to-carbon triple bond. Acetylene (C_2H_2, also known as ethyne) is the simplest alkyne. Thus, alkynes are the most reactive compounds but have the lowest energy content per unit mass among the three types of hydrocarbons. On the other hand, alkanes have the highest energy content per unit mass, but are the least reactive, making them less favorable for detonation than alkenes and alkynes.

3.1.13 Naphthas

Naphthas[50,51,52], also known as petroleum ether, are petroleum derivatives consisting of liquid mixtures of intermediate hydrocarbon products with densities below that of kerosene. Naphthas are used as feedstock to produce gasoline. They contain paraffins, olefins, naphthenes and aromatic compounds.

3.2 Fuels Selection for Pulse Detonation Engines

To be a competitive engine system, the PDE has to work on most if not all conventional fuels used in gas turbines. Theoretically, the PDE can run on any fuel, liquid or gaseous, provided that the combustor is at least one cell size in width. When choosing fuels for PDEs, one has to consider various factors, including engineering (combustion characteristics and gas dynamic), economic (availability, costs of production, transportation, storage and distribution), environmental and safety aspects. From an engineering standpoint, the parameters for selection of a fuel are fuel heating value, detonability, ignition time, ignition energy, adiabatic flame temperature and sensitivity with air. All of the above properties of a fuel, except for the former, can be expressed as a function of its detonation cell size[55]. For aircraft propulsion, the

preferred fuel must have high energy density for compact storage, and must be easy to mix with air by means of injectors or valves.

Detonations in flour mills and sugar factories attest to the fact that solid fuels can also be used to run PDEs. Solid fuels, such as coal dust, purified to remove sulfur and other harmful chemicals, may be viable for application in a ground based hybrid PDE electric power plants, in which the fuel is made into a finely ground powder form and is delivered into the combustion chamber in the form of a colloidal aerosol. Such an arrangement may not be able to achieve high repetitive rates and the complexity and added weight of the fuel delivery system would make this concept feasible for ground based power generation, which would make use of the available fuels more efficiently than a steam turbine based power plant driven by a coal-fired water-boiler.

Therefore, liquid fuels must also have a desired amount of volatility. While gaseous fuels are easy to inject and cause effective mixing with air, many gaseous fuels, for example hydrogen, require high-pressure storage with cooling and large-scale thermal insulation. Gaseous fuels may be preferable for short range or ground based applications due to space or weight constraints on aircraft. Hydrogen (and oxygen) is currently stored in the liquid form in rockets, which require cryogenics facilities and large tanks. The added complexities, weight and size take a toll on the payload and range of the rockets. Nevertheless, hydrogen has many advantages. It has a wide detonability limit, high energy-to-mass ratio, and is clean burning, producing few undesirable byproducts. Table 3.1 provides a short list of fuels in use today, along with their properties, including explosive limits, flash point, auto-ignition point, heat of combustion and cell size, compiled from various sources.

Table 3.1 List of a few well known fuels and their properties.

Substance	Formula	M	LEL (%V)[a]	HEL (%V)[a]	Stoicho-metric Vol (%V)[a]	Flash Point (˚C) (boil. pt.[b])	AIT (˚C)[c]	H.o.C.[d] (MJ/kg)	Cell size (mm)[e] Eq. Ratio =1, (T (K), p (atm))
Hydrogen	H_2	2.02	4	75	29.53	(-253)	520	119.720	10.9 (295,1)
Methane	CH_4	16.04	5	15	9.48	-188	537	50.031	280 (295,1)
Ethane	C_2H_6	30.07	3	12.5	5.65	-135	472	47.489	54 (293,1)[f]
Propane	C_3H_8	44.11	2.1	9.5	4.02	-104	495	46.336	51.3 (295,1)
Butane	C_4H_{10}	58.12	1.9	8.5	3.12	-74	480	45.742	75.1 (293,1)[g]
Pentane	C_5H_{12}	72.15	1.4	8	2.55	-49	260	45.348	NA
Hexane	C_6H_{14}	86.18	1.1	7.5	2.16	-23	225	45.098	51.1 (295,1)
Heptane	C_7H_{16}	100.21	1.05	6.7	1.87	-3	204	44.917	NA
Octane	C_8H_{18}	114.23	0.95	6.5	1.65	14	206	44.789	42 (373,1)
Decane	$C_{10}H_{22}$	142.29	0.75	5.6	1.33	46	210	44.595	42 (373,1)
Ethylene (ethene)	C_2H_4	28.05	2.7	36	6.53	(-103)	450	47.165	22.8 (295,1)
Propylene (propene)	C_3H_6	42.08	2.4	11	4.45	(-48)	460	45.777	NA
Acetylene (ethyne)	C_2H_2	26.04	2.5	100	7.73	(-84)	305	48.219	9 (295,1)
Benzene	C_6H_6	78.12	1.2	7.9	2.72	-11	560	40.571	126 (373,1)
Toluene	C_7H_8	92.15	1.2	7.1	2.27	4	480	40.932	NA
Napthalene	$C_{10}H_8$	128.19	0.88	5.9	1.71	79	526	39.428	NA
Methanol	CH_3OH	32.04	6.7	36	12.25	13	385	19.700	NA
Ethanol	C_2H_5OH	46.07	3.3	19	6.53	11	365	29.620	NA
Acetone (propanone)	C_2H_6CO	58.08	2.6	13	4.97	-18	465	29.032	NA
Avgas 100	Blends		1.2	7	NA		~250	44.000	NA
Jet A	~$C_{10}H_{23}$	167.31	0.6	4.7	NA	38	238	43.2	45 (408,1)
JP-4	Blends		1.3	8	NA	<35	246	43.900	45 (373,1)
JP-5	Blends		0.6	4.6	NA	60	241	43.100	NA
JP-7	Blends		0.6	4.6	NA	60	241	43.500	NA
JP-8	Blends		0.6	4.7	NA	38	238	43.300	NA
JP-10	$C_{10}H_{16}$	136.24	NA	NA	NA	55	245	42.200	60.4 (373,1)
Kerosene	~$C_{12}H_{24}$		0.6	5	NA	38~72	255~455	43.000	NA
Gasoline	Blends		1.4	7.6	NA	~-40	260	48.000	NA
Diesel	Blends		0.6	7.5	NA	~62	210	45.000	NA
Natural Gas	Blends	17	3.8~6.5	13~17	8.5	~-188	480~630	~54	NA
Coal Gas	Blends	NA	5.3	32	15.5~18		NA	NA	NA
Silane	SiH_4	32.12	1.4	?	NA	(-111)	20	NA	NA

Notes:

[a] Fuel-air mixture, Reference [50, 56]

[b] Boiling point provided where flash point is not available, Reference [50, 52, 56]

[c] Auto-ignition temperature, Reference [50, 52, 56]

[d] Heat of combustion, Reference [50, 52, 56]

[e] Cell size for stoichiometric fuel-air mixture (at temperature, pressure) - Reference [43]

[f] Reference [57]

[g] Reference [58]

3.2.1 Propane as an Ideal Fuel for PDEs

Propane is an ideal fuel for aircraft or automobiles as it has many advantages as a clean and versatile fuel. Propane, in the form of liquefied petroleum gas (LPG), and natural gas are already in extensive use worldwide in vehicles running on alternative fuels, including cars, buses, forklifts, sweepers and other factory-floor vehicles. The fact that propane liquefies easily and can be stored, transported and supplied without difficulty makes it an ideal fuel for everyday use.

Propane is produced from natural gas, which is a mixture of methane, ethane, propane and other light hydrocarbons, and from fractional distillation of petroleum[59]. Natural gas is found in vast quantities around the world, including in the US, Canada and Russia, which are three of the largest producers[60].

Propane has been widely used for detonation research, because it has high energy density (46.3 MJ/kg compared to 43.2 MK/kg for Jet-A, 43 MJ/kg for kerosene, 48 MJ/kg for gasoline and 45 MJ/kg for diesel) and has comparable detonation cell sizes to that of kerosene based jet fuels, such as Jet-A and JP-10. Therefore, many researchers have used propane as a surrogate fuel for liquid jet fuels in experimental detonation studies and PDE developmental research[61]. Since the combustor size of a PDE is determined by the cell size and DDT length, an engine designed for propane can also run on liquid jet fuels (and vice versa), with modifications on the fuel delivery system, including pumps and valves. Some of the advantages of propane are listed below.

- Propane is clean burning and produces significantly less carbon monoxide and smoke, compared to traditional fuels, such as gasoline and diesel[62].
- LPG based engines would produce the least amount of emissions of carbon dioxide and smog producing compounds, including nitrous oxide and ozone, compared to all other fuels presently in use in internal combustion engines[63].
- Unlike gasoline, diesel and aviation fuels, propane (or LPG) does not contain toxins or

carcinogens, such as benzene or toluene, which may be emitted into the atmosphere due to incomplete burning.

- Propane is not detrimental to soil or water as liquid propane will vaporize and disperse quickly if spilled outdoors.
- The ratio of propane's gaseous volume (specific gravity of 1.5 at 1 atm, 20 °C) to its liquid state volume (specific gravity of 0.504 at 1 atm, 20 °C) is about 270, while it is about 700 for water[63,64]. And propane can be stored in a stable liquid form at room temperatures in relatively simple, thin walled containers.
- Since propane is a gas at STP[63,64], it can be stored and pumped as a liquid and injected as a gas into engines. This is one of the reasons why internal combustion engines can be converted for propane use relatively easily. Figure 3.1 shows the vapor pressure vs. temperature curve for propane.
- Propane is also used as a refrigerant in air-conditioning and refrigeration systems. This particular application may be useful for cooling onboard systems on a propane based aircraft or vehicle, such as the cooling of valves, sensors, electronics and other critical parts.
- Propane is available commercially in disposable containers of various sizes, e.g., cans of 4 to 10 in. length are used for handheld torches, for cooking, etc., while larger cylinders of 5 to 500 lbs (2.27 to 227 kg) sizes are available for various applications, including cooking and heating. The small handheld cans are apt for powering small aircraft such as UAVs.
- Given that propane is commonly used and widely available, expanding the present propane industry to meet the needs of the transportation industry is a real possibility that has to be looked into. Propane is already in use in airports around the US to power service vehicles. The use of propane would also fit in well with PDE based engine systems.

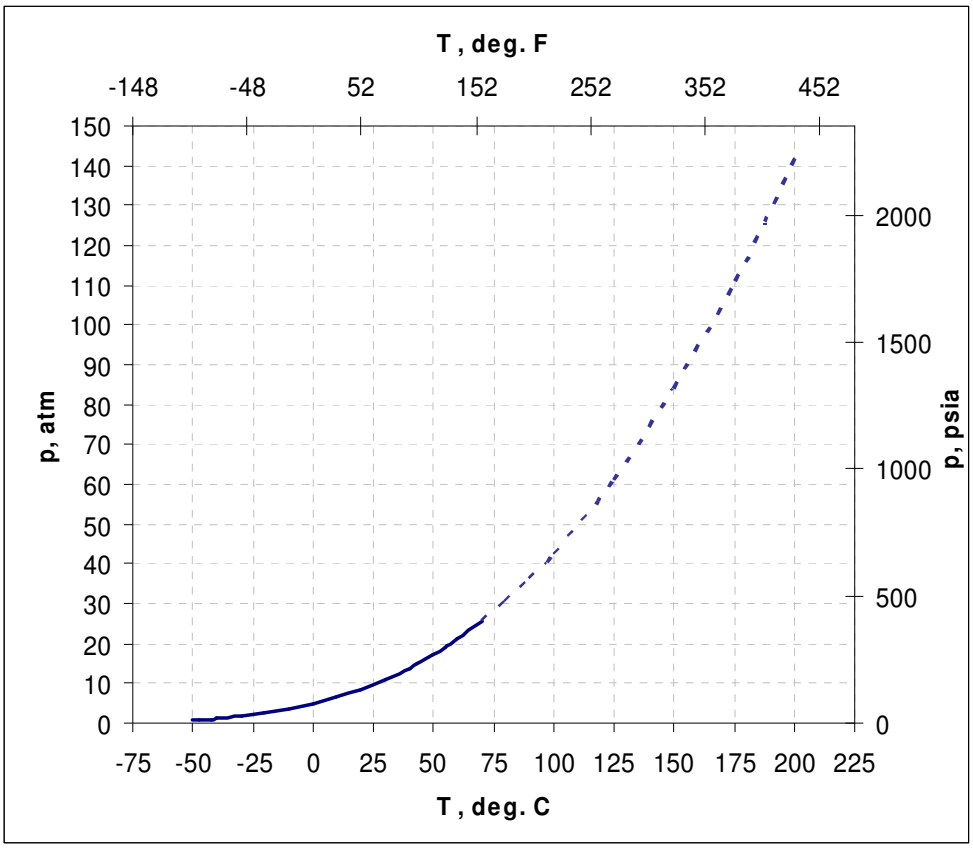

Figure 3.1 Vapor pressure of propane versus temperature, with the $p-T$ curve projected up to a temperature of 200 ℃[65].

3.3 Brief Review of Aviation Fuels

There are three types of liquid hydrocarbon fuels used for aviation, namely the aviation gasoline (avgas), jet fuels and missile fuels. Commercial aviation fuels are named with the Jet prefix, e.g., Jet A and Jet B, while the military fuels are classified as JP (jet propellant), e.g., JP-1 through JP-10. The JP fuels include both turbine and missile fuels. Table 3.2 shows a brief list of the various aviation fuels in the U.S.

Table 3.2 List of some aviation fuels[52,66].

Name	Grade	Octane No.	Heat of Combustion	Flash Point	Boiling Point	Aromatics	Naphthalenes	Olefins	Hydrogen	Comments
			MJ/kg (MJ/L)	℃	℃	% by Vol.	% by Vol.	% by Vol.	% by Mass	
Aviation Gasoline	80	80	43.5	~-40	170	0.1~5				Contains TEL, EDB*
	91	91	43.5	~-40	170					Contains TEL, EDB*
	100LL	99.5	44	~-40	170					Contains TEL, EDB*
	100	99.5	43.5	~-40	170					Contains TEL, EDB*
	82 UL	82	40.8	~-40	225					Contains TEL, EDB*
Turbine Fuel	Jet A		42.8	38	300	18.1	3			
	Jet A-1		42.8	38	300	18	3			
	Jet B (JP-4)		42.8	Low (<38)	270	8.1	3	5	13.5	Replaced by JP-8
	JP-5		42.6	60	300	19.1		0.5	13.4	
	JP-7		43.5	60	288	1.5			14.4	SR-71, YF-12
	JP-8		42.8	38	300	17.3	3		13.4	Similar to Jet A-1
(Thermally Stable)	JP-TS		42.8	43	260	9.9			14	U-2
Ramjet Fuel	RJ-4		-39	60-79	232			100		
Turbine Missile	JP-9		42.1 (39.573)	~21	300?					Replaced by JP-10
	JP-10		42.1 (39.40)	54.4	300?			98.5~100		
Rocket Fuel	RP-1		43.3	68	274	5		2		

*TEL, EDB Tetraethyl lead and ethylene dibromide

Avgas is used in piston engines and is derived from petroleum by blending various paraffins of between seven and eleven carbon atoms, along with additives to improve shelf life and to prevent knocking. Avgas is extremely volatile since its constituents have low boiling points; in addition avgas also has a low flashpoint temperature (i.e., the temperature at which the vapor pressure will be high enough to cause the fuel-air mixture to ignite when a spark is introduced). The above reasons make avgas dangerous to store, transport and supply. Also, at higher altitudes, the lower ambient pressures can cause avgas fuel to vaporize quicker, leading to fuel loss and also to become a potential hazard. Avgas cannot, therefore, be used for cooling the engine or for other onboard fluidics, such as the hydraulic systems. On the other hand, jet fuel is often used for cooling the engine and as the working fluid in onboard hydraulic systems. Gasoline and avgas are designed with slightly higher auto-ignition temperatures to prevent the fuel-air vapor from self igniting, such as from a hot spot within the engine. The octane number denotes the detonability of the fuel, with the higher rating indicating a lower likelihood of detonation. Knock-prevention additives, such as tetra-ethyl lead (TEL), are added to avgas to increase its octane number. However, due to the negative environmental effect of TEL, there is widespread consideration to switch to diesel powered piston engines for small to medium propeller-driven aircraft. Therefore, avgas is expected to become less desirable as a fuel in future. The anti-knock additives also rule out avgas as a possible fuel for PDEs.

In theory, a jet turbine can operate on a wide selection of the fuels available today. But jet engines do not need liquid fuels that vaporize at low temperatures, unlike piston engines. The fuel also has to survive higher temperatures, elevated altitudes and lower pressures without boiling off, since these reasons would make the onboard storage of fuel prone to explosions. Moreover, the presence of cavitation brought on by vaporization will critically affect fuel pumps and injectors. With the advent of gas turbine engines as the work-horse of the civil and military aviation sectors, there are now in existence many strict specifications and classifications for aviation fuels. Many of these specifications have been put in place by the U.S. military[52,66], which produced custom-made fuels to meet the exact performance requirements of their

aircraft. Quite a few of the specifications pertain to the additives blended in to the fuels to meet various needs, namely, to increase shelf life, prevent oxidation of the fuel constituents, reduce fuel volatility, lower the freezing point, prevent microbial growth, prevent corrosion of critical engine parts, prevent damage to seals, etc. The fuels are blended to achieve the required heat of combustion, thermal and electrical conductivity, flash point, minimum ignition energy, flammability limits, etc. All Jet and JP class fuels are made from kerosene with various additives and contain larger paraffin molecules. Jet fuels have also been made safer to store and handle, especially in heavy-traffic locations such as in airports and onboard aircraft carriers. A significant advantage of jet fuels over avgas is that the former do not contain harmful lead additives, as can be seen from Table 3.1. The various jet fuels are introduced below[52,66,67].

Jet A (freezing point -40 °C) and Jet A-1 (freezing point (-47 °C) are mostly pure kerosene while Jet B (freezing point -50 °C) has naphtha (precursor of gasoline) blended in to lower its freezing point. Jet A and Jet A-1 have a similar boiling point range (149 to 290 °C), while Jet B has a wider range (60 to 260 °C) and all three have the same heat content. Jet B is also equivalent to the military fuel JP-4, and is usually found only in extremely cold regions such as Alaska and Northern Canada. Jet A and A-1 are the most widely used aviation fuels in the civilian sector. Only a few researchers have considered using Jet A for PDEs[68].

JP-1[52,66] was a kerosene-based fuel introduced in 1944 by the U.S. military, with a freezing point of -60 °C and a flash point of about 43 °C. JP-2 and JP-3 had similar characteristics as JP-1 and were introduced in 1945 and 1947 respectively. These fuels were soon replaced with a fuel with better characteristics, such as lower smoke and higher ignition temperatures, to prevent accidental fires[66].

JP-4[52,66] was the U.S. Air Force's version of Jet B, introduced in 1951, composed as a mixture of kerosene and gasoline (naphtha derivatives) with a lower flash point and lower freezing point (-72 °C), to enable jet engines to operate at higher altitudes and in colder climes. However, the lower flash point made the fuel susceptible to fires. JP-4 was replaced with JP-8 in the late 1980s.

JP-5[52,66] was introduced by the U.S. Navy in 1952 to meet the safety requirements for use onboard aircraft carriers. This fuel, with a high flash point of 60 °C and a freezing point of -46 °C, is still in widespread use today by the U.S. Navy, especially on their aircraft carriers. The wide availability provides a valid reason for its potential use on PDE based aircraft.

JP-6[52,66] was designed specifically for the U.S. Air Force's XB-70 Valkyrie program in 1956 and was dropped soon after the aircraft program was decommissioned.

JP-TS[52,66] (thermally stable) was introduced by the U.S. Air Force for the U-2 in 1956 with a flash point of 43 °C and freezing point of -53 °C. This fuel is being replaced with the JP-8+100.

JP-7[52,66] was developed by the U.S. Air Force in 1960 for the YF-12 and its sibling, the SR-71. The fuel has a flash point of 60 °C and a freezing point of -43 °C. JP-7 also has improved thermal stability than earlier jet fuels. However, it is hard to ignite at low temperatures and the aforesaid aircraft required the addition of tetra-ethyl boron during the starting phase of the engine. This fuel is considered by many for PDE application[69].

JP-8[52,66] is the U.S. military version of Jet A-1, with extra additives for corrosion reduction and enhanced lubricity, first introduced in 1979. An improved version called the JP-8+100 was released in 1998 with better thermal stability. The U.S. military intends to use this fuel as a multipurpose fuel to power not just the aircraft, but also diesel-engined vehicles, tanks with gas turbine engines and other ground systems, as well as in heaters and stoves for personnel[52]. However, JP-8 has an unpleasant odor and is not agreeable to handle. It has caused adverse reactions in some people who have come into contact with it. JP-8 is used widely worldwide as well as by the U.S. Air Force, Army and NATO[67], and is considered by many to be a viable fuel for PDEs[70].

JP-9 and JP-10[52,66] were developed as turbine missile fuels by the U.S. Air Force for the Air Launched Cruise Missiles. These fuels have extremely high energy densities. JP-10 is mostly composed of a single compound, exo-tetrahydrodicyclopentadiene, with a minimum volumetric heat content of 39 434 MJ/m^3 (141,500 BTU/gal) which is about 11 % higher than Jet

A or JP-8. JP-9 is a blend of three compounds: methylcyclohexane, perhydronorbornadiene dimer, and exo-tetrahydrodicyclopentadiene, with a minimum volumetric heat content of 39 573 MJ/m^3 (142,000 BTU/gal). JP-9 has been replaced with JP-10. JP-10 is widely considered to be the prime fuel for PDE-based aircraft and many experimental and numerical studies have utilized JP-10[68,70,71].

In addition to the above fuels, the U.S. military also introduced liquid hydrocarbon fuels for ramjets: RJ-4, RJ-5 and RJ-6, of which only RJ-4 is still in active use; and rockets: RP-1, which is a kerosene-based fuel. These special fuels[52,66] are not as widely available as the conventional aviation fuels described earlier.

3.4 Ignition Time Delay of Fuels

The induction time or ignition delay is the time taken after the activation energy has been imparted to a mixture of fuel and oxidizer before the exothermic chemical reaction rate starts to increase very rapidly and energy is released in a very short period of time. The ignition delays of various fuels have been studied by reflected shock initiation in shock tubes[72-79]. In this method, the driven section of a shock tube is filled with a mixture of fuel and oxidizer, the temperature of which is raised very rapidly and held steady for a few milliseconds by means of a shock wave. The ignition delay time is identified as the period of time between the arrival of the shock and the initiation of ignition. The time of ignition can be determined by measuring one of many physical quantities, including pressure measured with a high frequency pressure transducer, emissivity of light by radicals such as OH, CH, or other species in the gas, the absorption of laser, UV or IR spectra by various species in the gas, or by the measurement of heat release[72]. If pressure measurements are used, the point of sudden rise in pressure at the wall of the shock tube is taken as the onset of ignition, as illustrated in Figure 3.2. The ignition delay times can be measured quite accurately with the above method and data for various fuels are available in the literature[72-79]. It is seen that ignition delay times have an inverse

relationship with temperature, pressure and concentration and a direct relationship with the concentration of diluents, such as nitrogen, argon, carbon dioxide, steam, etc.

In a PDE with a pre-detonator, a detonation wave moving in to a fuel-air mixture provides high pressures and temperatures, which can reduce ignition delay. However, to get the detonation process started in a PDE that is not equipped with a pre-detonator, while using fuel-air mixtures, it will take a significant amount of energy input to overcome the initial ignition delay. The factors that can affect ignition delay in the main combustor of a PDE are the proper mixing of fuel and air, the amount of energy input to the mixture by the ignition system and the initial pressure and temperature of the mixture. Figure 3.3 shows a schematic of the combustion stage of a pulsed detonation combustor. Since the filling and purging stages take much longer times (tens of milliseconds), the combustion and blowdown periods have to be shortened to a few milliseconds each in order to achieve high repetition rates. If the ignition takes longer to initiate, the DDT process is also delayed, which further delays the detonation and blowdown stages. If the ignition delay is too long, DDT process may even fail completely. This suggests that the ignition delays have to be in the range of microseconds to enable the combustion to be completed within a few milliseconds.

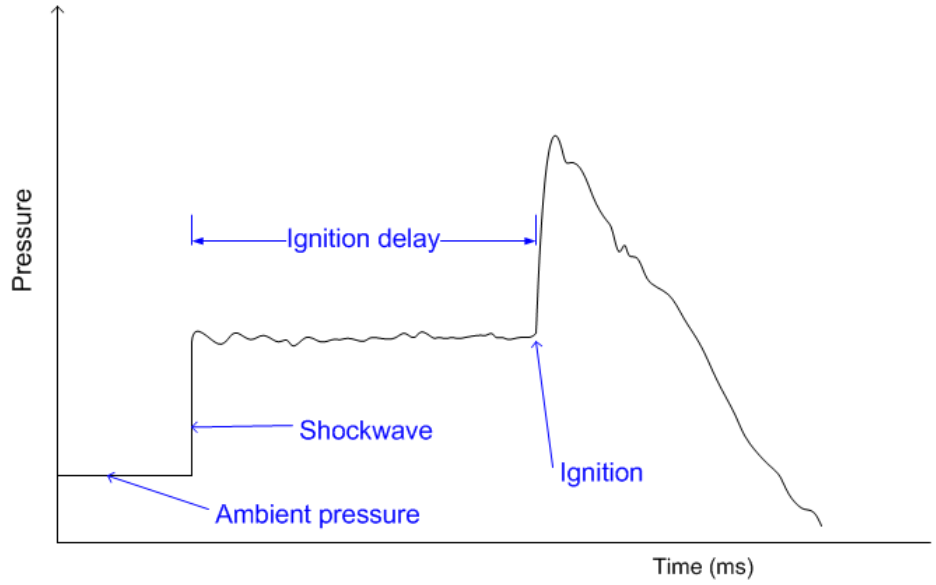

Figure 3.2 Schematic of ignition time delay between the arrival of the reflected shock wave and the onset of ignition in a shock tube[72,73].

Ignition delays of hydrogen-air mixtures have been reported to be less than 1 μs at 2000 K to about 1 ms at 1000 K[80]. However, if the hydrogen is not properly mixed the delay is seen to increase significantly. The introduction of cold hydrogen jets injected into the compressed air behind a shockwave in a shock tube was found to be between 0.5 ms at 1600 K to about 15 ms at 800 K[81]. There is a marked increase in ignition delays at temperatures lower than 1000 K. The large ignition delay was found to be due to two factors. The cold compressed hydrogen expanded on entry into the shock tube, reducing the temperature of the flow. A finite amount of time was required for mixing of the hydrogen with air, seen by the difference in time delays seen from premixed hydrogen-air mixtures. Nevertheless, the ease of ignitability of hydrogen and the fast mixing of hydrogen with air are clearly demonstrated.

Propane-oxygen ignition delays are reported to be as low as a 0.25 μs at 1400 K and about 1.5 μs at 1200 K[82], showing that higher oxygen concentration also helps in reducing ignition times. This factor comes into play in pre-detonators. Propane-air mixtures are shown to

have ignition delays of about 1 μs at 2000 K and about 3 μs at 1000 K, once again demonstrating the efficacy of propane as a fuel for PDEs[75].

Jet fuels have longer induction times than simpler gaseous hydrocarbons, such as methane and propane[74,79]. Premixed Jet-A and JP-8 mixtures in air are reported to have similar ignition delays, from about 2 μs at close to 1700 K to about 4 ms at 870 K (15-30 atm, equivalence ratio of 1)[74]. Kerosene is also reported to have similar ignition delays[83-87]. However, when the fuel is not premixed and the fuel is dispersed as droplets in the air, the ignition delays of increase by one to two orders of magnitude. A 0.7 mm diameter kerosene droplet is shown to have an induction time higher than 1 s at about 650 K, and close to about 70 ms at 1000 K[84]. Clearly, the induction time is much longer than the residence time within the PDE combustor. Therefore, to operate a PDE on liquid fuels, serious thought has to be put into reducing the ignition delays of liquid fuels, in order to be able to achieve high operating frequencies. It may require the implementation of a number of schemes, including pre-mixing chambers, efficient injectors that produce reduced droplet sizes, preheating of the liquid, the air or the fuel-air mixture and the blending of additives to the fuel or the fuel-air mixture.

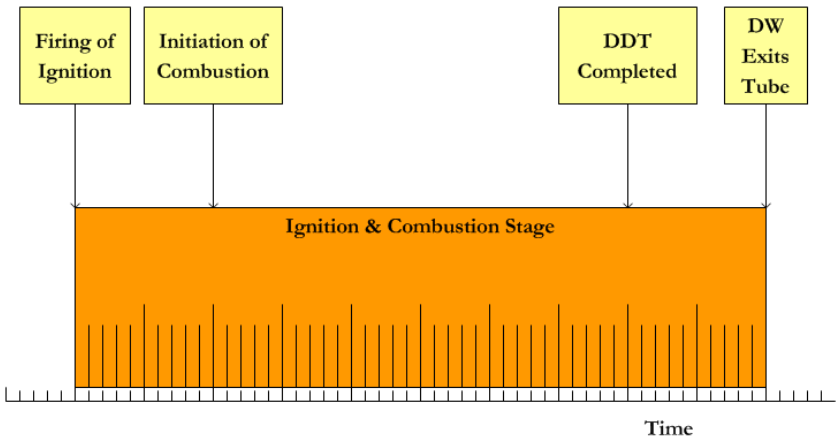

Figure 3.3 The combustion stage of the PDE is expanded to show the various processes that occur within it. If the ignition delay increases, the combustion stage may fail or be lengthened. As a result, the PDE cannot achieve the required cycle speed of the engine and thus, cannot produce the required thrust.

3.5 Reduction of Ignition Delay Times of Hydrocarbon Fuels

3.5.1 Reduce Droplet Size

As stated earlier, the ignition delay of fully vaporized liquid fuels have been reported to be in the range of a few microseconds. If the fuel is sprayed into fine droplets, the smaller the droplet size, the larger is the surface area and the fuel-air interface region. The smaller droplets of lower masses are able to absorb heat from the surrounding air more quickly giving rise to an increase in the rate of evaporation of the fuel. In addition, the larger fuel-air interface enables a higher rate of reaction. A number of studies have shown the direct relationship of droplet size with ignition delays and ignition energy[72,74,78,79,84]. It is possible to achieve micrometer sized droplet sizes using fine-slit, high-pressure injectors, which are further discussed in Section 8.6.

3.5.2 Increase Temperature and Pressure

Ignition delay has been shown to be indirectly related to temperature and pressure. Thus, raising the initial temperature of the fuel, air or the mixture reduces the ignition delay as well as the ignition energy requirements. The relationship between ignition energy and initial temperature can be seen from Figure 7.1.

3.5.3 Increase Ignition Energy

The ignition delay is indirectly related to the amount of energy discharged into the reactant mixture to bring about the ignition[72,74]. In a study of ignition systems, higher energy ignition has been seen to reduce the ignition delay in stoichiometric propane-air mixtures, as explained in Section 7.4.

3.5.3 Blending of Nitrates, Propane, Hydrogen or Oxygen

Many studies have shown that addition of small amounts of more sensitive fuels or oxidizers to heavier fuels can shorten the ignition delays[72,73]. Propane and ethane added to methane has shown benefits in bringing about faster ignition, as have hydrogen, hydrogen

peroxide and nitrogen dioxide. Nitrogen-based additives ($(CH_3)_2N_2$, CH_3ONO, CH_3ONO_2, N_2F_2, $n\text{-}C_3H_7NO_2$, etc.) have been shown to reduce the ignition delays and the DDT lengths significantly[68,86]. However, these additives are not practical for a propulsion system. Nitrous oxide (N_2O) is added to gasoline in racecars to increase power output and performance. The drawback is the added weight and volume of extra additives that have to be carried on board, which is not desirable for aircraft. Addition of CH_3NO_2 and H_2O_2 to heptane ($n\text{-}C_7H_{16}$) and oxygen mixtures were not shown to improve combustion or ignition delays[88]. This is because the oxygen already makes the mixture very sensitive and no further additives are required.

Detonation studies of JP-10 with multiple additives, including CO, H_2, methane, ethylene, acetylene, hexane along with some oxygen and nitrogen, were shown to be beneficial[68,89].

3.5.4 High Temperature Pyrolysis of Heavy Hydrocarbons

While it is known that high temperatures significantly reduce induction time, high temperatures can be used to crack heavy hydrocarbons into smaller hydrocarbon molecules and hydrogen by pyrolysis using electric arc discharges or very high temperatures. Pyrolysis of kerosene[87], jet fuel, and specifically JP-10 were studied for PDE application[85,90] and the results showed reduction in induction time and improved detonability for heater temperatures in excess of 1273 K. At such high temperatures, higher concentrations of hydrogen, methane, acetylene, ethene, etc., were found. However, this requires very huge amounts of energy, possibly in the form of electric energy, to be input into the heater. Therefore, large and heavy power supplies, heating elements, batteries, etc. will be required onboard. In addition, a Shchelkin spiral was also found to be needed for DDT. Therefore, this method does not appear suitable for flight applications.

3.5.5 Hydrogen Blending

Mixing hydrogen with kerosene in high speed flows have been shown to improve burning and to reduce the ignition delays (and ignition energy requirements) significantly in many studies[91-97]. Compared to nitrates or propane, blending of hydrogen would be the best option for reducing the ignition delay of jet fuels because hydrogen is more sensitive and it, being a gas, is easy to inject and mix with the liquid fuel-air mixtures. Addition of hydrogen would reduce the induction time, detonation cell size and shorten the DDT time[97]. In addition, hydrogen addition would make ignition of the fast-moving flow within a PDE combustor easier to accomplish at lower energy levels, using a low-power ignition system, as explained in Section 7.1.

Hydrogen does not need to be stored on board, but can be generated as needed because the mass of hydrogen required would be very small compared to that of the fuel or air. There are currently two available technologies that have already been demonstrated successfully to produce hydrogen in ample quantities:

1. Electrolysis of water in the presence of catalysts[98-100]
2. Plasma reformation of the hydrocarbon fuel by means of a plasmatron[101-107].

A plasmatron is a device that uses plasma, generated by a high-voltage, low-energy power source, to break hydrocarbons in the presence of air into hydrogen and carbon monoxide.

$$C_nH_m + \frac{n}{2}O_2 + \text{plasma} = nCO + \frac{m}{2}H_2 \qquad (3.1)$$

The plasmatron was originally proposed for automobiles, to improve the combustion efficiency of engines, thereby increasing power output as well as reducing the formation of NOx and harmful hydrocarbons due to incomplete burning[102,103,107]. In another application, the hydrogen and carbon monoxide generated in a plasmatron are added to the exhaust gases of diesel engines, which are reduced by an exothermic reaction to form carbon dioxide and water[107].

Plasmatrons are small in size and consume low amounts of power. For example, a

plasmatron weighing 3 kg with a volume of 2 L and consuming about 50 to 300 W of power is able to produce 30 to 50 liters per minute of hydrogen gas from diesel[105]. The researchers claim that about 15% of the heating value of liquid fuels, such as gasoline and diesel, is used up for the fuel reformation process.

The advantage of employing electrolysis device or a plasmatron to produce hydrogen on demand is that hydrogen storage, which requires extreme cooling, pressurization and a large storage volume, can be eliminated completely, thereby also removing the associated safety concerns. In its place, hydrogen is stored inside the fuel itself or in water, both of which are stable, safe and compact. In a PDE-based aircraft, a plasmatron or a water-electrolysis apparatus could supply hydrogen gas to a small pump, which boosts the pressure at the fuel manifold to a higher level. The fuel injectors then deliver the hydrogen to the combustors at the required flow rates during the fill stage of the PDE. Figure 3.4 shows a schematic of how the hydrogen circuit would be implemented.

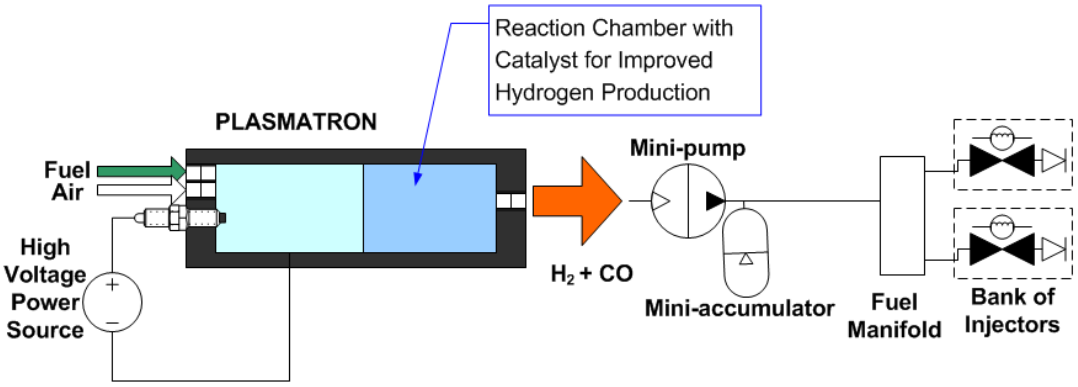

Figure 3.4 Schematic of a plasmatron-based hydrogen gas generator for use onboard a PDE-based aircraft.

The benefits of adding small amounts of hydrogen to a fuel-air mixture can be easily demonstrated numerically. Table 3.3 shows the results of the addition of small concentrations of hydrogen to propane-air mixture obtained by C-J Detonation calculations using the CEA

code[42]. It is seen that with the increase of hydrogen, the pressure and density ratios decrease. But the temperature ratios and CJ detonation velocities are seen to increase with increasing hydrogen concentration. The loss of pressure may not too adverse, as the increased post-detonation total temperature will translate to a pressure increase in constant volume combustion. The hydrogen enrichment technique is a case for further experimental study.

Table 3.3 C-J detonation properties obtained from the CEA code for propane with small concentrations of H_2.

T_1 (K)	300									
p_1 (atm)	1									
$C_3H_8 + nH_2 + (5+n/2)(O_2 + 3.76N_2) = 3CO_2 + (4+n)H_2O + (5+n/2)*3.76N_2$										
Conc. Of Reactants in moles				γ_1	a_1	p_2/p_1	T_2/T_1	ρ_2/ρ_1	Mach No.	CJ Velocity
C_3H_8	H_2	O_2	N_2		(m/s)				M_1	(m/s)
0	1	2.38 air		1.4014	408.1	15.497	9.817	1.804	4.8179	1966
0	1	0.5	1.88	1.4004	408.7	15.478	9.808	1.8041	4.8163	1968.4
1	0	5	18.8	1.3667	340.1	18.123	9.399	1.8106	5.29	1799.4
1	0.01	5.005	18.8188	1.3668	340.2	18.119	9.399	1.8106	5.2894	1799.5
1	0.02	5.01	18.8376	1.3668	340.3	18.116	9.399	1.8106	5.2887	1799.7
1	0.1	5.05	18.988	1.3672	340.9	18.086	9.403	1.8105	5.2837	1801
1	0.25	5.125	19.27	1.3678	341.9	18.033	9.408	1.8104	5.2745	1803.4
1	0.5	5.25	19.74	1.3687	343.6	17.949	9.418	1.8102	5.26	1807.3
1	0.75	5.375	20.21	1.3696	345.2	17.87	9.426	1.81	5.2464	1811
1	1	5.5	20.68	1.3705	346.7	17.797	9.435	1.8098	5.2335	1814.5
1	5	7.5	28.2	1.3797	363.8	17.028	9.534	1.8079	5.0987	1855
1	10	10	37.6	1.3854	375.3	16.573	9.603	1.8067	5.0175	1883.2
1	15	12.5	47	1.3887	382.1	16.324	9.644	1.806	4.9726	1900.2
1	20	15	56.4	1.3907	386.6	16.167	9.672	1.8056	4.9441	1911.5

3.6 Summary

Propane is a good choice as a fuel for PDE based aircraft because of its wide availability and usage, ease of storage and transportation and, above all, its ease of injection and mixing with air. Propane is widely available in a variety of packaging. Propane, which is a gas at STP, can be safely stored as a liquid in thin walled containers with no cooling required. The detonation cell sizes of propane -air mixtures are in the same range as that of aviation fuels, such as Jet A, JP-10, etc. Thus, a detonation chamber designed for propane-air can also

use aviation fuels and vice versa. Propane can also be blended to aviation fuel to reduce ignition delay and improve DDT.

Liquid aviation fuel sprays have to have an SMD of about 3 to 10 μm to produce detonations in air. Larger droplet sizes have longer ignition delays. The rate of vaporization of the liquid fuel can be increased with temperature of the fuel or air. The ignition delay can be decreased by increasing the temperature and pressure, reducing the droplet sizes and by blending of nitrates, propane, hydrogen and oxygen. Hydrogen blending is a very viable method of reducing ignition delay and also enhancing ignition and DDT. The hydrogen can be produced by electrolytic reformation of the hydrocarbon fuels or electrolysis of water. Only a small amount of hydrogen is required to be blended into the fuel.

CHAPTER 4

EXPERIMENTAL SETUP

During the course of this study, five PDE apparatuses were designed, built and tested. The setups are described in some detail below.

4.1 Bantam Pulsed Detonation Engine

This compact engine was designed by Kumar[108]. The author was involved in the assembling and testing of this engine. The objective of this project was to develop a compact multi-cycle PDE running near stoichiometric propane-oxygen mixtures. A schematic of the set up of the PDE is shown in Figure 4.1.

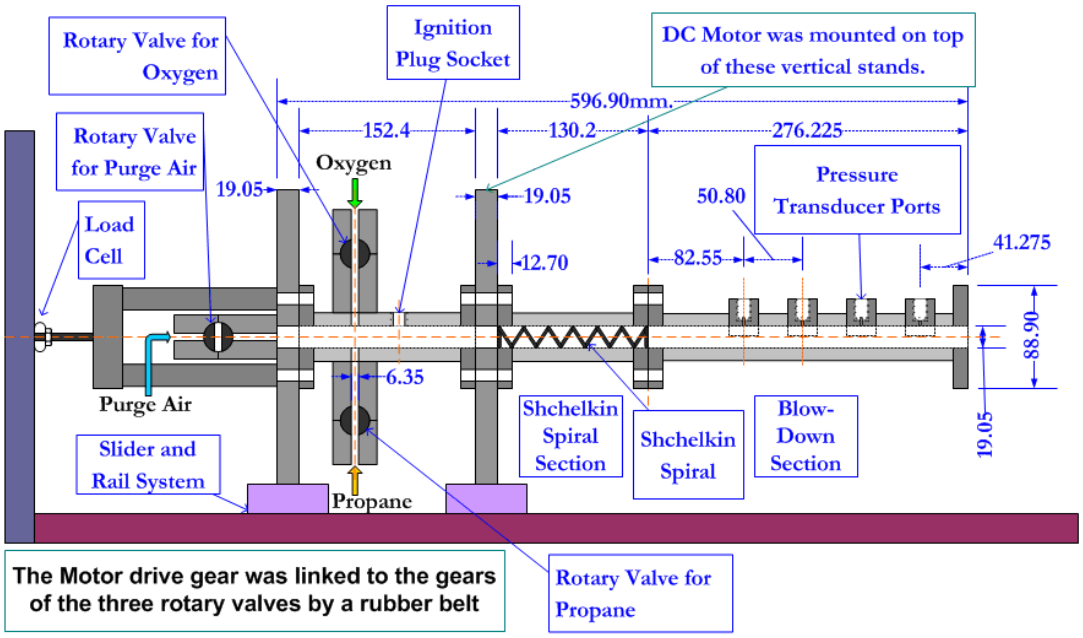

Figure 4.1 Schematic of the Bantam PDE.

The combustor, which had an internal diameter of 0.75 in. (19.05 mm), was composed of short flanged tube sections, each tube bored out of mild steel cylindrical rods. The flanged

sections could be bolted together and allowed for relatively easy assembly and dismantling. The overall length of the internal length of the combustor was a little under 60 cm. The engine was not water cooled as the run times were intended to be short, lasting about 20 seconds to less than a minute.

The fuel, oxygen and purge air were delivered by means of a rotary valve system. The rotary valve had three separate channels, one each for propane, oxygen and air. Each gas channel had a rotating spindle which had a 0.25 in. (6.35 mm) diameter orifice in it. The flow rate was set by tuning the supply gas pressure regulators to meet the appropriate volumetric flow rate ratio of propane to oxygen of 1:5. The rotary valve was driven by a variable speed dc motor. A gear was attached to the motor drive shaft, which was connected to a gear on each of the three spindles by means of a rubber belt. Each complete turn of a spindle provided two valve-open phases and the corresponding two valve-closed phases, making for two complete time periods. The purge air valve was shifted 90° out of phase with the other two valves. This allowed the purge air to be pumped in with the fuel and oxygen valves being shut-off, followed by the injection of propane and oxygen in the filling stage. The speed of the engine was determined by the speed of the motor, which could be manually fixed by means of a speed controller. A magnetic pickup sensor was added to the valve system, so that when the propane-oxygen valves were at full-open positions, the signal to fire the ignition was given to the ignition controller. The propane and oxygen lines were outfitted with flashback arrestors, which prevented any accidental flare-ups traveling back into the supply lines. The gas supply connections on the final leg of the gas lines used flexible hoses (reinforced steel braided rated for 2000 psig with ¼ in. fittings), which enabled the PDE to move freely without restriction.

The blow down section was attached at the end of the PDE and it contained four pressure transducer ports situated 2 in. apart, as shown in Figure 4.1. The pressure transducers used for the study were PCB model 111A24 piezoelectric pressure transducers rated for 1000 psig, which were enclosed in PCB model 064B02 water jackets for cooling.

These water jackets required the pressure transducers to be recessed inside them for added protection. The 111A24 transducers have a natural frequency of approximately 450 kHz.

An intermediate flanged section held a Shchelkin spiral in place. The spiral was a stainless steel helical spring that was cut to the length of the section. The whole PDE assembly, including the dc motor and valve system, was mounted on a slider and rail mechanism, as shown in Figure 4.1, which enabled the setup to be moved freely in the direction of the flow. A piezoelectric load cell (PCB model 201B05, 500 lbs rating) was mounted at the rear end of the PDE against a thrust stand. The slider system and the load cell allowed the thrust developed by the PDE to be measured. The output signals from the piezoelectric pressure transducers and the load cell were conditioned through a PCB 483A signal conditioner prior to being sent to the data acquisition system.

The ignition system was a dual-voltage arc-ignition system that used a three-electrode igniter. The details of this system are presented in Section 7.2. The data acquisition system employed for this study was the 12-bit Model 9200 from DSP Technology, Inc. It included the Model 2812 100 kHz 8-channel digitizer. The DAQ has two memory modules, the Model 5204 512 kilo-sample module and the Model 5005 2 mega-sample module. The sampling period was set to 1 second only. The results of this study are presented briefly in Chapters 6 through 8.

4.2 PDE Mark 1

This PDE[109] was designed by T.H. New and built at the National University of Singapore's Temasek Laboratories. It was delivered to the ARC for assembly. The auxiliary systems including fuel and gas delivery system, ignition, control and DAQ, etc. were designed and assembled at the ARC. The aim of this study was to understand the effect of parameters of the Shchelkin spiral, such as pitch, wire thickness (blockage ratio) and length, on DDT. The fuel and oxidizer chosen were propane and oxygen respectively.

A schematic of the PDE set up is shown in Figure 4.2. The detonation tube was manufactured from ASME Schedule 80 stainless steel pipe sections of various lengths with

flanges welded to both ends, so that they could be mounted together by means of nuts and bolts. The pipes had an outer diameter of 33.5 mm and an inner diameter of 24.3 mm. The detonation tube was thus divided into four detachable sections, namely, the gas injection section, the ignition section, the Shchelkin spiral section and the blow-down section which contained the pressure transducer ports. Two Shchelkin spiral sections were made available, one of 304 mm length and the other of 594 mm in length, to enable the testing of two lengths of spirals. The length of the PDE could therefore be varied between 1134 mm (L/D = 46.7) and 1424 mm (L/D = 58.6).

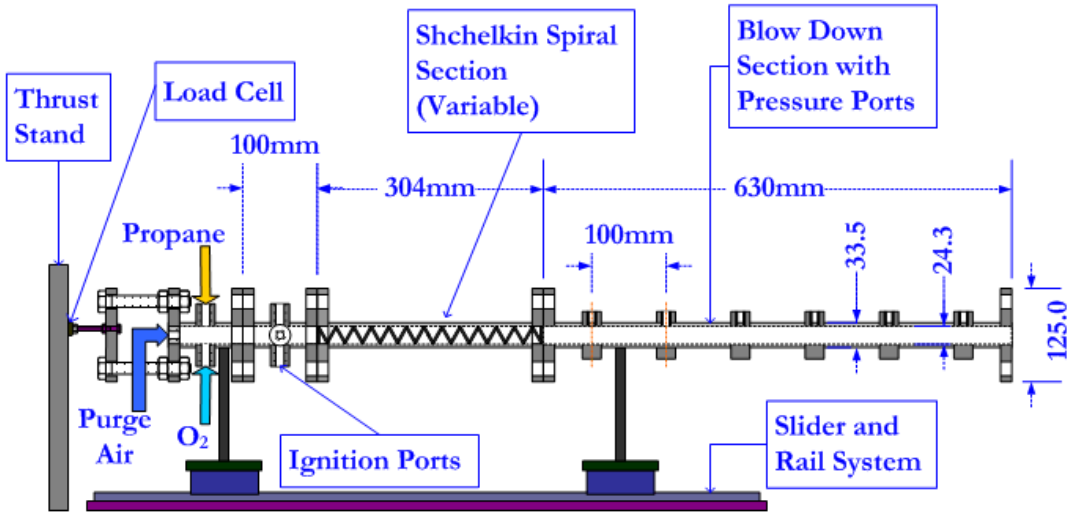

Figure 4.2 Schematic of PDE Mark 1.

A rotary valve system was employed to supply near stoichiometric oxygen and propane gases and pressurized air for purging the combustor. The rotary valve consisted of one spindle with three orifices of 6.35 mm (0.25 in.) which could rotate within a larger housing. Two of the orifices, used for propane and oxygen lines, were perpendicular to the other, which was used for purge air. This system, which is schematically shown in Figure 8.2, enabled purge air to be pumped in off-phase from propane and oxygen injection. One complete rotation gave two complete engine cycles. The rotary valve had a gear attached to the spindle which was rotated

by a variable speed dc motor rated at 0.5 hp. The motor's speed controller ran off the 120 V, 60 Hz mains and sent a rectified dc output to the motor. The speed of the motor determined the cycle frequency of the PDE. An optical sensor was used to detect the position of the valve, whereby it would cause a timing control circuit to send a square wave pulse to the ignition system's control circuit. The ignition was timed to fire when the propane-oxygen valves were fully open. Compressed air was supplied at 150 psig (11.2 atm) while oxygen and propane were supplied from gas bottles. The oxygen pressure was regulated to about 85 psig (6.8 atm) and the propane pressure was set to about 42 psig (3.86 atm). Both propane and oxygen lines were fitted with flashback arrestors for safety. The gas supply was connected to the PDE by means of flexible hosing that allowed the PDE to move freely on a slider-rail mechanism that it was mounted on, as shown in Figure 4.2.

Two types of ignition systems were tested in this study. The previous high-energy arc-ignition system and a low-energy, high-voltage, automotive-based ignition system were used. The igniters consisted of three separate plugs, namely, a high-energy electrode, a low-energy high-voltage electrode and a ground electrode, made from 14 mm steel bolts, as shown in Figure 4.3. The high- and low-energy igniters had ceramic tubes inserted into orifices made at the center of each bolt and fixed in place with epoxy. Tungsten rods were then pushed through the ceramic tube and glued with epoxy, such that about 0.25 in. of the rod was exposed from the bottom end of the bolt. The low-energy, high-voltage electrode had thicker ceramic insulation (0.375 in. vs. 0.25 in for the high-energy, low-voltage electrode) to prevent the spark shorting to the ground, from the tungsten rod via the bolt body, because the whole PDE assembly was grounded. The ground electrode was made by inserting a tungsten rod straight through an orifice in the bolt. The tungsten rods employed in the igniters were 3/32 in. diameter 2 % lanthanated tungsten rods used for TIG welding. The advantage of using bolts for the igniters was that the spark gap could be adjusted by screwing the bolts in or out. The spark gap between the high-voltage electrode and the high-energy electrode was set to be about 2 mm,

while the gap between the high energy electrode and the ground electrode was about 4 to 5 mm. When the high-energy igniter was not needed, its port was plugged up with a bolt.

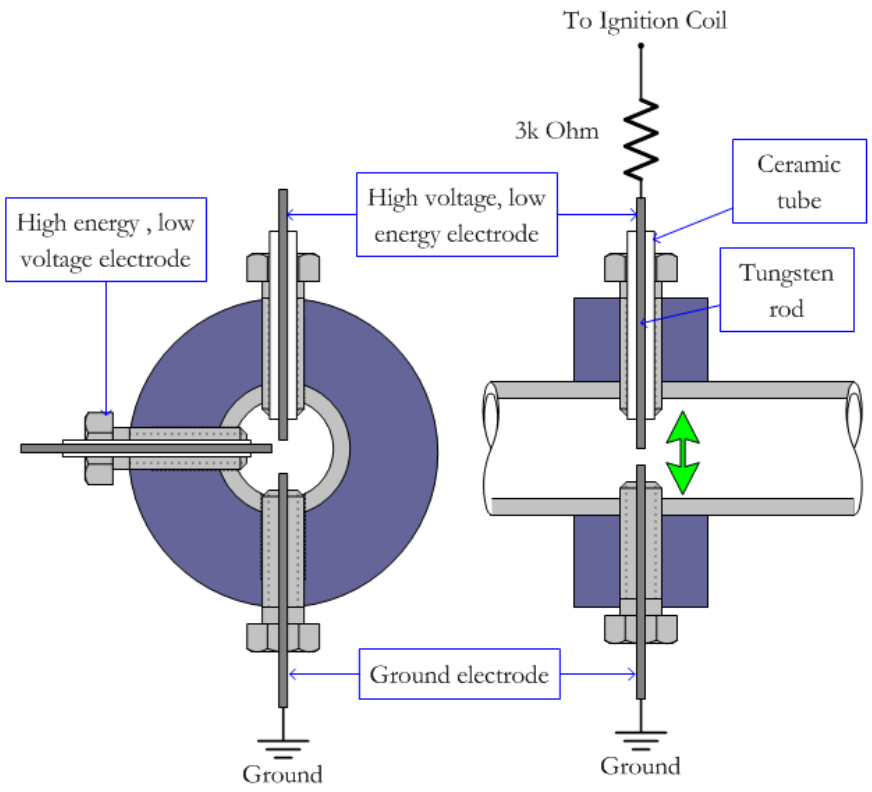

Figure 4.3 Schematic of the ignition plugs used in PDE Mark 1 and Mark 2. In the Mark 2, the high-energy, low-voltage electrode was not used.

The diagnostics included dynamic pressure measurements inside the combustor, temperature measurement of the external tube and the exhaust, and the thrust measurements. Pressure measurements were made with the help of six piezoelectric dynamic pressure transducers (PCB model 111A24, 1000 psig rating), which were enclosed and recessed in PCB 064B02 water jackets for cooling. K-type thermocouples were used to measure external wall temperature and the exhaust gas temperature. The thrust developed by the PDE was measured by means of a piezoelectric load cell, model 201B05 rated at 500 lbs, from PCB Piezotronics Inc. The PDE was restrained and pre-tensioned back against the thrust stand, with

the load cell sandwiched in between, by means of rubber cords. The output signals from the piezoelectric pressure transducers and the load cell are conditioned through a PCB 483A signal conditioner prior to being connected to the data acquisition system. The exhaust of the PDE was directed outside the building into open air.

Data were acquired on a National Instruments DAQ. It consisted of two 16-bit PXI-6133 cards installed inside a PXI-1042-Q chassis, which was connected to a remote PC by means of a 100 m long fiber-optic cable through its MXI-4 communication device. Each PXI-6133 card had an 8-channel BNC 2110 connection box onto which the transducers were connected by means of coaxial cables. The pressure, thrust and temperature signals were sampled at 100 kS/s for 10 s periods. Most of the tests were usually of 15 to 30 s duration, but a few tests went over 1 minute. NI LabVIEW 7.0 was used to program the data acquisition system.

Although water cooling was not integrated into the design of the PDE, the detonation tube was externally cooled by wrapping the tube in wet cloths which were continuously wetted by running tap water. The results of the PDE Mark 1 study are presented in more detail in Section 5.1.

4.3 PDE Mark 2

This PDE and the DDT-devices were designed and built at the National University of Singapore's Temasek Laboratories by T.H. New, K.F. Chui, K.S. Lim and H.M. Tsai[110]. The engine, its electronic valves and various DDT mechanisms were shipped over to the ARC. The author was involved in the engine's assembly, testing and analysis. The main aim of the study was to test various DDT devices, including Shchelkin spirals, slotted sleeves, converging-diverging nozzles, etc. for their efficiency in inducing DDT. The secondary objective was to test electronic valves and ignition systems for application on PDEs. Propane and oxygen were chosen as the fuel and oxidizer for the study.

The main detonation tube was made from ASME Schedule 80 stainless steel pipe with an i.d. of 24.3 mm and an o.d. of 33.4 mm, in the form of four detachable flanged sections that

could be bolted together as shown in Figure 4.4 to form one continuous combustor with an overall length of about 80 cm, giving it an L/D ratio of 32.9. The four sections were the gas injection section, the ignition section, the DDT section and the blow-down section, which contained the pressure transducer ports.

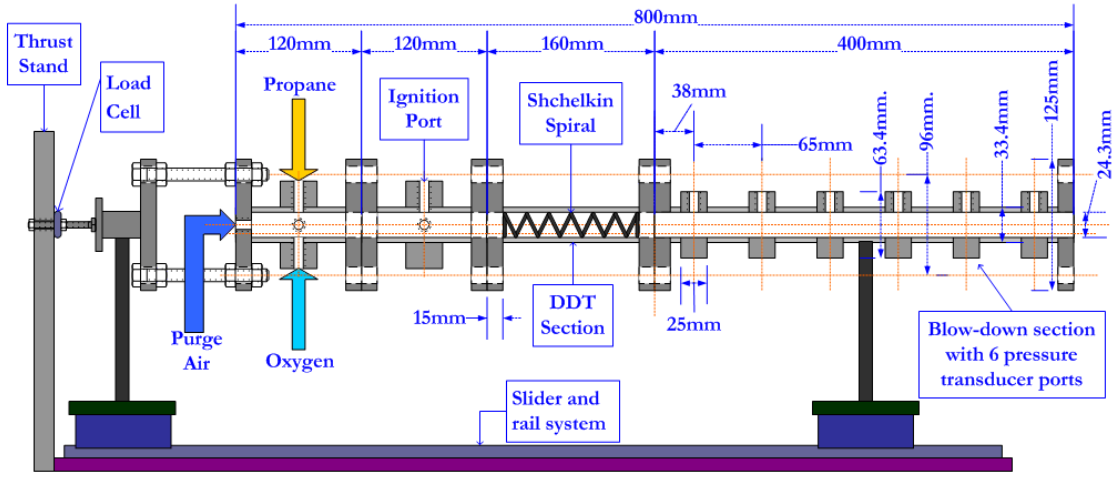

Figure 4.4 Schematic of PDE Mark 2.

The gas injection section contained four ½ in. FPT tapped ports located on a thick flange, in a perpendicular fashion so that the gases entering the tube impinged on each other to improve the mixing of propane and oxygen. Three ports were allocated to oxygen injection and one was reserved for propane. Since the volumetric ratio of propane to oxygen for stoichiometric condition is 1:5, the proper flow rates were achieved by regulating the oxygen supply pressure to about 85 psig (6.8 atm) and that of propane to about 42 psig (3.86 atm). Purge air was injected in from a ½ in. FPT port on the rear end wall at 85 psig (6.8 atm). The DDT section was approximately 160 mm in length. The flanged construction allowed the DDT devices to be easily inserted into the tube and reassembled before testing and then quickly disassembled for inspection right after the test. The 400 mm long detonation blow-down section housed six pressure transducer ports spaced 65 mm apart, as shown in Figure 4.4.

The gas injection was performed through gaseous fuel injectors from Alternate Fuel Systems Inc., Calgary, Canada. Their AFS Gs60-05-5-c series valves were rated for 550 kPa and a maximum frequency of 50 Hz. These solenoid valves are designed for use in automobile engines that run on propane or other alternate fuels. The valves are claimed to have a response time of close to 2 ms. The valve driver and controller run on 12 V dc power supply, with 8 A peak current and 2 A holding current ratings. The controller could be configured to take 5 V TTL signals to time the valve operation. For this study, the operating frequency was kept to 10 and 15 Hz, although 20, 25 and 30 and 35 Hz tests were performed to check their functionality at higher operating frequencies. At higher frequencies, the mass flow rates could not be sustained with the existing gas supply lines. Each of the six gas injectors were installed on individual water-cooled housing, each of which also had a check-valve screwed into the port of the gas injection section of the PDE. Cooling water was supplied at tap pressure and exhausted into a water tray underneath the PDE setup. The propane and oxygen supply lines were fitted with flashback arrestors for safety. Half-inch i.d. flexible hoses were used to make the final connection between the gas supply fixtures and the PDE, enabling the PDE to move freely on its base. Compressed air was supplied at about 90 psig, whereas propane and oxygen were supplied from gas bottles at about 44 psig and 90 psig respectively. The exhaust of the PDE was directed towards the exhaust chamber of the hypersonic shock tube facility at the ARC. The whole PDE setup was mounted onto a slider and rail mechanism that allowed the PDE to move smoothly when unrestrained, allowing the thrust to be measured.

The ignition system used for this study was a low-energy inductive ignition based on those found in automobiles. It consisted of an ignition driver circuit (Mallory HyFire Ia, Part No. 29026A) and an ignition coil (Mallory Promaster Coil, Part No. 24440). Together, they were rated to emit sparks at 135 mJ, although this was reduced for the PDE tests with a resistor. The ignition system was powered by a 12 V lead acid automotive battery. The ignition plugs were assembled from 14 mm metric thread bolts and were arranged in a fashion similar to that shown in Figure 4.3. There were two plugs, a high-voltage plug and a ground plug. The high-voltage

plug was constructed by first inserting a ¼ in. ceramic tube through an axially drilled hole in the bolt, with about 0.25 in. of its length protruding out of the end of the bolt. Then, a 5/32 in. diameter 2% lanthanated tungsten rod was inserted through the ceramic tube with about 0.25 in. of it projecting outside the end of the ceramic tube. The ceramic tube and the tungsten rod were glued in place in the bolt with high-strength epoxy. The ground plug only had the tungsten rod inserted right through the concentric hole with about ¼ in. of it projecting out of the end of the bolt. The tungsten rods were those used for TIG welding. The spark gap could be adjusted by screwing the bolts in or out. The spark gap was kept at about 2 to 3 mm. A 3 kΩ, 25 W high-power resistor was placed in series with the high-voltage electrode to reduce the current and energy output of the ignition coil. More details about the ignition system are discussed in Section 7.3.

Diagnostics were performed with six PCB 111A24 piezoelectric dynamic pressure transducers, rated at 1000 psig, with a natural frequency of 450 kHz. Each pressure transducer was enclosed in PCB 064B02 water-jackets. A load cell (PCB 201B05, 500 lbs) was mounted on a thrust stand at the rear of the PDE. The load cell required some pre-compression to function properly. This was achieved by restraining the PDE back tightly against the load cell with rubber cords during the tests. The output signals from the piezoelectric pressure transducers and the load cell were conditioned through a PCB 483A signal conditioner prior to being connected to the data acquisition system. The exhaust gas temperature was monitored with a K-type thermocouple. The signals from the transducers were collected on a National Instruments data acquisition system, which also simultaneously sent out the control signals for the valve and ignition. The DAQ consisted of a PXI-1042Q chassis with two S-series PCI-6133 16-bit resolution 8-channel data acquisition cards installed; each card was capable of a simultaneous sample-and-hold rate of 2.5 MS/s. Each card had a BNC-2110 connection box on which transducers lines could be connected. Coaxial cables were used to connect all transducers to the BNC-2110 sockets. The sampling rate was set at 240 kS/s for a period of 5 s of data writing, during which time the data would be written in text form and saved on a host

computer. The test times ranged from 15 to 30 seconds. The computer was linked with the 1042Q chassis by means of a 100 m long fiber-optic cable to provide electromagnetic interference (EMI) shielding to the data signals. LabVIEW 7.0 was used to create programs for data acquisition and for the valve controller TTL generator (counter output).

This PDE design also did not consider water cooling. As a result, the external parts of the detonation tubes were cooled by wrapping wet pieces of cloth on them and continually wetting the cloths with running tap water. Various DDT devices as well as the clean tube configuration were tested and their results are discussed in detail in Section 5.2.

4.4 PDE Mark 3

4.4.1 PDE Structure

This PDE[111] was designed by the author and built at the ARC to test a number of elements of interest, including ignition, a new type of spiral structure with water-cooling and also the integration of a PDE with an automotive turbo-charger. Also, this PDE was tested with hydrogen in low-frequency tests. The turbo-charger study was extended by mating a small ac generator to the turbo-charger's drive shaft as a proof-of-concept demonstrator to show that PDEs can be applied for electric power generation.

The PDE was made in five modules, including a gas injection and igniter module, an additional ignition module, a water-cooled spiral section, a blow-down section with ports for pressure transducers, constant area sections for additional length and a diverging conical nozzle for connection with the turbocharger, as shown in Figure 4.5. The overall length was close to 1 m, with a 19.05 mm (0.75 in.) i.d. The gas injection and ignition module was a 88.9 mm (3.5 in.) diameter round section with 50.8 mm (2 in.) depth, made out of mild steel. The gas inlet ports were cut so that the inlets meet the internal cavity at a tangential fashion as shown in Figure 4.6. This geometry was adopted to give the incoming gases a swirling motion as they entered the combustor, which would enhance the mixing of the fuel and oxidizer.

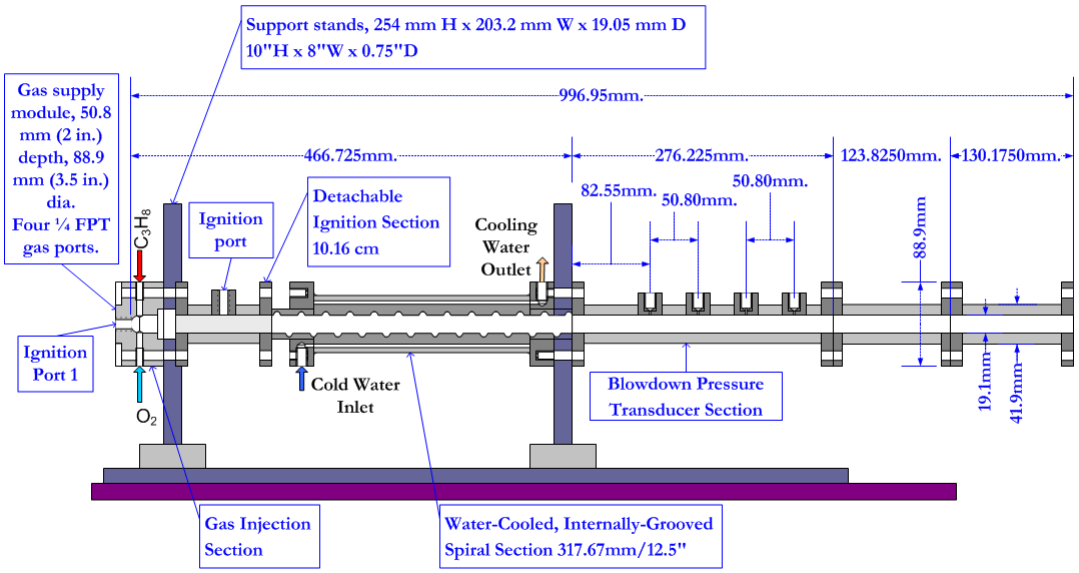

Figure 4.5 Schematic of PDE Mark 3.

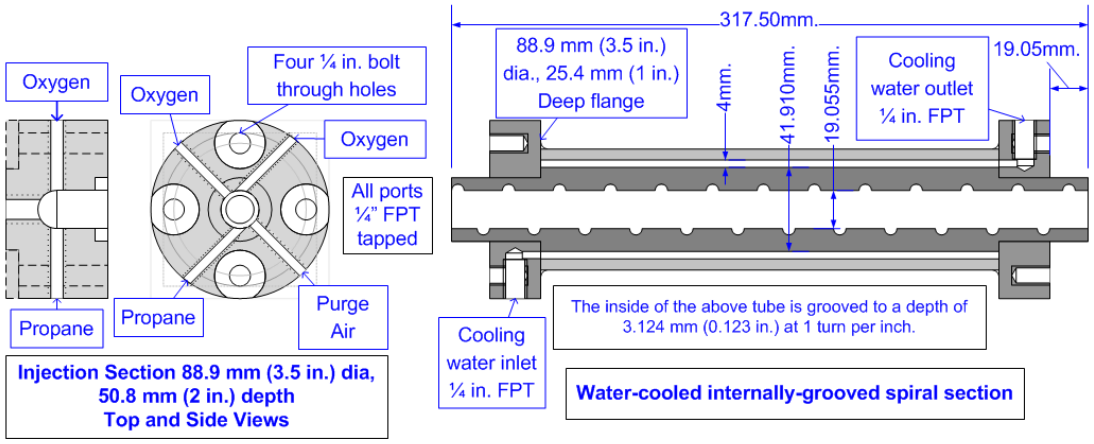

Figure 4.6 Schematics of the gas injection module and the spiral section of PDE Mark 3.

The additional ignition section provided the flexibility to fix the igniter downstream of the gas inlet or at the end wall of the combustor. The spiral section was made by cutting a groove on the inside of a mild steel tube (19.05 mm (0.75 in.) i.d. and 41.91 mm (1.65 in.) o.d.) to a depth of 3.124 mm (0.123 in.) at a pitch of 1 turn per inch. Two flanges of 88.9 mm (3.5 in.)

diameter and 25.4 mm (1 in.) width were welded to the ends as shown in Figure 4.6 with 19.05 mm (0.75 in.) extending out on either side. The two flanges had ¼ in. (6.35 mm) tapped bolt holes and ¼ in. FPT cooling water ports in them. A 1.5875 mm (1/16 in.) thick stainless steel sheet was folded over the tube with a small gap for the water passage in between and welded in place, as shown in Figure 4.6. The spiral section was symmetrical and could be installed in either direction.

The blow-down section had four pressure ports placed 5.08 mm (2 in.) apart as shown in Figure 4.6. This section and the additional ignition section were taken from the Bantam PDE, after its testing had been completed. There were two additional constant area extensions made of 123.825 mm (4.875 in.) and 130.175 mm (5.125 in.) lengths, as also shown. In addition, a 304.8 mm (12 in.) long water-cooled, constant area section was also made for the PDE-turbocharger integration study, to extend the length of the PDE, so as to slow down and cool the flow before it hit the turbo-charger. The pressure ports were 16 mm deep to accommodate water-cooling adapters for the pressure transducers and also have a ¼ in. bore from the bottom of the socket to the interior surface of the combustor so that more surface area of the pressure transducer could be exposed to the flow inside.

4.4.2 Gas Injectors

The gases were injected using solenoid fuel injectors, used in the previous study, namely the AFS Gs valves from Alternate Fuel Systems, Inc. Calgary, Canada. The valves enabled the precise control of the PDE frequency and timing using TTL signals generated in the data acquisition system and they were remotely controlled with a PC. The propane and oxygen lines contained flashback arrestors for safety. The final connection to the PDE from the gas supply lines were made with flexible hoses. All gas lines had check valves placed right after the fuel injectors to protect them from the high pressures developed during the detonations. Although these check valves caused a pressure drop and reduced the flow rates, they are very important for the safe operation of the PDE.

4.4.3 Ignition System

The ignition system comprised of a Mallory Hyfire 1A ignition driver and Mallory ProMaster 29440 coil, with rated spark energy of 135 mJ. The ignition driver is powered by a 12 V automotive lead acid battery. The ignition driver was triggered by means of a transistor control circuit that accepted TTL signals from the DAQ. Thus, the ignition timing could be precisely controlled remotely by the user from the DAQ PC. The spark plugs used were Bosch Platinum tipped automotive spark plugs (6234 model). These spark plugs have a built-in resistance of 3.18 $k\Omega$, ensuring that the spark current is reduced and the resulting electromagnetic interference (EMI) does not notably corrupt the weak transducer signals.

4.4.4 Diagnostics and Control

The diagnostics of the test apparatus was performed with the help of a National Instruments DAQ consisting of a 1042Q chassis that contained a pair of 8-channel, 16-bit 2.5 MS/s, simultaneous sample-and-hold, S-series PXI-6133 cards. The DAQ was connected to a remote PC via a fiber-optic cable which ensured EMI free signal transmission. The various sensors could be monitored in real time and the solenoid valve fuel injectors of the PDE could be operated remotely from the PC through the DAQ.

The pressure inside the combustion chamber was measured with four PCB piezoelectric dynamic pressure transducers (model 111A24, 1000 psig maximum, 450 kHz resonant frequency) which were encased in water cooling adapters (064A01 recessed sensor and 064B02 flush sensor models). The signal conditioner for the pressure transducer was a PCB model 483A unit which converted the charge output of the transducers to voltage waveforms. For the turbo-charger-generator experiment, additional instruments were used, including one differential pressure transducer for measuring flow rate of the compressor air output (Honeywell Micro Switch model number 164PC01D37) and a pair of K-type thermocouples to measure temperature of the PDE tube surface and of the flow exiting the PDE

or turbocharger. The voltage output of the generator was also measured through a 1:4 voltage divider, as shown in Figure 4.7.

Gas flow rates were measured in these tests with the help of critical flow nozzles from Flow-Dyne Engineering, Fort Worth, Texas. These nozzles were fitted with T-type thermocouples and static pressure transducers from Omega, namely a PX302-200GV (200 psig full scale) model and a PX302-300GV (300 psig full scale) model. Control and monitoring were performed with programs created with National Instruments' LabVIEW 8.0 through the remote PC. The programs enabled the control and fine-tuning of the PDE frequency and the timings of the valves and ignition, as well as the sampling rate of the data acquisition process.

4.5 PDE Integration With Turbocharger and Generator Study

This study was performed as a proof-of-concept of deriving electric power from a hybrid PDE-turbine system. A turbocharger and small ac generator were mated to the PDE, as shown in Figure 4.7.

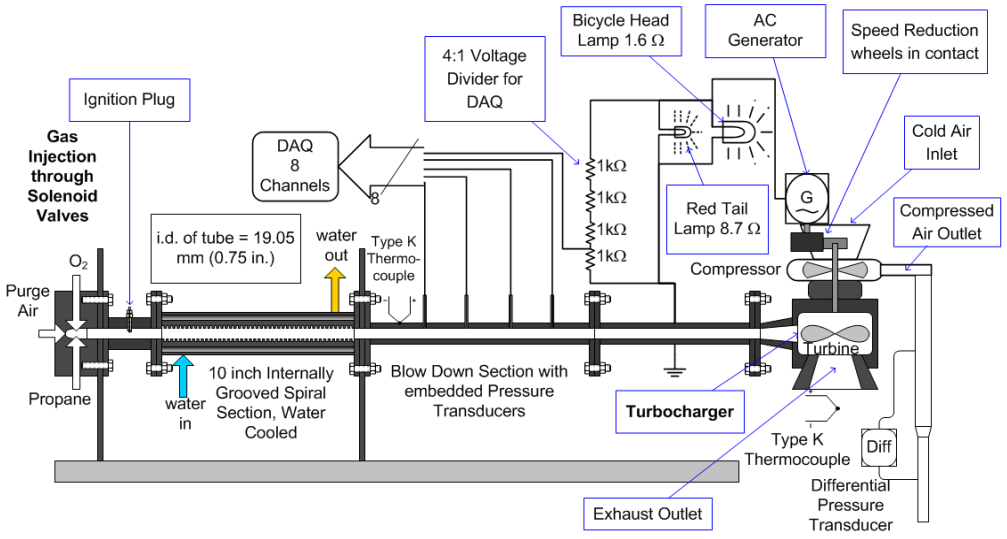

Figure 4.7 Schematic of the PDE-turbocharger-generator setup.

4.5.1 Turbocharger

The turbocharger used for this study was a BorgWarner Turbo Systems model K03 (part number 53039880029) that is used in Volkswagen Passat 1.8T and Audi A4/A6 1.8T model cars. The turbocharger had a single-stage radial flow turbine and a single-stage radial flow compressor coupled to the same axial shaft. The manufacturer's specifications for this turbocharger states that the compressor can deliver a maximum air flow rate of 0.17 kg/s and is recommended for automotive engines of up to 150 kW (200 hp) power rating. The turbine inlet port had and i.d. of 40 mm while its outlet port had an i.d. of 65 mm. The compressor inlet port had an i.d. of 36 mm and the outlet port had an i.d. of 38 mm. The turbine specifications stated a maximum operating temperature of 1050°C. The maximum operating speed was said to be 200,000 rpm. The turbocharger was mounted at the exit of the PDE such that the exhaust flow was directed downwards after passing through the turbine, as shown in Figure 4.7. Thus, the flow took a 90° turn as it traveled through the turbine. In the compressor, cool air entered the compressor axially from the top of the turbocharger and exited in a radial direction to the compressor blades. At rotational speeds beyond 200,000 rpm, the flow at the compressor blade inlet can reach sonic velocities at which point the air flow is choked. To avoid this predicament, the device has a built-in control system that opens a waste gate whereby the flow to the turbine is bypassed to the exhaust, thereby reducing the air flow to the turbine and consequently, its speed of rotation. For this study, the waste gate was firmly bolted shut as it was determined that the flow rates of an intermittent PDE are lower than that of a 4 cylinder auto-engine running at over 3000 rpm. It is extremely important to supply the turbocharger with oil to constantly cool and lubricate the bearings during its high-speed operation, and water or coolant to keep the housing and the components cool. Oil was delivered by means of an oil pump from a 1980's model Dodge truck, which was turned by an electric motor at a constant speed such that the oil pressure was maintained at about 40 psig (3.74 atm).

Cooling water was supplied at the utility tap pressure. A specially built nozzle was required to allow the mounting of the turbine inlet of the turbocharger, with an i.d. of 40 mm, to the exhaust of the PDE, which had an i.d. of 0.75 in. (19.05 mm). An additional water cooled section 9 in. (228.6 mm) in length with a 0.75 in. (19.05 mm) i.d. was also added to the end of the PDE tube. The air flow rate of the compressor was obtained by passing the flow through a Venturi tube and by measuring the differential pressure.

4.5.2 Generator

The generator chosen for this study was a bottle dynamo used on bicycles and was rated at 6V, 3W. The dynamo was a brushless ac generator which consisted of a 2-pole permanent magnet rotor and a wire wound stator armature having a dc resistance of 4.2 Ω. The magnitude of the voltage output is proportional to the strength of the magnet, the number of turns in the windings and the speed of rotation of the rotor:

$$E = 2\pi f N \Phi_m \sin(2\pi f t) = E_m \sin(2\pi f t), \quad E_m = 2\pi f N \Phi_m \tag{4.1}$$

where E is the output voltage, f is the rotational frequency, N is the number of turns in the coil winding, Φ_m is the magnetic flux of the magnet, measured in Webers, and E_m is the maximum amplitude of the voltage at a given speed of rotation. There will be a measurable voltage drop across the armature windings due to its internal resistance, but the voltage output across the output terminals of dynamos usually lie around 6 V when used in typical bicycle applications. Bicycle dynamos are operated at a few hundred to a few thousand rpm as they are powered by the moving wheels of the bicycle, whereas turbo-chargers are designed to spin at up to 200,000 rpm. Therefore, speed reduction was necessary to couple the bicycle dynamo to the turbocharger. The speed reduction was achieved by using rubber wheels of different diameters. A 1.85 in. (47 mm) diameter rubber wheel was attached to the dynamo rotor and a 0.56 in. (14.22 mm) diameter steel disk was welded to end of the shaft of the turbocharger at the compressor's cold air inlet. The dynamo was then mounted using clamps and brackets

such that its rubber wheel was in contact with the steel disk of the turbocharger and the motion was transferred by means of friction, as illustrated in Figure 4.8. This method proved to be adequate for the short run times expected, as well as for the purpose of this study. The effect of slip between the shafts of the two machines was neglected. The turbocharger was expected to have a slight reduction in speed due to the small loading caused by the dynamo. The dynamo's output terminals were connected to a bicycle headlamp (1.6 W, 22.5 W) and a red tail lamp (8.7 W, 4W) in parallel and to the DAQ through a 4:1 voltage divider, as shown in Figure 4.7. Since the voltage can be measured and the resistances of the loads are known, the current and consequently the power output can be found by Ohm's law. The total parallel resistance of the two lamps $R_{//}$ is 1.351 W. The lamps are considered to be purely resistive loads allowing for a simple analysis of the dynamo's output. In the following equations, I_{RMS} is the RMS current, V_{RMS} is the RMS of the output voltage which for a sinusoidal waveform can be expressed as below; and P is the power output.

$$V_{RMS} = \sqrt{2}\,E_m \tag{4.2}$$

$$I_{RMS} = \frac{V_{RMS}}{R_{//}} = \frac{V_{RMS}}{1.351\Omega}; \quad P = \frac{V_{RMS}^2}{R_{//}} = \frac{V_{RMS}^2}{1.351\Omega} \tag{4.3}$$

An advantage of using an ac generator is that the rotational speed can be determined from the output voltage frequency, without having to measure the speed of the generator or turbocharger. If N_D is the rotational speed of the dynamo rotor in rpm, f is the frequency of the ac voltage in Hz and p is the number of pairs of poles, then the rotational speed of the turbocharger N_T can be easily calculated by substituting in the dimensions of the speed reduction wheels into the following relation.

$$N_D = \frac{120f}{p} = \frac{120f}{2} = 60f; \quad \therefore N_T = N_D . \frac{1.85in.}{0.56in.} = 3.3N_D \tag{4.4}$$

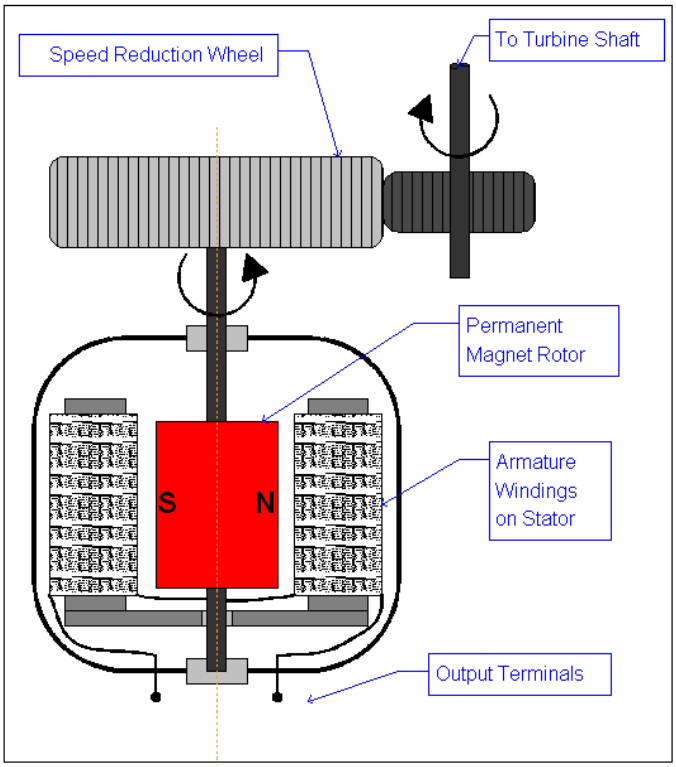

Figure 4.8 Schematic of the ac generator with the speed reduction wheels.

4.5.3 Results of the PDE-Turbo-Generator Study

The PDE was run at 15 Hz with propane and oxygen supplied at an equivalence ratio of $\phi = 1.2$, with a total mass flow rate of the propane-oxygen mixture being 0.0057 kg/s. The signals from the pressure transducers and the voltage output of the generator were sampled at 500 kS/s for 1 s periods. The data acquisition process was looped every 3 to 5 seconds, during which time, the data captured during the 1 s period were written onto the hard drive of the PC. Figure 4.9 shows the output voltage of the generator. The data acquisition commenced about 3 to 4 seconds after the PDE had been started, with the turbine at rest. It is seen in Figure 4.9 that the amplitude of the waveform climbs to a peak value of about 8.5 V and remains steady for a few seconds. Figure 4.10 depicts the initial 1 s of the run time, showing the sinusoidal waveform growing in amplitude and frequency as the generator builds up speed. After about 15 s of run time, the speed reduction wheels lose contact and the generator stops running. At its

peak, the generator produced 26.2 W of power at a frequency of 641.5 Hz, corresponding to a turbine speed of 127,015 rpm. Table 4.1 shows the generator output, and the rotational speeds of the generator and the turbine at the beginning and end of each 1 s acquired data block shown in Figure 4.10. The mass flux of the compressor was found to surpass 0.055 kg/s, demonstrating that a turbine and compressor could be used to self aspirate a PDE. Since the PDE was run in a fuel-rich state, combustion was observed to be taking place within and outside the turbocharger. An orange-yellow flame could be observed at the exhaust of the turbine. The temperature of the flow at the turbine exit was measured to be as high as 800°C. The detonation wave speeds, obtained by performing time-of-flight calculations with the dynamic pressure readings, indicated velocities in excess of the C-J velocity of 2440 m/s, showing that the grooved spiral successfully induced DDT within the short combustion chamber.

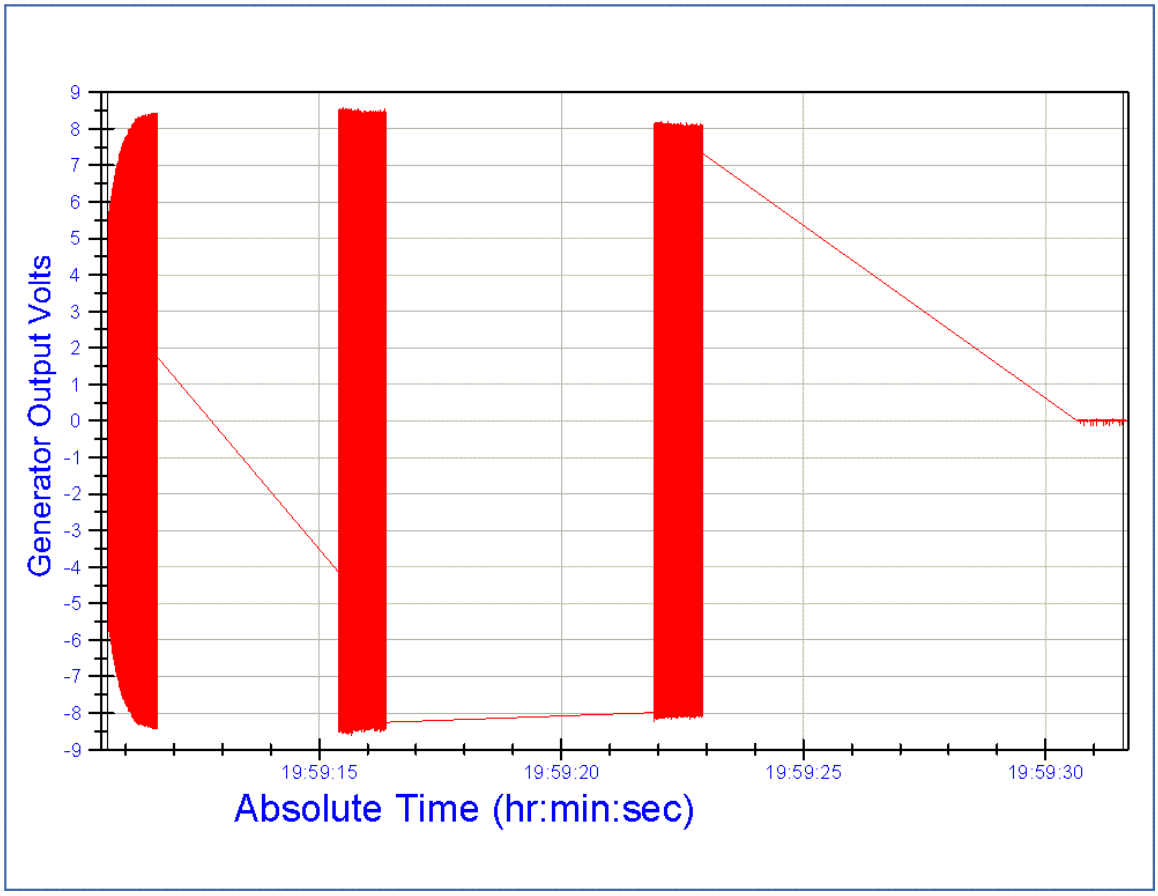

Figure 4.9 Output voltage of the generator acquired by the DAQ at 500 kS/s in 1 s periods. The gaps in between the blocks are due to the time delay taken by the PC in writing the collected data onto the hard drive. The output grows in amplitude to a peak of about 8.5 V and remains steady for a few seconds. After about 15 s of run, the speed reduction wheels lose contact and the generator stops running, resulting in the 0 V flat line towards the end of the chart.

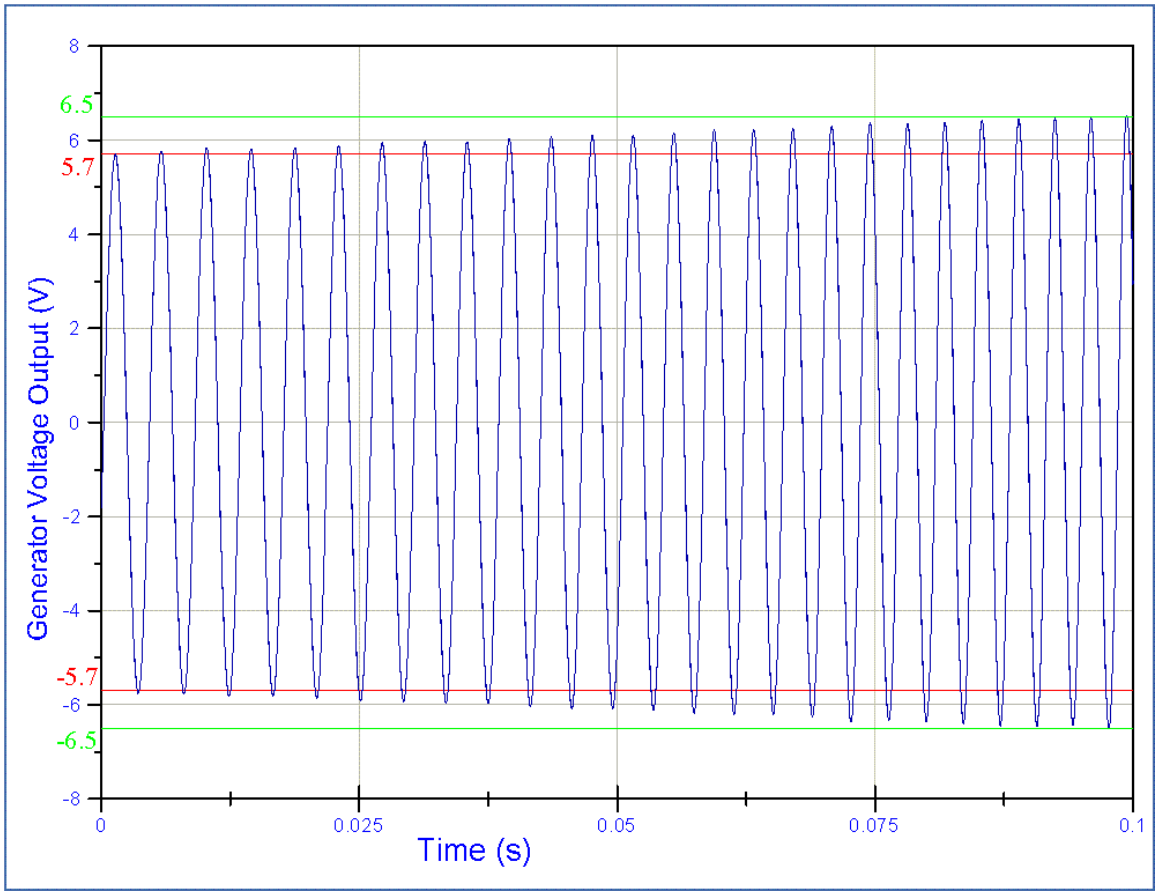

Figure 4.10 Voltage output of the generator showing a sinusoidal waveform that is growing gradually in amplitude and frequency, as the angular velocity of the turbine and generator increases.

Table 4.1 Results of the PDE-turbocharger-generator system test, with PDE running at 15 Hz on propane and oxygen at $\phi = 1.2$ and mass flow rate of 0.0057 kg/s. The time shown in the table corresponds to that of Figure 4.10, which is the actual time of the day the test was performed on.

Time (h:m)	Time (s)	Peak Voltage	V_{RMS}	Freq. of Output (Hz)	Power (W)	Generator Speed (rpm)	Turbo Speed (rpm)	Compressor Flow Rate (kg/s)
19:59	10.6562	5.7	4.03	225.124	12.02	13,507	44,575	0.0464
19:59	11.6562	8.41	5.95	621.922	26.18	37,315	123,141	0.0526
19:59	15.3906	8.42	5.95	641.491	26.24	38,489	127,015	0.0539
19:59	16.3902	8.34	5.90	600.519	25.74	36,031	118,903	0.0543
19:59	21.9219	8.11	5.73	501.458	24.34	30,087	99,289	0.0553
19:59	22.9219	8.01	5.66	484.447	23.75	29,067	95,921	0.0516

4.6 The Dual-Stage PDE: PDE With Pre-Detonator

This PDE[112] was designed by the author and built at the ARC to study the various techniques and engine systems that would make a fully functional PDE closer to reality. The objectives of this PDE are listed below:

- To test various techniques that will produce consistent detonations in a fuel-air mixture in the multi-cycle mode of operation, including Shchelkin spiral, pre-detonator with smooth area change and improved fuel-air mixing.
- To use liquid fuel-air mixtures in a multi-cycle PDE.
- To attain higher operating frequencies than previous tests, in the range of 20 to 50 Hz.
- To attain long run times and increase the endurance of the PDE. Previous test runs were limited to 20 seconds or up to 1 minute. With the water-cooled PDE, the run times may be extended to several minutes. This will enable the development of platforms that can yield 30 minutes to 1 hour of test time.
- To generate higher thrust as described by the scaling law, i.e., thrust is proportional to the area of the detonator.
- To test fuel injectors and multiple injector schemes to bring about better fuel mixing and combustion.
- To create a platform to test a variety of fuels. The bigger i.d. of 10.16 cm (4 in.) is larger than the detonation cell sizes of most fuel-air mixtures, such as propane, kerosene, jet fuel, etc. Thus, this new platform could be used to test many fuels.
- To compare a conventional low-energy ignition system with a novel high-energy plasma ignition system.
- To test and compare sensors that may be used within a PDE, which may be able to sustain longer test times than the previously used piezoelectric pressure transducers, which have a

low tolerance to heat and cannot sustain long-duration testing. Improved sensors are vital to the development of an effective control system that can be applied in an operational PDE.

The dual-stage PDE's main physical structure consists of the following parts: a pre-detonator, a 30° nozzle, a main combustor with a swirl-injector block and liquid fuel mixing chambers. These are briefly explained below. A schematic of the main body of the dual-stage PDE is shown below in Figures 4.11 and 4.12.

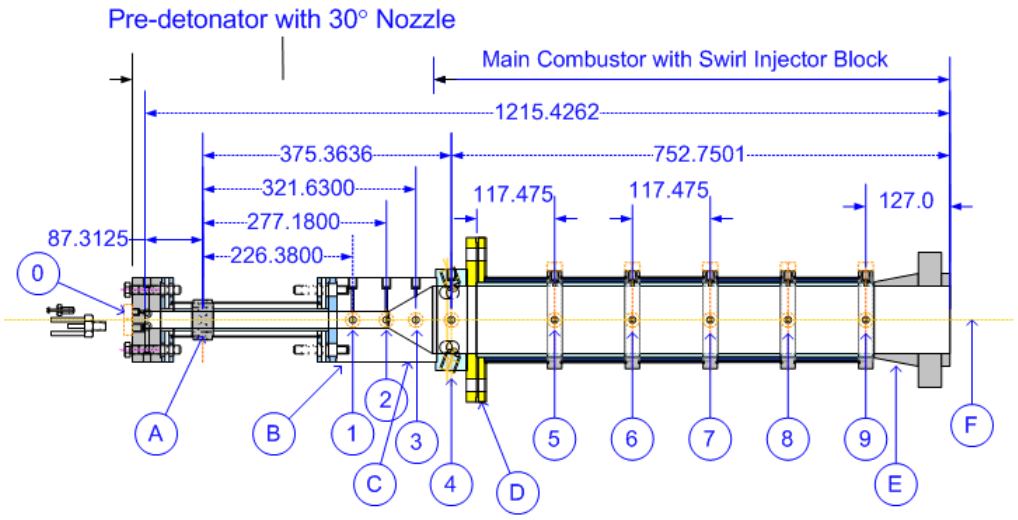

Figure 4.11 Schematic of the dual-stage PDE showing the dimensions and the locations of transducers. All dimensions indicated are in millimeters.

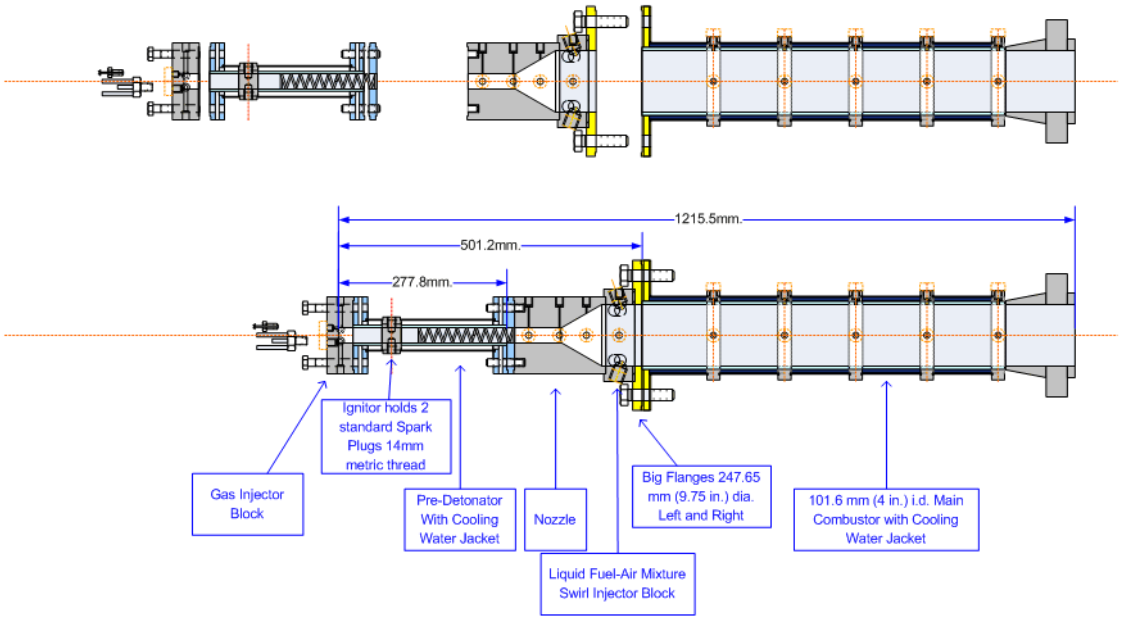

Figure 4.12 Schematic of the dual-stage PDE showing the various parts. All dimensions indicated are in millimeters.

4.6.1 Pre-detonator

The pre-detonator design was chosen because of its simplicity. At the cost of a small amount of oxygen carried on board, the pre-detonator provides an effortless means of igniting the propane-oxygen mixture quickly with low energy sparks, and makes it possible to transmit an accelerated detonation wave into a less energetic fuel-air mixture. The main piece of the pre-detonator consists of a 25.4 cm (10 in.) schedule 80 stainless steel tube of 25.4 mm (1 in.) i.d. and 33.2 mm (1.3 in.) o.d., rated at 171 atm (2500 psig) at 380°C (750°F) according to ANSI/ASME B 31.1 standards. In addition, the flanges and collars added to the pipe will lend strength to the pre-detonator, which will experience very high pressures and temperatures continuously. Carbon steel flanges (127 mm/5 in. diameter and 18.79 mm/0.74 in. thickness) are welded to both ends of the tube. The two flanges hold ¼ in. water-bearing tubes, acting as inlets and outlets for the water jacket that envelops the tube. The ignition plug holder is welded

to the tube 63.5 mm (2.5 in.) from the inlet end. The carbon steel gas injection block has four inlets, one for propane, two for oxygen and one for purge air, with the orifices opening tangential to the cross section of the tube. The gases enter the tube in a swirl pattern, which enhances mixing. There is also a pair of transducer ports, for one optical and one pressure transducer, on the back wall.

The pre-detonator has the option of being fitted with a 152.4 mm (6 in.) long Shchelkin spiral, which is made by winding a 304 stainless steel circular rod of 3.97 mm (5/32 in.) diameter with a pitch of 1.6 cm per turn, as shown in Figure 4.12. The spiral is welded to a flange that enables it to be bolted to the flange of the pre-detonator. The blockage ratio of the spiral is calculated to be 52.73%, which is in the region found to be most effective in reducing DDT run-up distance[109,110]. The Shchelkin spiral is used to over-drive the detonation wave so that it may be successfully transmitted through the nozzle without decoupling[32,33]. The pre-detonator is enclosed in a water-jacket for cooling, with four ¼ in. water inlets and four ¼ in. water outlets. The igniter sockets hold two regular 14 mm thread automotive ignition plugs simultaneously. The ignition plugs are both connected to the same automotive ignition system based on a Mallory ignition driver (HyFire III-A, Part No. 630, 135 mJ inductive ignition system) and a Mallory ignition coil (Part No. 24440). Only one plug will fire at a time and the redundancy ensures that if one plug fails, there is another one to take over. The same ignition sockets were also used for testing high-energy arc igniters, which were manufactured to fit the same sockets. A comparison of the ignition systems is provided in Section 7.4.

4.6.2. 30° Nozzle

The nozzle was designed to transmit the detonation wave with minimal loss of velocity. It was found that larger diverging angles or abrupt transition of area cause detonation waves to decouple, due to the excessive curvature of the detonation wave and the cooling of the flow due to the rapid expansion[72,113]. If the transition angle is very large, for over-driven detonations, the critical diameter condition moves from $d_c = 13\lambda$ to $d_c = 26\lambda$[72]. Therefore, the pre-detonator

will have to be larger for such cases. However, smaller angles result in a longer nozzle and larger volume, which requires more reactant. In addition, the nozzle had to be milled out of a solid steel block, while providing access for transducers and connectors. Long nozzles are difficult to machine and would weigh more. Thus, 30° was found to be the best compromise. The nozzle has three pairs of transducer ports that will enable the detonation velocity to be monitored during the transition through the nozzle. The nozzle is illustrated in the schematic of the PDE assembly shown in Figures 4.11 and 4.12. As mentioned above, by overdriving the detonation with a Shchelkin spiral before it expands through the nozzle, the detonation would only lose a small amount of energy and still come out strong enough to detonate the fuel-air mixture in the main combustor.

4.6.3. Main Combustor with Swirl Injector Block

The main combustor was fabricated from a welded stainless steel tube with 101.6 mm (4 in.) i.d. and 6.35 mm (0.25 in.) wall thickness, and was cut to a length of close to 711.2 mm (28 in.). Five collars have been welded to it, 114.3 mm (4.5 in.) apart, as seen in Figures 4.11 and 4.12. The 25.4 mm (1 in.) wide carbon steel collars hold pressure and optical transducer ports and contain orifices for water to circulate through them, and also provide additional strength to the tube. The combustor tube is covered with a layer of sheet metal in between the collars, forming a water cooling jacket. Water is pumped in through four tubes bored into the wall of the main flange on the left and the water exits the cooling cavity through four tubes welded to the last collar on the right hand side of the tube.

At the left hand end of the main combustor is the swirl injector block, which has four ports through which a fuel-air mixture is pumped in. The gas inlet ports are cut into the carbon steel structure such that the flow enters tangential to the cross section of the tube and at 20° to the normal to the surface, as seen in Figure 4.13, giving it a downstream axial velocity component. Thus, the fuel-air mixture enters the combustor in a forward moving, helical swirling pattern, thereby enhancing mixing as the flow moves downstream. Four injection ports

allow for the rapid filling of the combustor, making it possible to run the PDE at high frequencies. There is a pair of transducer ports, one for pressure and one for either an optical transducer or an ion detector, located on the swirl injector block, as seen in Figure 4.13. The main combustor is designed to be usable on its own as a detonation tube, by capping off the flanged inlet and adding an igniter. The end flange allows for additional tube to be added to extend the length of the PDE, so as to test fuels with longer DDT lengths.

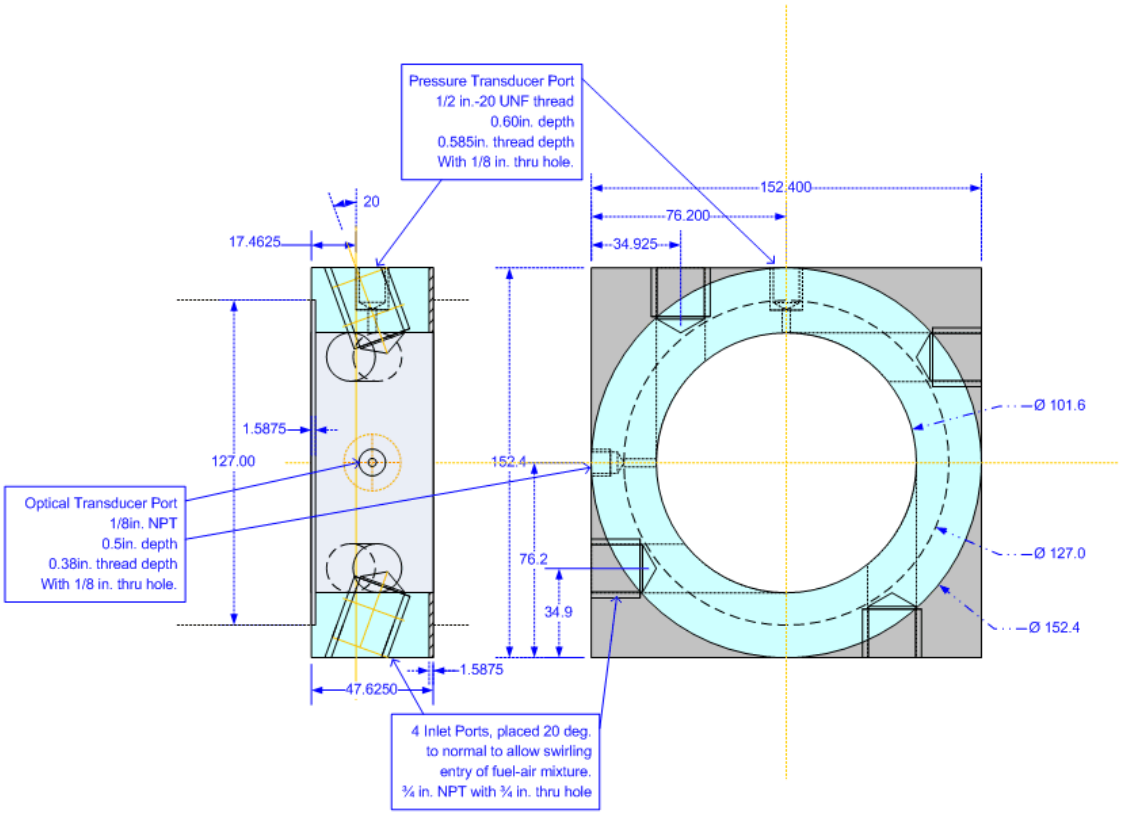

Figure 4.13 Schematic of the swirl injector block. All dimensions indicated are in millimeters.

4.6.4. Gas and Fuel Injectors

The gases are injected by means of the previously used gas injectors, the AFS-Gs series valves from Alternate Fuel Systems, Inc., Calgary, Canada. These valves have their own electronic driver unit, which enable the valves to be controlled by TTL signals. The valves are rated for 12 V dc, with a peak in-rush current of 8 A and a mean hold current of 2 A.

The liquid fuel injectors procured for this study were direct injection gasoline injectors from Denso Corporation that are used as OEM equipment in Lexus IS-300 2007 model cars. These valves inject fuel in a fan shape directly into the cylinder during the intake stroke of the engine, unlike earlier designs where the gasoline is injected into an air stream in a plenum chamber located before the inlet valves[114]. The new valves are rated for 14 MPa (2000 psig). Since they are located on the engine itself, these injectors are designed to function in high temperature and pressure environments. The valves spray fuel in a V-shaped fan that is also inclined at 30°to the axis of the valve.

The original electronic driver unit of the Denso valves is not easily customizable for use with the DAQ because it operates in conjunction with the car's onboard computer. Therefore a power transistor based driver circuit that accepts TTL signals from the DAQ was built in-house. This circuit, which is shown in Figure 4.14, requires a power supply of 50 to 60 Vdc and a steady-state current of 2 A per valve. The Denso injectors are claimed to be able to atomize liquids to a Sauter's mean diameter (SMD) of approximately $10\,\mu m$ at 10 MPa injection pressure. A sample valve was tested using pressurized water at room temperature and the SMD of the spray was measured using a Malvern Insitec Ensemble Particle Concentration and Size (EPCS) meter, which uses laser diffraction to measure particle size. The focal length of the lens of the EPCS meter is 450 mm and it can detect particles ranging from 2.25 to 1000 μm in size. The SMD of water injected at 10 MPa injection pressure were found to be around 26.17 μm. However, these results could not be reproduced with kerosene. An analysis of valve performance is presented in Chapter 8.

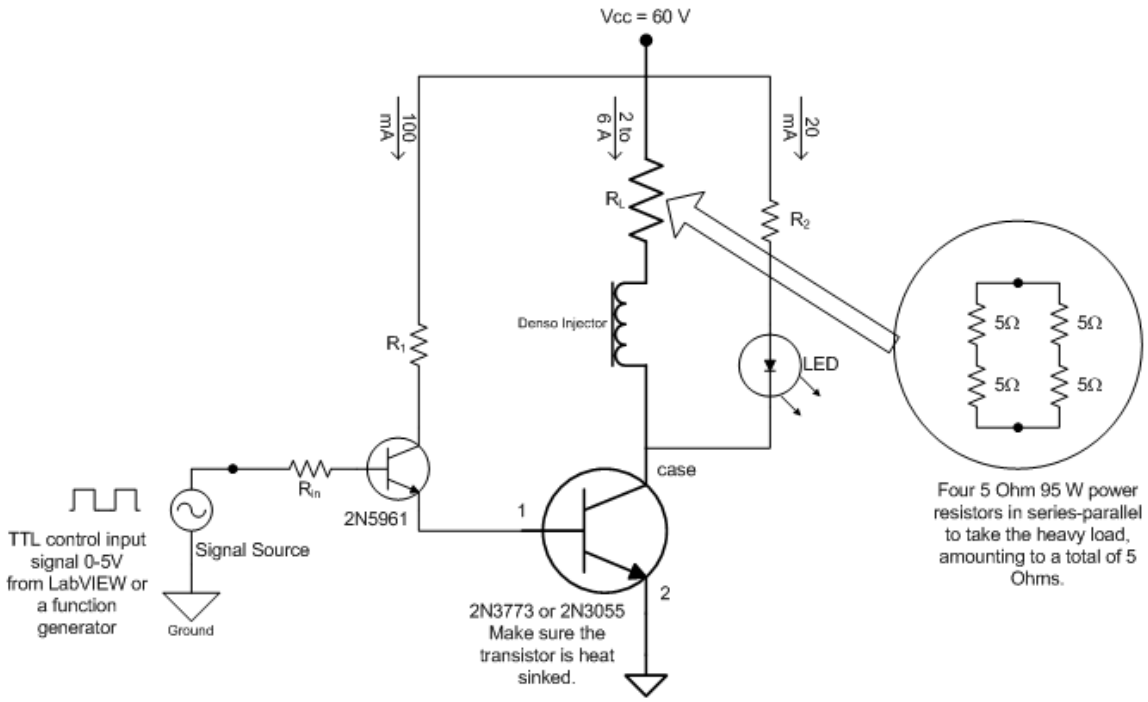

Figure 4.14 Circuit diagram of the driver circuit developed for the Denso gasoline injectors. The value of the resistors used for R_1 and R_{in} was 1 kΩ, while R_2 was 2 kΩ.

4.6.5. Liquid Fuel Mixing Chamber

There were two identical liquid fuel mixing chambers made, although the main combustor could accommodate four such devices. The liquid fuel mixing chambers were made from 50.8 mm (2 in.) diameter 304 stainless steel tubes. In each mixing chamber, two tube sections of 152.4 mm (6 in.) length were welded to either side of a steel plate with 6.35 mm (¼ in.) perforations, as shown in Figure 4.15. One side of the mixer contains a heating element while the other side holds the Denso fuel injector. Cold air is pumped in through the flange on the heater side of the mixer, using an AFS Gs valve. The air heating coil was made by wrapping 6.35 mm (¼ in.) copper tubing over a water heater element rated at 1400 W, 120 Vac. The heater is powered by means of an auto-transformer and regulated using a thermostat, making it possible to modulate the temperature of the heating coil. The temperature of the air coming out of the heater should not be high enough to ignite the liquid fuel. The heating coil's thermostat

prevents the mixing chamber from heating up beyond the required temperature. The mixing chamber was designed to have cold air injected in at pressures of 4.40 to 7.12 atm (50 to 90 psig), which would then be heated up as it passes through the heating element. As the now warm air flows through to the liquid fuel side of the mixer, it will encounter the fan shaped fuel spray being injected by the Denso valve, causing them to mix and form a gaseous mixture before being injected into the main combustor. A check valve is mounted on the exit of the mixing chamber so that flow is not returned into the chamber during the combustion process. Both the AFS Gs gas valve and the Denso valve are to be opened simultaneously to prevent liquid fuel from coming into contact with the heating element

Liquid fuel is pumped using a nitrogen based pressure system, similar to the schematic shown in Figure 4.16. A Swagelok 1000 cm^3 stainless steel pressure vessel is filled with liquid fuel. Nitrogen, at a high pressure, is manually regulated and fed into the chamber to pressurize the fuel to the required value. All inlets and outlets to the pressure vessel are connected through high-pressure (137-205 atm/2000 to 3000 psig) pneumatic valves, which are driven by air from low-pressure (4.4-11.2 atm/50 to 150 psig) solenoid valves, enabling the supply lines to be controlled remotely. The pressurized fuel then passes through a coil placed in a vessel of hot water. The temperature of the liquid fuel is adjusted to the desired set point by regulating the water heater. The water heater consists of heating elements activated by a variable thermostat, which is powered from an auto-transformer connected to the 120 Vac mains. The warm fuel is then supplied to the Denso injectors mounted on the mixing chambers. The main combustor is designed to take four such mixing chambers, allowing the PDE to be filled at high speeds and making it possible to operate at a high cycle frequency.

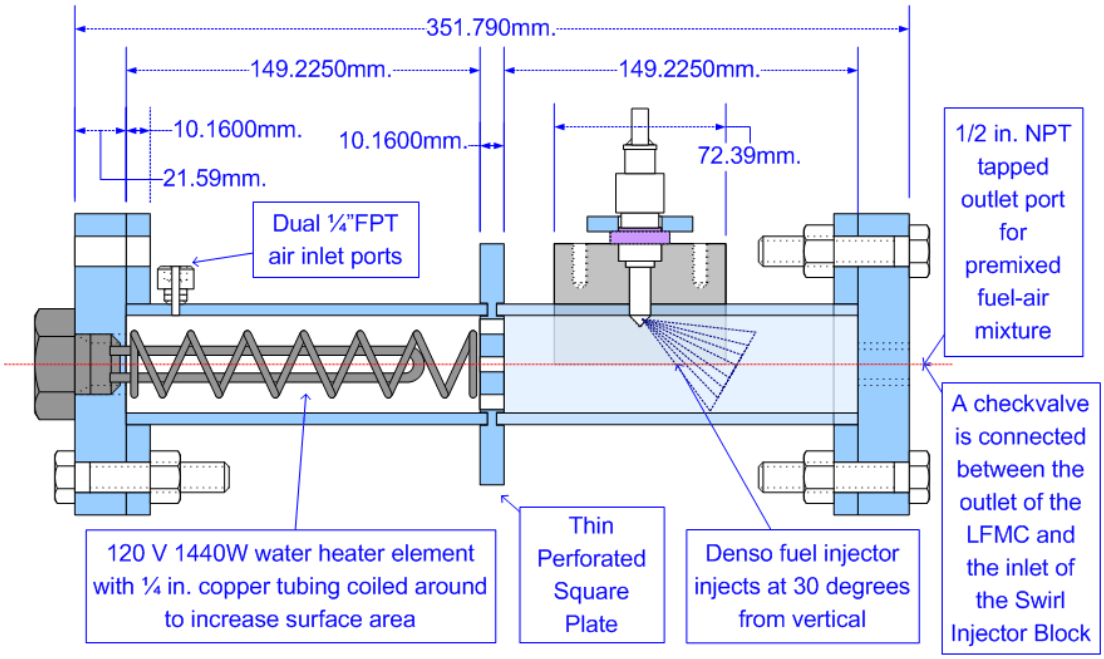

Figure 4.15 Schematic of the liquid fuel mixing chamber.

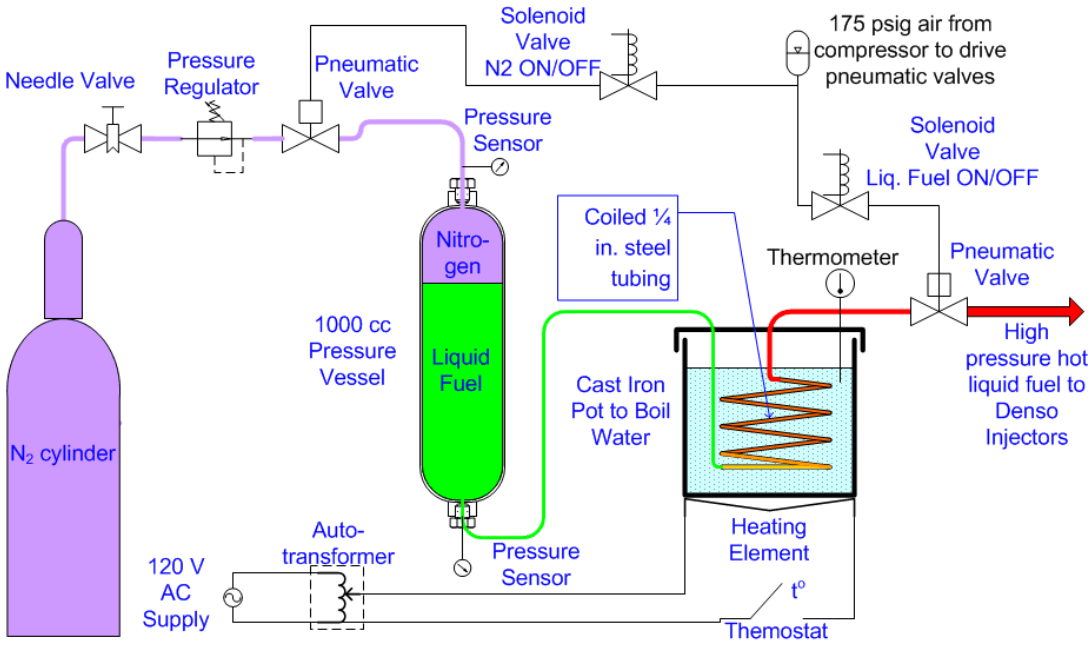

Figure 4.16 Schematic of the liquid fuel pumping system developed for the dual-stage PDE.

4.6.6. Diagnostics, Data Acquisition and Control System

The data acquisition service was separated and assigned to two independent systems. The internal diagnostics of the combustor was performed with piezoelectric pressure sensors (PCB 111A24, 1000 psig, 450 kHz natural frequency, with PCB 483A signal conditioner), ion detectors and photo-detectors. Schematics of the ion detectors and the photo-detectors used in this study, along with circuit diagrams of their amplifiers, are shown in Figures 4.17 and 4.18 respectively. The amplifiers of the ion detectors and the photo-detectors were designed to produce a 0-10V signal that could be directly sent to the DAQ. The signals from the above three sensors are sampled at very high sampling rates, 1 to 2.5 MS/s, so as to be able to determine the detonation properties with clarity. These signals were assigned to a high-speed DAQ based on the National Instruments PXI architecture. This system consists of a PXI 1042Q chassis that contains a pair of 8-channel, 16-bit, 2.5 MS/s S-series PXI-6133 cards. The DAQ is connected to a remote high-end PC via a fiber-optic cable which ensures smooth, EMI-free signal transmission. The performance of the PC was enhanced with 4 GB of RAM and a four hard-drive RAID 0 system, in which each hard-drive was a 100 GB, 7200 rpm unit. This PC also was used to control the valves and ignition timing by means of TTL signal generator programs. The larger amount of RAM allowed the data acquisition programs to run, while also running the valve and ignition timing control programs. The RAID 0 system allowed large amounts of data to be written at a fast rate.

The second DAQ was a slower PC-based system. The hardware included two PCI-6024E cards (E series, 200 kS/s maximum, 12 bit) and one PCI-6221 card (M series, 250 kS/s maximum, 16 bit). Each of the cards had 8 differential channels which could also be configured as 16 single-ended channels. The differential channels are preferred for improved noise immunity, but this arrangement reduces the number of available channels. The slower DAQ was used to measure signals from various sensors, including thermocouples (J-type, K-type and T-type), heat flux sensors, static pressure transducers for flow rate measurement and a

microphone for sound pressure level. These signals were acquired at varying sampling rates, 1 kS/s, 5 kS/s and 10 kS/s, as required. The sampling rates were set at the beginning of the tests. Gaseous flow rates were measured with the help of Flow-Dyne critical flow nozzles. The nozzles were fitted with T-type thermocouples and static pressure transducers from Omega, which included a model PX302-200GV (200 psig full scale) and a model PX302-300GV (300 psig full scale) transducers. The liquid fuel pump and supply lines were monitored with a pair of Omega PX319-3KG5V (3000 psig full scale) static pressure transducers.

The DAQ and the control programs were composed using LabVIEW 8.2. Further analysis of the relevant data and the more significant results obtained in the course of this study are presented in Chapters 7 through 9.

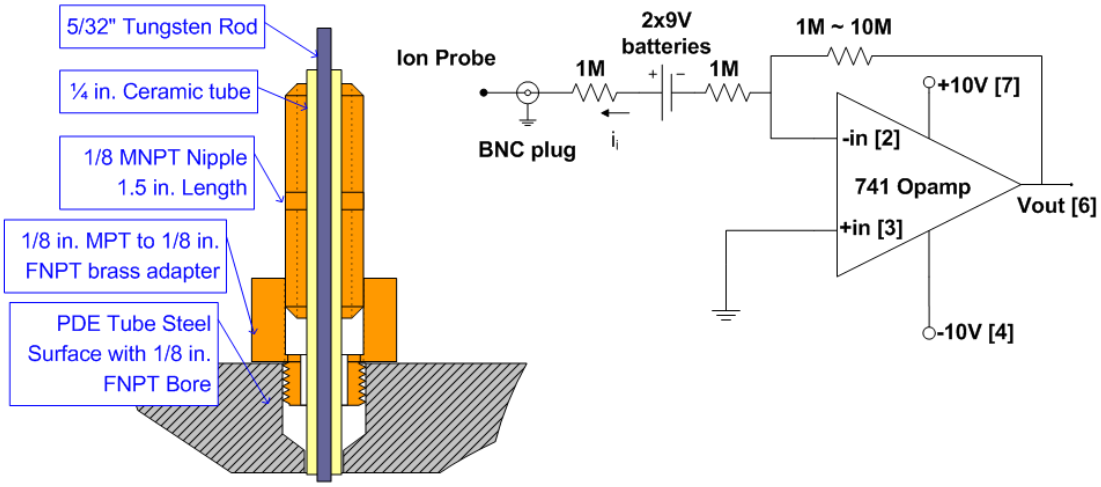

Figure 4.17 Schematic of the ion detector and the circuit diagram of its amplifier.

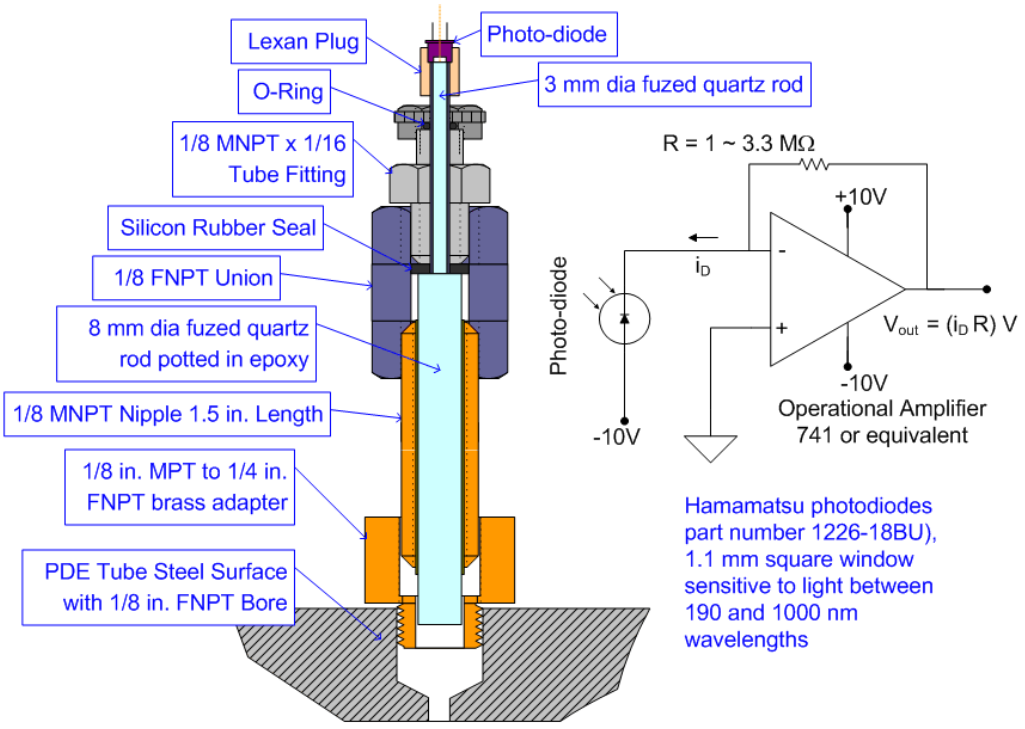

Figure 4.18 Schematic of the photo-detector and the circuit diagram of its amplifier.

CHAPTER 5

EXPERIMENTAL STUDY OF DEFLAGRATION-TO-DETONATION TRANSITION DEVICES

5.1 DDT Devices

As mentioned in Chapter 2, deflagration-to-detonation transition (DDT) is a process by which a deflagration flame front is gradually accelerated to form a supersonic detonation wave. As the flame is pushed downstream by the expansion of the burnt gases behind it, the flame front becomes curved and wrinkled by the effects of the boundary layer in front of the flame, flame instabilities and turbulence[33]. As a result, the surface area of the flame grows which increases the rate of reaction of the fuel and oxidizer. Thus, the rate of release of energy is amplified causing the flame front to be accelerated at an even faster rate. Finally, the increased energy release leads to the formation of one or more localized explosions and the transformation of the flame into a detonation wave.

It has been verified that placing certain obstacles in the flow significantly reduces the DDT run-up distance. These objects are called DDT devices. The effect that DDT devices generate is to increase turbulence and the thickness of the boundary layer in the flow and to create instabilities in the flame front[33,115]. The most commonly used device is the Shchelkin spiral, which is named after K.I. Shchelkin, who discovered it, while studying the effects of wall roughness on detonation, in the late 1930s. The Shchelkin spiral is essentially a helical spring made from thick rigid wire, as shown in Figure 5.1. The parameters of the spiral are length, blockage ratio and pitch. The blockage ratio of the spiral or any cylindrical DDT device is given in terms of its internal and external diameters, d and D respectively, and thickness t, as follows.

$$BR = \frac{\text{Area covered by device}}{\text{Total internal area of tube}} = \frac{\left(D^2 - d^2\right)}{D^2} = \frac{4t\left(D - t\right)}{D^2} \tag{5.1}$$

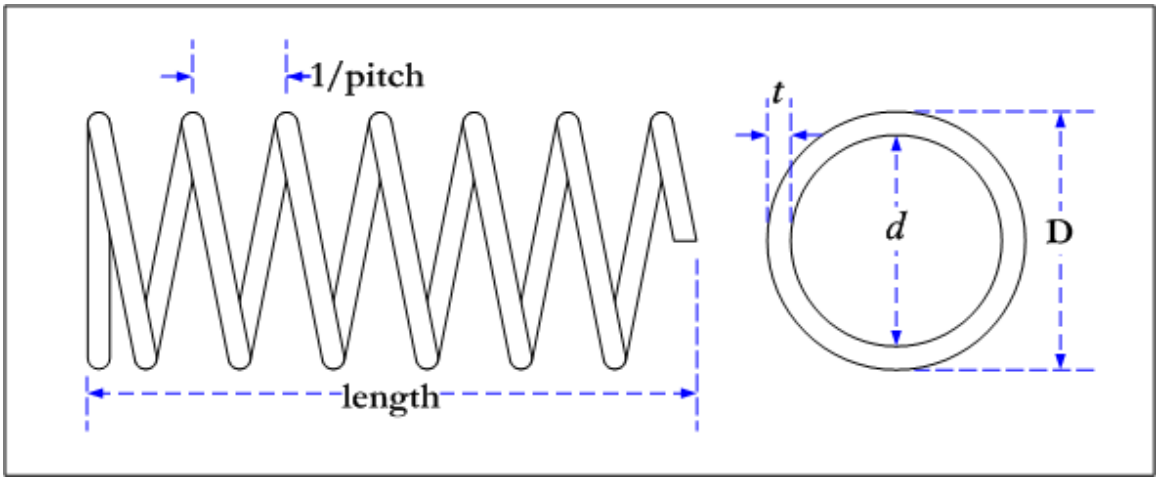

Figure 5.1 Schematic of the Shchelkin spiral, showing the various parameters used to specify it.

Other DDT devices include orifice plates, converging-diverging nozzles, sleeves with ridges, grooves or holes, etc. Figure 5.2 shows the schematic of the two types of orifice plates that have been studied in PDE applications, namely the single orifice and the multiple orifice types. To calculate the blockage ratio of orifice plates, the area covered by the orifice plate is taken as the difference between the total internal cross sectional area of the combustor tube and the sum of the areas of all the orifices on the plate. Orifice plates have been studied in extensively in PDE setups[35,115-121]. The advantages of the orifice plates are:

- They are very robust and durable, compared to thin wired springs.
- They are easy to manufacture and install.
- High blockage ratios are easier to achieve with orifice plates. Some studies mentioned earlier have used BR in the range of 0.6 to 0.85. Spirals would have to be very thick to match the same BR.
- One or two high BR orifice plates have been seen to produce DDT in a short distance.

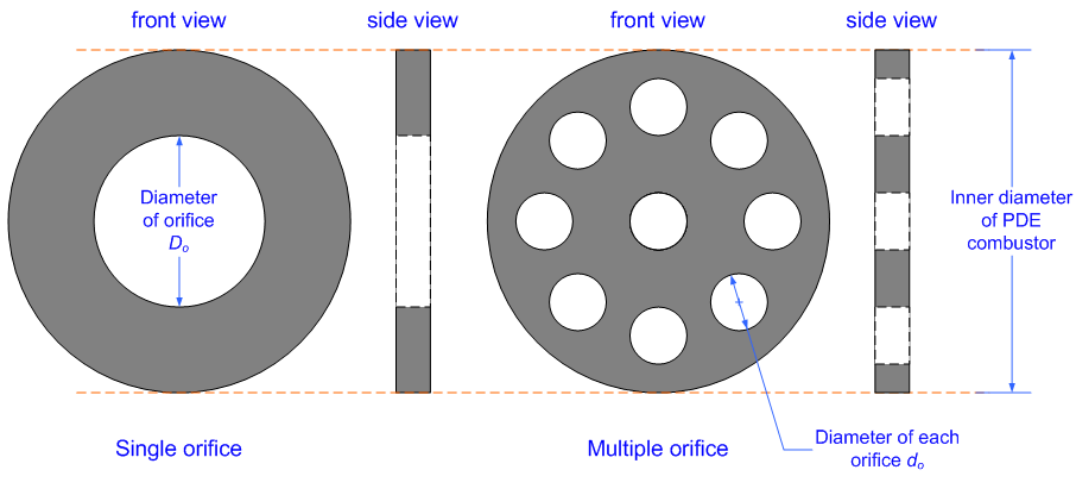

Figure 5.2 Schematic of orifice plates.

5.2 Study of The Effect of Shchelkin Spiral Parameters on DDT

The effect of Shchelkin spiral was tested on the Bantam PDE, the PDE Mark 1 and the PDE Mark 2. In PDE Mark 3, the spiral was grooved into the wall of the detonation tube, to study its effectiveness and its survivability. The detonation tube of the PDE Mark 3 was also water-cooled by means of a water jacket. In all the above cases, the flow rates were maintained for near stoichiometric propane-oxygen mixtures at various cycle frequencies, not exceeding 15 Hz.

5.2.1 Effects of Shchelkin spiral blockage ratio

Table 5.1 shows a list of eight test cases performed on PDE Mark 1, including the various blockage ratios and spiral lengths. All the listed test cases were run at 10 Hz. The first five cases show a clean tube baseline configuration, as well as four cases where the BR is increased while keeping the length of the spiral constant at 304 mm. It was observed that the detonation peak pressures (von Neumann pressures) and the corresponding plateau pressures behind the shock increase as the blockage ratio is increased. When compared with the clean tube, base-line configuration, there is an increasing trend in pressures, wave speeds, as well as

thrust as the blockage ratio is increased. In the case of the clean tube configuration, detonation was observed between the first two transducers as seen from the TOF velocity. However, the wave quickly dies down to subsonic speeds. The lower blockage ratios could not achieve detonation at all. The highest BR (55.6 %) gave the best results in terms of pressures, detonation velocities and thrust among these five cases. While the plateau pressures behind the shock is in the region of 5 to 15 bar for the clean tube and lower BR cases, for the 55.6 % BR case, the pressures behind the shocks are seen to be roughly about 10 to 15 bar and even increases to 30 bar as the wave progresses along the tube. Among the first five cases, the presence of strong detonations also shows an effect in the thrust developed. In the case of the highest BR, a peak thrust of 120 N per cycle is observed. The thrust is very small for lower blockage ratios, but once again it shows an increasing trend with BR. This means that BR in excess of 50 % brings about DDT quicker. Therefore, if the spiral is shorter, the BR should be at 50 % or higher to reduce the DDT run-up distance.

Table 5.1 List of test cases and results in brief.

Wire Diameter	Spiral Length	Blockage Ratio	Spiral Pitch	Maximum Det. Wave Speed	C-J Velocity	Top Thrust Recorded		Comments
(mm)	(mm)	(%)	(mm)	(m/s)	(m/s)	(N)	(lbf)	
0	304	0- base line case	0	2500	2350	15	3.4	Failing detonation
2.3	304	34.7	5.4	1200	2350	15	3.4	No detonation
3.2	304	46.2	3.6	1250	2350	55	12.4	No detonation
3.5	304	49.8	3.6	2000	2350	100	22.5	No detonation
4	304	55.6	3.1	2500	2350	120	27	Galloping detonation
0	594	0- base line case	0	1200	2350	15	3.4	No detonation
2.3	594	34.7	5.4	2500	2350	220	49.5	Galloping detonation
3.5	594	49.8	3.6	2500	2350	190	42.7	Galloping detonation

5.2.2 Effects of Shchelkin spiral length

A longer detonation tube is used for the last three cases of Table 5.1 which includes the clean tube and two BR cases. For these cases, the spirals with smaller BR that failed to give detonations earlier, were extended to 594 mm in length and compared with a clean tube combustor of the same length. It is seen that as the length of the spirals are increased, DDT occurs further downstream. There is an improvement in the detonation pressures also, as the plateau pressures increase from about 15 bar to 30 bar towards the exit. One significant observation is that the detonation is seen to increase in speed, and then decelerate till it goes below C-J velocity. In some cases, this trend is repeated twice before the detonation exits the tube. This phenomenon is suspected to be a galloping detonation and is known to occur at the detonation limits and is thought to be caused by improper filling or mixing. Therefore, proper valving and mixing of fuel with air is critical to the proper working of the PDE, especially at high speeds, when the residence times of fluid in the combustor is shorter. The thrust levels in the last three cases are also significantly higher than in the first five cases, due to the larger amount of mass flow being expelled during each cycle at high pressures. This is a case of volume scaling of the PDE, i.e., increasing thrust by increasing the volume of the PDE whilst keeping frequency constant. Interestingly, in the seventh case, the peak thrust observed during the tests is seen to be 220 N/ cycle, which is higher than the last case where the thrust is only 190 N. This is most likely an anomaly. However, it is true that large blockage ratio causes more drag and a reduction in thrust. But the likely cause of this one case is the unsteady effects of the hardware, including the fill rates of the motorized valves, timing, etc.

5.3 Comparison of Various DDT Devices

In the PDE Mark 2, the performance of various DDT devices was compared against the baseline clean tube configuration, including Shchelkin spirals, slotted sleeves, dimpled sleeves, converging-diverging nozzles, etc., as shown in Figure 5.3. The length of the sleeve-shaped devices was limited to 160 mm, while the converging-diverging section was set at 60 mm.

These tests were run with propane and oxygen mixtures at near stoichiometric conditions at 15 Hz, as this was found to be optimum in terms of speed and flow rates and the maximum number of engine cycles that could be captured by the DAQ in a 5 s window. Table 5.2 shows the parameters of the various devices tested.

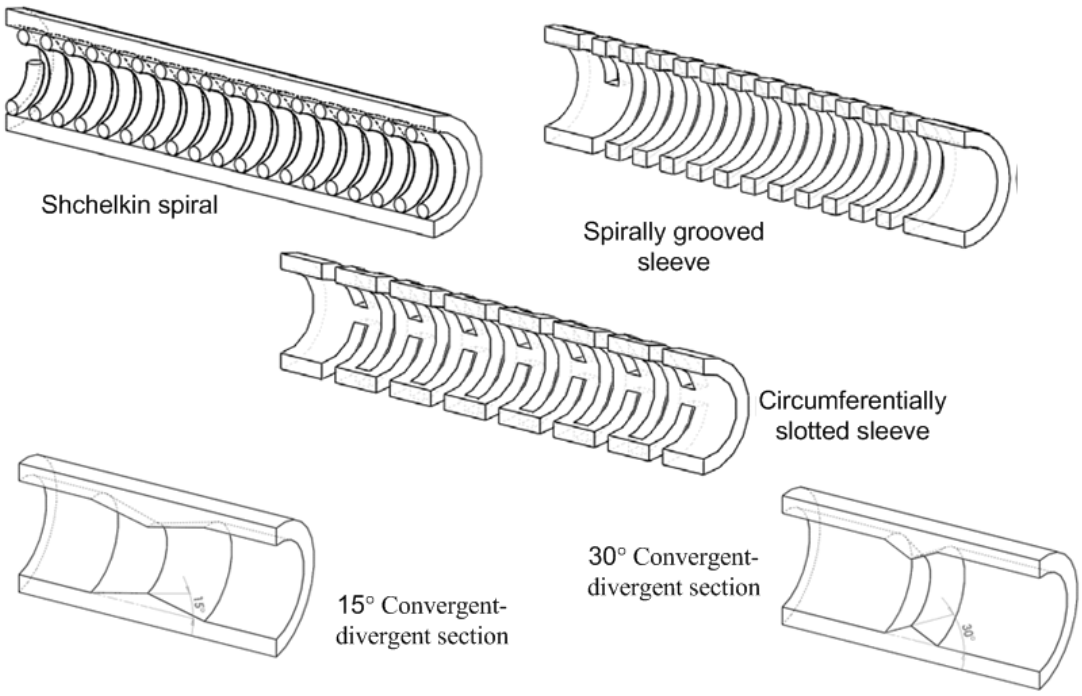

Figure 5.3 Schematic of the various DDT devices tested on PDE Mark 2.

Table 5.2 Dimensions of the DDT devices tested on PDE Mark 2.

DDT Device	Blockage Ratio (%)	Length (mm)	Outer Dia (mm)	Wire width (mm)	Wire depth (mm)	Pitch (mm/turn)	L/D
Shchelkin Spiral	55.56	160	24	4	4	8	6.7
Circ. Groove	61.46	160	24	5	4.55	10	6.7
Helical Groove	61.46	160	24	5	4.55	10	6.7
15° CD section	50%	60	24	17.2			
30° CD section	50%	60	24	17.2			

Figure 5.4 (top) shows the average TOF velocities of the detonation waves as well as the success rate of the devices. An engine cycle was deemed successful if the detonation TOF velocity met or surpassed the C-J detonation velocity of 2360 m/s for propane-oxygen at the stoichiometric state. It is seen from the results, that the clean tube produced the highest TOF velocities and in a consistent manner. The reason arrived at for this phenomenon was that propane and oxygen forms a highly reactive mixture when mixed at the right proportions that readily detonates. The solenoid valves were able to supply a much better mixture close to an equivalence ratio of 1, which the previous rotary valves could not match. However, the pressures and the wave speeds of the clean tube are seen to decline more rapidly as the wave progresses downstream.

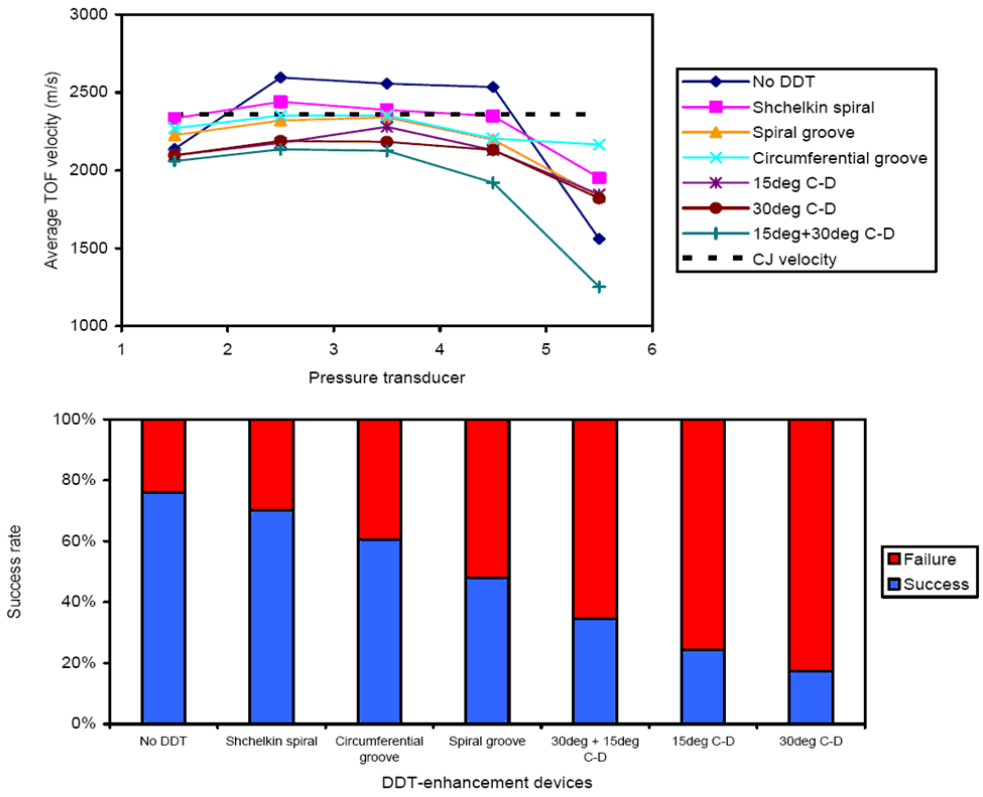

Figure 5.4 (Top) The average TOF velocities for various DDT devices tested at 15 Hz. (Bottom) Success rate for the various devices at 15 Hz. Success is defined as the case when TOF velocity is greater than the C-J velocity of 2360 m/s.

The Shchelkin spiral is again seen to be the better choice of DDT device over the slotted sleeves. As seen in the table, the BR for the spiral is quite high, being 55.56%. Therefore, it is able to induce DDT quickly. However, the sleeves have higher BR and it is possible that their lengths need to be altered to enhance DDT. Therefore, the length of these DDT devices was deemed to be too short with an L/D of only 6.7, and so it was concluded that longer DDT devices would have been better. It is also possible that the geometry of the slots were not optimum and that spirals or multiple rings work better, as seen in studies elsewhere[115-117].

The converging-diverging (CD) sections did not produce satisfactory DDT results. Their TOF velocities were close to C-J when used singly but were worse off when used in tandem. Perhaps the gradual decrease in area is less conducive to detonation unlike the abrupt changes in the Shchelkin spirals and orifice plates, that tend to induce turbulence and cause the flame surface to wrinkle and enlarge, whereby the chemical reaction is able to spread out more rapidly. The CD section can be considered to be similar to an orifice plate or one loop of a Shchelkin spiral, with 50 % BR. Therefore, multiple instances of these CD devices with the same or lower BR in the range of 40 to 50 % may produce better results. The advantage of the CD sections is that they are more robust than the thin wired spirals or thin walled grooved sleeves. Therefore, they will last longer in a detonation environment. On the negative side, the higher BR will cause larger drag and reduction in the thrust.

All the TOF velocities show a decline in velocity and complete failure of the detonation towards the exit. The reason for this is the inhomogeneous concentration of propane and oxygen near the exit is that the mixture becomes diluted near the exit and it is also possible that the gas valves could not sustain full filling of the tube at the chosen frequency and duty cycle, although they could provide a good mixture for most of the tube volume.

5.4 Discussion

It is seen from tests conducted here and from literature that Shchelkin spirals are very effective in bringing about DDT in very short distances, with the DDT length having an inverse relationship with BR. BR greater than 50 % are most effective. Similar to spirals, other geometries have also proved to be successful. The key appears to be the BR. The device could be in the shape of rings, slotted sleeves or orifice plates to bring about DDT. However, BR larger than 50 % also has a detrimental effect on flow dynamics. They create drag during the purging, filling and blowdown stages. Orifice plates with high BR come under heavy stress during the blow-down phase, because they take the brunt of the force on them. Therefore, orifice plates should be reduced in size to about 50 % BR or lower. If the BR is reduced, then the number of orifice plates or the length of the DDT device can be increased to achieve the same effect. The longer device may be preferable for longer engines and also to dissipate heat. Shorter engines would require shorter DDT devices with high BR.

But Shchelkin spirals have to be made robust and actively cooled to prevent damage to their structure. The Shchelkin spirals from PDE Mark 1 suffered irreparable damage after only a few seconds of run time. Therefore, the good data acquired were only from the first few seconds. After that, the spirals were either broken or ejected out. This is clearly seen in Figures 5.5, 5.6 and 5.7.

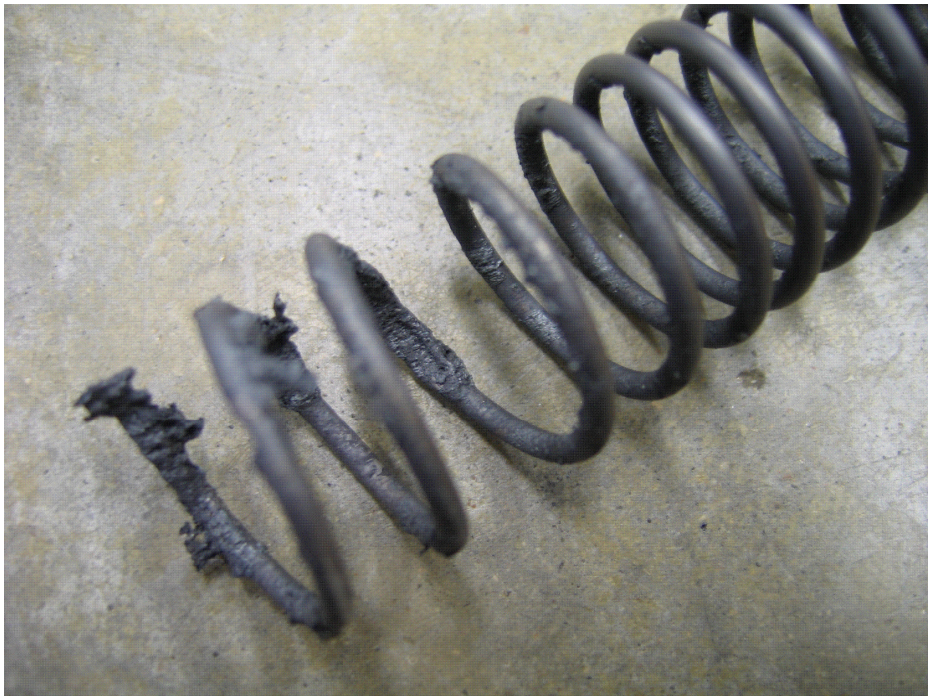

Figure 5.5 A sample Shchelkin spiral after testing in the PDE Mark 1 showing evidence of massive wear and deformation.

Figure 5.6 Fragment of a Shchelkin spiral after testing the PDE Mark 1.

Figure 5.7 The remains of a Shchelkin spiral that fused together after testing within PDE Mark 1.

In addition, DDT devices can cause hot spots to occur on them, which can lead to pre-ignition and misfiring of the PDE. This is undesirable. Therefore, purging and cooling is especially critical for DDT devices. It was seen in the tests that the part of the combustor housing the Shchelkin spiral is the hottest part of the tube, as clearly visible in Figure 5.8, where the spiral section is shown to be glowing red hot during a test run that lasted about 15 s. If the tests were carried on for longer periods, the section would have been damaged. Therefore, cooling the tube is extremely important.

If the DDT devices are integrated into the engine structure with active cooling, they will survive longer. However, sleeve shaped devices that can be dismantled and replaced would be a benefit for engines intended for long duration use with regular scheduled maintenance.

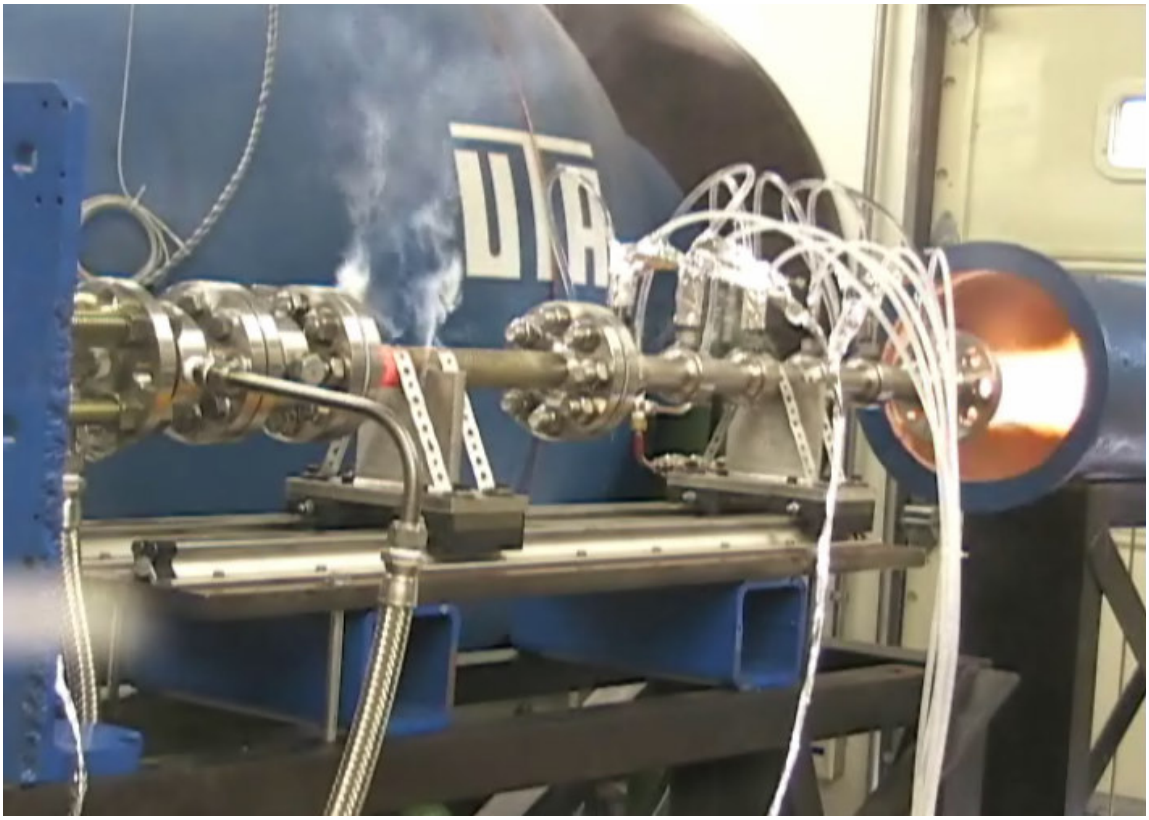

Figure 5.8 Picture of the PDE Mark 1 undegoing a test, using stoichiometric propane-oxygen mixture at 10 Hz. The Shchelkin spiral section is seen to glow red hot with smoke rising from the area due to the burning of epoxy applied to the exterior of the tube.

5.5 Summary

The Shchelkin spiral has been found to be the most effective at BR in excess of 50 % in bringing about DDT in a shortest possible distance and time. However, Shchelkin spirals suffer severe damage due to the high temperatures and pressures and also retain heat which may lead to pre-ignition and misfiring of the PDE. Thus, active cooling of the spiral section is required. Moreover, the spiral may be made by cutting grooves into the inner walls of the detonation tube or inserted as a replaceable sleeve. Also, injection of pressurized liquid through the interior of a spiral is another way to accomplish the cooling of the device. However, this last method requires complex sealing and pressurization of the cooling fluid.

In addition to Shchelkin spirals, the orifice plate is a good choice as a DDT device because of its simplicity of design. It is seen from a review of literature that high BR greater than 75 to 85 % can bring about DDT with just one or two orifice plates. Moreover, cooling conduits can be made into the plates to actively cool them.

CHAPTER 6

STUDY OF PRE-DETONATOR DESIGN

6.1 Introduction

It is known that detonation can be initiated in a less energetic mixture by imparting a large amount of energy to it, such as in the form of an arc discharge or from a pre-detonator. In the latter case, a more energetic mixture is detonated and allowed to transmit the detonation into a weaker mixture. The advantage of the pre-detonator is that a smaller amount of fuel-energizer, such as oxygen, is required to be spent to bring about detonation. Therefore, the ignition system of smaller energy and power ratings can be used to initiate the combustion, as is explained in Chapter 7, allowing considerable savings in the form of weight and complexity of the systems. Also, the components of higher energy ignition systems, the circuitry and especially the igniters, experience damage to a high degree and have shorter durability. Hence, a pre-detonator could also be to PDEs what a flame holder is to gas turbine engines.

Various pre-detonator shapes have been studied so far, including the shapes shown in Figure 6.1. The main parameter that determines the size and geometry of the pre-detonator and the main combustor is the cell size of the mixtures that is to be used in them. The diameter of the pre-detonator must meet the minimum requirement of one cell width of the mixture for a constant area tube. The diameter requirements are further discussed in the sections below. The length of the pre-detonator must be long enough to achieve DDT. It may also be necessary to over-drive the detonation within the pre-detonator before transmission to the less sensitive mixture, which may require some additional length.

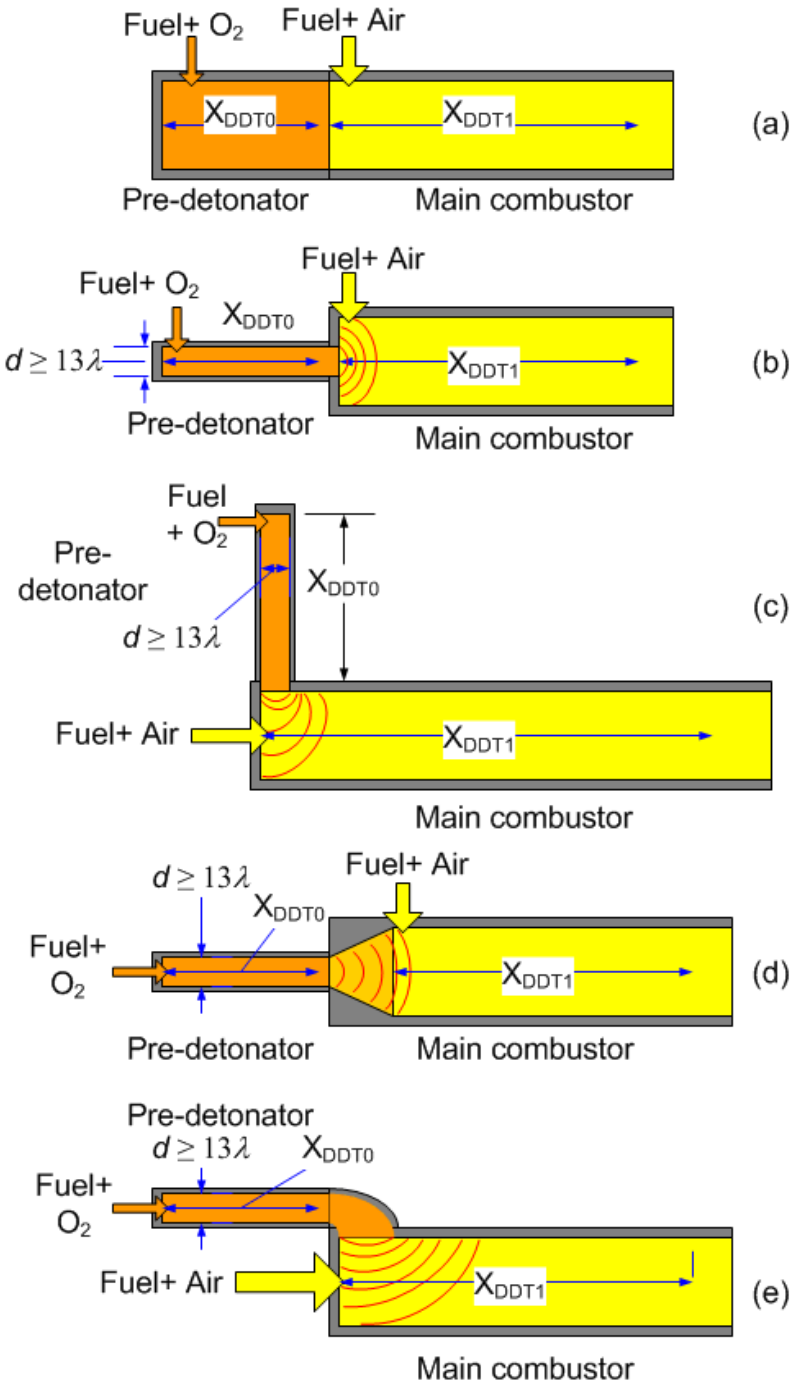

Figure 6.1 Schematics of various pre-detonator designs: (a) constant area, (b) abrupt area change, (c) abrupt area change at right angle to main combustor, (d) pre-detonator with a smooth area change nozzle to main combustor and (e) pre-detonator with smooth bend.

6.1.1 Effect of tube diameter and length on DDT and Pre-detonator Length

For stoichiometric mixtures, the DDT distance is shown to follow a relationship expressed as

$$X_{DDT} = Kd^{a} \tag{6.1}$$

where X_{DDT} is the DDT distance, K and a are empirically derived constants and d is the diameter of the tube[33,34]. The value of a is found to be between 0.41 and 0.5. However, for non-stoichiometric mixtures, this relationship alone does not hold and other dynamics, such as dissipation of detonation wave energy, flame acceleration and amplification factor (the ratio of turbulent flame velocity to the laminar flame velocity) also have to be considered. In such cases, the DDT distance may be expressed as

$$X_{DDT} = Kd^{a}C(\phi) \tag{6.2}$$

where $C(\phi)$ is an empirically derived correction factor and a function of the equivalence ratio ϕ. The above relationships can be obtained from literature or compiled from experimental observations and utilized effectively in the design of pre-detonators.

6.2 Constant Area Pre-detonator

Li studied the transmission of an overdriven detonation from a highly sensitive fuel-oxidizer mixture (propane-oxygen) to a less energetic mixture, (propane-air) in constant area shock tube type apparatus[32,33]. A wide range of test cases were studied by varying the equivalence ratios of the mixtures in the pre-detonator (between 0.9 and 1.1) and the main combustor (between 0.6 and 1.8) and the length of the pre-detonator section. In all the test cases, the detonation wave velocity is seen to undergo a drastic attenuation of speed as it goes through the less energetic mixture, and hovers near the C-J detonation velocity of the secondary mixture. As long as the equivalence ratio of the secondary mixture remains in the region of 0.9 to 1.1, the detonation is seen to transmit successfully. In some cases, a galloping detonation, i.e., gradual deceleration followed by acceleration, and the repetition of this

phenomenon is also observed. The detonation velocity of the secondary mixture decreases as equivalence ratio is reduced from 1.1 to 0.9. The detonation transmissibility is once again seen to be dependent on the cell size of the mixtures. As the equivalence ratio of the secondary mixture departs from the optimum range of 1 to 1.1, the cell size of the transmitted detonation wave grows in size, until it gets larger than the minimum tube diameter or the diameter of the tube and the detonation fails.

A constant area pre-detonator will require the input of larger amounts of oxidizers or fuel sensitizers, such as oxygen. Therefore, for more practical applications it is advantageous to use a smaller area pre-detonator, as seen in Figures 6.1 (b), (c) and (d). Constant area pre-detonators may be used with the hydrogen-blending fuel-sensitizing concepts discussed earlier in Section 3.5.3.

6.3 Pre-detonator with Abrupt Area Change

To transmit a detonation from a tube with a smaller cross section to one with a larger cross section, the criterion is that the smaller tube must have a critical minimum diameter of $d_c = 13\lambda$. Moreover, the larger tube must meet the minimum diameter ($d_m \geq \lambda$) and the optimal equivalence ratio ($0.9 \leq \phi \leq 1.1$) required to propagate a detonation. The minimum diameter has previously been stated as $d_m \geq \lambda/\pi$, but it is safer to have a larger diameter to ensure that no spinning or galloping detonations are developed, as these are unstable and tend to die out quickly. Smaller pre-detonators also will require less volume of fuel energizers, such as oxygen or hydrogen.

For the pre-detonator with an abrupt area change[122-125], two other points to be considered in their design are as follows.

- Degree of overdrive: The detonation wave in the pre-detonator has to be overdriven above the C-J velocity before expanding into the larger chamber in order for it to be transmitted successfully and drive the weaker mixture to detonation. To achieve this,

the pre-detonator has to be slightly longer than X_{DDT} and the application of DDT devices in the pre-detonator may be necessary[33].

- Degree of overflow: Experimental studies using the pre-detonator shape shown in Figure 6.1 (c) have shown that the energetic mixture has to overlap into the main combustor in order for the detonation to transmit successfully[126]. Therefore, the fuel and oxidizer injection in the pre-detonator has to be designed to account for the amount of mixture overlap.

6.4 Pre-detonator with Smooth Area Change

Khasainov et al.[127] and Thomas et al.[128] have studied the transmission of detonation through a smooth area change nozzles of various angles. They found that detonation transmission occurs for angle less than 45° without major or irrecoverable failures of the detonation, as seen from the smoked foil records shown in Figure 6.2. In the top most picture in Figure 6.2, it is seen that for a 10° nozzle, following an initial enlargement of the cellular structures at the entrance of the nozzle, the cells look similar in size and shape to the cells within the first tube. This shows that the detonation is transmitted without much change in strength. For the 25° and 45° nozzle cases, the cells around the sides of the nozzle are seen to be enlarged, while the cells in the center are smaller than the original and form a fan shape in the center of the nozzle. Thus, the detonation gets concentrated in the center and is then transmitted in the fan shaped area, till finally the cells at the end of the nozzle are at about the same size as in the original tube.

Conical nozzles may be preferable to nozzles with abrupt area changes because of the absence of sharp edges. The dual-stage PDE is built similar to the design shown in Figure 6.1(d). The nozzle angle has to be chosen so that the length and volume of the nozzle is not excessive, while keeping the angle small enough. Table 6.1 shows the relationship between angle and the length and volume of a nozzle expanding from 25.4 mm (1 in.) up to 101.6 (4 in.).

The angle of the pre-detonator was chosen to be 30° as this value results in a nozzle with a relatively short length and small volume.

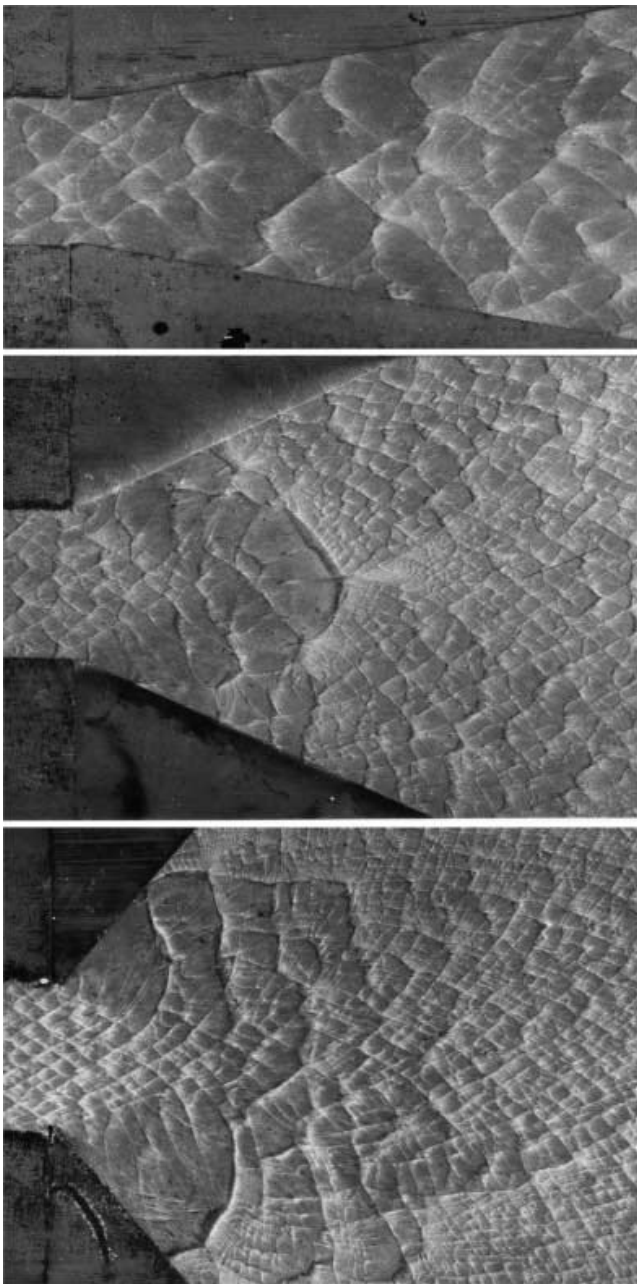

Figure 6.2 Photographs of smoked foil records from detonation propagating through smooth nozzles in $C_2H_2 + 2.5O_2$ mixtures. (Top) 10°, 4.0 kPa, (middle) 25°, 8.0 kPa and (bottom) 45°, 10.6 kPa.[128]

Table 6.1 The length and volume of a nozzle that expands from 25.4 mm (1 in.) to 101.6 mm (4 in.) for angles from 0° through 45°.

Angle (°)	Length (cm)	Vol. (cm^3)	Length (in)	Vol. (in^3)
5	44.35	1,544.64	17.46	94.26
6	36.92	1,285.76	14.53	78.46
7	31.60	1,100.62	12.44	67.16
8	27.61	961.56	10.87	58.68
9	24.50	853.23	9.64	52.07
10	22.00	766.41	8.66	46.77
11	19.96	695.23	7.86	42.43
12	18.25	635.78	7.19	38.80
13	16.81	585.35	6.62	35.72
14	15.56	542.01	6.13	33.08
15	14.48	504.35	5.70	30.78
16	13.53	471.29	5.33	28.76
17	12.69	442.02	5.00	26.97
18	11.94	415.91	4.70	25.38
19	11.27	392.47	4.44	23.95
20	10.66	371.29	4.20	22.66
22	9.60	334.48	3.78	20.41
24	8.71	303.53	3.43	18.52
25	8.32	289.81	3.28	17.69
26	7.96	277.08	3.13	16.91
28	7.30	254.16	2.87	15.51
30	6.72	234.07	2.65	14.28
35	5.54	193.00	2.18	11.78
40	4.62	161.05	1.82	9.83
45	3.88	135.14	1.53	8.25

During tests of the dual-stage PDE, it was observed that the 30° nozzle had an accelerating effect on the detonation wave. The velocity of the detonation wave would shoot up as it traversed the nozzle and then fall sharply to below C-J as the detonation entered the main combustor which was filled with propane-air mixture. The fall in velocity was ascribed to the poor fuel-air ratio of the mixture in the main combustor. The sharp rise in velocity could be due to the expansion of the supersonic flow exiting the pre-detonator. The fan shaped concentration of the cells at the center of the 25° and 45° nozzles shown in Figure 6.2, suggests the same increase in detonation velocity. Figure 6.3 shows a plot of the detonation velocity obtained in a study comparing a high energy arc-discharge ignition system (HEIS) with a high voltage low energy system (HVLEIS) (See Section 7.3.2).

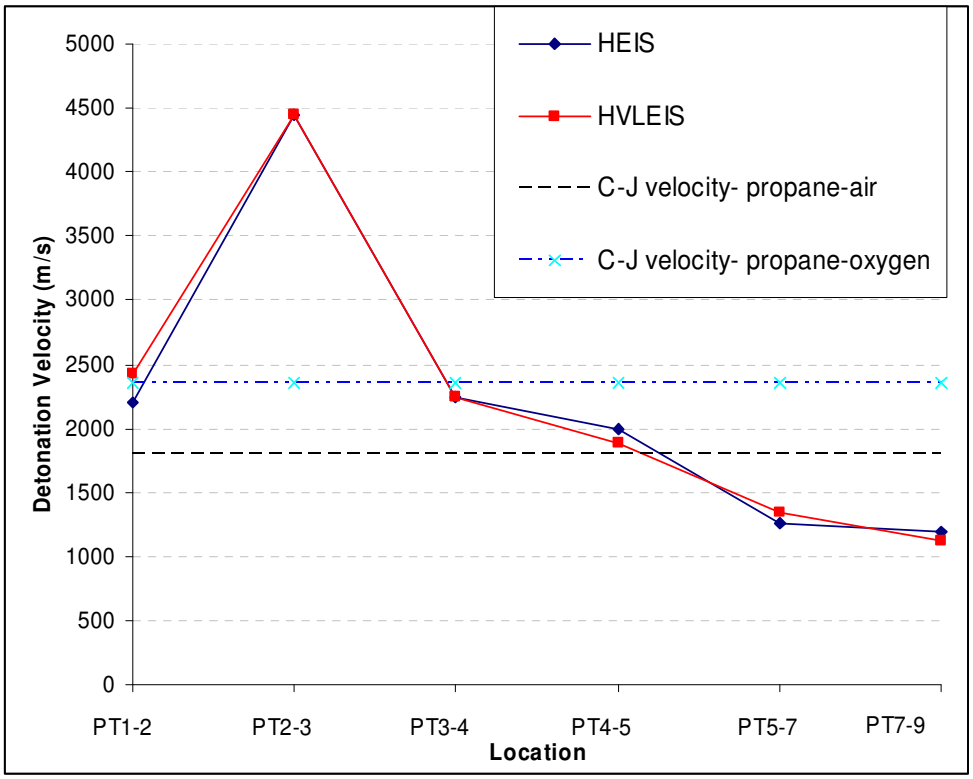

Figure 6.3 Test results from the Dual-Stage PDE with pre-detonator and 30° nozzle for stoichiometric propane-oxygen mixture. The abscissa shows location between two pressure transducers. The velocity of the detonation wave going through the nozzle (PT1-2 and PT2-3) spikes up sharply and then decreases as it encounters the propane-air mixture in the main combustor.

6.5 Pre-detonator With Smooth Curving Bend

The back end-wall of the combustor is where the air inlets and valving mechanisms may be located. Therefore, it may be advantageous to have the pre-detonator located at a different location, in order to make way for the valving, ignition and other associated mechanisms. A useful design that would be applicable under such circumstances would be a ducted pre-detonator or a pre-detonator with a bend that transitions into the main combustor in a smooth fashion, as shown in Figure 6.1 (e).

Thomas et al.[128] have studied the transmission of detonations through 90° smooth bends. It was observed from the study that at lower initial pressures, the detonation may weaken and fail. Figure 6.4 shows the smoke foil records from tests conducted with

stoichiometric acetylene-oxygen mixtures at various pressures. As the detonation goes around the bend, the cell structure is seen to enlarge and become irregular. After the bend, the cell sizes are seen to be larger in size for the lower pressure cases.

For a pre-detonator that uses a 90° smooth bend to connect to the main combustor, the fuel-oxidizer mixture must be carefully selected so that the diameter of the pre-detonator is greater than 13λ and the equivalence ratio should be maintained in the region of 0.9 to 1.1 to keep the cell width as small as possible. Maintaining the pre-detonator at a higher pressure than the main combustor with an overflow of the mixture from the pre-detonator into the main combustor would ensure successful transmission of the detonation wave. The detonation should also be overdriven with the help of DDT mechanisms before entering the bend.

Frolov et al.[130] studied the initiation of detonation in helical tubes with one or more coils. They used Shchelkin spirals to bring about the detonations before transmitting it into a larger combustor. The usage of long spiraling tubes with one or more loops would reduce the over-all operating frequency due to the increased filling time. Hence long coiled tubes may be applicable for slow-speed engines or ground-based power generation. However, short coiled pre-detonator tubes with more energetic mixtures may be applicable for higher speed engines.

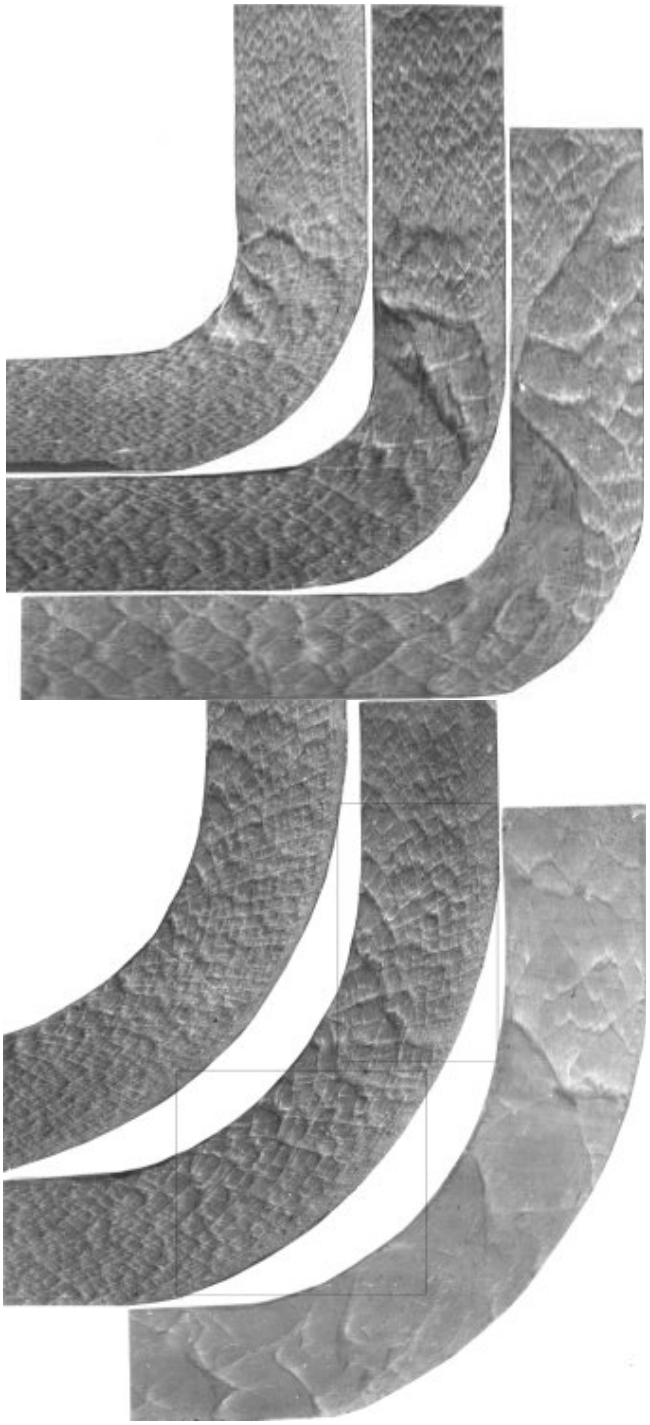

Figure 6.4 Smoked foil records of detonation propagation in 15 mm channels containing $C_2H_2 + 2.5O_2$ mixtures, with the flow going from top right to bottom left. Pressures increase from left to right. (Top) 20.0, 10.6 and 8.0 kPa respectively, (bottom) 13.0, 10.6 and 4.0 kPa respectively. [128]

6.6 Summary

The compact pre-detonator design, in which a smaller diameter pre-detonator is coupled with a gradually expanding nozzle to the larger main combustor, was studied and found to be effective in transmitting detonation from the propane-oxygen mixture within the pre-detonator to propane-air mixture within the main combustor. The pre-detonator concept can be successfully employed in higher speed engines, at the cost of carrying a fairly large quantity of oxygen on board, as ignition and DDT are achieved rapidly. The ignition can be accomplished with just a single low energy igniter that is recessed to protect it from the detonations.

Other pre-detonator geometries were discussed to show how a pre-detonator can be implemented in case of space or size constraints, including the right-angled, the smooth-bend and the U-bend pre-detonators. Also, spiral shaped pre-detonators can be used for the benefit of compactness.

CHAPTER 7

STUDY OF IGNITION SYSTEMS FOR THE PDE

7.1 Brief Introduction of Ignition Systems

Electrical ignition systems can be broadly classified as high-voltage low-energy (HVLE) ignition and high-energy (HE) ignition systems. The low-energy ignition systems are used in internal combustion engines on automobiles, motor cycles, lawn mowers, etc. In such systems, a resonant circuit or a capacitive storage circuit sends a short pulse to a transformer (ignition coil) which multiplies the voltage about a hundred fold to about 40 to 50 kV, causing a spark to occur at the discharge terminals of a spark plug or igniter. HVLE ignition systems are typically rated from as high as about 150 mJ to as low as about a few tens of mJ. The spark duration is in the range of 50 to 100 μs , giving them a power rating of less than 300 W.

7.1.1 High-Energy vs. Low-Energy Ignition Systems

HE ignition systems are rated in the range of about 1 to 20 J[1,132]. The ignition systems used on gas turbine jet engines are HE systems[1]. They rely on large inductors or heavy storage capacitors to generate a pulse across the primary of a transformer, which sends a corresponding stepped-up pulse to an igniter. A strong arc lasting about 100 μs or more is produced at the igniter. A typical ignition system used in a gas turbine engine, found on a typical passenger aircraft, is rated at 12 J. If this system would fire a strong arc lasting 50 μs, the power output would amount to 240 kW. The output voltage at the igniters is usually about 2 to 3 kV, but the current rating can be higher than 100 A. This high amount of current flow and power rating can produce excessive heat, which causes increased wear. Therefore, HE ignition systems, such as those on gas turbine engines, are usually not fired frequently. In a gas turbine

engine, the igniters are fired a few times at the starting of the engine only. The igniters in gas turbines have a semi-conductor layer at the firing end that erodes away with each discharge. Therefore, the igniters have to be inspected regularly, e.g., Rolls Royce recommends inspecting gas turbine igniter plugs every 200 hours[1], while the U.S. Army recommends inspecting igniters every 500 - 1000 hours[133]. HE igniters are rated to last for about a quarter million discharges only because the wear is significant during each firing[134]. For this reason, all aircraft engines are fitted with two identical ignition systems, with separate igniters, as protection against igniter failure.

By contrast, low-energy ignition systems used in automobiles and other engines have to fire during every cycle of the engine and yet spark plugs in automobiles routinely last upwards of 100,000 miles. PDEs also require continual firing, since it works in a pulsed mode. In addition, the temperatures and pressures inside a PDE are higher than in deflagrative engines. As a result, HE igniters, which already have to dissipate their own heat, also have to withstand the tremendous amounts of heat generated in a PDE. Therefore, HE ignition systems would be impractical for a PDE that has to run continuously for several hours.

7.1.2 Size and Weight of Ignition Systems Based on Power Rating

Even though ignition systems are rated in Joules, electrical systems, even the ones inside the ignition system itself, are rated in terms of power and not energy. The size and weight of the equipment depends on the amount of power (voltage and current) it can handle and the heat it needs to dissipate. Also, higher power-rated components, such as capacitors, transformers, etc., have shorter life spans due to increased wear.

Neglecting efficiencies, the heat generated in an electrical circuit is equal to the power output, as shown.

$$\frac{dQ}{dt} = P_E = V_E I = \frac{V_E^2}{R} = I^2 R \,. \tag{2}$$

More than half the power generated by an ignition circuit is wasted in the cables, capacitors, inductors and other components. Only the rest of it actually goes out to the igniters. The efficiency of converting mechanical energy to electrical energy is very poor. For example with a turbine engine operating at 50 % thermal efficiency, and a generator operating at its maximum of 75 % results in only 37.5 % conversion efficiency. This is the highest a turbine-generator system can achieve. Much of that energy is again wasted in storage and transmission.

Circuits rated for higher power require thicker wires, larger capacitors, inductors, resistors and semiconductor components to carry larger currents and to dissipate the heat generated. Thus, high power circuits are large and heavy. The size and weight of electric power transformers depend on their power rating, operating voltage, percentage regulation (the ratio of change in output voltage from no load to full load condition to the full load voltage; lower regulation percentage ~3% is preferred), dielectric requirement, operating frequency, etc. For a larger power rating, larger amount of heat is created due to the higher current flow, thus requiring more surface area to dissipate the heat. Transformers larger than a few kW may require active or passive cooling materiel and the winding and core has to be made heat resistant, all of which adds to the weight and size. A higher voltage requires thicker insulation material and the insulation of the winding wire has to be improved as well, once again increasing the size and weight. The core material is selected based on the operating frequency. Low frequency power transformers (<1 kHz) use tape wound or laminated silicon steel cores. Moderate frequency transformers (<10 kHz) are usually used in audio equipment and have cores made of tape wound or laminated nickel iron. High frequency transformers (>10 kHz) are not used for power transmission and have small cores, made from ferrite ceramics.

The frequency of a transformer can be shown to be inversely proportional to the size and weight of the transformer[135]. The frequency of a transformer is given by

$$f = \frac{Z}{2\pi M_E} \tag{7.3}$$

where f the frequency of the ac voltage in Hz, Z is the impedance in Ω and M_E is the mutual inductance of the transformer in Henry (H). The mutual inductance may be expressed as

$$M_E = \frac{N_1 N_2 A \mu}{l} \tag{7.4}$$

where N_1 and N_2 are the number of turns in the primary and secondary windings respectively, A is the area of cross section of the core, μ is the magnetic permeability (H/m) and l is the length of the core in m. At higher frequencies, the impedance increases due to skin effect. Therefore, the mutual inductance is lowered for high frequency applications by reducing the area of cross section, weight of the core and the number of turns. This is the reason power supplies on board aircraft are designed for 115 V, 400 Hz, to make use of lighter transformers and power conversion equipment. Thus, it is evident that a HE ignition system would be much heavier and larger in size than a LE ignition system. However, other techniques, such as using a pre-detonator or blending in additives to sensitize the fuel, can be used in combination with a LE ignition system in a PDE if weight and size constraints are present.

7.1.3 Ignition Energy Requirement

The minimum ignition energy required for many hydrocarbon fuel vapors in air is between 0.2 and 1 mJ with a spark gap of 0.4 cm[52,136]. The minimum ignition energy for sprays of aviation fuels in air at 1 atm is given in Figure 7.1. The energy required for ignition increases as the concentration of the fuel in air departs in either direction from stoichiometric state. The ignition energy is also directly related to the temperature and pressure of air. At high altitudes and as the velocity of the air flow increases, to in the order of hundreds of meters per second, the minimum ignition energy rises dramatically to above 10 J[1]. Low energy sparks can be blown away by a fast moving fuel-air mixture. Higher concentration of oxygen decreases the ignition energy requirement and increases the detonability of the mixture.

Turbojet engines have two HE igniters with independent HE driver circuits to bring about relighting of the flow in the combustor in case of a flame blowout during flight. The redundancy is for protection in the event of failure of any one igniter. However, in some systems, both igniters are fired simultaneously for added energy input into the fuel-air mixture, in order to bring about fail-safe ignition. This is a critical requirement for aircraft engines, as all aircraft are subject to accidental blowout of their engines during high altitude flight or maneuvering.

For PDEs, relighting has to occur at every cycle, because the flame is extinguished at the end of the blowdown stage and the combustor is purged and refilled with fresh air and fuel. The speed of the flow may be high, especially for engines operating at high frequencies, where the air flow speed can approach sonic velocity. Therefore, it is imperative that the ignition system have the capability to deliver enough energy to bring about ignition. The operation of a PDE depends on the exact timing of its valve operation and the firing of the ignition. If the ignition does not occur at the required point in time, detonation may not occur within the allotted time period or may fail altogether and no power will be generated during the cycle. Figure 7.2 shows the various stages of the PDE cycle along with an expanded view of the combustion stage. If the detonation and blowdown occurs later than their pre-designed times, they may merge with the purge stage. Thus, the engine may not cool down to the required equilibrium level and may cause pre-ignition to occur during the next filling stage. Therefore, without an intelligent monitoring and control system constantly checking the state of the engine, ignition failure can lead to failure of the engine. If detonation fails or is delayed, there must be a system that purges the chamber to clean out and cool the combustor, so as to prevent pre-ignition.

With continual high speed use, it has been shown that HE igniters wear away quickly and, therefore, may disintegrate mid-flight. Therefore, some kind of a flame holder may be required for ignition in a PDE. In place of one or two HE igniters, an array of smaller, lighter LE igniters may be used to bring about ignition of the mixture by imparting energy in a distributed fashion. Another approach would be to use hydrogen as a pilot flame, which can be initiated

using low energy ignition. Therefore, once again, the advantage of hydrogen for use with hydrocarbon fuels is demonstrated[92,93].

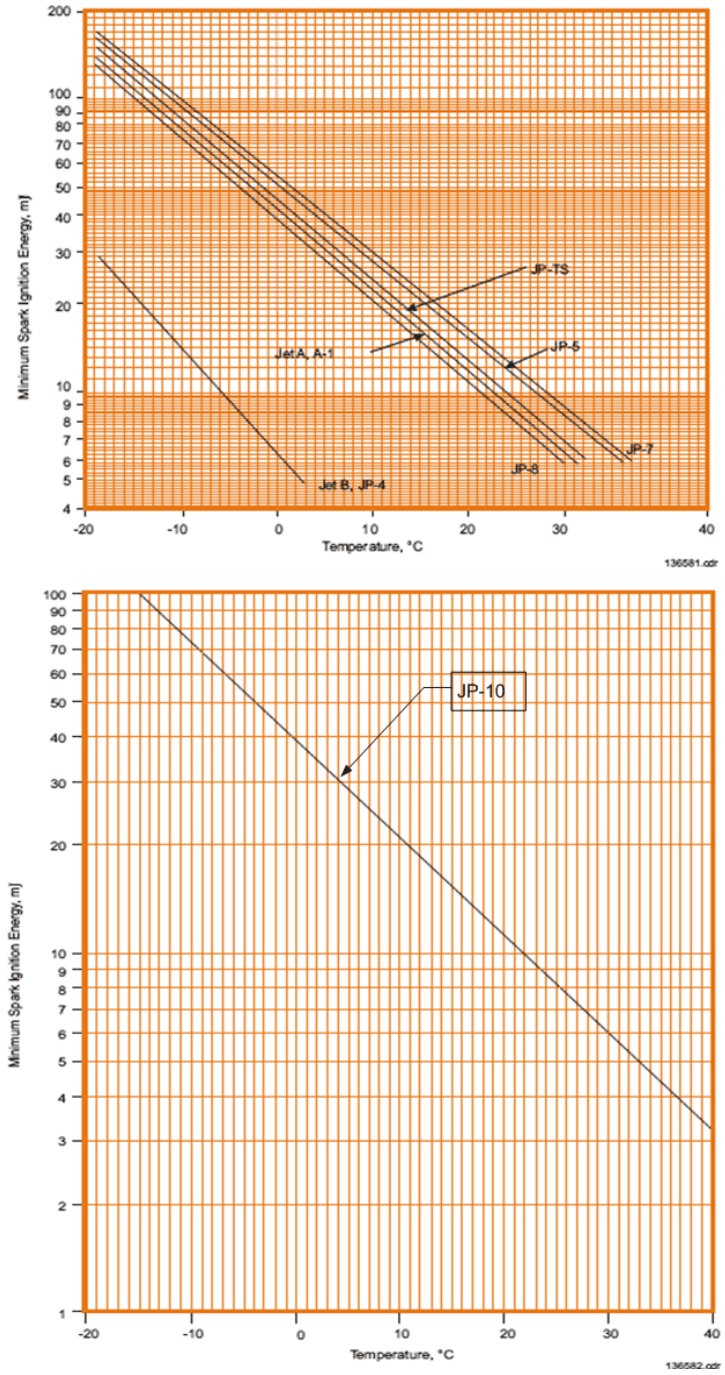

Figure 7.1 Minimum spark ignition energy of various jet fuel sprays in air at 1 atm[52].

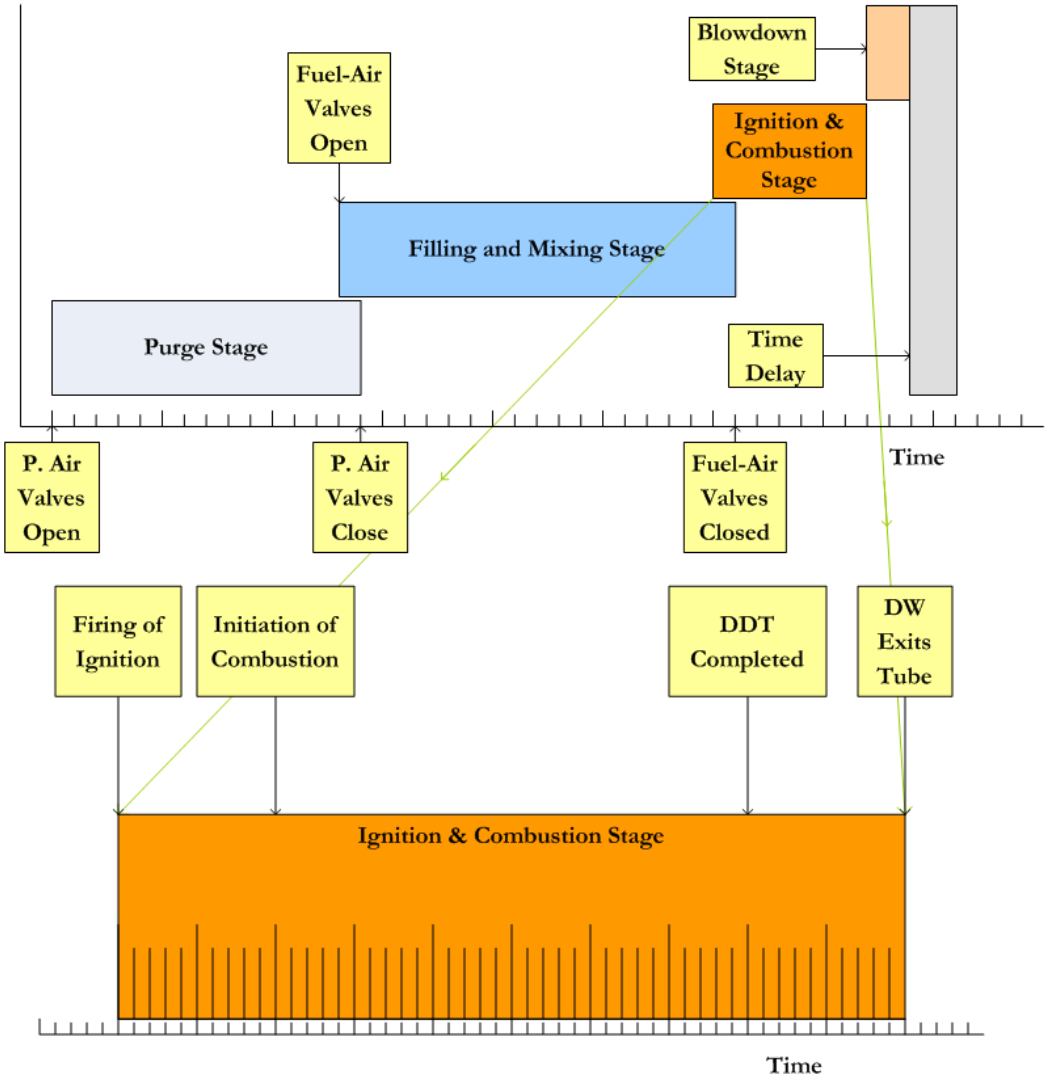

Figure 7.2 Schematic of the PDE timing. The combustion stage is expanded to show the ignition phase. If the ignition cannot be achieved in as short a time as possible, the detonation may not occur within the time allotted to the combustion stage. The delay after the blowdown stage is optional.

7.1.4 Ignition Noise

The ignition spark is a big contributor to noise on automobiles. In the lab, the ignition noise inundates all the signal lines. In order to cut down on EMI generated by ignition sparks, manufacturers of spark plugs add a resistor inside the plugs to reduce the ignition energy. The

Bosch Platinum Series spark plugs used on PDE Mark 3 and the dual-stage PDE have a dc resistance of about 3 kΩ. For the HVLE spark plugs designed for PDE Mark 2 and PDE Mark 3, a resistance of about 3 kΩ was found, through trial-and-error, to be an optimum value that produced minimal interference on transducer signal lines while maintaining sufficient spark strength. The HE arc ignition had a larger noise signature on the transducer lines. In a dry run of the HE arc ignition system on the PDE Mark 1, the interference in the signal was found to be so strong that it covered the entire range of the input, from -10V to +10V. A sample pressure trace from a dynamic pressure transducer which was contaminated by the arc ignition is shown in Figure 7.3. Since the arc persists for a longer duration than the LE spark, the interference also persists for a similar period.

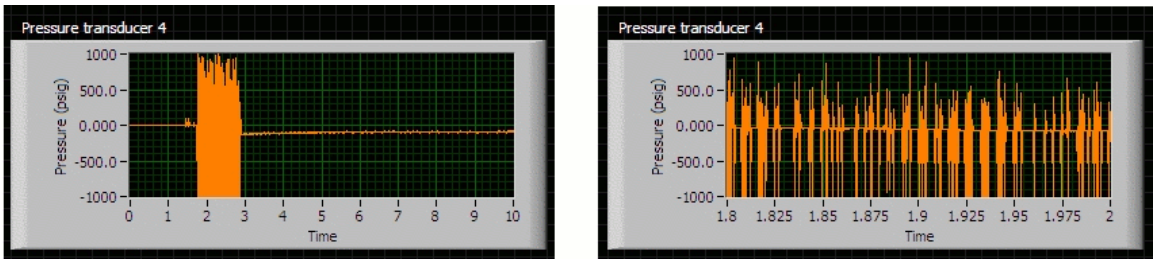

Figure 7.3 Pressure history from a no-flow test of PDE Mark 1 with the HE ignition system turned on for about 1.25 s shows very high intensity EMI when the ignition is fired. The picture on the right is an expanded view of a 0.2 s window of the chart on the left. The interference from the arc ignition covers the entire range of signal amplitude, -1000 psig to +1000 psig, corresponding to -10V to +10V.

The ignition EMI can be mitigated by using shielded cables, by shielding all the circuits and instruments and properly grounding all the instruments and the data acquisition system. Care must be taken to avoid ground loops. Using differential input channels with shielded DAQ devices also reduces EMI. Nevertheless, the ignition noise of the spark plug or arc igniter can still be seen on the traces from all the pressure transducers, ion detectors and photo-detectors, in the form of a tiny blip on the signal time plots, as seen in Figure 7.14, later in this chapter. Since the ignition causes this small peak to appear at exactly the same time in all the signal records, it can be used for determining the time of firing of the ignition spark or arc. Thus, this marker can be used for computing the ignition delay or DDT times.

7.2 Study of the High-Energy Arc Ignition System

The HE arc ignition system was used in early PDE studies at the ARC[22,24,25] and on the Bantam PDE and the PDE Mark 1. It was a dual-voltage system consisting of a HVLE system and a medium-voltage HE system. Detailed circuit diagrams of this system are available in Appendix B. On the HE side of the circuit, a continuously variable autotransformer was used to supply power from the mains (120 V, 60 Hz) to a step-up transformer. The output of this transformer was rectified and stored in a capacitor bank. By varying the output voltage of the autotransformer between 0 and 120 V, the capacitor bank could be charged to a voltage between 0 and 2000 Vdc. The capacitor bank could then be discharged periodically through the igniter by triggering an silicon-controlled rectifier (SCR) at the required pulse rate. The HVLE circuit was based around an automotive ignition system. It contained an inductive ignition driver unit from Mallory Ignition (Mallory HyFire 1A, Part No. 29026A, peak spark energy of 135 mJ) and an ignition coil (Mallory Part No. 24440). The output of the ignition coil could go as high as 40 to 50 kV. A central control circuit was used to trigger the HE arc ignition and the HVLE ignition circuits simultaneously using a TTL signal.

The igniter had three electrodes, a high-voltage low-energy (HVLE) electrode, which could be smaller in size, a thicker high-energy electrode, and a thick ground electrode, as shown in Figure 7.4. The igniter was constructed such that the HE electrode would be placed closer to the ground electrode. By itself, the HE electrode's voltage level is too low to break the potential barrier of the air-gap between the ground and itself. Therefore, it needed the HVLE spark to overcome the potential barrier and allow the current to flow in the form of an arc. The capacitor bank consisted of two sets of electrolytic capacitors, a primary set consisting of five $50\,\mu F$, 440V capacitors in series (labeled A through E in Figure B.1 in Appendix B), and a secondary set of similar capacitors (labeled F through J in Figure B.1). When the SCR is triggered, the current flows from the primary to the secondary capacitors causing them to be charged up to the same voltage level. At this point, the secondary capacitors are ready to be

discharged through the igniter. When a TTL clock pulse is sent to the main control circuit, it triggers the HVLE ignition system to fire a spark from the HVLE electrode. This spark is the end result of the breakdown of the potential barrier of the air-gap between the HVLE electrode and the ground electrode. Thus, the HE electrode, being at a lower voltage, can easily overcome the resistance and fire an arc through the air-gap to the ground electrode. The spark and the HE arc happen in rapid succession in a matter of about 50 μs. After the main control circuit triggers the ignition, it sends another signal to the SCR control circuit, which triggers the SCR and causes the secondary capacitors to be charged up once again and await the next spark. The delay between the two signals (trigger for the HVLE system and trigger for SCR) was created by means of a 556 timer IC in the main control circuit. The delay was set by adjusting the values of a timing resistor and capacitor. This dual-voltage ignition system was capable of firing at up to 120 Hz, because the rectifier could charge the capacitor bank at twice the supply frequency of 60 Hz. However, it was only run at a few tens of Hz to limit the current draw and to prevent the components from overheating.

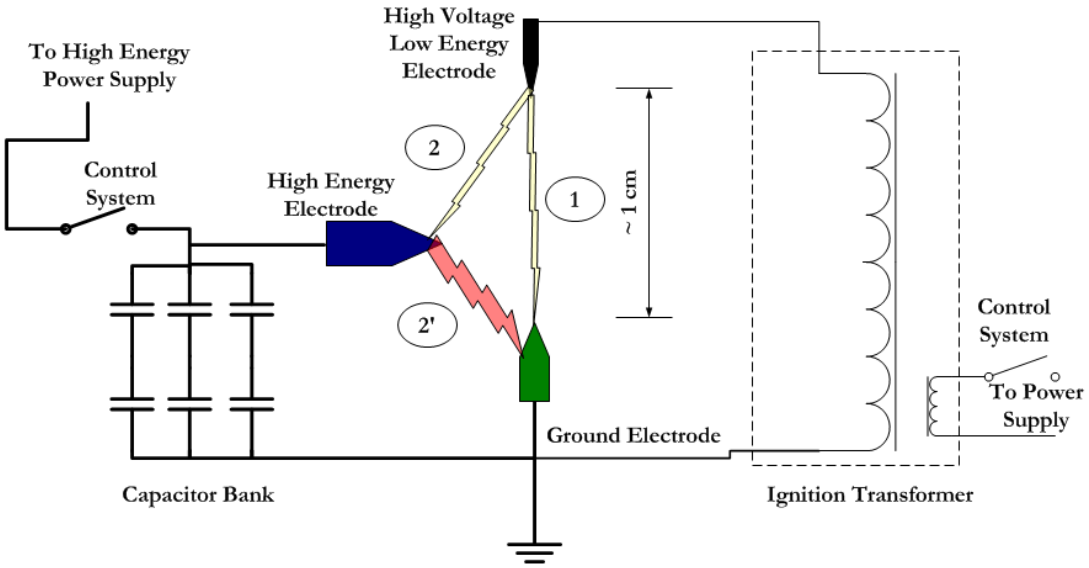

Figure 7.4 Schematic of the HE arc ignition system used on the Bantam PDE, PDE Mark 1 and earlier PDE studies.

7.2.1 High Energy Dual Voltage Igniters

7.2.1.1 Generation 1 Igniter

The HE igniter developed for the Bantam PDE is as shown in Figure 7.5. It was made of mild-steel with the electrodes made from tungsten rods (1/16 in. diameter) sheathed in ceramic tubing. This igniter was screwed into the PDE combustor and it protruded into the flow. The construction of the igniter was not very robust as the thin electrodes were mounted on thin and weak structures. The igniter was small and did not have any form of cooling to dissipate the tremendous amounts of heat generated by the arcs as well as the detonations. As a result, the igniter did not last long and was easily destroyed after about 15 to 20 s of test time. Figure 7.6 shows pictures of the igniter before and after testing within the Bantam PDE with stoichiometric mixtures of propane and oxygen.

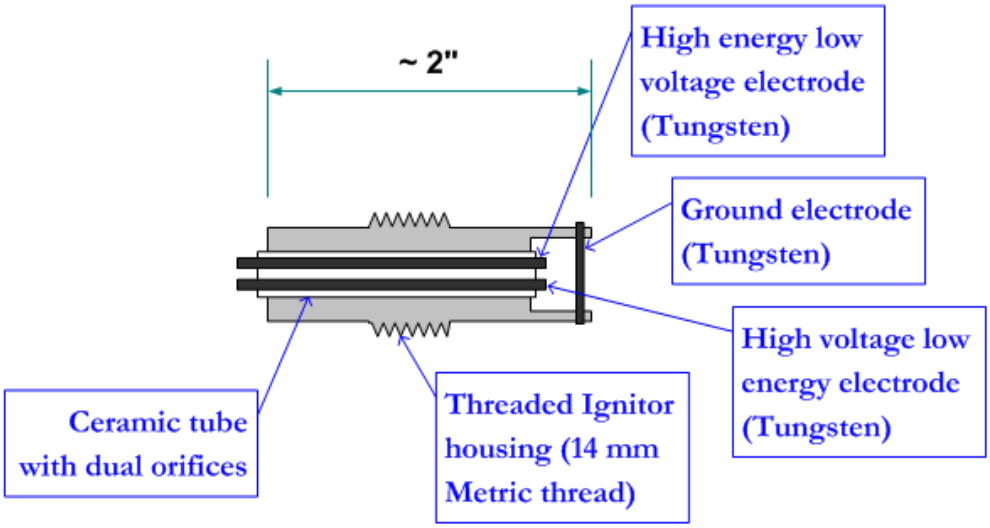

Figure 7.5 Schematic of the igniter used on the Bantam PDE for the HE arc ignition system.

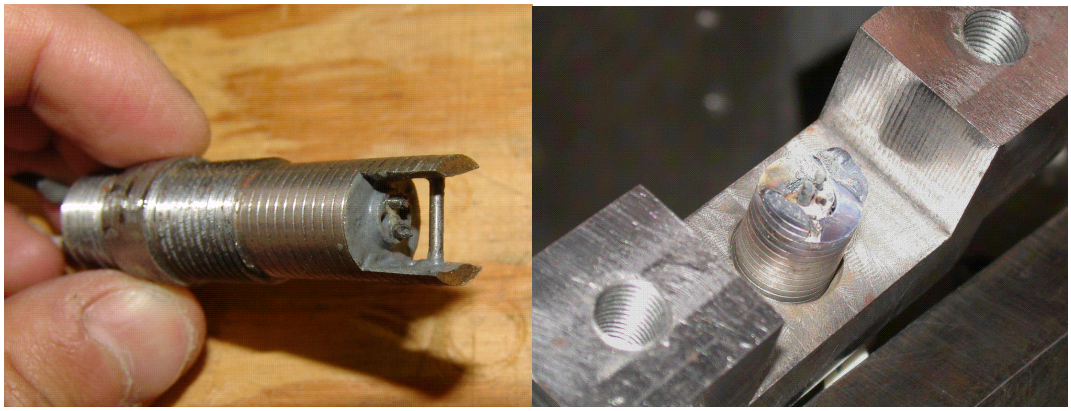

Figure 7.6 The HE igniter developed for the Bantam PDE before testing (left), and after about 20 s of testing with a propane-oxygen stoichiometric mixture (right).

7.2.1.2 Generation 2 Igniters

The next generation of igniters was developed for the PDE Mark 1 and was also used on the PDE Mark 2, although only the HVLE igniter and the ground electrode were used on that PDE. This design consisted of bored out bolts with ceramic tubes inserted through and glued in place with epoxy, as shown in Figure 7.7. The electrodes were made from 2 % lanthanated tungsten rods (5/32 in. thick) that are employed as electrodes in TIG welding. The HVLE electrode had thicker ceramic insulation to prevent the spark from shorting to the grounded body of the bolt. The ground electrode did not have a ceramic tube as no insulation was necessary for grounding. The design of these electrodes was more robust, and the spark gap could be adjusted easily by screwing the bolt in or out. But because they were exposed in the line of the flow within the PDE, they suffered from erosion of the tungsten rods, as visible in Figure 7.8, and had to be rebuilt after about four to five test sessions, each lasting about 20 s long.

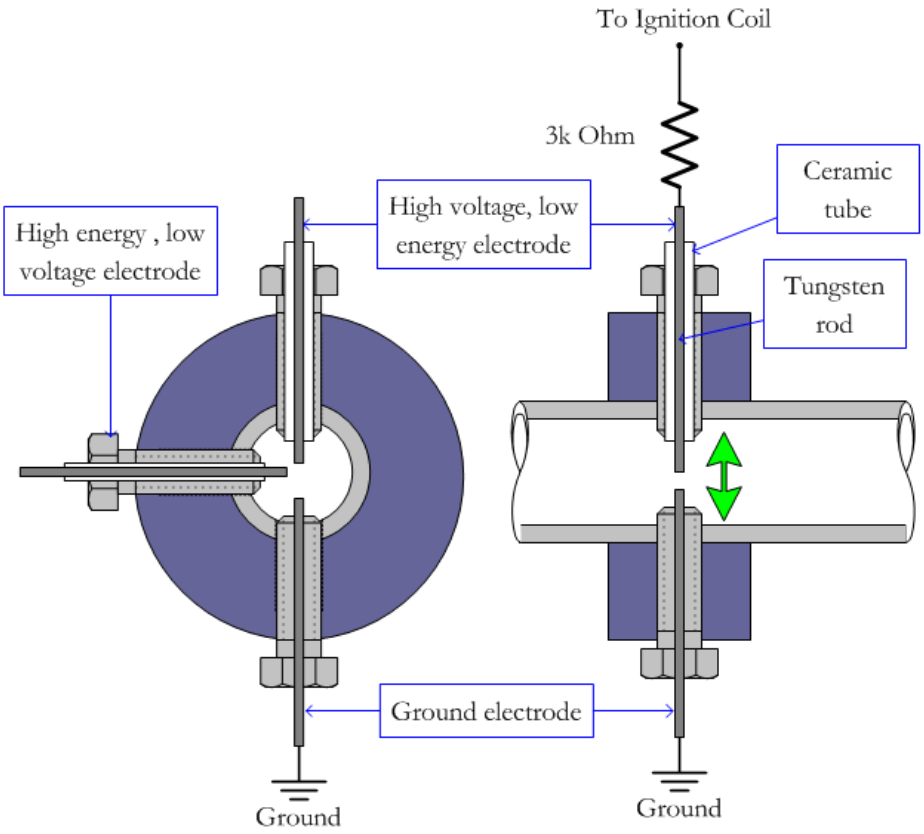

Figure 7.7 Schematic of the igniters used in HE and HVLE ignition used on PDE Mark 1 and PDE Mark 2.

Figure 7.8 The electrodes used for HE and HVLE ignition on the PDE Mark 1 and the PDE Mark 2 suffered erosion as a result of the detonation. The electrode in the center is the HVLE electrode, while the electrode on the left hand side is the ground electrode. The erosion is obvious when one compares the shape of the two ends of the tungsten rods.

7.3 Study of High-Voltage Low-Energy (HVLE) Ignition System

On the PDE Mark 2, the PDE Mark 3 and the dual-stage PDE, the HVLE ignition system was used by itself to bring about ignition. The HVLE ignition system consisted of the Mallory ignition driver unit (inductive type, Mallory HyFire 1A, Part No. 29026A, peak spark energy of 135 mJ) and an ignition coil (Mallory Part No. 24440). The driver unit was later replaced on PDE Mark 3 with a newer unit, the Mallory HyFire IIIA, Part No. 630, which is also a 130 mJ system.

The ignition plugs used for PDE Mark 3 and the newer Dual Stage PDE were Bosch Platinum Plus brand automotive spark plugs. These spark plugs have a built-in resistance of about 3 $k\Omega$. Before inserting the plug, the spark gap was widened manually to about 2 mm, by

prying the ground electrode apart with a screwdriver. However, these also suffered major damage when they were screwed in with the electrodes protruding in to the line of the flow. On the PDE Mark 3 and the dual-stage PDE, it was found that when they were recessed with the electrodes hidden away inside the igniter port of the pre-detonator, as shown in Figure 7.9, the electrodes survived the tests with no damage, even after repeated trials. The recessed spark plug work only because oxygen was used as the oxidizer. In tests with propane and air, ignition was not observed to occur. However, with hydrogen and air, the recessed spark plug produced consistent ignition, once again showing that the addition of hydrogen with low energy ignition is a viable method

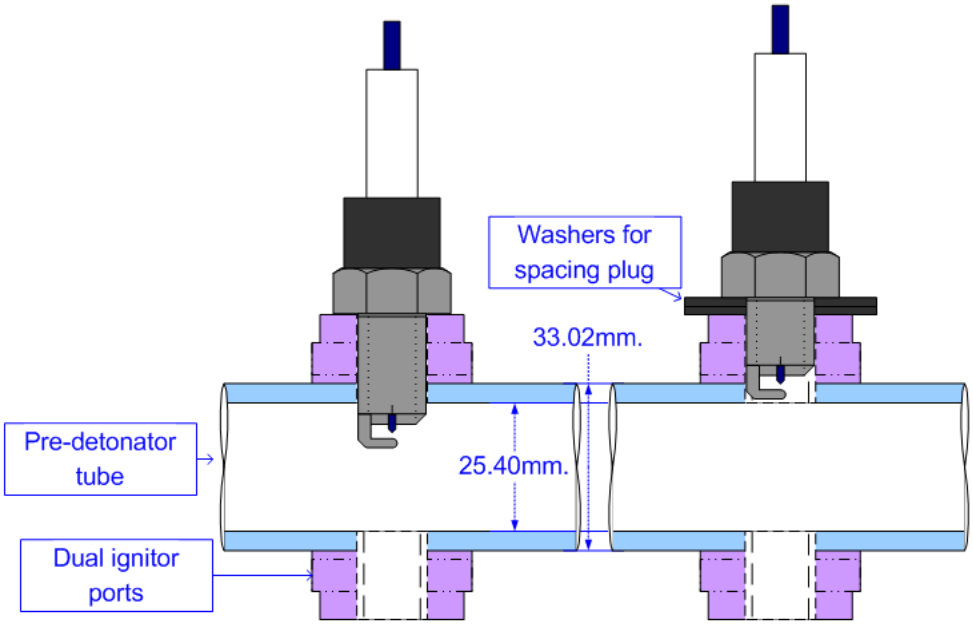

Figure 7.9 Schematic of the placement of the automotive igniter used in the PDE Mark 3 and the dual-stage PDE. The recessing of the igniter protected it from being damaged by the detonations within the 10 to 20 s run time.

7.4 Comparison of HE Arc Discharge with HV LE Ignition in Pre-Detonator of The Dual-Stage PDE

A series of tests were performed to study the advantages and disadvantages of using a HE arc discharge ignition system over a HVLE automotive ignition system in the pre-detonator of the dual-stage PDE. The igniter of the HE ignition system was of a coaxial design, as shown in Figure 7.10. It had a core electrode made of tungsten, sheathed in a ceramic tube and encased in an aluminum housing. It had a threaded mounting section that enabled the igniter to be screwed into a standard 14 mm automotive ignition plug socket. The HE ignition power supply had an autotransformer, to selected the input voltage between 0 and 120 Vac, and a 1:4 step-up transformer. The output of the step-up transformer was rectified and stored in a capacitor. A switching circuit then delivered this stored power at the required frequency to the igniters. A schematic of the power supply circuit is shown in Figure 7.11. Because the voltage across the igniter terminals was low, about 500 to 675 V, it was not high enough to overcome the potential barrier of the air-gap and start the conduction of current. Therefore, a solution of graphite was required to be applied to the face of the igniter to initiate the flow of current. Once the graphite starts conducting, it vaporizes due to Ohmic heating and a plasma is developed over the face of the igniter. Then an arc discharges rapidly and gets projected into the flow in the vicinity of the igniter. The power supply was designed to accept from one to ten balanced igniters of the above type. The power supply was capable of supplying up to 100 J of energy per discharge.

For the tests mentioned above, the voltage was limited to about 600 V. Each arc discharge created a peak current flow of 675 A and lasted about 400 μs, amounting to an energy level of about 81 J per discharge. Two arc igniters were balanced with resistors and connected in parallel so that they could fire simultaneously.

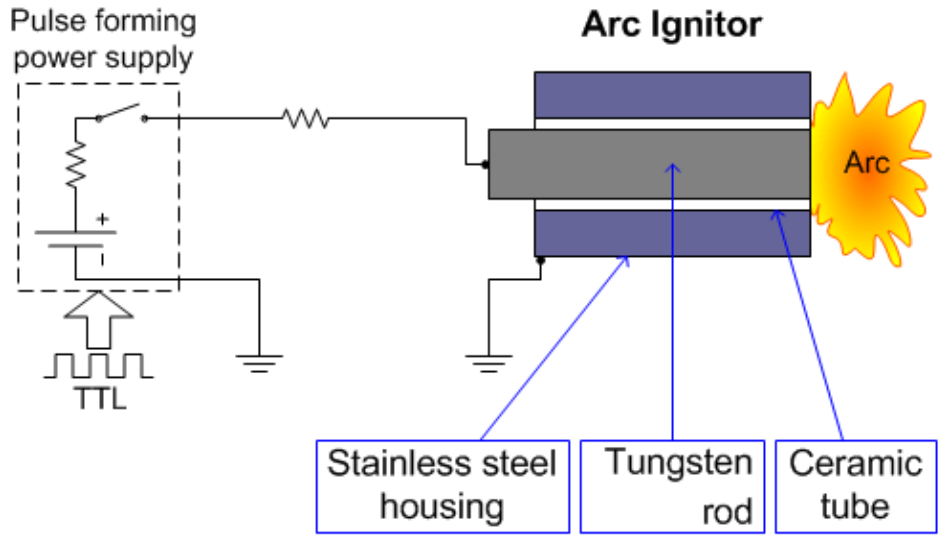

Figure 7.10 Schematic of HE arc discharge igniter used in the pre-detonator of the Dual-Stage PDE.

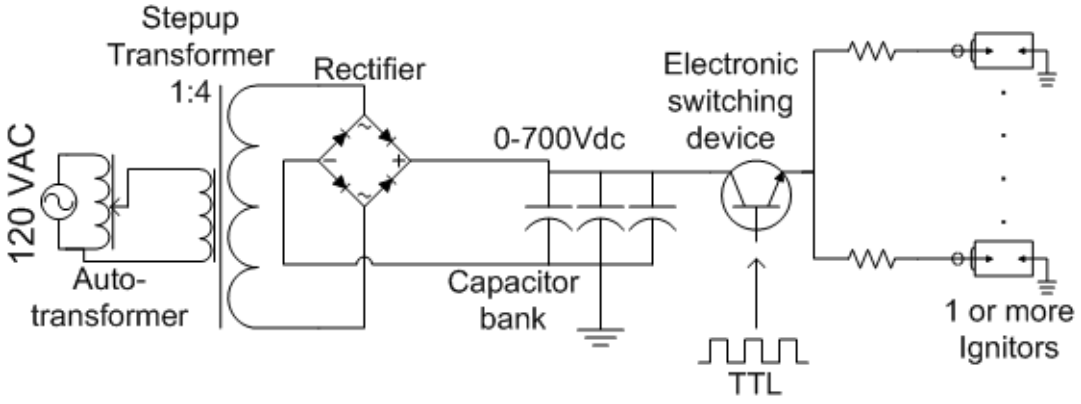

Figure 7.11 A schematic of the HE ignition circuit is shown.

7.4.1 Test Format

The dual-stage PDE was tested with the HE igniters and the original low energy ignition system each at 1 Hz, 5 Hz and 10 Hz. The PDE set up is as shown in Figure 7.12, with two igniters inserted into the ignition ports in the pre-detonator which used propane-oxygen

mixtures. Following the pre-detonator was the 30° nozzle that expanded the flow into the main combustor where propane and air was injected in through the swirl injector block. For each test, the fill time of the valves (obtained by changing the duty cycle of the TTL) were slightly modified to get optimum gas flow rates. Typical duty cycles were 50 % for purging, 45 % for fuel-oxidizer filling followed by the ignition at the end of the filling stage with 5 % left over for the combustion and blowdown. At frequencies higher than 5 Hz, the gas flow rates reduced significantly because the tubing and gas supply system used for the PDE were too small (being only ½ in. tubing and tube fittings) and could effectively maintain proper flow rates only for 5 Hz or less. As a result of the sagging flow rates, it is seen that thrust and pressures reduce as frequency is increased from 1 Hz to 10 Hz. At 10 Hz very low thrust is obtained. Nevertheless, the HE igniters were seen to outperform the low energy ignition system at all frequencies.

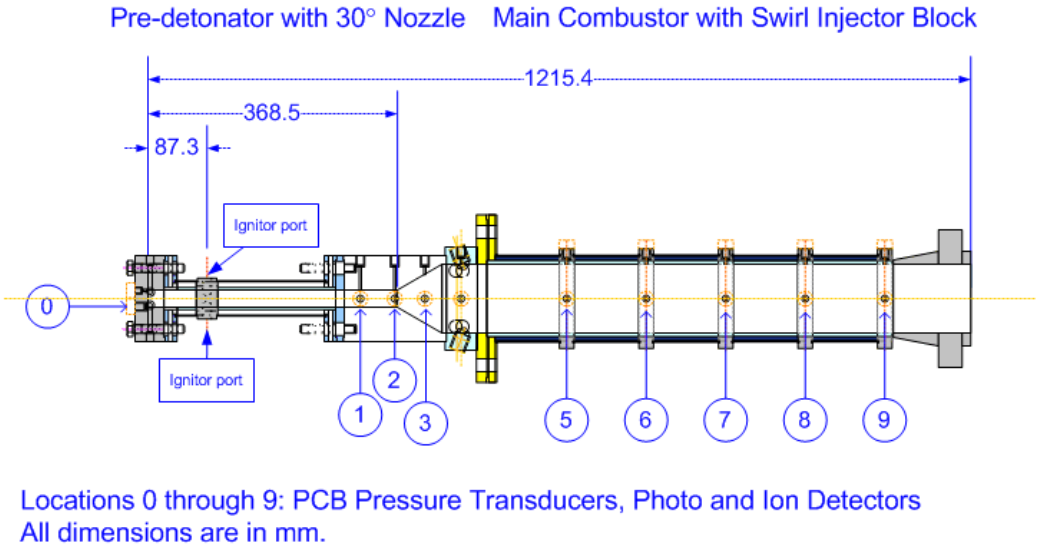

Figure 7.12 Schematic of the Dual-Stage PDE with pre-detonator, showing the location of the igniters and the pressure transducer ports.

7.4.2. Results of HE Arc Igniters and HVLE Spark Plugs Tests

1. With the HE arc discharge ignition, more energy is imparted to the fuel-oxidizer mixture enabling it to detonate quicker and more consistently. The two HE igniters delivered a high energy impulse, in the order of 80 J, to the quiescent mixture in the pre-detonator enabling it to rapidly reach detonation. On the other hand, the LE ignition system only produce sparks of about 100 mJ. Because propane-oxygen mixtures are very sensitive, even low energy is enough to initiate detonation.
2. With the HE arc discharge ignition, detonation induction time is reduced even for a highly sensitized mixture such as the propane-oxygen mixture. Figures 7.14 through 7.17 show the readings from the pressure transducers, ion detectors and photo detectors for the 1 Hz and 10 Hz tests. It was seen that the time between the start of the discharge, and the arrival of the detonation wave at pressure transducer 1 (PT1) is considerably less for the HE system, indicating that the induction time is shorter for the HE arc discharge system. The ignition times are presented in Table 7.1.
3. The detonation pressures and the velocities obtained from the TOF method are slightly higher for the HE ignition system than the HVLE system, as seen in Figures 7.14 through 7.17. There does not seem to be a big payback in terms of improved detonations in the main combustor of the PDE where propane and air is injected in, despite putting in much higher energy by means of the HE arc discharge ignition system. The detonation is seen to die out rapidly in the main combustor in all cases, as seen in the TOF velocity plot shown in Figure 7.13.
4. The thrust produced by the PDE is slightly higher for the HE system than the HVLE system, as seen in Table 7.1. At 10 Hz, even with the poor flow rates causing detonation failure to occur, the HE system managed to achieve consistent thrust for every pulse, although the thrust is much lower than for the lower frequency cases.

5. When near stoichiometric propane-air mixtures are injected in the pre-detonator, the HE system was able to ignite the mixture. However, the HVLE system was not able to ignite the flowing mixture of propane and air. Even though the HE system enabled ignition to occur, the deflagration could not be successfully propagated through the pre-detonator (and expansion nozzle) into the main combustor, because the i.d. of the pre-detonator is much smaller than the cell size of propane-air mixtures. The 1 Hz test with the HE system showed thrust as high as 55 lbs per pulse for near stoichiometric propane-air mixtures.

Despite the small advantages that the HE arc discharge ignition system was able to demonstrate, there does not seem to be a significant improvement for the extra addition of energy. In addition to the extra weight and electric power consumption, the HE system also causes added wear and tear of the circuit components and igniters. Therefore, it is evident that the HVLE ignition system combined with DDT mechanisms and other techniques for shortening the ignition delay would be better suited for PDE application.

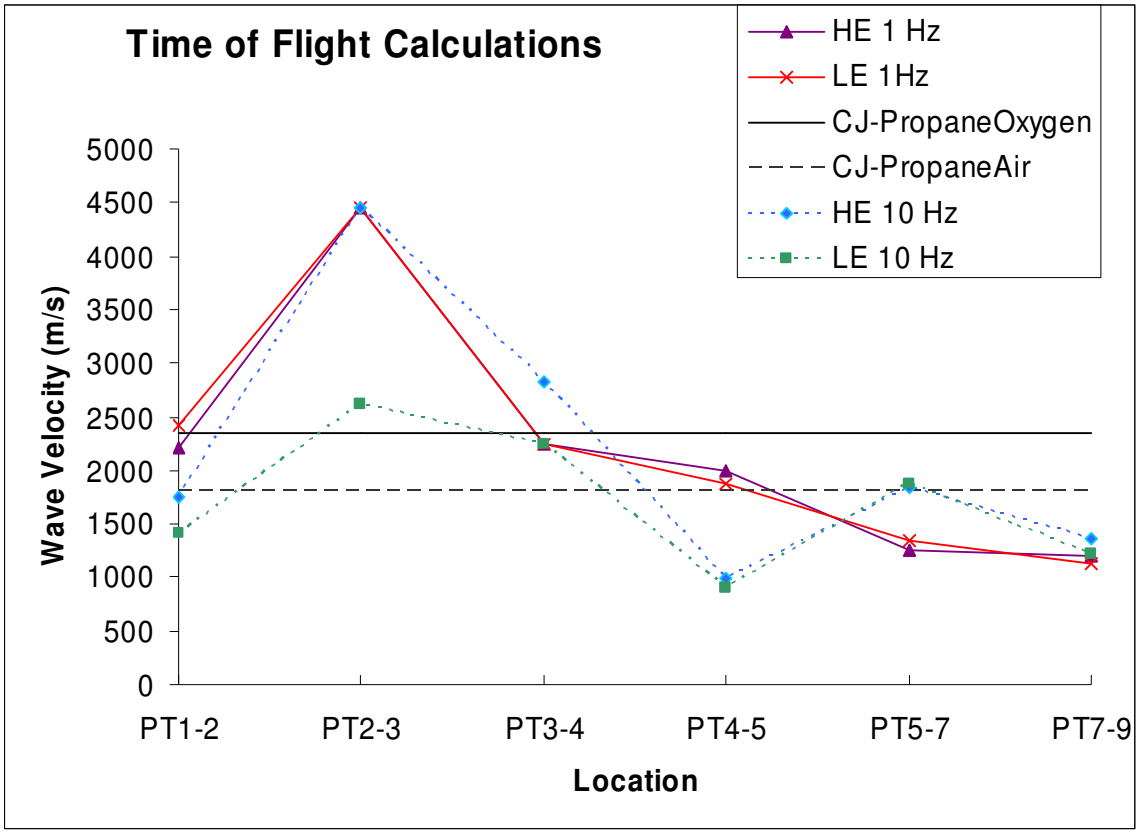

Figure 7.13 Time of flight calculations for PDE operating at 1Hz and 10 Hz. The detonation velocities are only slightly higher for the HE arc discharge ignition system in the 1 Hz case, but there is a significant improvement in the 10 Hz case, when the flow rates were not properly maintained.

Table 7.1 Comparison of thrust measured for the HE arc discharge ignition system and the HVLE ignition system. The one instance for the 1 Hz test where the HVLE system attained higher thrust is well within the margin of error. The ignition delay, determined from the time taken for detonation to arrive at PT1 after the ignition has been fired, is smaller for the HE system.

Igntion System	Frequency	Average Peak Thrust		Ignition Time
Units	Hz	lbs	N	s
HE	10	23.3	103.6	0.000606
HE	1	101.2	450.2	0.000531
LE	1	22.1	98.2	0.000685
LE	10	102.1	454.2	0.000587

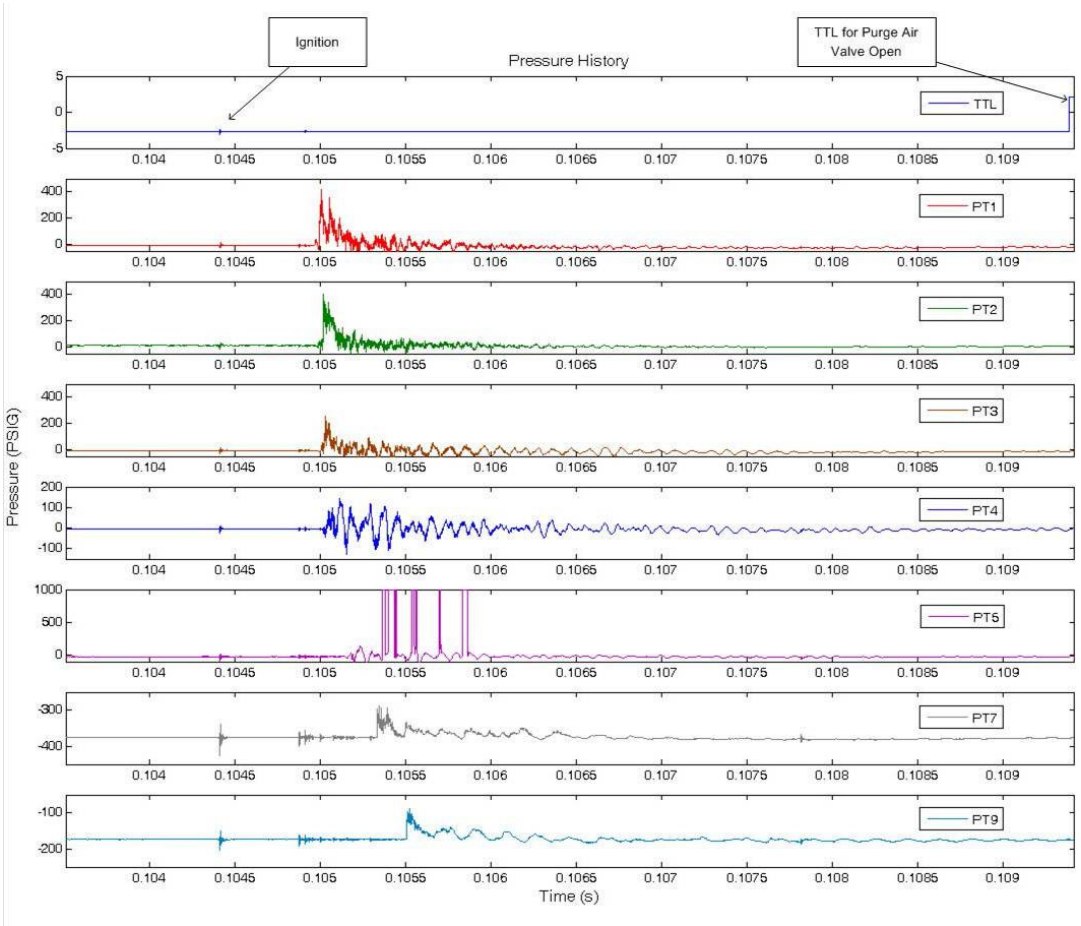

Figure 7.14 History of the TTL signal and the pressure readings for a test of the dual-stage PDE with the HE arc discharge ignition system at 10 Hz. The noise caused by the ignition is seen in all signal traces indicating the position of the ignition firing. The time of ignition can also be calculated from the TTL signal time. The rising edge of the TTL signal for the purge air valves to open is shown in the chart on top. The pre-detonator was filled with stoichiometric propane-oxygen, while the main combustor used a propane-air mixture.

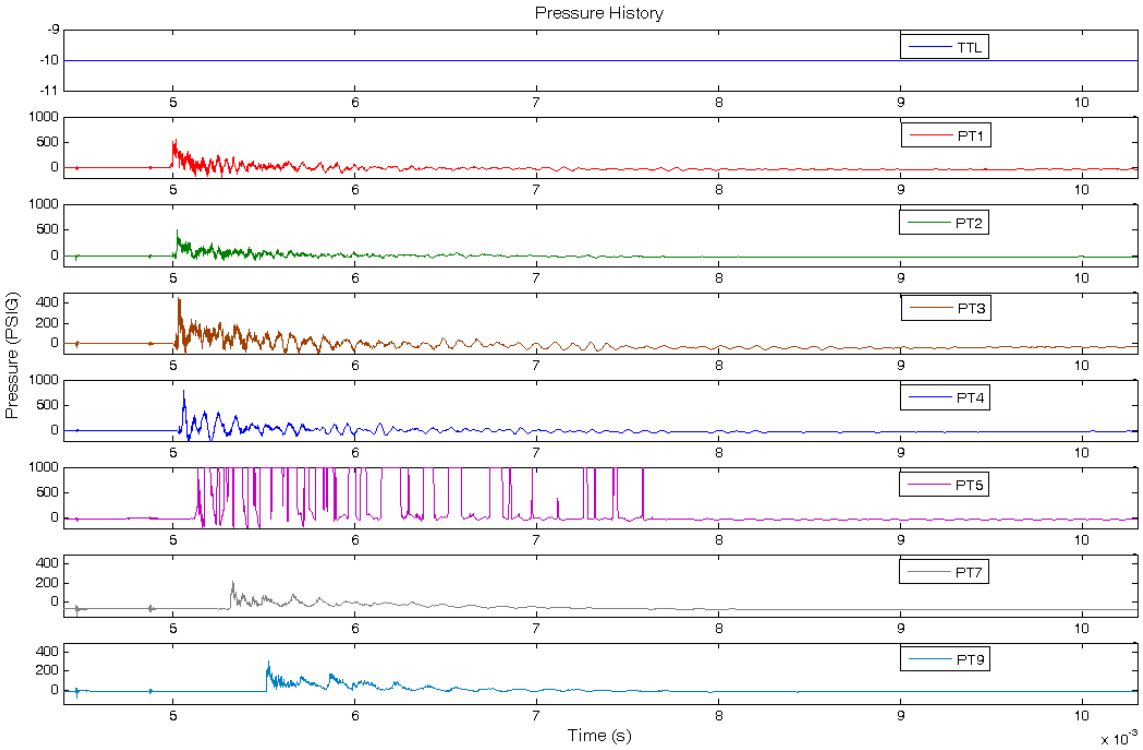

Figure 7.15 Pressure history for PDE test with the HE arc discharge ignition system at 1 Hz. The reading of PT6 is awry due to mechanical vibrations affecting the electrical connection of the transducer. The pre-detonator was filled with stoichiometric propane-oxygen, while the main combustor used a propane-air mixture.

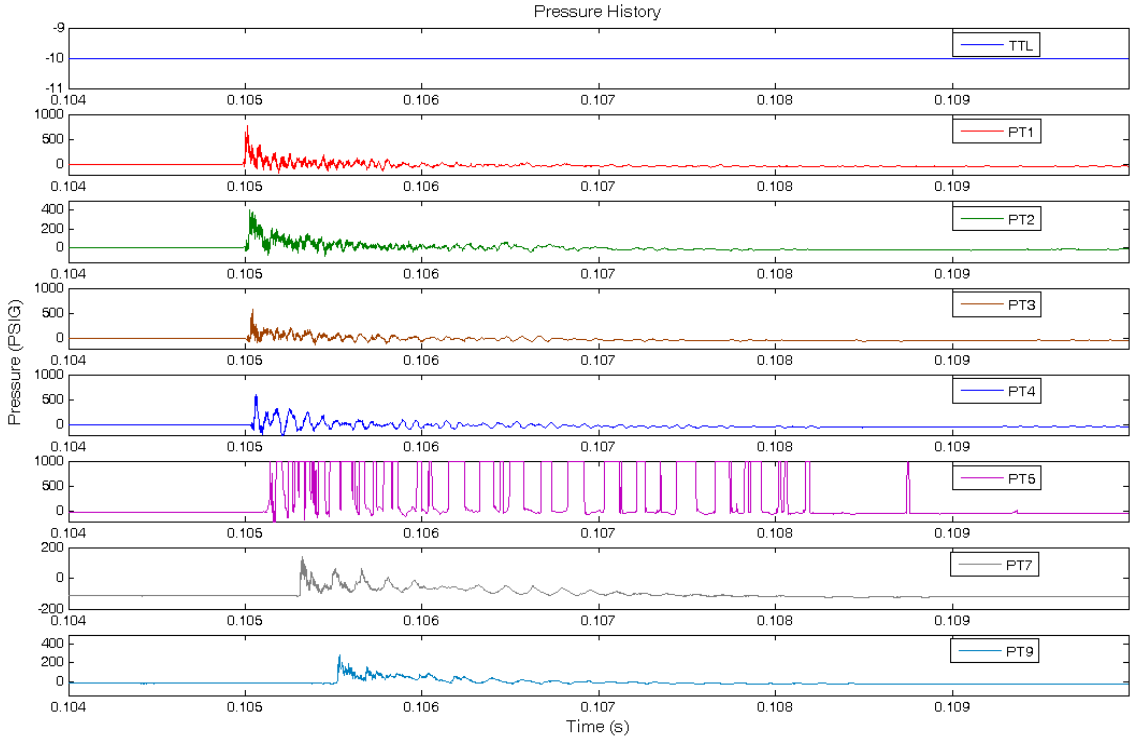

Figure 7.16 Pressure history for PDE test with the HVLE ignition system at 1 Hz. The reading of PT6 is awry due to mechanical vibrations affecting the electrical connection of the transducer. The pre-detonator was filled with stoichiometric propane-oxygen, while the main combustor used a propane-air mixture.

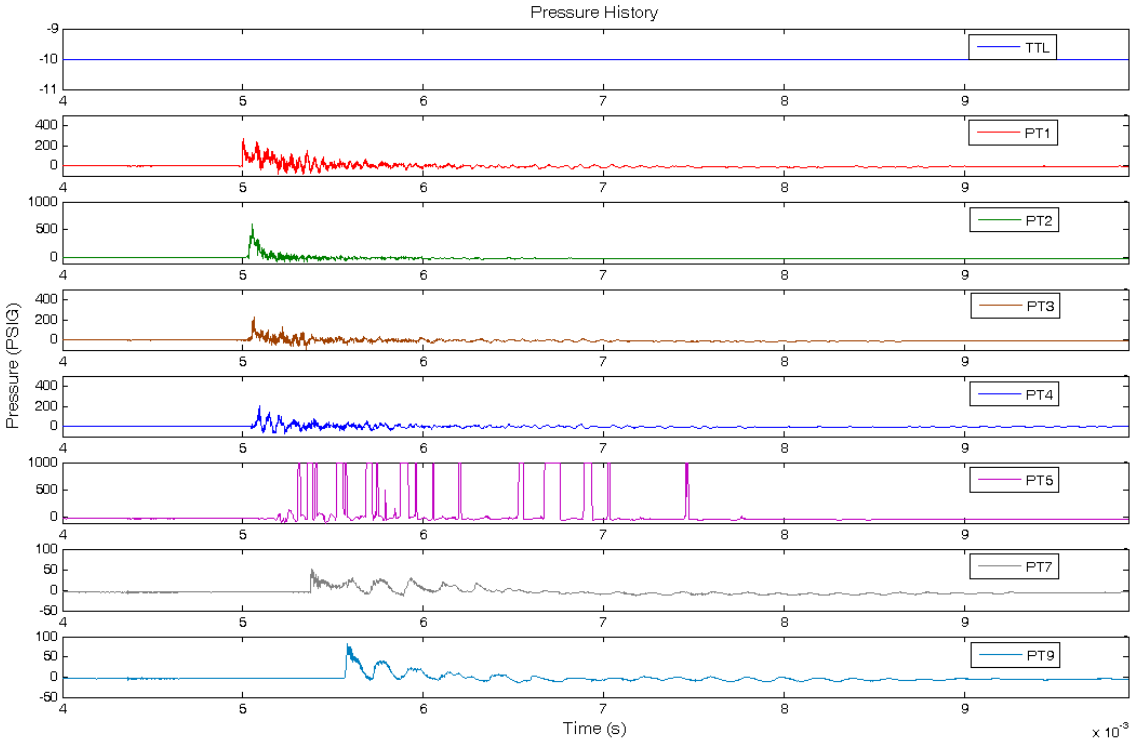

Figure 7.17 Pressure history for PDE test with the low-energy system at 10 Hz. The reading of PT6 is awry due to mechanical vibrations affecting the electrical connection of the transducer. The pre-detonator was filled with stoichiometric propane-oxygen, while the main combustor used a propane-air mixture.

7.5 Corona Discharge for Pre-ionizing Air Flow

Corona discharge in air creates plasma which is visible as a bluish-white glow around the high voltage electrodes. The plasma contains free electrons and ions, which will react more readily with the fuel-air mixture, thereby reducing the ignition energy requirement. If the power is high enough (0.1 to 14 J), the streamers in the discharge can ignite a reactive mixture. In a combustible mixture, corona discharge has been found to reduce the induction time and the DDT time[137-143]. Corona discharge is recognized as a means to produce large amounts of ozone in air[144]. Because ozone is very reactive, it can lower the activation energy and increase the reaction rates of combustion. Studies in internal combustion engines have shown improvements in the ignition time and the combustion of the fuel-air mixture with the addition of

ozone into the air intake[145]. In fact, ozone is also known to react at cryogenic temperatures with hydrogen. Therefore, the presence of ozone is likely to be advantageous to detonation. Corona discharge and ozone generation is currently being used to reduce NOX in automobiles and factory exhausts[146]. In addition to the lowering of ignition energy and enhancement of the reaction, ozone also improves the detonation properties of a fuel-air mixture, including higher pressure and temperature ratios, .higher speed of sound for the mixture, etc. Table 7.2 shows the results of C-J detonation calculations for propane performed using the CEA code[42]. It is seen that very small amounts of ozone enhances the pressure, temperature and density ratios across the detonation wave, and increases the detonation velocity.

A corona discharge can quickly progress to an arc discharge if the current is not limited especially if the air is static or slow moving. Many researchers have used high-powered corona discharges to initiate ignition[138-143]. However, such systems are nothing but HE ignition systems which generate large amounts of heat and require large power supplies to drive the circuits. The associated circuits will also be very large and bulky. This is counterproductive to PDEs for flight applications, where the aim is to produce smaller, lighter and faster engines.

The scheme that is being described here is a corona discharge unit that is supplemented by a HVLE ignition system. For this application, it is necessary to limit the corona current, so that the energy discharged into the air is not enough to initiate ignition and the power consumed remains in the region of a few W to a few hundred W. Such a corona discharge mechanism can be implemented either in the air inlets to ionize the incoming air flow or incorporated into the geometry of a DDT. The DDT devices can be designed to serve as both detonation enhancing obstacles and as electrodes for the corona discharge, as shown in Figure 7.18. The incoming air is thus charged with ions and ozone, which when mixed with fuel will require a lower ignition energy to ignite. Therefore, a small HVLE igniter will be sufficient.

In previous studies at the ARC, corona discharge was induced in supersonic flows in a shock tube, with a single knife-edge electrode, 4.76 mm wide and 19.05 mm long, inside a steel tube of 1.63 in. i.d. (41.25 mm)[147]. The electrode separation was about 10.32 mm. At about 12

kV, the corona current was less than 50 μA, which amounts to a very tiny power dissipation of 0.6 W. The transformer used in this power supply was rated at about 750 VA, but it was very much under-utilized. Therefore, a much smaller and lighter power supply could have also been used. However, it shows the range of power required to generate corona in a given geometry. The ionization level can be improved by increasing the number of electrodes or the surface area of the electrodes. Higher ionization is obtained near sharper electrodes, which also work well for reducing drag in high speed flows. There are many parameters that can be adjusted to achieve optimum level of ionization, including the intensity of the voltage applied, frequency of the voltage (dc or ac), dimensions of the electrodes, number of electrodes and electrode spacing.

However, corona discharge may have a few drawbacks that will have to be considered if the technique is implemented in a PDE. Ozone oxidizes reactive metals, such as copper and iron, but not gold, platinum or iridium. Therefore, the corona discharge electrodes may have to be coated with these precious metals. Aluminum and stainless steel are also not attacked by dry ozone and are safe choices for constructing electrodes. In addition, the combustor may need a ceramic coating to protect the metallic surfaces against oxidation.

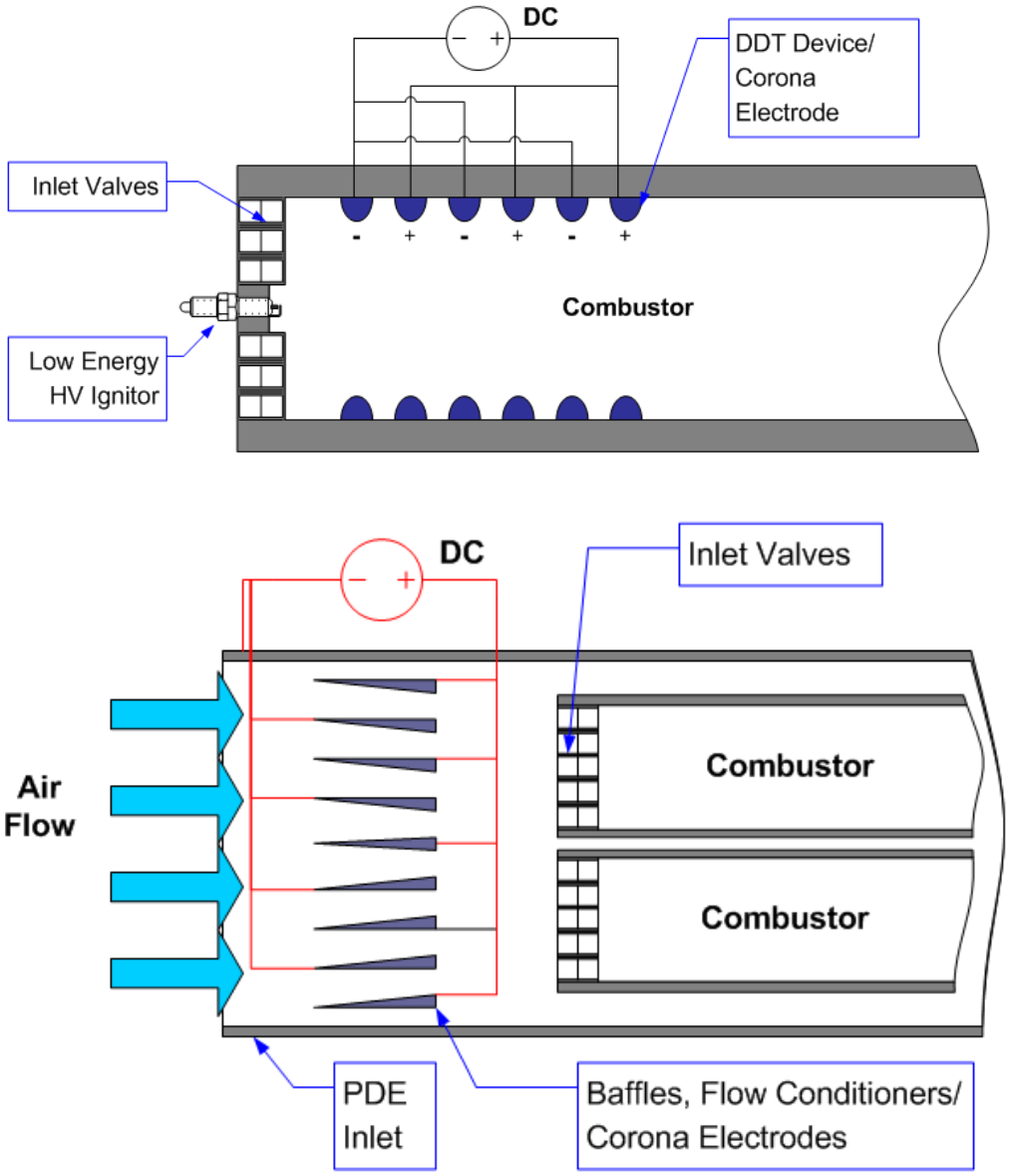

Figure 7.18 Corona discharge schemes are shown for PDE application. (Top) DDT devices are used as corona discharge electrodes, and (bottom) wedge shaped electrodes in the inlet can also serve as flow conditioners.

Table 7.2 Results of C-J detonation calculations of propane obtained from the CEA code, for various concentrations of ozone.

Fuel	C_3H_8		Reactants	Air, O_2+N_2, O_2+O_3+N_2								
T_1 (K)	300				Spec. heat ratio	Sound speed						
p_1 (atm)	1											
Concentration of Reactants in moles					γ_1	a_1	p_2/p_1	T_2/T_1	ρ_2/ρ_1	Mach No.	C-J Velocity	% Ozone
C_3H_8	Air	O_2	O_3	N_2		(m/s)				M_1	(m/s)	by mole or vol.
1		5			1.2917	307.8	35.951	12.742	1.8571	7.6569	2356.6	0
1	23.8	-	-	-	1.3679	339.7	18.148	9.409	1.8105	5.2919	1797.4	0
1		5		18.8	1.3667	340.1	18.123	9.399	1.8106	5.29	1799.4	0
1		4.666625	0.22225	18.8	1.3652	339.2	18.367	9.465	1.8118	5.3285	1807.4	1
1		4.8	0.13333	18.8	1.3658	339.6	18.269	9.439	1.8113	5.3131	1804.2	0.5836
1		4.85	0.1	18.8	1.366	339.7	18.233	9.429	1.8111	5.3073	1803	0.4332
1		4.925	0.05	18.8	1.3664	339.9	18.178	9.414	1.8109	5.2987	1801.2	0.2133
1		4.9625	0.025	18.8	1.3666	340	18.151	9.406	1.8107	5.2943	1800.3	0.1058
1		4.97	0.02	18.8	1.3666	340.1	18.145	9.405	1.8107	5.2935	1800.1	0.0845
1		4.985	0.01	18.8	1.3667	340.1	18.134	9.402	1.8107	5.2918	1799.7	0.0421
1		4.9925	0.005	18.8	1.3667	340.1	18.129	9.4	1.8106	5.2909	1799.6	0.0210

7.6 Summary

High energy (HE) and low energy (LE) ignition systems were studied. The HE igniters have many drawbacks, including larger and heavier power supply components, significant wear and tear on the system and the igniters with reduced durability of the igniters, wastage of power as heat in the circuit and in the igniters, such that a sizable portion was not being transmitted to the flow, and increased EMI. However, HE ignition was able to reduce the ignition delay. The LE ignition is found to ignite mixtures of propane and oxygen in tubes of 19.05 mm and 25.4 mm i.d., hydrogen and oxygen and hydrogen and hydrogen-air mixtures in tubes of 19.05 mm i.d. However, propane-air mixtures could not be ignited using the LE ignition. Therefore, the following two methods may be used to allow ignition within a PDE using LE ignition. The first suggestion is to use an array of LE igniters firing simultaneously so that the combined energy of the array is enough to initiate ignition. The second method is to blend hydrogen into the fuel to reduce ignition energy and time and to promote DDT. LE igniters also can be protected against detonation induced damage by recessing the igniters. Once again, the recessed igniters can only bring about ignition if hydrogen or other fuel sensitizing agents, such as oxygen, are blended into the fuel in the ignition zone.

In addition to LE ignition, low power corona discharge may be used to impart energy to the air flow, to pre-ionize the air prior to fuel injection and mixing and to generate small quantities of ozone. Ozone is known to be a very reactive oxidizing agent that can reduce ignition delays and increase the reaction rates of fuels. Thus, for a PDE running on fuel-air mixtures, a LE ignition with hydrogen blending and DDT devices can bring about fast and successful ignition and DDT.

CHAPTER 8

STUDY OF VALVES FOR PDE GROUND DEMONSTRATOR

Once the internal geometry of a PDE has been defined and assembled, there are only two ways to control the processes within the combustor and to ensure whether there will be successful detonations or not. One is through the valves for controlling the flow of fuel and oxidizer, and the other is through the igniter, whereby energy is added to the mixture. These two topics are dealt with separately, with the ignition system being discussed in Chapter 7. Some researchers have analyzed valveless PDEs[148,149]; however, this is not viable for a practical aircraft engine, as throttling cannot be performed without valves. Operating the PDE in a resonant mode limits its speed and range of operations and may not be easy to control.

Many researchers have used rotary valves in their experimental PDE setups[150] and also for computational analysis of PDEs and their integration with inlets and nozzles[151]. Earlier experimental studies of multi-cycle PDEs at the ARC were performed on combustors fed through rotary valve systems. In this course of study, two PDE setups used rotary valves, namely the Bantam PDE and the PDE Mark 1. Schauer et al.[152] have used the overhead-cam and cylinder head assembly of an automobile engine to supply fuel and air to PDE combustors, which were essentially long tubes fitted into the engine cavity of the automobile engine and instrumented with pressure or other types of sensors. This approach has also proved successful in tests up to 20 Hz, but it is bulky and heavy and is not practical for a flight vehicle.

8.1 Mechanical vs. Electrical Systems and Mechatronics

Mechanical systems are rugged and generally have long service lives. They are also predictable, in that before a part breaks down, it will show signs of wear, e.g., increased play in levers, wider hysteresis, etc., and emit sounds indicating the state of the system, e.g., bearings

get tighter and the sound of machines get louder with time. Therefore, it is possible to know when to replace or service the part. However, mechanical systems tend to be bulkier and slower to respond. Even the fastest machines, have response times in the ms range.

Electrical and electro-optical systems tend to be smaller and quieter and have better energy conversion efficiencies. They can have a wide range of response times, from ns to ms or more as desired by the designer. A big advantage of electrical systems is that the current and voltage characteristics can readily tell the state of the system. By measuring the current and voltage, e.g., one can tell what the speed of rotation of a particular motor is. Therefore, electrical systems can reduce the number of sensors needed for feedback control. Also, electrical systems are easier to control and monitor remotely.

There is an increasing trend towards integration of electronics and mechanical systems, known as mechatronics, which has given rise to the more electric vehicle (MEV) and the more electric aircraft (MEA) concepts. Electromechanical actuators are widely used in present day aircraft, allowing for the interfacing of intelligent control systems with the physical systems, bringing about dramatic improvement in control and the design of smarter aircraft with improved fuel efficiencies. It is also expected that modern electro-mechanical systems will help make PDEs a reality.

Some of the fastest electro-mechanical systems are found in Formula 1 engines, such as the Cosworth CA2006 V8 engine (2400 cc, 755 BHP) which is rev-limited to 20,000 rpm, or 333.33 rps or 167 cycles/s. (Presently, F1 regulations have reduced the rpm limit to 19,000 rpm.) Such a high repetition rate is not possible without an intelligent engine management control system. The above engine uses electronic (solenoid driven) fuel injectors that must be capable of cycling at such high speeds. The piston-cylinder configuration has been refined over the period since its discovery and is the best known sealable machine that can deliver extremely high pressures in pumps or work under very extreme pressure and temperature environments without spillage in heat engines, while moving at high speeds. The advances in tribology and the introduction of improved lubricants have greatly benefited the development of

high speed pumps and engines. The advantages of piston-cylinder systems can also be adapted for rotary valve systems.

In this chapter, two types of valve systems will be studied for their effectiveness for possible implementation in PDEs. They are

1. Motorized rotary valve
2. Solenoid driven valve

8.2 Rotary Valves

The advantages of rotary valve systems are:

1. They can be built to tight tolerances.
2. They can withstand high temperatures and pressures.
3. They can operate at moderately high speeds. For example, a single rotary valve, similar to the one shown in Figure 8.2, rotating at .20,000 rpm would result in 667 open and close operations per second.
4. The air flow path through the rotary valve has a fewer number of obstructions than a .poppet valve. Therefore, higher mass flow rates are possible, with lower loss of pressure. Poppet valves are used in the intake and exhaust valves found in automobile engines and in solenoid type valves. This is the biggest advantage over solenoid valves.

The drawbacks of rotary valves are:

1. They need a sensor to pick up the position and velocity of the valve.
2. Rotary valves cannot modulate the duty cycle of the valve open-time, i.e., the period of valve opening is dependent on the frequency of rotation and the area of the opening. Therefore, as the valve rotates faster, the open-time period reduces. Thus, less mass flow rate is possible at higher

speeds. This demonstrates an inverse relationship of flow rate with frequency, which is not desirable for PDE operations at higher speeds.

To make up for the reduced open time, the pressure at the inlet of the valve has to be increased. The mass flow rate is proportional to the square root of the difference in pressure between the inlet and the outlet. Therefore, for a doubling of mass flow rate, pressure has to be increased by four times. The above relationship is obtained from the orifice flow model, such as shown in Figure 8.1[153]. Mass flow rate $\dot{m}$, is proportional to the pressure difference, the area of the orifice A, and an empirical discharge coefficient c_d.

$$\dot{m} = c_d \rho A \sqrt{\frac{2(p_1 - p_4)}{\rho}} \tag{8.1}$$

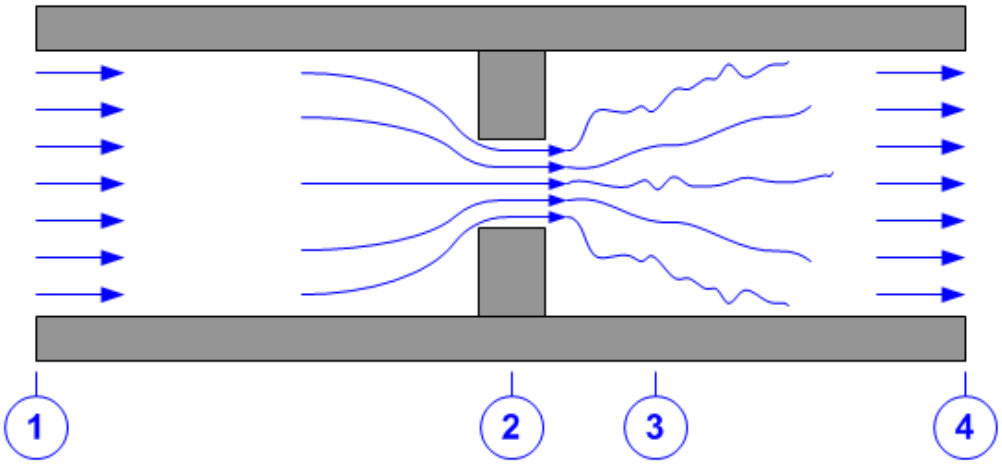

Figure 8.1 Schematic of the flow through an orifice[153].

A better alternative to the continuous duty motor is a stepper motor, which can be controlled in fractions of a degree. Therefore, the valve can be kept in the open position for a longer duration, as required by the control system. This also removes the need for an additional sensor, since the stepper motor controller will have motor shaft position at all times. Thus, the valve speed and duty cycle can be modulated as desired.

A successful implementation of this concept of modulated valve timing is found in automobile engines and is known as continuously variable valve timing (CVVT) which is found

in engines from almost all major car manufacturers today. Honda, for example, has an electronically controlled CVVT system that they call VTEC[154], once again demonstrating the ingress of mechatronics into traditionally, all-mechanical systems. The VTEC system uses cams to vary the timing of the poppet valves during operation by allowing the poppet to stay open for longer periods. The camshaft is driven by the crankshaft of the engine through timing belts, gears and chains. This technique can be applied to PDEs, in which the camshaft can be driven by the turbine of a hybrid PDE-turbine system. Mechanical or electro-mechanical variable valve timing techniques have the benefits of the years of trials and refinements in industry.

8.3 Experimental Rotary Valves Used in PDE Tests

The rotary valve systems used in previous studies at the ARC for gas injection were of the type shown in Figure 8.2. Their construction was simple consisting of a spindle mounted within a rectangular housing so that it was free to rotate. The spindle had one or more orifices perpendicular to its axis. When the orifice on the spindle lined up with the ports in the housing, the gas could flow through, as shown in the figure. The spindle was driven by a dc or universal motor either by gears or by a belt-and-pulley system. The rotary valve used in the Bantam PDE and the PDE Mark 1 had two orifices at right angles to one in the center, as shown in Figure 8.1 on the left. This allowed the outer orifices and their ports to be used for propane and oxygen and the central off-phase orifice to be used for purge-air delivery.

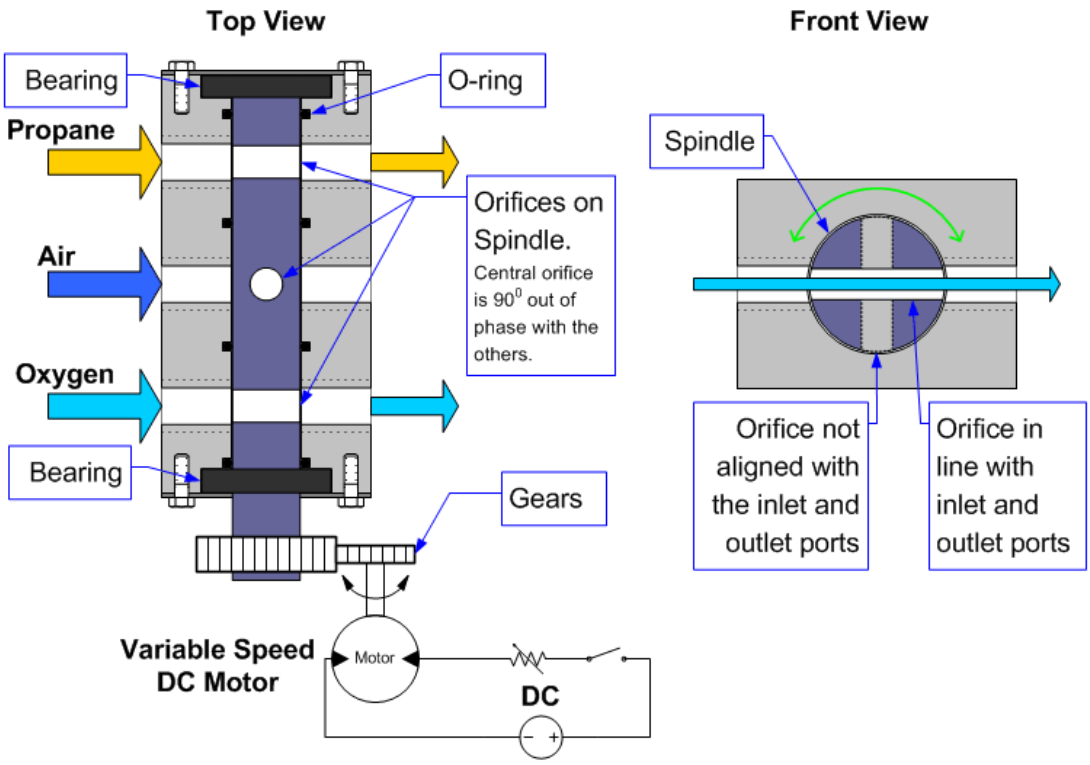

Figure 8.2 Schematic of the rotary valve system used in the PDE demonstrators.

The drawbacks of this type of rotary valve system are listed below:

1. The rotor needed a magnetic or optical sensor to detect the valve position.
2. The sensors were prone to EMI due to the proximity of the motor.
3. The motor caused vibrations. If the rotors and the motor were not matched or aligned properly, strong vibrations were produced.
4. Because the valve spindle and the housing were not made to exact tolerances, there was huge leakage, and cross contamination between the channels. In a three-channel design, the leakage caused the oxygen and propane lines to be contaminated with air and vice versa. Thus, high pressures could not be used.
5. The rubber o-ring seals were not suitable for sealing in a rotational motion. An alternate sealing method, such as piston rings, would be required to prevent leakage and excessive wear of the seals.

6. If the housing was tightened too far, the spindle would not move properly and the motor would need to be driven with a higher current to achieve higher speeds. This caused the motor to overheat quickly. The deformation in the housing, due to the over-tightening, caused excessive friction on the spindle. Therefore, more attention needs to be paid during the design and construction of the parts to ensure a perfect fit.
7. The frequency of the PDE was set by the speed of the valve motor. Each rotation of the spindle produced two sets of fill-fire and purge stages. The motor speed could not be controlled accurately and only speeds close to the desired value were obtained. For example, if 10 Hz was desired, the motor speed was set as close as possible to 5 rotations per second, but the speed would change during the operation and the pulse width would therefore change from one moment to the next due to changing friction, pressures on the spindle, vibration of the motor, etc. Also, the motor speed control exhibits non-linear behavior at the low range. Therefore, low speeds could not be achieved on these motors. A stepper motor drive for the rotor would overcome this deficiency.
8. The duty cycle of the valve open or close stages could not be changed due to the preset geometry. Because the size of the orifice and ports are fixed, the area of the opening depends only on the area of the orifice and ports and the speed of rotation of the spindle, as shown in Figure 8.3. At higher speeds, the period that the valve stays open is shorter. As a result, if the pressure is held constant, the flow rate reduces considerably.
9. The belts and gear drive system had significant slippage, as a result of which the valves would quickly go out of synchronization and the PDE would misfire and function abnormally. This was once again a result of improper machining. Gears and timing belts and chains are widely used for valve timing in automobiles and they last about 60,000 miles (100,000 km) before they need servicing. Therefore, more attention has

to be paid during the design, manufacture and assembly of rotary valves to ensure smooth and precise operations.

Due to these shortcomings, solenoid valves were used for later PDE set ups. However, rotary valves are still good for PDE applications, provided they are made to very precise standards.

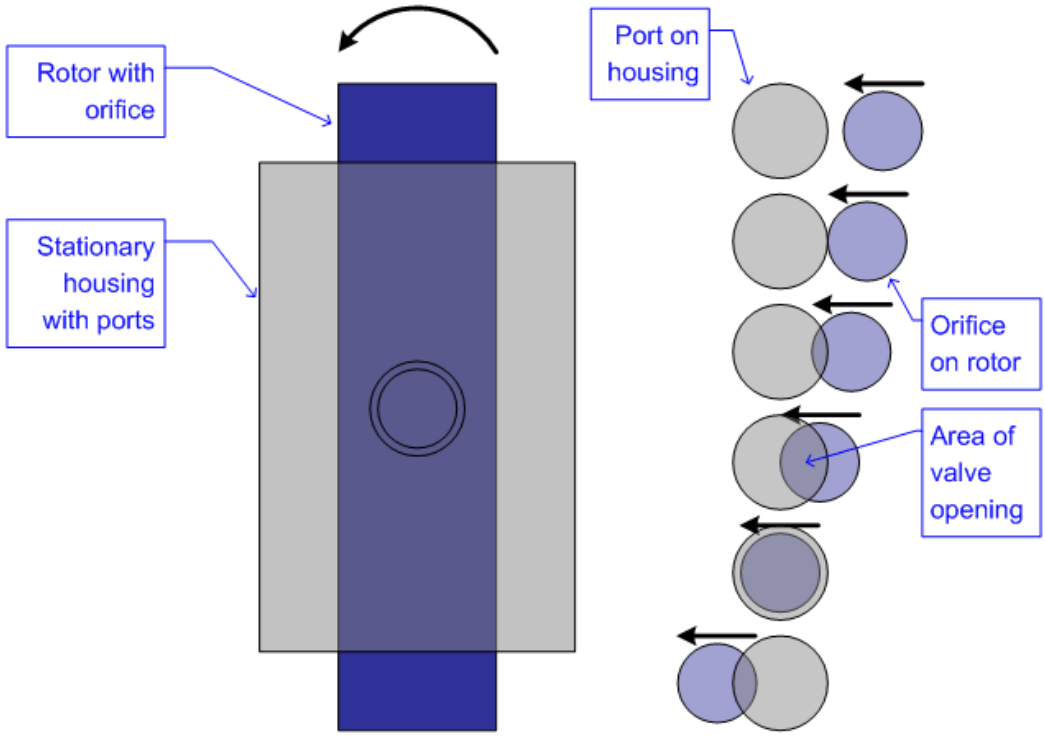

Figure 8.3 Schematic of the rotary valve showing the variation in the area of the valve opening as the rotor is spun (right).

8.4 Application of Solenoid Valves in PDE Ground Demonstrators

8.4.1. Gaseous Solenoid Valves Used in the PDE Mark 2, the PDE Mark 3 and the Dual-Stage PDE Apparatus

As mentioned earlier, the solenoid valves used for supplying the various gases (including air, oxygen, propane and hydrogen) to the PDEs were the AFS Gs series gas

injectors from Alternate Fuel Systems, Inc., Calgary, Canada. The AFS Gs series valves are actually low-flow valves, meant for use in the engines of buses and trucks, with each injector only injecting a small volume into one cylinder, of the order of 1000 cm^3 per engine cycle. Therefore, multiple valves were needed for the PDEs. In the case of the PDE Mark 2, three such valves were used for oxygen, one for propane and two for purge air. In the pre-detonator of the dual-stage PDE, two valves were used for oxygen service, one for propane valve and two for purge-air. In the main combustor up to four valves were needed for each gas due to the large volume of that section (5792 cm^3).

The AFS valves and the ignition were controlled using TTL signals generated by the DAQ. A typical TTL waveform for three channels (purge air, fuel-oxygen filling and ignition) would look like Figure 8.4. The TTL logic-low voltage level is given as between 0 and 0.8 V, whereas the logic-high voltage level is given as between 2 and 5V. The rise and fall times between a logic high and a logic low is in the region of 50 ns or less for most National Instruments' devices. The rise/fall times of the TTL is negligible compared to the response time of the valves and the TTL signals may be assumed to be perfectly rectangular for all practical purposes, as shown in Figure 8.4. The AFS valves have a 2 ms response time. Since the PDE test frequencies were almost always less than 15 Hz (about 30 ms time period for filling or purging), the opening and shutting of the valves were assumed to follow the TTL signal, although the closing of one set of valves overlapped with the opening of another set of valves. That is, as the purge air valves closed at the end of the purging stage, the oxygen, propane and air valves opened for the beginning of the fuel-oxidizer filling stage. This is illustrated in Figure 8.5.

A typical timing control program, devised in LabVIEW for this study, would generate TTL pulses for each device set, with each TTL signal coming from a separate counter channel on the DAQ. Therefore, one channel was reserved for the purge air valves, one for the fuel and oxidizer valves, one for the ignition and another for controlling other valves, if they operated at a different time. The fuel and ignition valves controllers were configured to follow the purge air

valve timing by a preset delay, as shown in Figure 8.4. The program was set up in such a way that the operating frequency could be entered in Hz while the duty cycle of each component and the time delay in between each component could be entered in as percentages and the program would compute the timing automatically. Once the required values were entered in to the program, the PDE could be run with the click of a mouse button. The LabVIEW based control program allowed the precise control of the valves and ignition and thus the PDE operation with relative ease. The ignition was the fastest process, occurring in a few μs, followed by the combustion and blowdown, all of which took only a few ms, on the order of 5 to 10 ms.

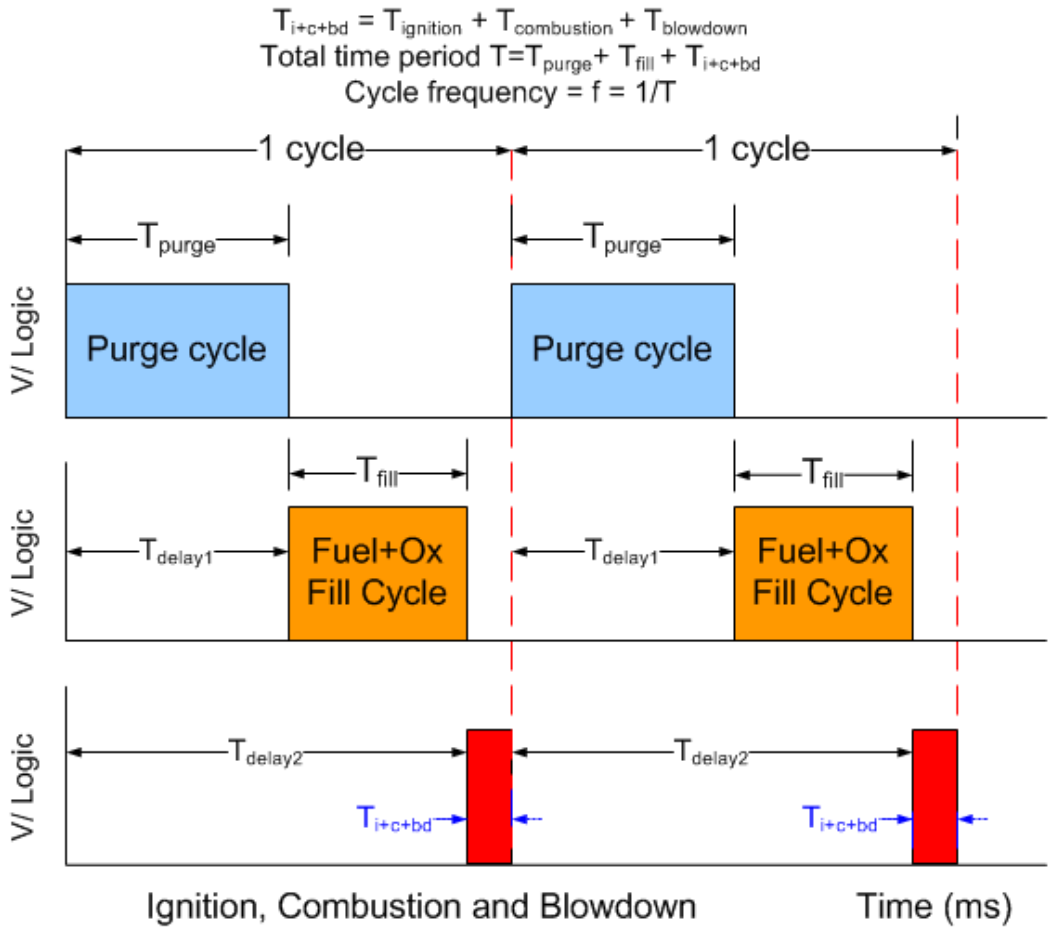

Figure 8.4 A typical TTL output from the PDE control program, for a three device setup. The valves are assumed to open and shut in line with the TTL, because the response times and the rise/fall times of the TTL signals are negligible compared to the time period of operation. In reality, the closing and opening of valves overlap.

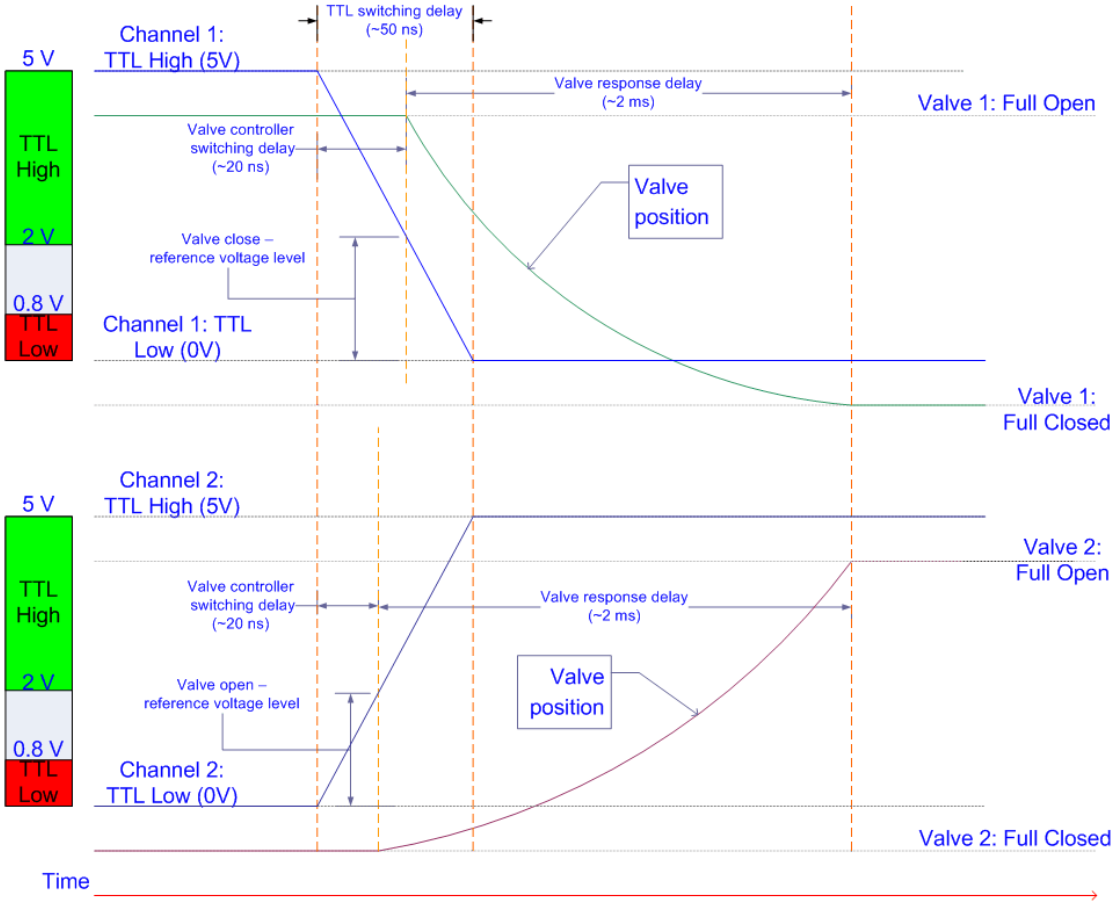

Figure 8.5 Schematic of the TTL signals and valve operations for a two valve system. As one valve is closing, another is opening and their actions overlap. The time axis is not drawn to scale.

8.4.2 Solenoid Valves for High Speed Fuel Injection in PDEs

The schematic of a typical two-way, normally-closed solenoid valve is shown in Figure 8.6. It has a magnetic core plunger that is sealed at its ends, allowing it to shut off the exit orifice when it is resting in the closed position. When the coil is energized, the core is pulled up toward the center of the coil and the orifice is opened to allow fluid to exit through the orifice into the outlet.

Because the fluid has to make a sharp turn to exit the valve, there will be severe loss of momentum and pressure inside the valve. High mass flow rates are not possible due to this obstruction. Most electrical fuel injectors used in automobiles today are similar in operation to

the above model. They are designed to inject a small amount of liquid into the engine at regular intervals. Therefore, solenoid valves should only be reserved for the injection of fuels or or for the addition of small amounts of oxidizers or fuel sensitizing agents in a pre-detonator. To increase the mass flow rates, multiple valves channeled from a common manifold or a common-rail may be operated in tandem. For handling the large amounts of air flow in a PDE, rotary valves are still the better choice.

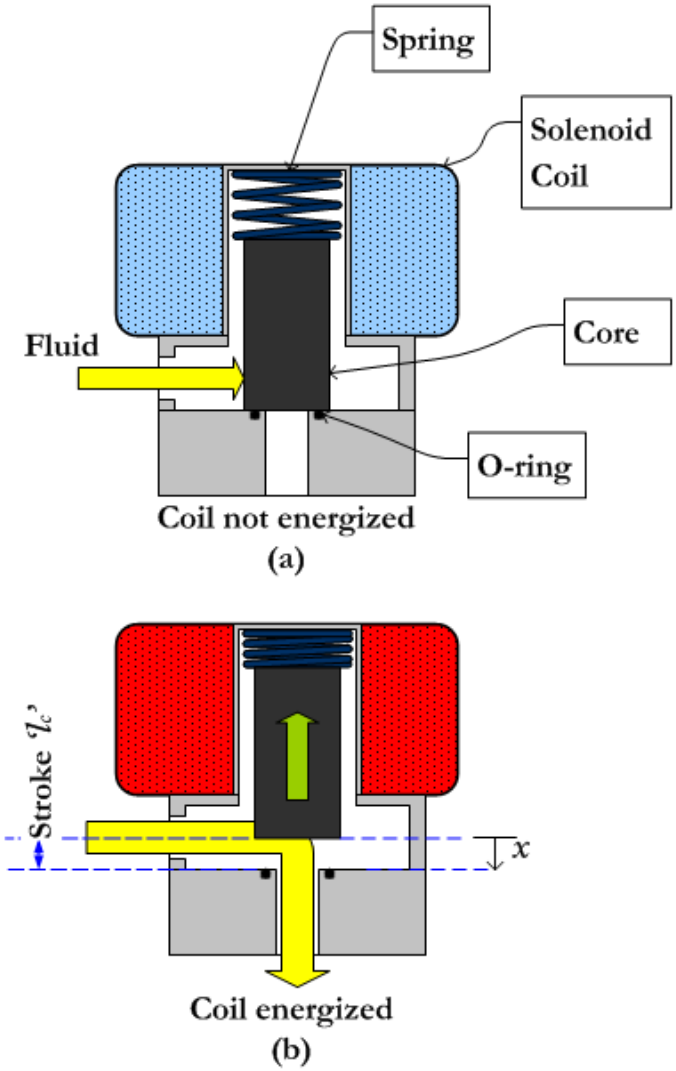

Figure 8.6 The schematic of a two way, normally closed solenoid valve.

8.4.2.1 High Speed Actuation of Solenoid Valve

Lu et al.[156] performed experiments on driving a solenoid valve at high frequencies, with the aim of applying this technique in PDEs. The idea was to drive the solenoid with a higher than rated voltage pulse, at high frequencies, to allow the solenoid core to saturate quickly and pull the valve open rapidly. At low frequencies, the valve would open faster with the higher voltage. However, at higher frequencies, the response was delayed and there was a significant phase lag, as shown in Figure 8.7 (a).

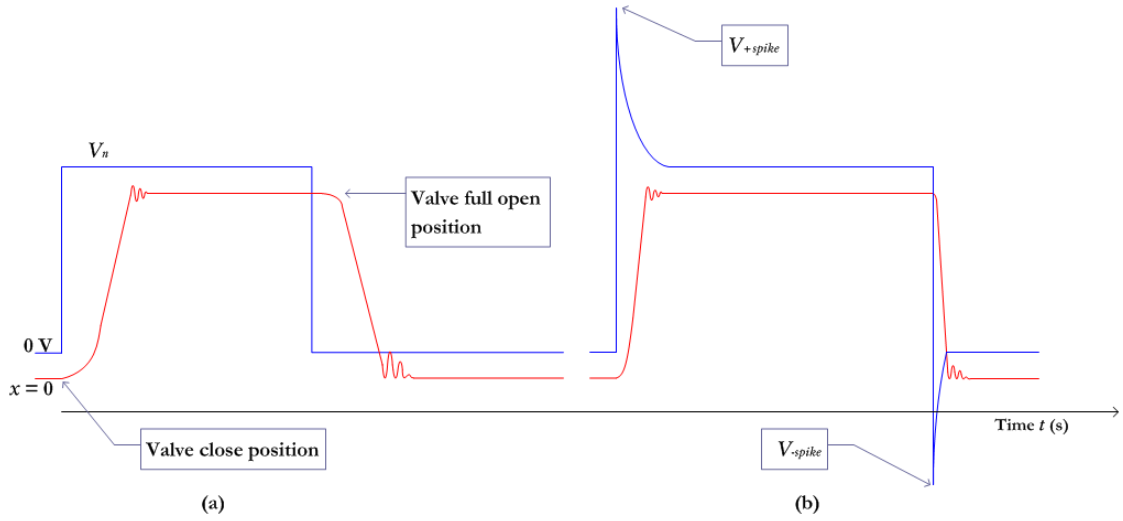

Figure 8.7 (a) The response of a solenoid valve to the application of a voltage pulse, and (b) reaction of the solenoid valve when a modified voltage pulse is applied.

The commonly used notations in electromagnetic circuit analysis are presented below. The magnetic field strength H of a coil of N turns, length l and radius R is given by

$$H = \frac{NI}{l} = \frac{NI}{2\pi R}. \tag{8.2}$$

The magnetic field strength and the flux density B are related by

$$B = \mu H = \mu_0 \mu_r H = \frac{\mu NI}{2\pi R} = \frac{\mu N}{2\pi R}\frac{V}{Z}. \tag{8.3}$$

Equation (8.3) shows that the flux density and the magnetic field strength of a coil are directly proportional to the current flowing in the coil I and the voltage V applied across it. Figure 8.8

shows the typical $B-H$ curve of ferromagnetic material, such as iron, steel, etc. Initially B increases almost linearly with H. H can be increased by driving the coil with an increasing voltage, since current is proportional to the voltage V and inversely proportional to the impedance Z of the coil. But, as B reaches saturation, any further increase in voltage only drives up the current and yields no further growth in the flux density. As the voltage is increased beyond the point of saturation, the current will increase dramatically, causing the coil to heat up and possibly burn up. This is the major cause of solenoid coil failure and also for failure in transformers. Therefore, it is important not to linger in the saturation region for too long. Also, the heating reduces the magnetization of the core, as explained in the section below. Thus, continuous duty solenoids are not run into the saturation region to prevent burnouts or wear of the coil and its insulation.

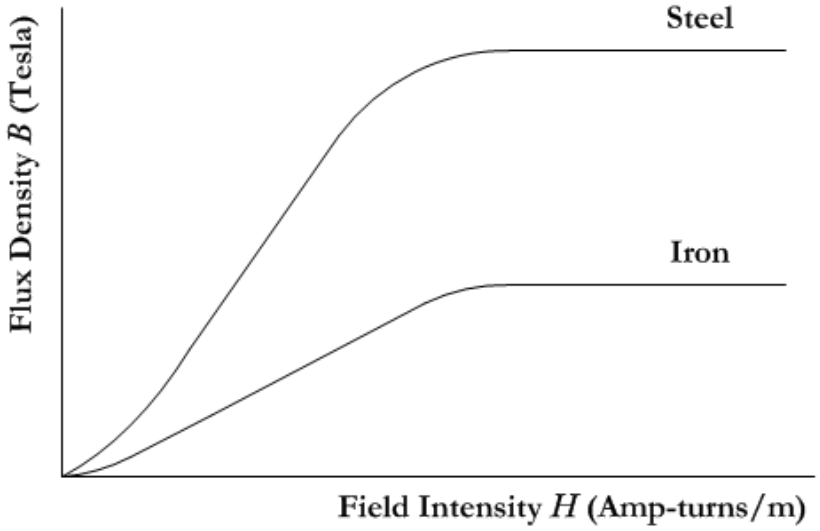

Figure 8.8 The typical B-H curve of ferromagnetic materials is as shown above. As H is increased, B reaches saturation and flattens out.

For fast switching solenoid valves, the B-H curve will show a hysteresis, as shown in Figure 8.9. As the voltage supply to the coil is cut off, the magnetic flux still persists inside the core and the plunger core does not immediately return to the non-energized location. As a

result, the solenoid response time is affected by the hysteresis causing a phase lag in the valve position, as shown in Figure 8.7 (a).

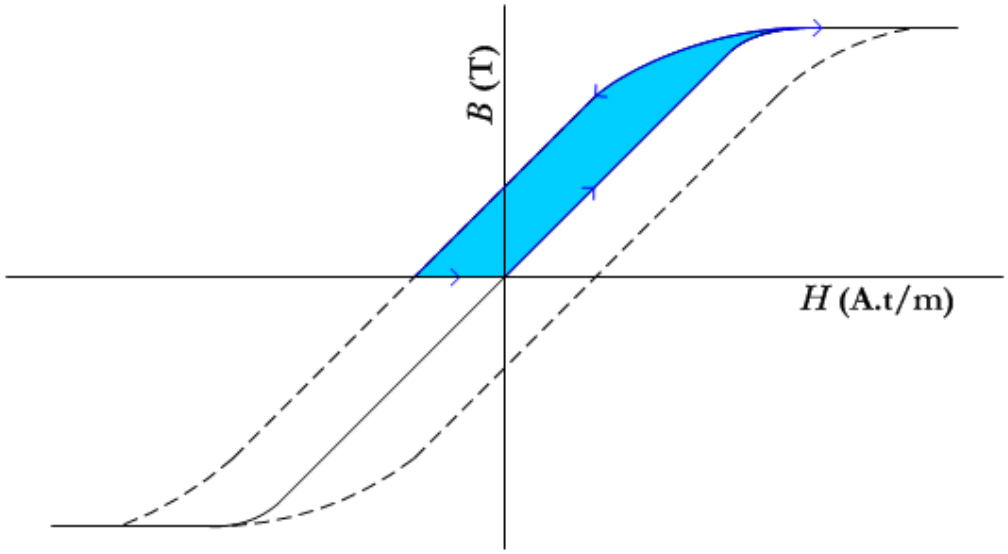

Figure 8.9 A schematic of the B-H hysteresis loop of a ferromagnetic material shown using dashed line. The shaded region represents the path taken if a voltage waveform similar to that shown in Figure 8.7 (b) is used to drive a solenoid coil.

In order to remove the remnant magnetic flux inside the core, the magnetic field intensity has to be driven past zero, into the negative region, as shown by the shaded region in Figure 8.9. This can be done by using a voltage waveform of the form shown in Figure 8.7 (b), in which a sharp negative peak is added to the square shaped pulse. The positive spike causes the magnetic flux to saturate momentarily and drive the core up quickly. On the return journey, the negative spike causes the core to de-magnetize and return rapidly to the non-energized location, assisted by the spring force. Another reason why such a waveform is required may be explained by looking at the force-stroke curve and the force-current curve, shown in Figure 8.10. When the core is extended fully, the magnetic force on it is very weak. Therefore, a higher voltage spike at this point would help it to move faster by driving up the intensity of the force.

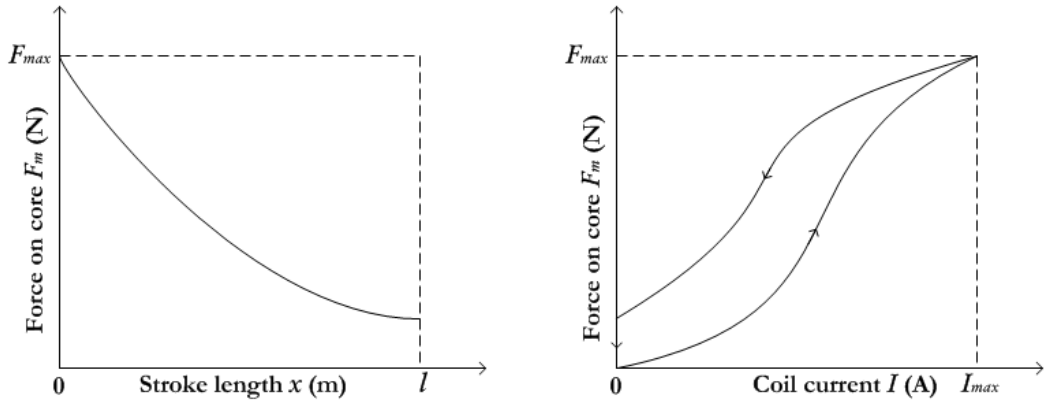

Figure 8.10 The force-vs.-position of core curve, along with the force-vs.-coil current curve of a solenoid valve.

8.4.3 The Negative Effect of Heat on Solenoid Valves

A major problem with magnetic circuits is that they cannot handle high temperatures very well. High temperatures reduce the magnetic flux carrying ability of a ferromagnetic material, as shown in Figure 8.11. If the temperature is increased, the magnetization decreases until it completely vanishes at the Curie temperature. Curie temperature, named after Pierre Curie (1859 – 1906), is the temperature at which ferromagnetic materials become paramagnetic, i.e., they cannot be magnetized beyond that temperature. The Curie temperatures of a few ferromagnetic elements are provided in Table 8.1. Although electromagnetic or magnetic devices are never operated at close to the Curie temperatures of their constituent materials, high temperatures can affect the operation of such devices.

Since the magnetic strength of the coil and the core weakens at higher temperature, more current is required in the coil to provide the same magnetic force required to drive the valve open. But higher currents cause a further increase in temperature, which further compounds the problem. Therefore, solenoid valves cannot be used for very high temperature fluids as the valves become inefficient at higher temperatures. The resistance of the coil also increases with temperature and reduces the current resulting in a loss of magnetic force at higher temperatures. As a result, the voltage has to be increased to get the required higher

currents. Thus, solenoid valves have to be actively cooled to operate at higher frequencies and heavy loads.

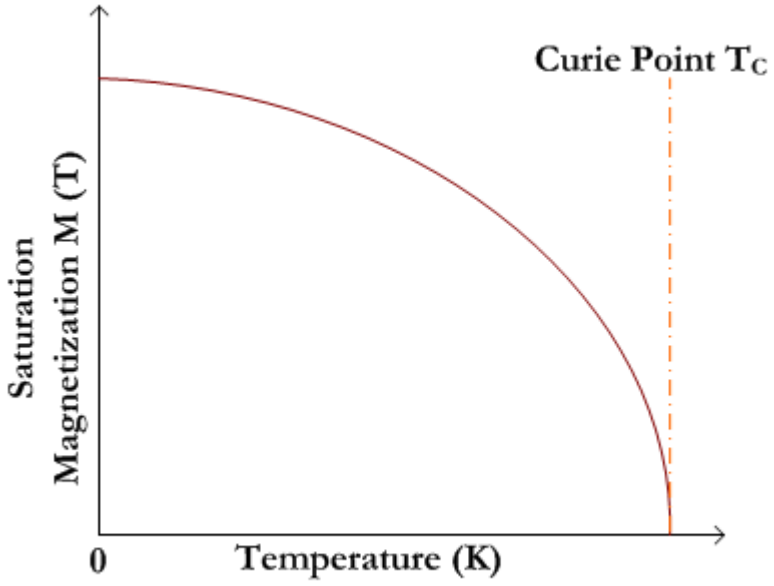

Figure 8.11 The typical magnetization vs. temperature curve of a ferromagnetic material.

Table 8.1 Curie temperatures of a few ferromagnetic elements.

Material	Curie Temperature (K)
Cobalt	1388
Iron	1043
Nickel	627

8.5 Achieving The High Flow Rates Required For PDE Operation

The sizing and selection of the valve system will depend on the amount of mass flow required, which is again dependent on the thrust requirement. The amount of mass flowing out of a valve is directly related to how long the valve stays open. Therefore, it can be shown that the total mass flow from a valve is inversely proportional to the frequency, because the valves are open for shorter periods of time as the frequency increases. The mass flow (out of a purging or filling valve in a PDE) can be expressed as

$$m = \dot{m}\, dT = \dot{m}\frac{\text{duty cycle}}{f} \tag{8.4}$$

where dT is the valve open time, f is the frequency of operation and the duty cycle is the fraction of the time period the valve remains open. The effect of this drop in mass flow is detrimental to the PDE operation as the combustor is not filled fully during the valve-open periods and the detonation fails. The effect of the mass flow drop is clearly seen in Figure 8.12, which shows the results from a study by Meyers[25]. It was seen that as the frequency was increased while holding the gas supply pressures constant, the detonation would fail.

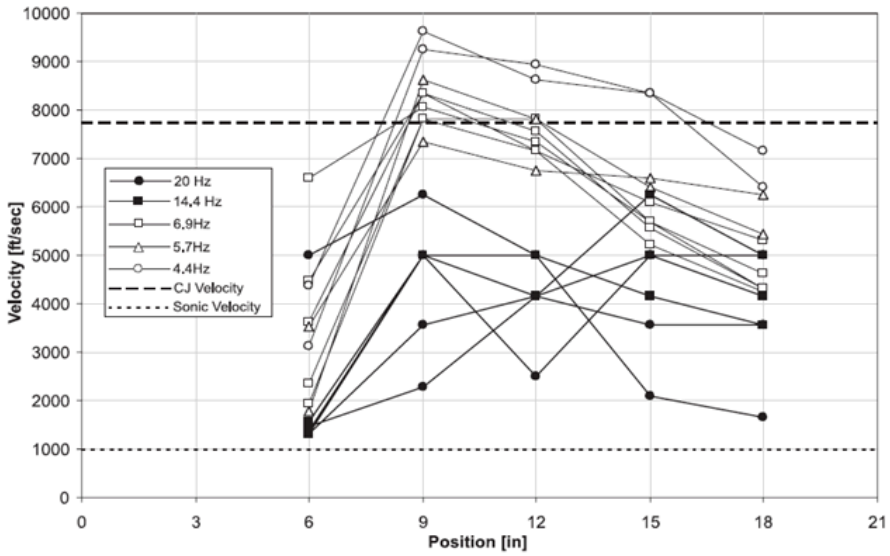

Figure 3.32. Average velocity plot for Shchelkin spiral installed configuration with C_3H_8=43 psig and O_2=146 psig

Figure 8.12 Results of from an earlier study of a multi-cycle PDRE performed at various frequencies. It is seen that as frequency is increased the detonation fails due to improper filling of the combustor[25].

To overcome this drop in mass flow rates at higher frequencies, the number of valves has to be increased or the pressure at the inlet of the valves has to be increased. The pressure increase would be significant because it was shown in Equation (8.1) that mass flow rate is proportional to the square root of the pressure difference across the valve ($\dot{m} \propto \sqrt{\triangle p}$).

To get an estimate of the flow rates required, a simple analysis as described below can be performed on a PDE combustor operating at 1 atm and 300 K. The air is assumed to flow in through one inlet at the front end of the combustor. The air flow occurs twice at the same velocity, once for purging the tube and once for filling the tube. At the end of the filling stage (during which time the fuel would have been injected and mixed in), the ignition and combustion and blowdown processes occur. A period of 5 ms is given for the three processes, which is a realistic value based on experimental results. Now the maximum flow rates and frequencies can be calculated. The frequency f is given by

$$f = \frac{1}{T_{purge} + T_{fill} + 5\ \text{ms}} \tag{8.5}$$

where T_{purge} is the time period for purging and T_{fill} is the time period for filling. The volumetric flow rate Q is given by

$$Q = \frac{\pi D^2}{4}.\not{V} = \frac{\pi D^2}{4}.aM = 272.74\,D^2 M \tag{8.6}$$

where D is the internal diameter of the PDE combustor, $\not{V}$ is the velocity of the flow entering the combustor, a is the speed of sound and M is the Mach number of the flow. The speed of sound at sea level (347.27 m/s) is taken for this calculation. Figure 8.13 illustrates the relationship between combustor inlet Mach number and the volumetric flow rate of air Q, for tube diameters of 2 in. (50.8 mm), 3 in. (76.2 mm) and 4 in. (101.6 mm), showing a linear trend.

If the air is filled into the combustor from the back end, the time it takes for a flow to travel through the combustor of length L is given by

$$T_{purge} = T_{fill} = \frac{L}{aM} \tag{8.7}$$

Therefore, assuming a 5 ms period for combustion and blowdown of the exhaust, the frequency f can then be described as

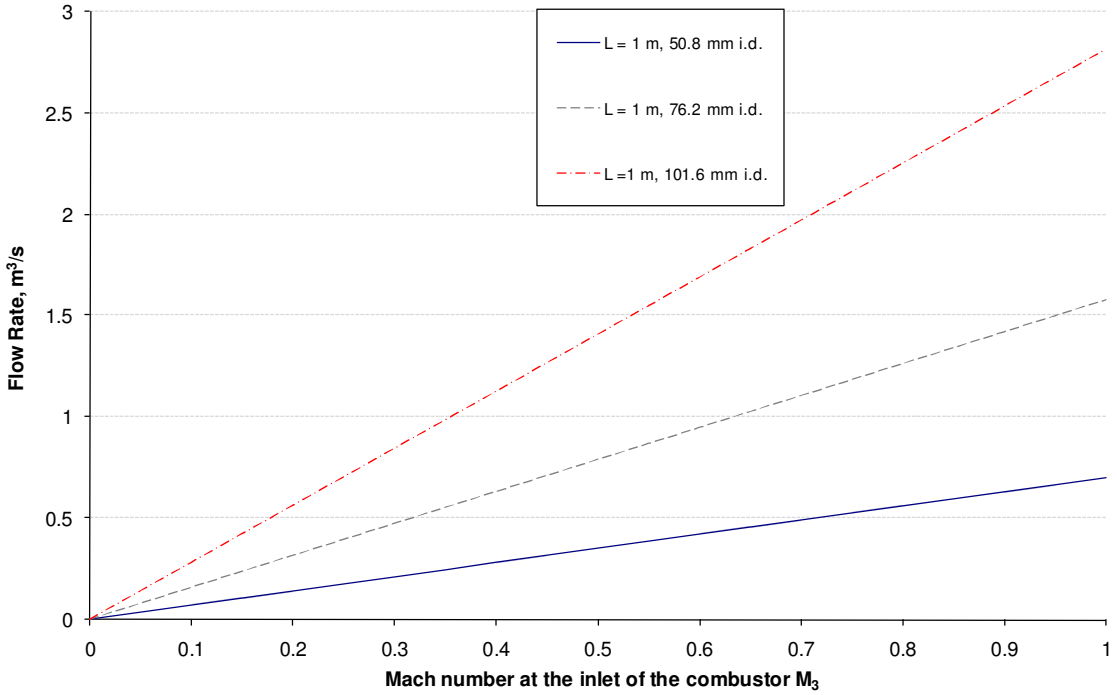

Figure 8.13 The air mass flow rate vs. combustor inlet Mach number for a 1 m long combustor of various diameters, calculated at 1 atm, 300 K. Air flows twice in a cycle, once for purge and once for filling, followed by a 5 ms window for ignition, combustion and blowdown.

$$f = \frac{1}{T_{purge} + T_{fill} + 5\ \text{ms}} = \frac{1}{\frac{2Ma}{L} + 5\ \text{ms}} \tag{8.8}$$

Friction is neglected in the above analysis. Figure 8.14 shows the relationship between Mach number at the inlet of the combustor and the attainable frequency for tubes of different lengths. It clearly demonstrates that at low inlet velocities, high frequencies cannot be achieved. Therefore, the inlet and the valving should be designed to allow for optimum flow at the highest possible velocities. Another inference from the results is that single point filling from the back wall will not be able to produce high frequencies. Multiple locations, side wall filling and purging will be needed for high speed PDEs.

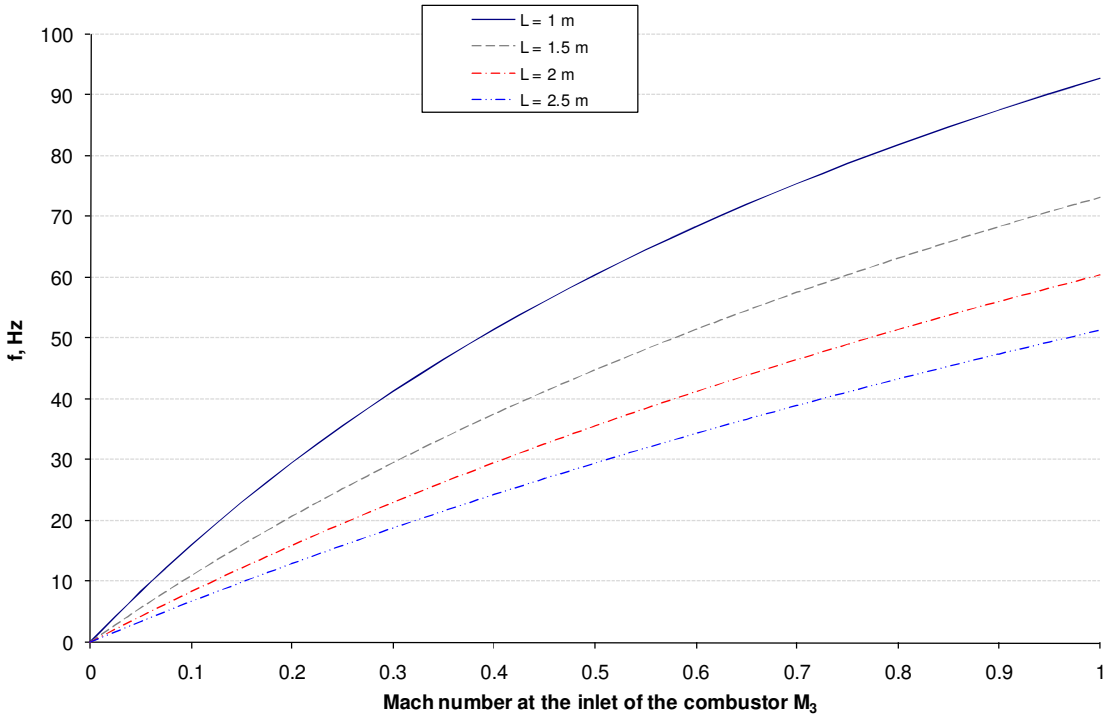

Figure 8.14 The frequency attainable when the combustor inlet Mach number is given is shown in the frequency vs. Mach number plot for various combustor lengths. Air flows twice in a cycle, once for purge and once for filling, followed by a 5 ms window for ignition, combustion and blowdown. Calculations were done for air at 1 atm and 300 K whilst neglecting friction.

For filling air, the schemes illustrated in Figures 8.15 and 8.16 can be adopted to achieve higher flow rates and operating frequencies. Multiple valves along with bleed air entering the combustor along the length of the combustors through valves located on the sidewall enable the combustor to be filled much more rapidly than from a valve at the back wall. The fuel valves have to be positioned along the side wall to enable optimum mixing. This design can be refined using CFD and inverse-design optimization techniques.

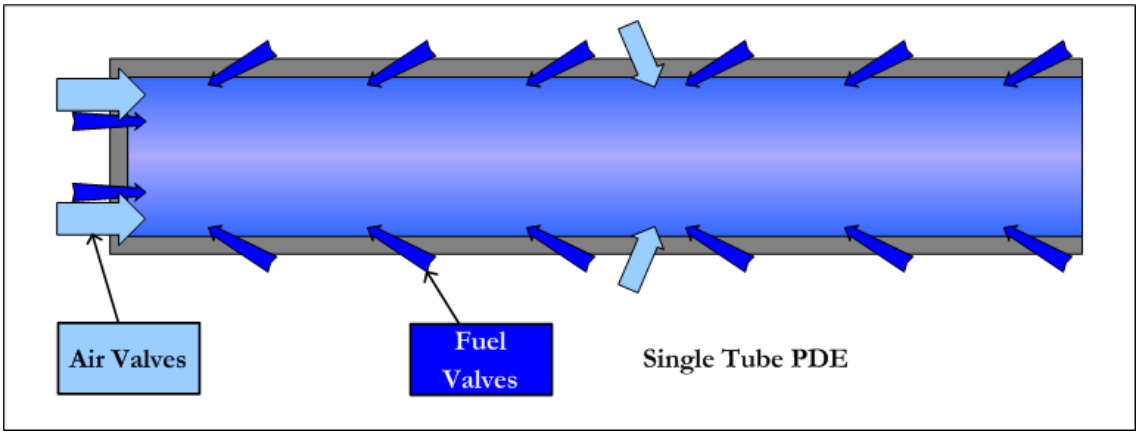

Figure 8.15 Schematic of inline side wall fuel injection to increase filling and mixing speed on a single tube PDE. Bleed air is also fed in at a downstream location to increase airflow rate.

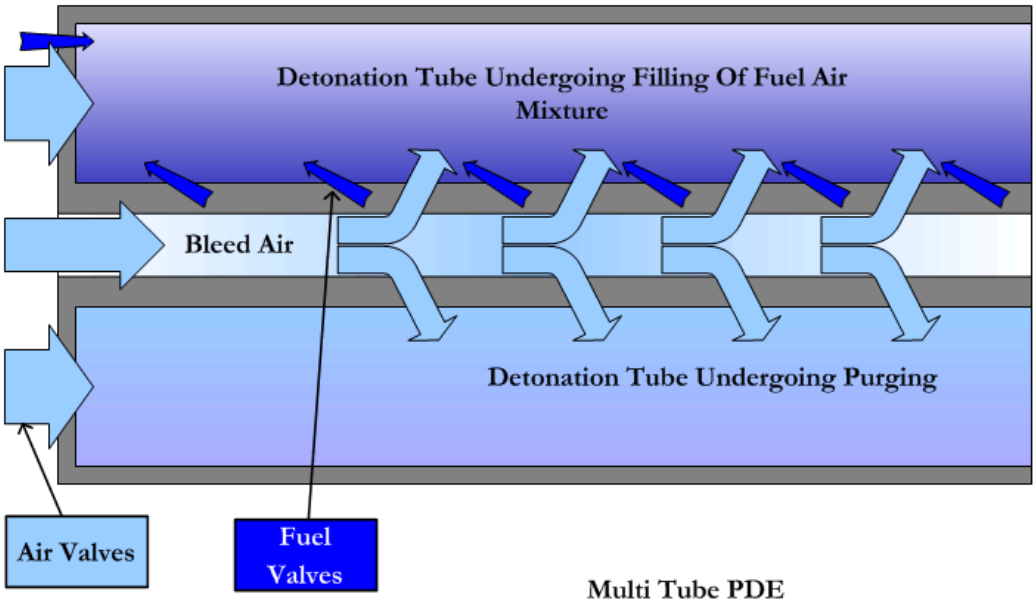

Figure 8.16 Schematic of a multi-combustor PDE with sidewall fuel and air injection. Since the U-shaped curve of cell size-vs.-equivalence ratio, as seen in Figure 2.10, has the minima at an equivalence ratio of 1 to 1.1, this is the region that the fuel injection should strive to reach. Equivalence ratio close to 1.1 may be desirable for shorter DDT distances.

8.6 Gasoline and Diesel Fuel Injectors for PDE Application

In this study, Denso direct injection (DI) gasoline valves[114,157], which are used in Lexus IS-300 2007 model cars, were tested with kerosene. However, they did not provide sufficient misting of the fuel, as much of the fuel came out as liquid. This could have been due to damage of the slit nozzles because an earlier test with water at 10 MPa showed Sauter mean diameter (SMD) values in the region of roughly 10 to 120 μm for a majority of the particles. However, that demonstrates that gasoline injectors cannot be used for PDEs where detonations may damage the nozzles. DI injectors are solenoid operated valves that inject gasoline directly into the engine during the air intake stroke, which is a low pressure stage. The DI injectors are designed to operate with fuel line pressures of about 20 MPa (2900 psi) or less. The injectors have thin slit nozzles of about 0.26 mm width and the high pressure creates a rapid expansion that vaporizes the fuel as they are injected in fan-shaped spray patterns. Typical SMD sizes quoted are in the range of 10 to 100 μm for gasoline.

As mentioned earlier in Section 3.4, the ignition delay of fuel droplets in the millimeter range can be from a few milliseconds to a few seconds, whereas at around 10 μm, which is in the optimum range of SMD for detonations[186], the ignition delays drop to a few fractions of a microsecond. Moreover, for detonations in jet fuel to occur, the SMD is known to be about 3 μm for fuel-air mixtures and about 10 μm for fuel-oxygen mixtures[186]. Therefore, a capable injector is needed to vaporize kerosene or jet fuel. Diesel injectors may work much more effectively than DI gasoline injectors with kerosene or jet fuel (which have lower densities and slightly lower surface tension values than diesel[52]), because in diesel engines, the fuel is injected into the engine cavity at the end of the compression stroke, under much higher pressures than gasoline engines. Common-rail diesel injectors (CRDI)[158] are designed to operate with fuel line pressures reaching as high as 200 MPa (29,000 psi). The diesel injectors enable the fuel to be injected in the vapor form into the engine at the end of the compression stroke.

Moreover, such high pressure ratings mean that CRDIs may be able to survive the shock pressures in PDEs, where the pressures have not been reported to go beyond the range of 6.9 MPa (1000 psia) to 13.8 MPa (2000 psia). Direct diesel injectors are also designed to be directly mounted on the engine. However, cooling features for the valves will have to be provided for a PDE application.

Diesel injectors can be operated at high frequencies, capable of 50 Hz or more. In a PDE, an array of high-pressure diesel fuel injectors can be used, all firing simultaneously or in a series sequence to achieve optimum fill rates and mixing. One scheme that utilizes multiple fuel injectors to achieve faster fill rates at higher frequencies is as shown in Figure 8.17. In this configuration, two sets of valves are used, with each set being actuated only once per clock pulse. All the valves are connected to a common-rail type manifold carrying fluid at a high pressure. In a particular clock pulse, the first set of valves is actuated first, and then they remain idle for the second half of the period. During this time, the second set of valves is actuated. Thus, even though each set of valves only operate once per clock pulse, that is, at the same frequency as the clock pulse, the combined frequency of operation is twice the clock pulse rate.

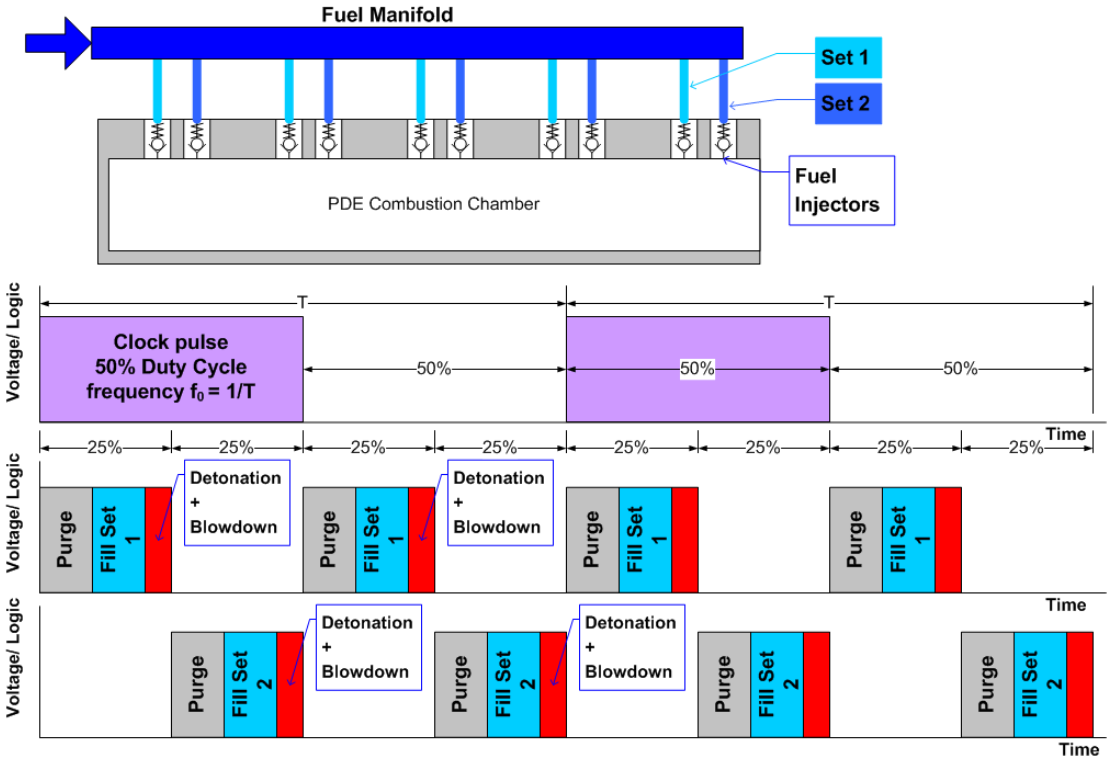

Figure 8.17 A schematic of the staggered injection scheme to increase the frequency of operation, along with the TTL control signals or timeline of valve operation. In one clock pulse, each set of valves operate only once, but the combination results in a frequency that is twice the clock pulse rate.

The nozzle of the valve can be designed to produce swirl shaped spray patterns. Studies using valve designs in which two fluids (liquid-liquid or liquid-gas) are injected simultaneously, through a coaxial nozzle, have shown to be successful at reducing droplet size and mixing[159,160]. This concept can be used in PDEs too, with some bleed air being used to assist in the liquid fuel injection. Furthermore, if fuel sensitizing agents, such as hydrogen, are added to the liquid fuel to reduce DDT distance and ignition delays, such dual fluid swirl-injectors would be an ideal choice.

8.7 Pressure Regulator to Prevent Line Pressure Drop and To Maintain Flow Rates

It is observed that when a large valve or multiple smaller valves are opened simultaneously, the pressure expansion travels back into the supply lines causing a drop in

pressure in the supply lines. If the supply lines are large in diameter, even small flow rates will drop the pressure; and unless the original supply pressure is very high, the drop will be significant. However, if the lines are small, the flow rates and the pressure loss are smaller. Figure 8.18 shows pressure and temperature readings taken at sonic nozzles located about 2 to 3 meters upstream of the injectors, which were mounted to the dual-stage PDE. It is seen that as the PDE is started at a frequency of 10 Hz, the pressure in the lines drop significantly, throwing off the fuel-oxidizer ratio that was set before the test. The line pressures can be seen to rise immediately after the PDE is stopped towards the right of the figure.

As explained earlier in Section 8.5, the mass flow is inversely proportional to frequency, because the valves are open for shorter periods of time. Since the mass flow rate is proportional to the square root of the pressure difference, the supply pressure has to be increased to meet higher flow requirements. Therefore, if a PDE is suddenly accelerated to a higher velocity, the pressure in the supply lines have to be boosted to meet the flow rates required.

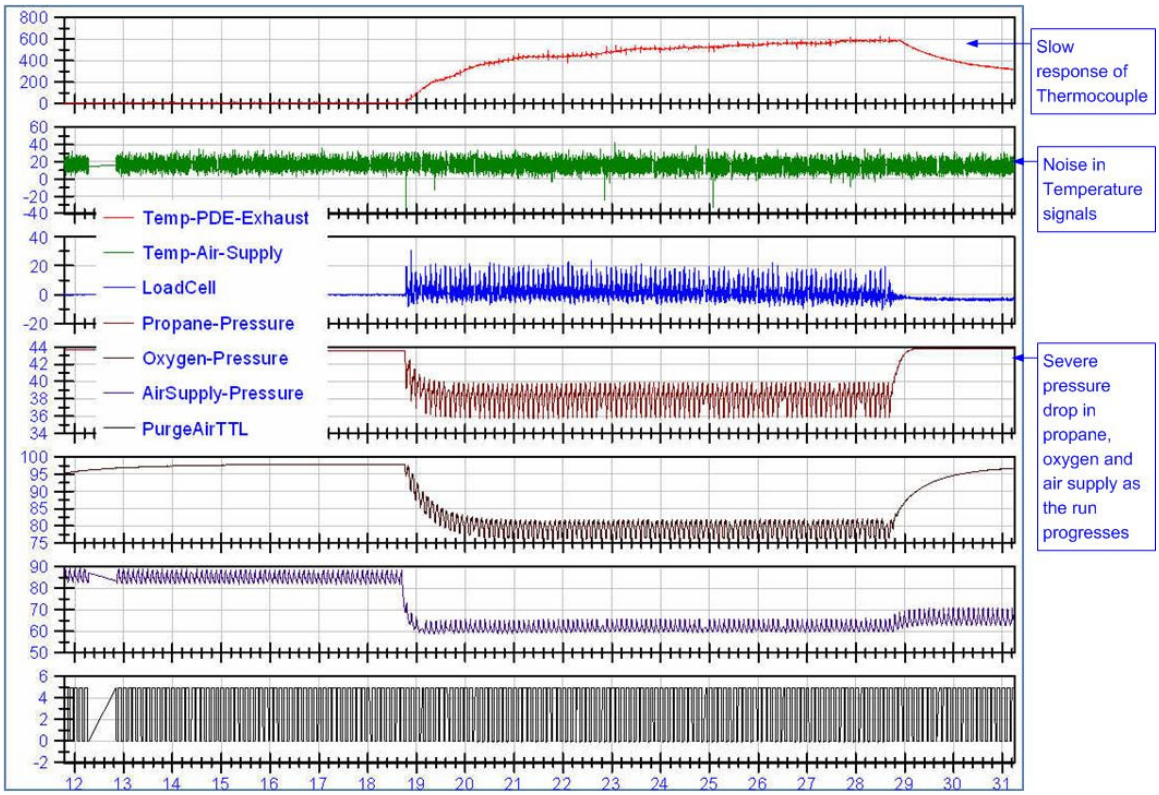

Figure 8.18 The dramatic drop in line pressures of propane, oxygen and air supply is seen during a test of the dual-stage PDE at 10 Hz. Also in evidence is the effect of the noise on the thermocouple signal as soon as the purge-air valves are turned on.

The above problems can be alleviated if a closed loop feedback pressure regulator is installed in the line. This sort of system requires a high pressure fluid pump to maintain a very high pressure in an accumulator upstream of the pressure regulator. A pressure sensor downstream of the pressure regulator monitors the pressure and then activates the pressure regulator to increase the supply pressure to the valves. Pulse width modulated (PWM) regulators are used in many industrial and vehicular applications. Such devices will be required in the fluidics system of PDEs. A schematic of such a system is shown in Figure 8.19. The line pressure will be adjusted to meet the mass flow rate required by the controller of the engine (or the aircraft).

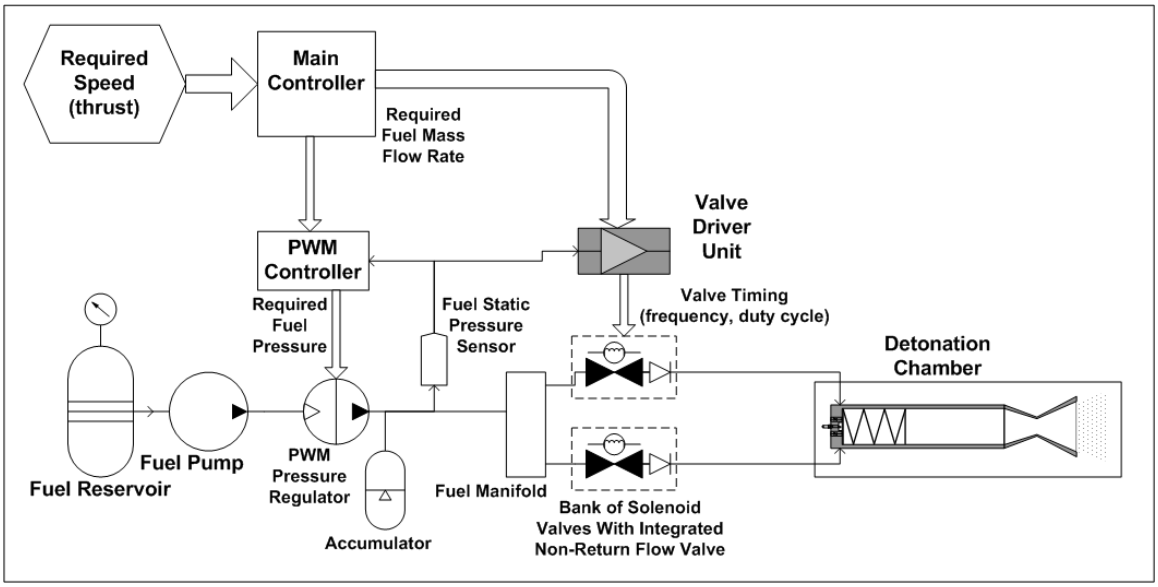

Figure 8.19 Schematic of a pulse-width-modulated pressure regulator system to control the line pressure on a PDE.

8.8 Summary

Rotary valves and solenoid valves were studied. The rotary valves were found to have problems with sealing, high friction and slippage of the rotors. These faults were ascribed to improper machining and design. However, a properly designed rotary valve can achieve high speeds and simple operation. If the rotary valve is rotated by means of a stepper motor, modulation of the valve cycles can be made possible. Rotary valves offer less obstruction to the flow and therefore can handle larger flow rates.

Compact gaseous and liquid-fuel solenoid valves were studied. The gasoline injectors studied were, however, not effective in vaporizing the fuel, possibly due to damage of the slit nozzles. The gaseous valves were effective in fast operations enabling the compact PDE Mark 2 to be run at speeds of up to 30 Hz. However, at higher speeds, valves positions were found to be out of phase with the control signals. One method has been suggested to enable high speed operation of solenoid valves. However, solenoid valves can be used for low flow rate fluids, such as fuels only. In a PDE, a combination of rotary valves, for air injection, and

solenoid valves, for fuel injection, will be required for the effective filling and purging of the engine.

In the study, it was found that at higher frequencies, the mass flow per cycle decreased if the supply pressures were held constant at the same pressures as at the low frequency runs. The reduced mass flow was identified as the cause of detonation failures at higher frequencies, because the detonation chamber was not being fully filled. Also, when the valves to the detonation chamber were opened, the supply pressures in the gas lines were seen to drop because the flow rates could not be sustained by the gas supply system. An electronically controlled pressure regulator along with a high pressure fluid pump can modulate the supply line pressures to meet the higher mass flow requirements at higher frequencies and offsetting any momentary drop in line pressure when the valves are opened suddenly.

CHAPTER 9

STUDY OF DIAGNOSTICS, INSTRUMENTATION, DATA ACQUISITION AND CONTROL SYSTEM FOR PDE GROUND DEMONSTRATORS

9.1 Requirements For a PDE Control System

It has been well established that single-shot experimental observations confirm C-J theory, as seen in Section 2.2. Therefore, it may be possible for a PDE to be operated and controlled using the C-J detonation relations as a basis, with the help of a fast-acting, closed loop control system. The processes that can be controlled, however, are entirely gas dynamic, such as initial pressure, temperature and mixture composition. In addition the ignition timing and energy level can also be controlled. The control of initial pressure and mixture composition are achieved by implementing proper valving and injection techniques. The mass of fuel entering the engine can be controlled by modulating the pressure in the supply lines and varying the duty cycle of the fuel valves. Similarly, the mass of air entering the combustor can be controlled by varying the duration of the valve-open time. The controller can, therefore, meter the amount of fuel-air entering the combustor and control the fuel-air ratio. The initial temperature can be controlled by designing the geometry to transfer heat from the engine to the fuel and incoming air (i.e., using fuel or air to cool the engine) or by using a heater to heat the fuel and air. The ignition energy can be controlled with the help of a variable-energy ignition source. Once the input parameters have been set for a particular cycle of the engine, a diagnostics system is required to determine if detonation has been successful by measuring the detonation wave speed and comparing it with the value computed for the initial conditions based on C-J properties. The controller can then determine and adjust the input parameters for the next cycle to meet the required thrust or speed.

9.1.1 Application of C-J Detonation Theory For PDE Control and Diagnostics

The control system needs measurements of properties of the air and fuel going into the engine, including pressures, temperatures and mass flow rates. The variables denoting the initial conditions in the combustor are given the subscript 1 and all post-combustion or post-detonation variables are given the subscript 2 in this analysis. The mass flow rates of air, $\dot{m}_a$, and fuel, $\dot{m}_f$, are required to determine the composition of the reactive mixture. The flow composition along with the initial pressure p_1 and temperature T_1 are needed to determine thermodynamic properties of the mixture in the combustor, including specific gas constant R_1, specific heat ratio γ_1 and specific heat capacity at constant pressure c_{p1}. Thus, these values can be expressed as functions of the mass flow rate and initial temperature as shown below.

$$R_1 = R_1(T_1, \dot{m}); \quad \gamma_1 = \gamma_1(T_1, \dot{m}); \quad c_{p_1} = c_{p_1}(T_1, \dot{m}) \tag{9.1}$$

The density ρ_1 and the specific enthalpy h_1 of the original reactive mixture can be obtained using the perfect gas law from p_1 and T_1 as

$$\rho_1 = \rho_1(p_1, T_1); \quad h_1 = h_1(p_1, T_1) \tag{9.2}$$

The net heat added per unit mass of fuel-air mixture ($q = h_1 - h_2$) is obtained as a function of the fuel's heating value, the initial temperature T_1 and the mass flow rates of fuel and oxidizer.

$$q = q(\dot{m}_f, T_1) \tag{9.3}$$

Thus, by measuring p_1 and T_1 and the flow rates, all the initial conditions can be computed, making it possible to compute the post-detonation conditions using C-J relations. The final states and flow properties can be expressed as functions of the detonation Mach number M_1 as shown below.

$$p_2 = p_2(M_1); \quad T_2 = T_2(M_1); \quad \rho_2 = \rho_2(M_1) \tag{9.4}$$

$$R_2 = R_2(M_1, \dot{m}); \quad \gamma_2 = \gamma_2(M_1, \dot{m}); \quad c_{p_2} = c_{p_2}(M_1, \dot{m}) \tag{9.5}$$

The detonation wave speed can be measured using a number of sensors, including dynamic pressure transducers, ion detectors, photo detectors, etc., using the time-of-flight (TOF) method and the Mach number can be calculated. If the measured wave speed is within an acceptable margin or error, the engine cycle may be deemed successful. Thus, the CJ relations and the minimum number of variables measured may be sufficient enough to effectively control a PDE with the help of a suitable control system as described above. It may be said that, for the successful implementation of PDEs in the near future three essential elements are required, namely, an intelligent control system containing a fast, compact computer, fast-acting, durable actuators (valves) and fast, accurate and precise sensors and instruments that can survive in the harsh detonation environment.

9.1.2. Digital Controllers and Diagnostics Instruments For PDEs

The sampling rate of sensor signals is based on the Nyquist-Shannon sampling theorem[161] which requires that a signal of frequency f must be sampled at a rate of $2f$ or more in order to prevent aliasing. A characteristic frequency f_c for a transducer can be defined as the inverse of the time period of the residence of a physical phenomenon over the sensing element of the transducer, i.e., $f_c = 1/t$. In the case of a detonation wave, t is the time required for the wave to traverse the width of the sensor, as shown in Figure 9.1. Thus, the smaller the sensing surface of the transducer, the higher is the characteristic frequency of the transducer for the particular physical phenomenon. Table 9.1 shows the range of characteristic frequencies for various wave speeds and sensor dimensions.

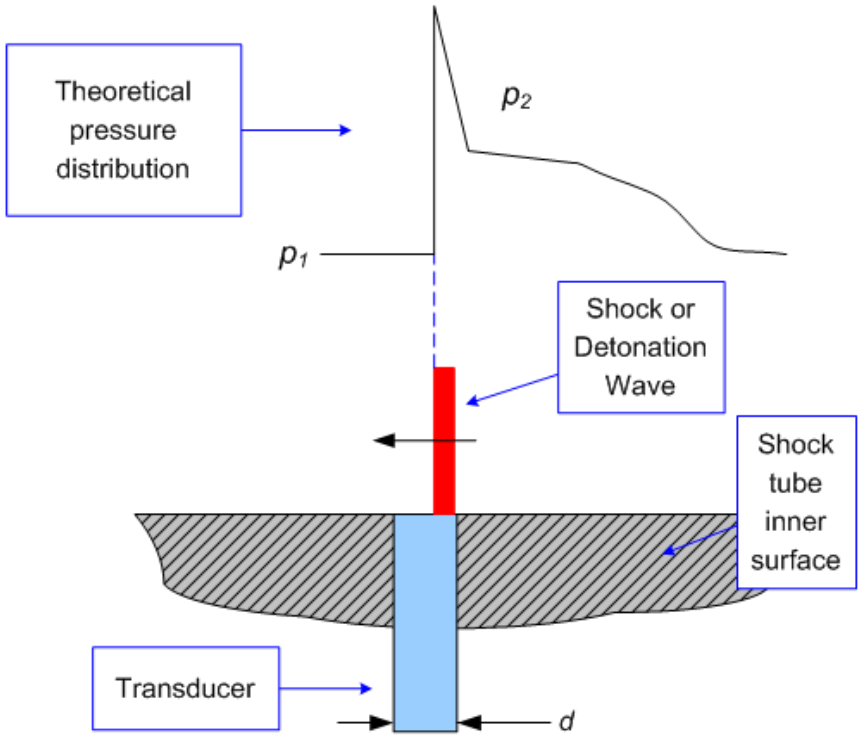

Figure 9.1 Schematic of a detonation wave moving over the sensing surface of a transducer, going right to left. The pressure profile before and after the wave is shown on top.

Table 9.1 Characteristic frequencies for various wave speeds and sensor widths.

	Velocity, m/s												
d, mm	**500**	**1000**	**1500**	**1750**	**2000**	**2250**	**2500**	**2750**	**3000**	**3500**	**4000**	**4500**	**5000**
0.1	5000	10,000	15,000	17,500	20,000	22,500	25,000	27,500	30,000	35,000	40,000	45,000	50,000
0.2	2500	5000	7500	8750	10,000	11,250	12,500	13,750	15,000	17,500	20,000	22,500	25,000
0.5	1000	2000	3000	3500	4000	4500	5000	5500	6000	7000	8000	9000	10,000
1	500	1000	1500	1750	2000	2250	2500	2750	3000	3500	4000	4500	5000
1.5	333.3	666.7	1000	1167	1333	1500	1667	1833	2000	2333	2667	3000	3333.3
2	250	500	750	875	1000	1125	1250	1375	1500	1750	2000	2250	2500
2.5	200	400	600	700	800	900	1000	1100	1200	1400	1600	1800	2000
3	166.7	333.3	500	583.3	666.7	750	833.3	916.7	1000	1167	1333	1500	1666.7
3.5	142.9	285.7	428.6	500	571.4	642.9	714.3	785.7	857.1	1000	1143	1286	1428.6
4	125	250	375	437.5	500	562.5	625	687.5	750	875	1000	1125	1250
4.5	111.1	222.2	333.3	388.9	444.4	500	555.6	611.1	666.7	777.8	888.9	1000	1111.1
5	100	200	300	350	400	450	500	550	600	700	800	900	1000
6	83.33	166.7	250	291.7	333.3	375	416.7	458.3	500	583.3	666.7	750	833.33
7	71.43	142.9	214.3	250	285.7	321.4	357.1	392.9	428.6	500	571.4	642.9	714.29
8	62.5	125	187.5	218.8	250	281.3	312.5	343.8	375	437.5	500	562.5	625
9	55.56	111.1	166.7	194.4	222.2	250	277.8	305.6	333.3	388.9	444.4	500	555.56
10	50	100	150	175	200	225	250	275	300	350	400	450	500

The detonation wave speeds can be measured by calculating the TOF velocity of the wave and this can be achieved with dynamic pressure transducers, ultra-fast thermocouples (1 μs response or better), photo-detectors (to detect the flame speed) and ion-detectors (to detect the flame or wave speed). All these sensors will be looked at in more detail in the following sections. Detonation velocity measurements require fast-acting sensors and higher sampling rates, because the detonation travels over the sensors at very high velocities in the range of 1500 to 2500 m/s. For example, the C-J velocity of a stoichiometric propane-oxygen mixture is 2357 m/s. At that speed, the detonation would traverse a 4 mm wide transducer in $1.7\,\mu s$, giving it a characteristic frequency of 589.25 kHz.

The choice of the transducer also has to take into account the response time and the natural frequency of the transducer. This can be done by looking at a magnitude vs. frequency chart and the corresponding phase difference vs. frequency chart for second order systems, as shown in Figure 9.2. Most transducers are designed to have a damping ratio of close to 0.7. It can be seen from the magnitude vs. frequency ratio chart that for a 5 % margin of error, the characteristic frequency must be only 60 % of the natural frequency ($f_c = 0.6 f / f_n$). Therefore, for the above example, the natural frequency of the transducer should be 982.08 kHz. And the sampling rate should be twice the characteristic frequency of 1178.5 kS/s. Thus, it is evident that the sensors used for the detonation wave diagnostics must be sampled at a high rate, 1 to 2 MS/s or higher.

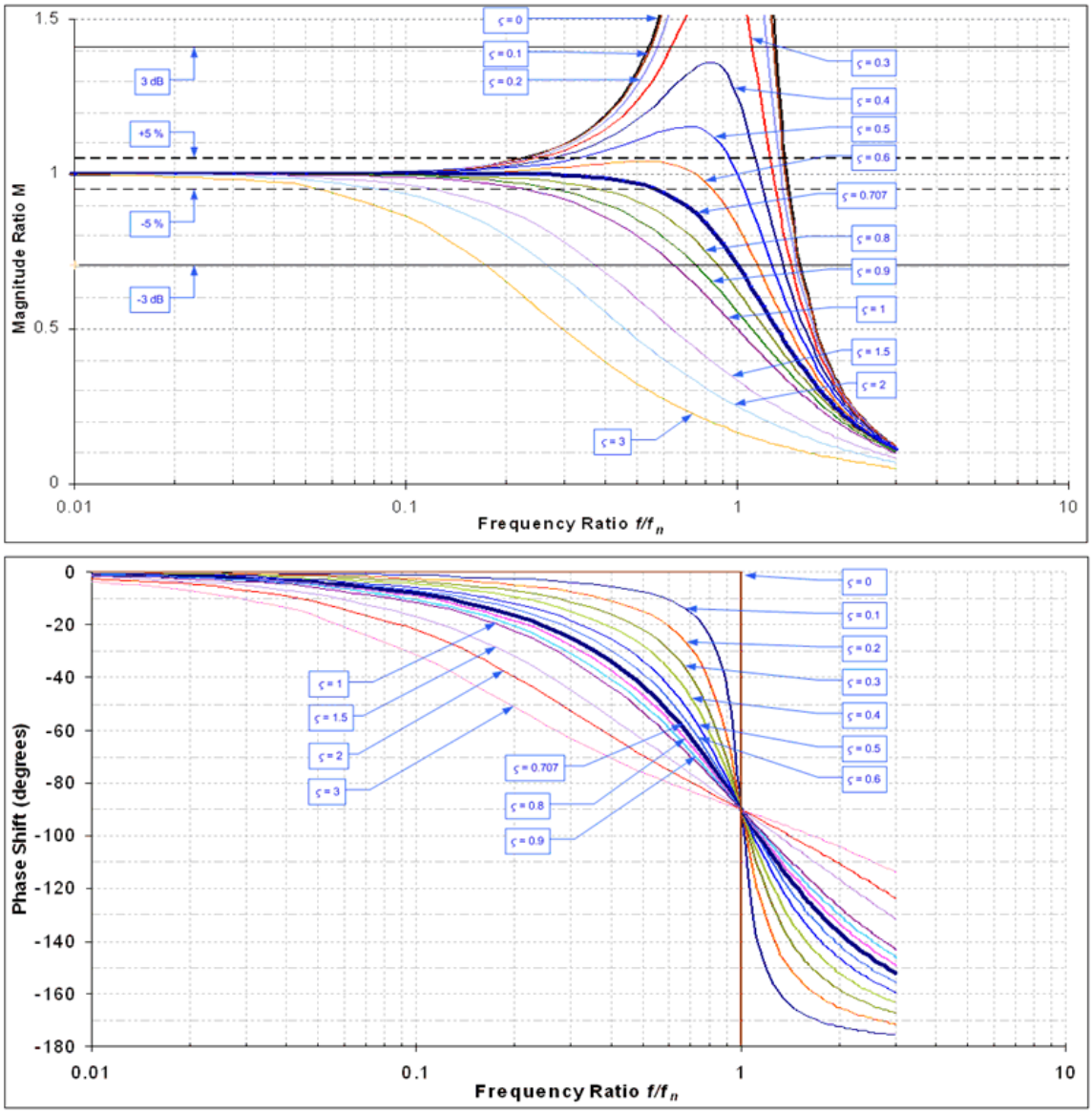

Figure 9.2 Plot of magnitude vs. frequency ratio (top) and phase shift vs. frequency ratio (bottom) for second order systems.

Pressure and temperature variation in the inlet ducts and in the engine during filling is relatively slow. The static pressure may fluctuate in the inlet ducts during valve operation, which occurs at the operating frequency of the PDE, with some higher harmonics present. The frequency of PDE operation shall not likely exceed a few hundred Hz. Therefore, the sampling rates for pressures and temperatures of the fluid flow to the engine can be set in the region of 1

to 10 kS/s. Mass flow rate sensors can also be sampled at the lower rate of 1 to 10 kS/s as the flow velocities are subsonic. The low frequency sensors can be multiplexed using one (or more) high speed sampling devices to conserve bandwidth of the DAQ. In addition, the transducers used for measuring the flow properties within the inlet and the supply ducts or tubes do not have to endure shock loading as opposed to the high pressures and temperatures that the sensors within the combustor are subjected to. Therefore, they do not need cooling or protective housings.

Thus, a typical diagnostics system will have various sensor systems being monitored at different sampling rates. This method of multiple sampling along with multiplexing techniques can save computing resources for a PDE controller.

9.2 Dynamic Pressure Transducers

The dynamic pressure transducers used in this study were the piezoelectric type model 111A24 from PCB Piezotronics, Inc. The transducers are rated to have a natural frequency greater than 400 kHz, with a response time less than 1.5 μs. The damping ratio is calculated to be in the region of 0.7 to 0.95. The pressure transducers have a range of 6895 kPa (1000 psi). Their operating temperature range is only -73 to 135 °C (-100 to 275 °F), with a flash temperature rating of 1649 °C (3000 °F). The operating temperature range is a very small window that is easily exceeded in combustion studies.

Piezoelectric transducers have fast response and small size, but they do not work well in high temperature environments. Piezoelectric transducers have a crystal element which is pre-stressed to a precise value. A schematic of the piezoelectric transducer is shown in Figure 9.3 (c). When the transducer is exposed to heat, the housing expands and the stress applied to the crystal element inside becomes distorted. As a result, the pressure readings show an increasing error, also known as thermal drift, which persists for as long as the transducers are exposed to the heat. The effect of thermal drift is clearly visible in Figure 9.4, which shows the pressure history from a 15 Hz run of the PDE Mark 2 with stoichiometric propane-oxygen

mixtures. The total test time of the PDE lasted about 15 s, and the 5 s long data capture process was started about 3 to 5 s after the engine was started. The initial thermal shock causes the output of the transducer to go to a low negative value which is then followed by a monotonic rise in the base pressure line with time. The PDE tests were limited to short durations because the piezoelectric transducers may get permanently damaged within a few minutes of continuous exposure to extreme temperatures. Therefore, for high temperature settings, these pressure transducers have to be installed inside a water-cooling envelope. There are two types of cooling enclosures available from the manufacturer, one that has the sensing surface flush with the enclosure, so that the pressure transducer is installed inside the combustor with the sensing surface exposed, and another that recesses the pressure transducer inside the housing. In the latter design, a small orifice extends from the face of the enclosure that is exposed inside the combustor, to the sensing surface of the transducer. The cooling enclosures may have circulation of high-pressure cooling fluid, as shown in Figure 9.3 (a) and (b), to increase the heat transfer rates, thereby extending the test time of the transducer. In some variations, the orifice is continually injected with an inert gas, such as helium, to cool the surface of the pressure transducer. The methodology of helium injection is shown in Figure 9.3 (a) in which both water cooling and helium bleed are incorporated into the transducer's cooling enclosure. The manufacturer claims that the helium, having a higher speed of sound than air, increases the response time of the recessed transducer configuration[162]. Helium bleed may also be adapted for PDE use by drilling a tiny helium injection channel into the port of the transducer, as shown in Figure 9.3 (b). This method can be applied to protect other kinds of transducers also, including photo detectors.

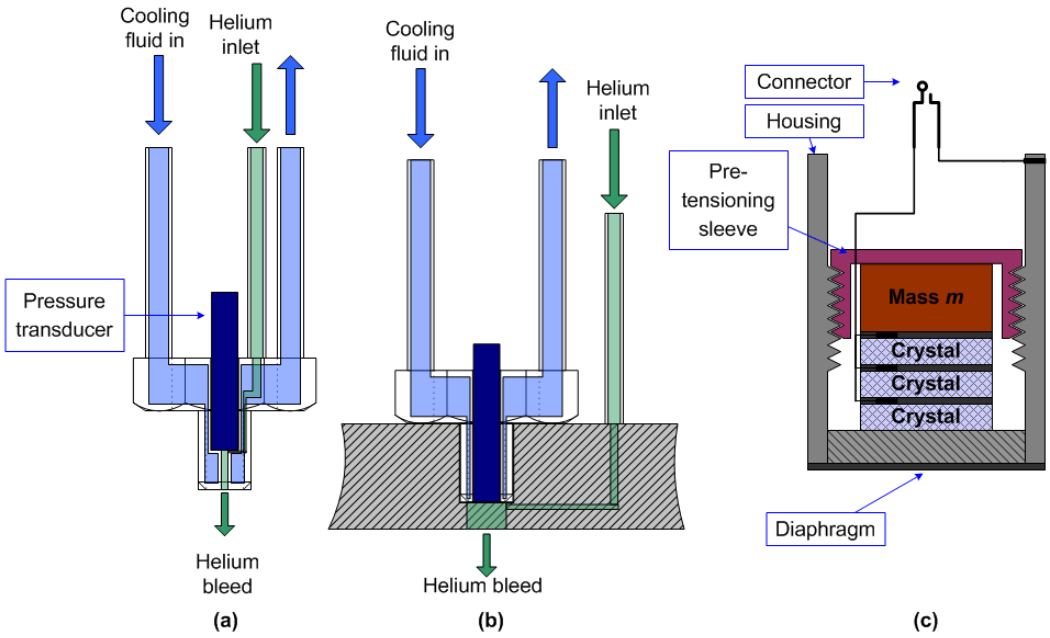

Figure 9.3 Schematic of a recessed water-cooling envelope (a) and a flush mounted water-cooling envelope (b) for pressure transducers are shown. The schematic of a piezoelectric pressure transducer is on the right hand side in (c). Figures (a) and (b) also show how helium bleed is used to protect the sensing surface from heat.

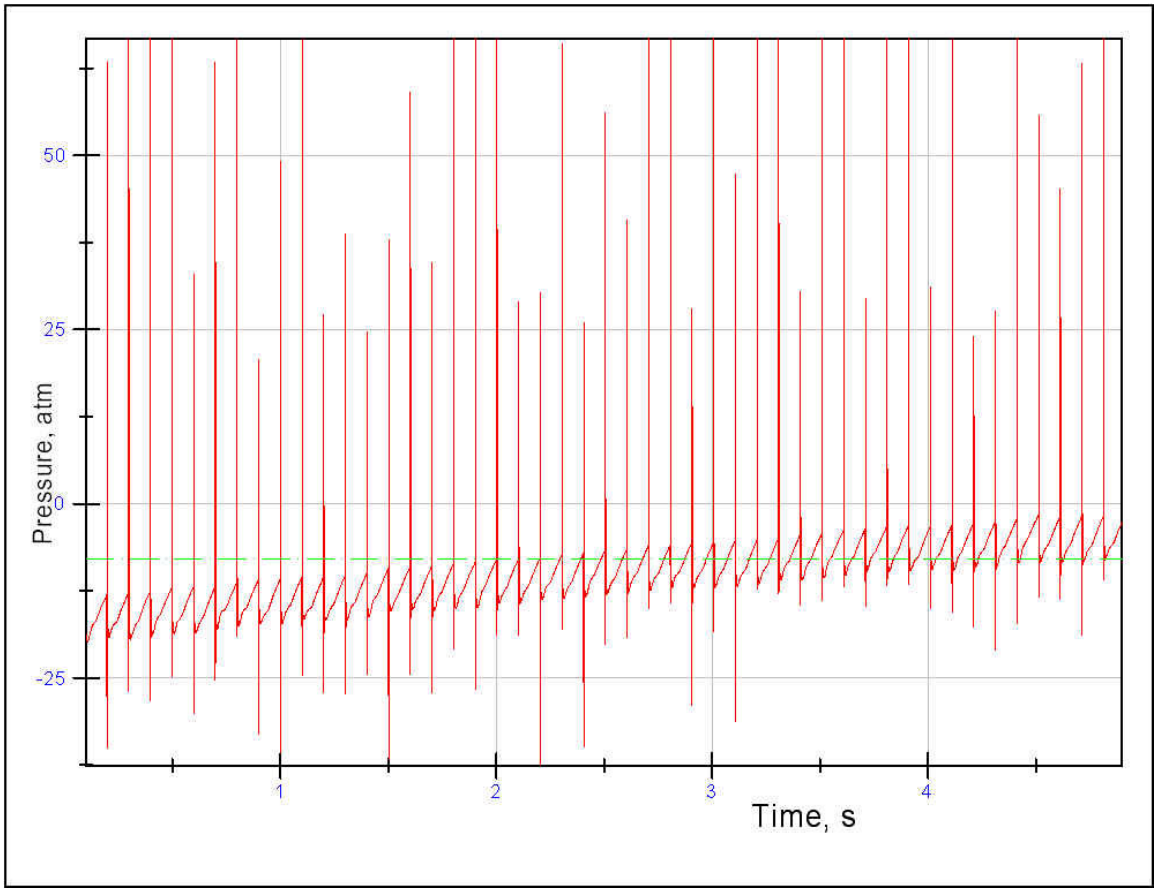

Figure 9.4 Pressure history from a 15 Hz test of the PDE Mark 2 with stoichiometric propane-air showing pronounced thermal drift in the readings.

The recessed cooling enclosure obstructs part of the sensing surface, as seen in Figure 9.2 (a) and Figure 9.5 (right), whereby only a small fraction of the original surface is visible through the orifice, effectively reducing the area of the sensing surface. As a result, the residence time of the detonation wave over the sensing surface is shortened, thereby increasing the characteristic frequency. The transducer has less time to respond to the impulse. The recessing also causes the transducer to produce an attenuated response to the pressure, such that the pressure peaks are lower than the flush-mounted versions. Furthermore, the dead air pocket inside the recess orifice acts as a damper to the pressure waves, which results in a reduction in the amplitude of the pressure waves. The column of gas in the recessing passage causes attenuation of the high frequency pressure fluctuations, including shock and detonation

waves, increases the rise time of the transducer and causes ringing to occur within it, as seen in Figure 9.7 (top). The attenuation increases as the frequency of the pressure fluctuations approaches the resonant frequency of the orifice[182-185]. The resonant frequency of the recessing passage depends on the type of gas trapped within it and its temperature. The recessing passage may be modeled as a closed end pipe whose depth is equal in length to the quarter wavelength of a resonant standing wave. Thus, the resonant frequency may be expressed as

$$f_n = \frac{a}{4h} = \frac{\sqrt{\gamma RT}}{4h} \tag{9.6}$$

where a is the speed of sound in the gas trapped within the passage, is the depth of the passage, γ is the ratio of heat capacity, R is the universal gas constant and T is the temperature of the gas. The rise time is about a third of the time period of the resonant frequency and may be expressed as

$$t_r \approx \frac{1}{3f_n} = \frac{4h}{3\sqrt{\gamma RT}} \tag{9.7}$$

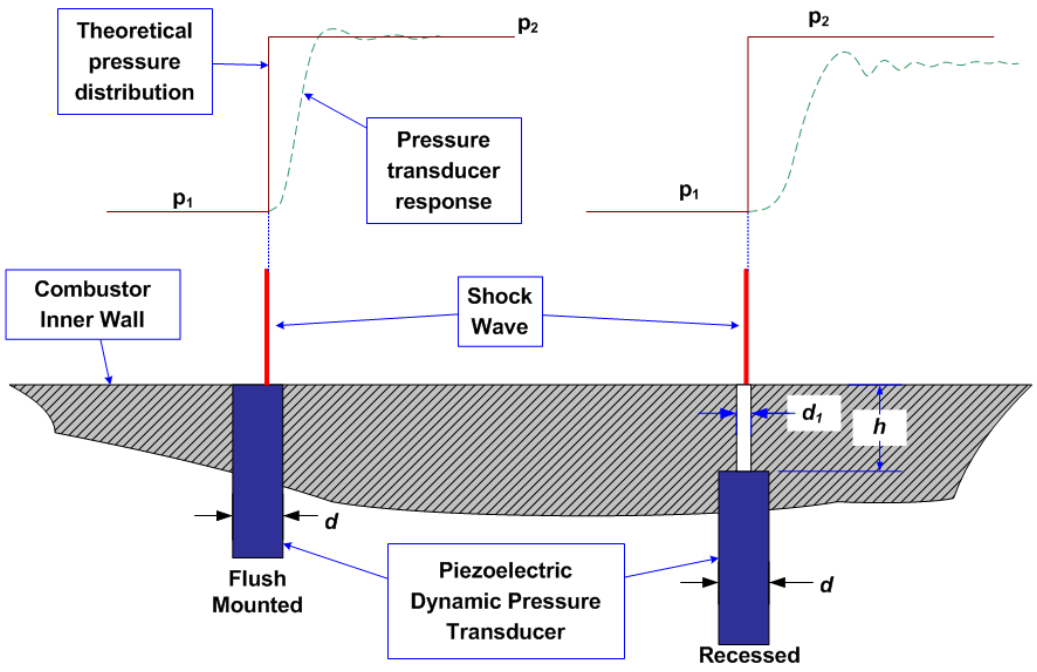

Figure 9.5 A schematic of the flush and recessed pressure transducer.

In summary, the effects of the cooling enclosure are:

1. Attenuation of the detonation wave pressure.
2. Reduction of sensitivity of the transducer.
3. Reduction in the response time of the transducer.

The effects of the recessing of the transducer can be seen clearly in Figure 9.6, where the recessed transducers show attenuated pressure traces, with less definition than that of the flush mounted transducers.

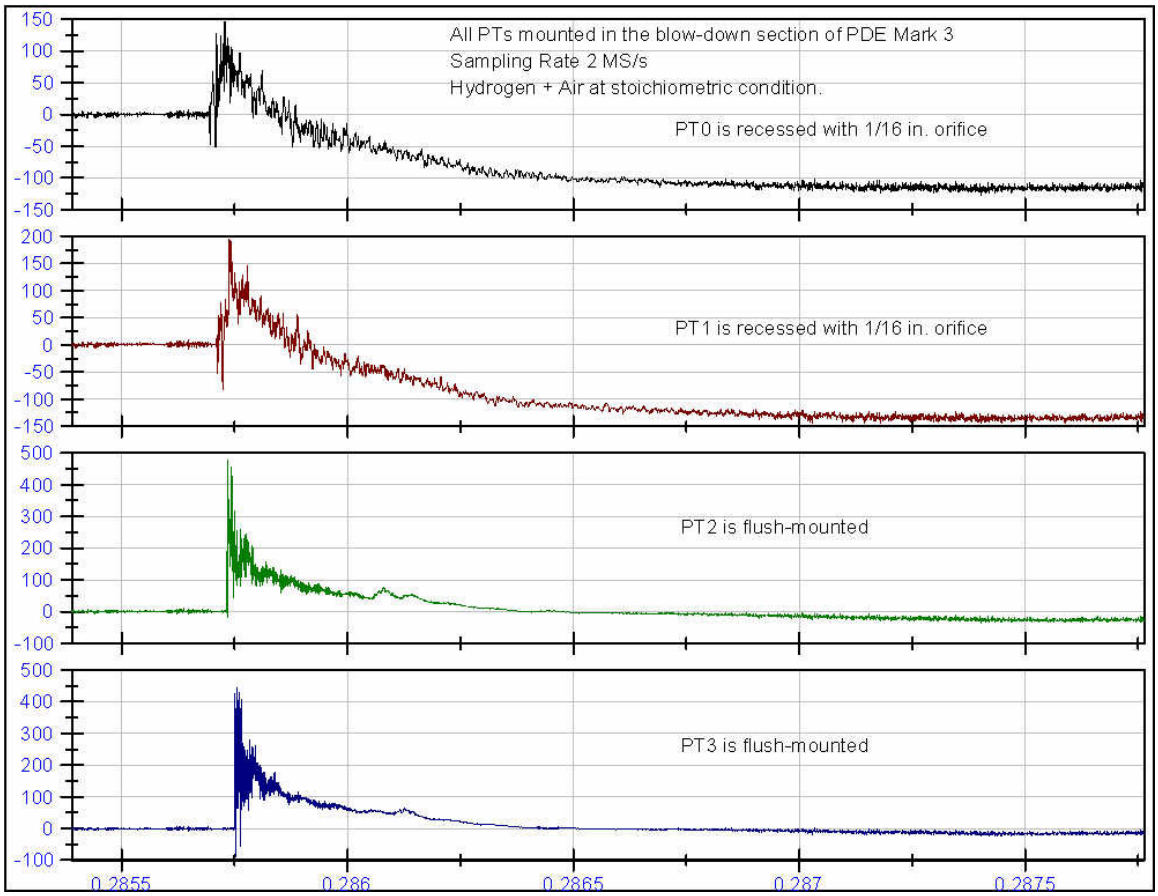

Figure 9.6 A sample pressure history from a test of the PDE Mark 3 running in single shot mode, showing the difference in pressure readings from flush-mounted and recessed pressure transducers. The recessed pressure transducers have delayed and attenuated pressures and less definition. The surface flush-mounted transducers show well defined and taller pressure waves.

However, the reduction in sensitivity and the attenuation of the pressure can be compensated by calibrating the recessed transducers against a flush mounted transducer to develop a correction factor that may be applied to the signals of recessed transducers[182]. Hence, the recessed actively cooled pressure transducers can still be recommended for PDEs for measuring detonation pressures and more importantly the detonation velocities. For TOF determination of wave speeds, faster-acting transducers, such as the PCB High Frequency Shockwave/Blast/Explosion range of pressure transducers with integrated electronics[162], may be suitable as these have rise times rated at less than 1 μs. Also, it is recommended that an

active cooling system, which is comprised of a miniature refrigeration system, be applied to cool the pressure transducers in a cooling enclosure. This type of system on a PDE could use propane as the refrigerant, as propane refrigerants are said to be more efficient than refrigerants, such as R134a, R22, etc.

Figure 9.7 shows the response of the same pressure transducer for two different sampling rates. The figure on top shows pressure history from a test using the PDE Mark 2, with a sampling rate of 240 kS/s. The figure on the bottom is from the PDE Mark 3 at a sampling rate of 2 MS/s. Both tests used stoichiometric propane-oxygen mixtures. It is clearly evident that the definition of the wave profile is much better at the higher sampling rate. The higher sample rate case on the bottom shows indications of wave reflections, while in the lower sampling rate case, it is difficult to make out any phenomenon clearly. The error in the TOF calculations associated with the lower sampling rate is also much higher[25]. Appendix D shows the calculated uncertainties in the TOF velocities for the various sampling rates.

The higher sampling rate of 2 MS/s results in more than an eight fold increase in the amount of data compared to the 240 kS/s case. At a sampling rate of 2 MS/s, if each sample is kept at the minimum size of 2 B, in the binary format, the size of the data file will be 3.8 MB/s per channel. However, the sample word sizes are usually about 4 B or 8 B, as the data packet has other information, including time, and sampling rate, error correction codes, etc. Higher precision formats may increase the size of each record or sample point to 8 B (64 bits) in the case of the double-precision floating point representation, or 80 bits in the case of the extended double-precision floating point representation. If mathematical operations are required to be performed on the data, including processes such as FFT, auto-correlation or cross-correlation, the storage and processing resources will be enormous if performed in real time. A dedicated mathematics processor will be required for speeding up the mathematical operations.

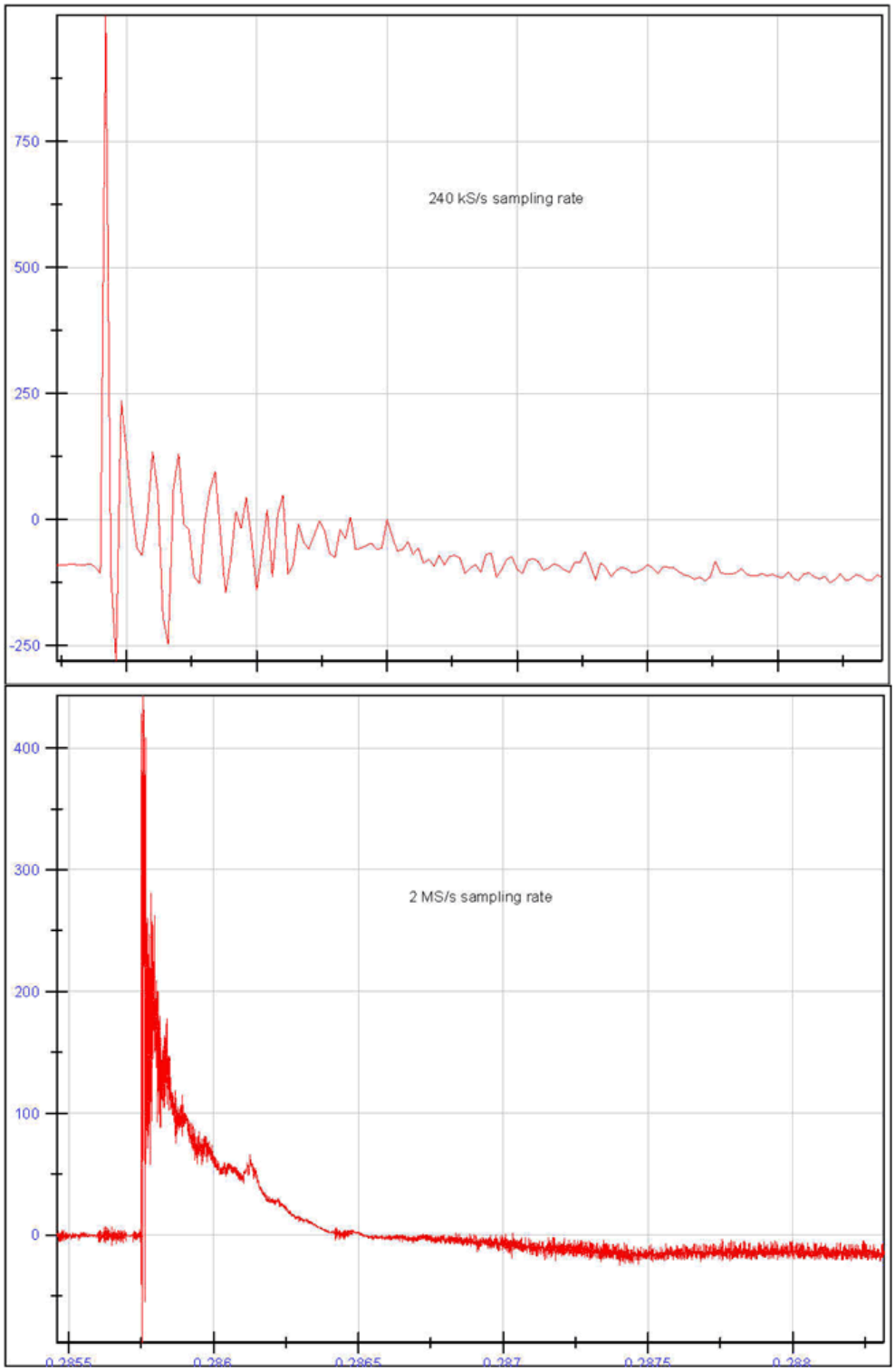

Figure 9.7 A sample single detonation wave pressure trace sampled at 240 kS/s (top) and 2 MS/s (bottom).

9.3 Optical Transducers

Optical transducers were also studied to detect wave speed by calculating the TOF speed of the flame front as it travels down the detonation tube. In a planar detonation wave, the flame front is coupled closely behind the shock wave. Therefore, a detonation wave passing a pressure transducer and a photo detector will produce sharp pressure and optical peaks respectively. The optical transducers used in this study were assembled, as shown in Figure 9.8. The sensors were Hamamatsu model S1226-BU silicon photo-diodes, which have a square shaped sensing window of 1.1 mm by 1.1 mm. These photodiodes have a spectral operating range of 190 through 1000 nm (violet to red) with a peak sensitivity at 720 nm (red) and suppressed infra-red sensitivity, as shown in Figure 9.9. For combustion, lower visible wavelengths and improved infrared sensitivity would have been preferable, but in this particular application, one of the objectives was to compare the pressure transducer output to the photodiode output for the visible spectrum only, by placing photo detectors and pressure transducers at the same axial locations along the detonation tube. Another aim was to detect the location of DDT by the simultaneous appearance of a sharp pressure spike and a bright visible light signal, which would confirm the coupling of the flame front with the shock front. Prior to DDT, the shock front detected by the pressure transducer would precede the bright flame front that the photo-diode would pick up. After the DDT, both the pressure and the optical transducers should give temporally coincident sharp peaks.

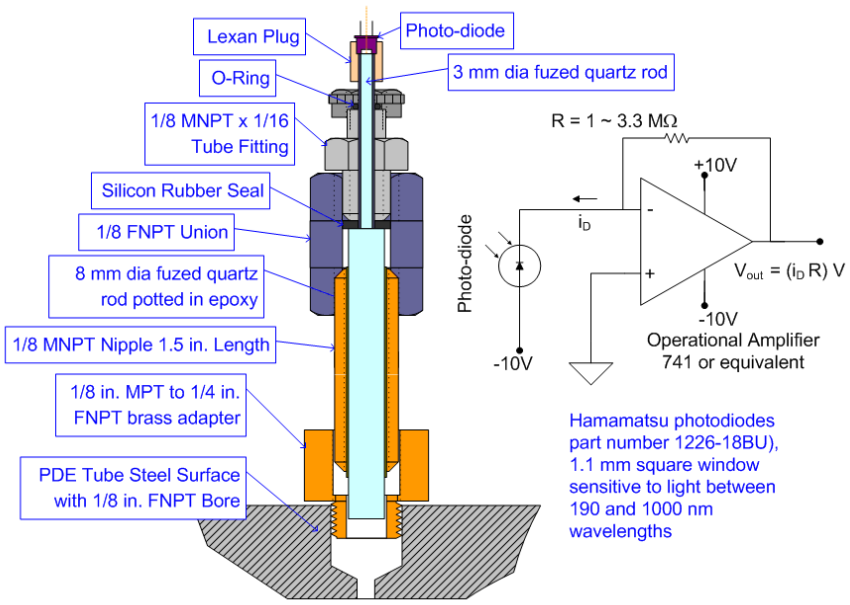

Figure 9.8 Schematic of the hand built optical transducers and the associated circuit diagram used in this study.

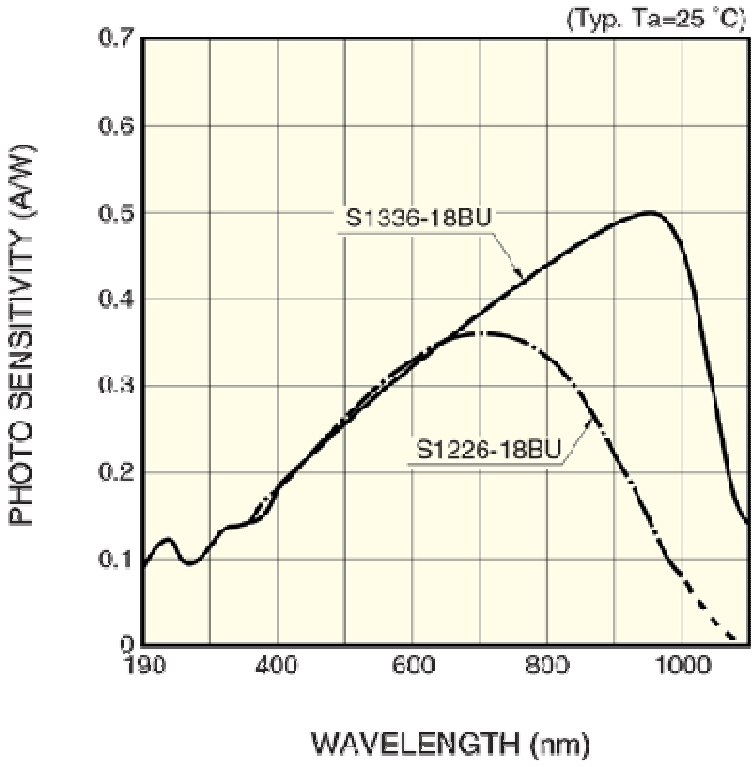

Figure 9.9 The spectral response range of the S1226-18BU photo-diode[163].

The main body of the optical transducer consisted of fused-quartz rods, which are transparent to light ranging from UV to IR. Fused-quartz is resistant to high temperatures and begins to soften only at a temperature of 1950°C. First, 8 mm, 38.1 mm (1.5 in.) long pre-cut and factory-polished fused-quartz rods were inserted into brass ¼ in. NPT nipples and secured tightly in place with epoxy. Another quartz rod of 3 mm diameter was cut and mounted on top of the other rod by means of a tube fitting with an o-ring to cushion the rod, such that the axes of the two quartz rods were in line, as shown in Figure 9.8. This allowed the smaller rod to be taken out when required by unscrewing the fitting. At the bottom end of the brass nipple, a 1/8 in. FPT to 1/8 in. MPT fitting was screwed on tightly. This fitting was used for mounting the transducer into the optical ports on the PDE. The pressure ports and the optical/ion transducer ports were located at the same axial locations along the length of the PDE. The photo-diode was mounted on top of the 3 mm rod by means of a Lexan mounting plug, as shown in Figure 9.8.

The main advantage of photodiode based optical transducers is the speed of response. Photo-diodes with response times much faster than that of piezoelectric pressure transducers are available. The rise time of the photodiode used here is quoted as 0.15 μs. The speed of the circuit is also dependent on the response time of the operational amplifier. In this case, a 741 operational amplifier (op-amp) was used to form a trans-impedance amplifier (also known as a current-to-voltage converter), as shown in Figure 9.8. The op-amp has a bandwidth of 1.5 MHz. The gain of the amplifier was set by the resistor R, which had a value in the range of 1 to 3.3 $M\Omega$. If the value of R is too high, the noise level will become elevated and small light signals will cause the amplifier to saturate. Therefore, the value of R should be kept to about 1 $M\Omega$. With lower amplifier sensitivities, it may be possible to resolve properties of the flame from the wavelength or intensity of the light.

With the above mentioned circuit, the optical transducer was much faster than the dynamic pressure transducer. This may pose a problem if used in tandem with pressure

transducers, because photo-diodes will respond first. If one is not aware of the mismatch in response times, the presence of an optical signal preceding a pressure signal may be interpreted as the shock following a flame front, when in fact the reverse is true. This effect can be clearly seen in Figure 9.10 in which the pressure and optical signals are compared. The pressure transducers and the optical transducers are mounted at the same axial locations along the PDE combustor. However, optical transducer number 2 is seen to respond before pressure transducer PT2 responds to the detonation.

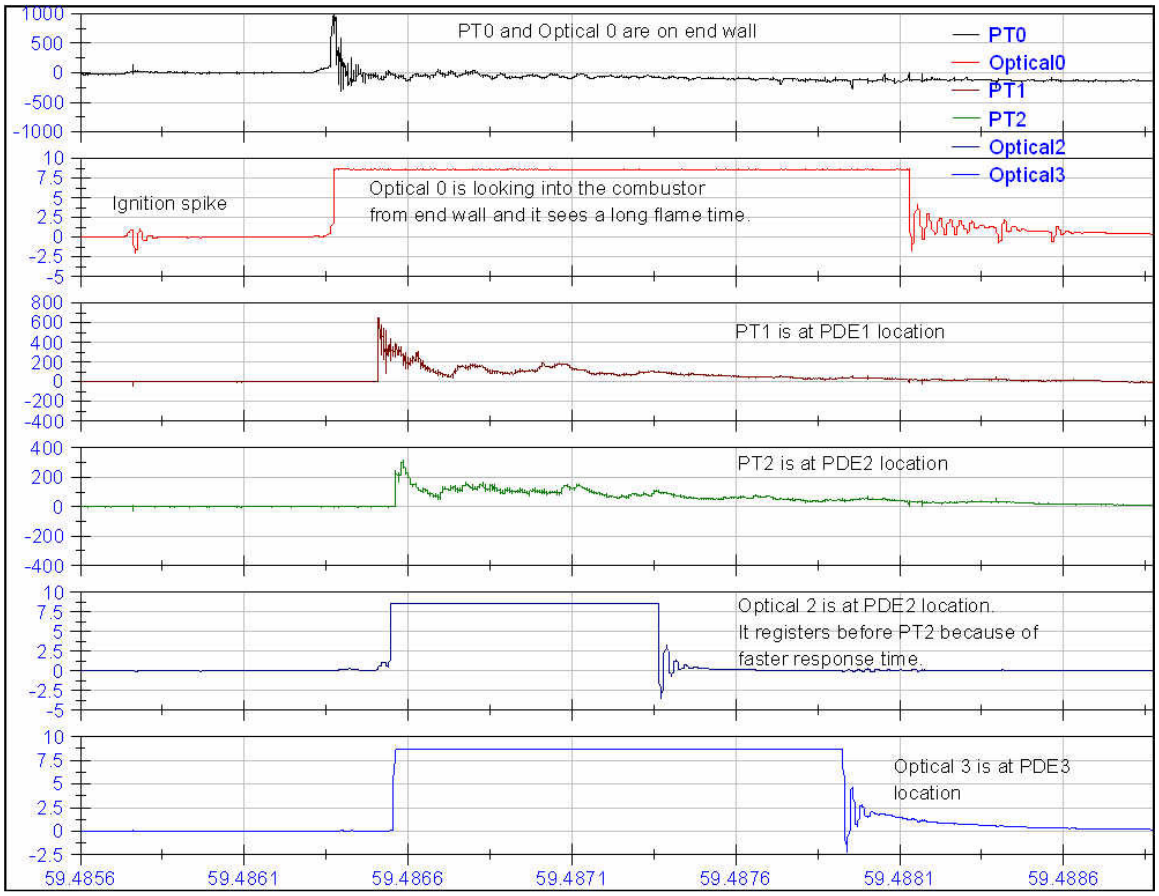

Figure 9.10 A typical set of signal history from the Dual-Stage PDE, showing data from the pressure and optical transducers. The PDE is running at 5 Hz. Although pressure transducer (PT2) and optical transducer (Optical 2) are located at the same axial point on the PDE, the optical transducer shows the step response first due to the faster response of its circuit. See Figure 4.11 for sensor locations.

The optical transducer has some disadvantages. They are difficult and time consuming to build by hand and to make them resistant to the detonation environment. Moreover, if purchased pre-assembled from a manufacturer, optical transducers are likely to be expensive. It is difficult to get a polished flat cut surface on the quartz rod without losing some transparency. The optical transducers are difficult to cool. In this study, the external exposed metal surfaces were wrapped in a wet cloth. The biggest disadvantage of any optical diagnostic system used in combustion environments is that the optical window will get covered up with soot, which will gradually diminish the optical clarity of the glass window. The sensitivity of the transducer will gradually reduce to zero. Therefore, the optical ports need to be cleaned before each test. This is a cumbersome and time-consuming process.

9.4 Ion Detectors

Ion detectors in the form of Langmuir probes are widely used to measure plasma properties, such as ion and electron density and electron temperatures. The electron density is obtained from the probe current and voltage and the electron temperature is determined from the slope of the voltage-current curve, if the voltage is swept across a range of values[164]. Langmuir ion probes are effective in weakly ionized plasma, such as flames, shock waves and detonation waves. The probes are very simple in construction, consisting of a pair of metallic electrodes (dual electrode type) inserted into the region occupied by the plasma, as shown in Figure 9.11 (left). Single probe circuits are also used, as shown in Figure 9.11 (right). The circuit requires a biasing voltage of the order of 10 to 100 V dc applied between the probes, (or probe and ground in case of the single probe type), a resistance to limit the current in case of a short circuit, typically in the 10 kΩ to 1 MΩ range, and a current measuring device, such as an ammeter, that can detect currents in the μA or nA range. The current detected will be proportional to the voltage and the surface area of the exposed electrode[164].

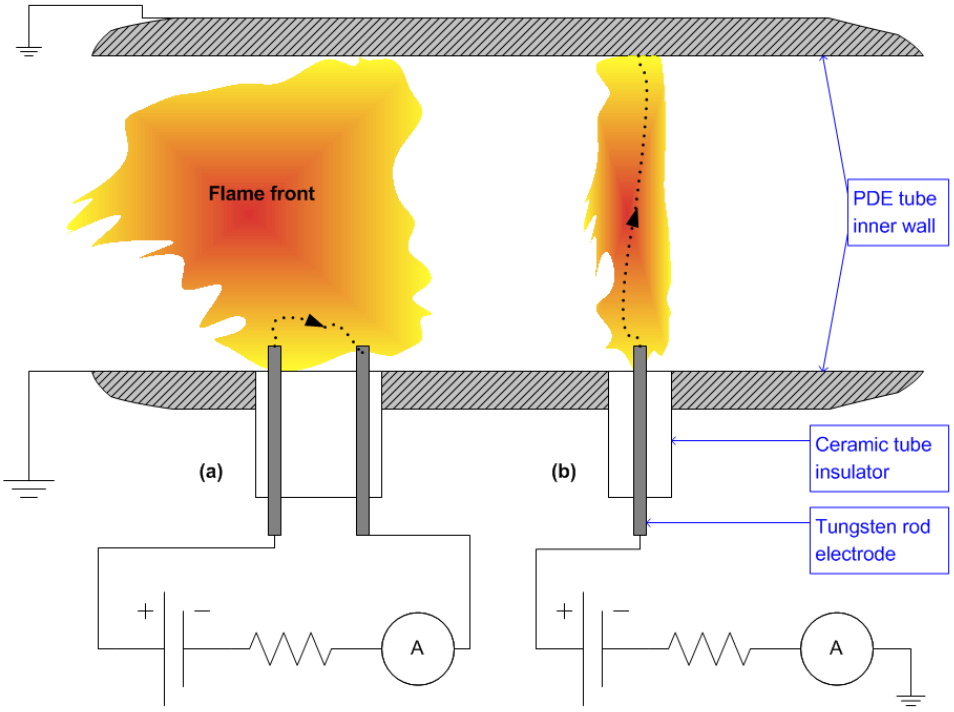

Figure 9.11 A schematic of the dual probe (left) and the single probe (right) ion detectors.

In the single-probe circuit, the electrode is biased with respect to the ground, which is the body of the combustor. When a flame bridges the gap between the probe and the body ground, a current flows through the circuit and the flame, caused by the movement of electrons and ions in the flame. This circuit can also be used to detect a shock wave or a detonation wave, which makes a contact between the probe and the body of the tube. If the single probe is biased positive with respect to ground, it will attract more electrons, which are less massive than the positive ions and will therefore be more sensitive.

A dual-probe circuit will have two probes biased against each other and a flame or wave completes the circuit by coming into contact with both the probes at once. Dual probe circuits can have one probe grounded to the body ground or left ungrounded and kept floating off the grounded body of the tube or combustor. The latter may be preferable in some cases which have floating power supplies. In most cases, all metallic apparatus are usually connected to a common ground, by virtue of the mechanical fittings and fasteners. Dual probes usually are

slightly larger in size, as the two electrodes have to be insulated from each other and the body. And the probes have to be inserted such that the two electrodes are perpendicular to the direction of flow, so that the wave joins the gap between them as it passes by them.

If the electrode is small in size of the order of 1 mm in width, its spatial resolution will be high and can then be used to pin point the shock or detonation wave. However, its sensitivity will be low, due to the reduced surface area. Therefore, the amplifier gain will have to be set very high. This introduces another problem in the form of increased noise, i.e., a low signal-to-noise ratio. Therefore, a balance between resolution and noise will be required. If the probe is used for detection of shock or detonation wave only, then the sensitivity can be set high, so that the first presence of the wave causes the output to shoot up to the saturation level. Then this spike can be used for TOF calculations with the readings from other ion probes located down-stream.

The temporal resolution is inversely proportional to the absolute value of the charge of the particles q and the electric field intensity E and directly proportional to the speed of sound a and the mass of the particles m. The response time of the probe can also be expressed in terms of the drift velocity of the ions as[165,166]

$$t \propto \frac{a\,m}{q\,E} \tag{9.8}$$

The resulting response times can be in the order of a fraction of 1μs, with a bandwidth of 1 to 10 MHz

In this study, single electrode probes of the type shown in Figure 9.11 were used in the dual-stage PDE. The probes were hand crafted by inserting 5/32 in. thick 2 % lanthanated tungsten rods through ¼ in. ceramic tube insulators and fixing them in place with epoxy. These ceramic tubes were then inserted into ¼ in. NPT brass nipples. At the bottom of the nipple, a 1/8 in. NPT brass fitting was screwed on to serve as the mounting end, which could be fitted with the help of a wrench into the ion/optical transducer ports on the PDE, which were all 1/8 in. FPT tapped, and located at the same axial locations as the pressure transducer ports. The extra

fitting also served to protect the nipple from damage when the transducer is repeatedly removed or mounted.

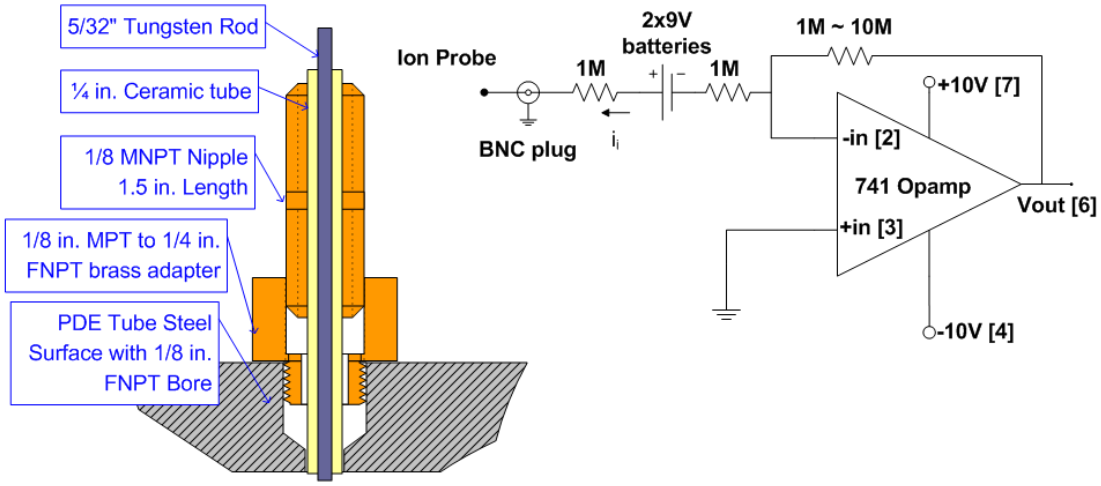

Figure 9.12 Schematic of the ion probe and the amplifier circuit used for detonation wave detection.

The tungsten electrode and ceramic tubing were fixed such that the ceramic tube extended just a mm into the inner volume and the tungsten electrode protruded about 3 to 5 mm into the inside of the tube, when the probe housing was screwed tightly into the port. The outside metal surface of the probe was then wrapped in cloth which was continually wetted during the tests, to cool the probe.

The circuit used for this study was a trans-impedance amplifier, or current-to-voltage converter. The output voltage is directly proportional to the probe current and is equal to the feedback resistance times the current, in other words the gain of the amplifier is equal to the value of the feedback resistance. The feedback resistance value was set at 1 $\mathrm{M}\Omega$, after experimenting with various values up to 10 $\mathrm{M}\Omega$. At higher gains, noise is amplified significantly and small signals can cause the output of the amplifier to saturate to 10 V. The amplifier circuit was made using a 741 op-amp, which has a bandwidth of 1.5 MHz. The response time of the probe is therefore dependent only on the amplifier and the electron drift velocity. Since electrons move very fast, the response time of this probe is expected to be in

the range of a fraction of 1 μs. Therefore, these ion probes are very suitable for the detonation chamber wave speed measurements. A sample signal history from a 5 Hz test of the dual-stage PDE is shown in Figure 9.13, showing that ion detector readings can be used for TOF velocity calculations.

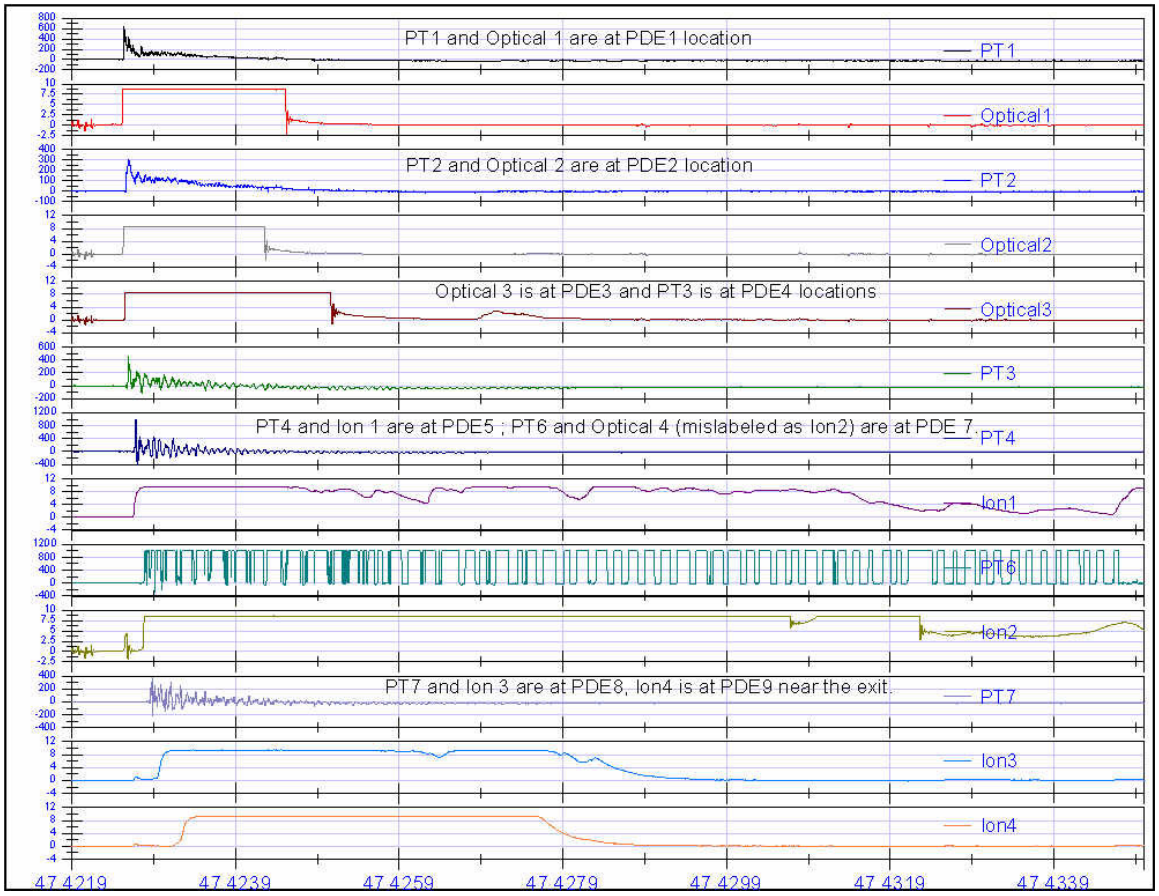

Figure 9.13 A sample signal history from a dual-stage PDE test at 5 Hz showing pressure, optical and ion sensor readings. PT6 is affected by some unknown ringing, but the optical transducer located at the same point also shows a reading for the same location. Comparing the readings of PT7 and Ion3, it shows that the ion detector is able to detect the pressure wave, but it also detects a flame out following the pressure wave front. See Figure 4.11 for sensor locations.

In many newer cars, the spark plug serves a dual purpose. It is used to ignite the fuel-air mixture, but for the next three stages, in which it usually sits idle, the spark plug is now used to monitor the conditions within the engine by applying it as an ion detector[167]. A dual-stage

circuit; with a high-voltage circuit for the ignition and a low 50 to 100 V circuit for the ion detection; separated by a varistor or other isolation to protect the low voltage side, makes this dual purpose igniter possible. The ion probe current can be expressed as a function of the pressure.

The application of spark plugs as ion detectors in PDEs has been studied[165,166] to test whether they can be used to read pressure accurately with the aim of replacing the pressure transducer with ion probes that can withstand the detonation pressures and temperatures. The relationship that was developed was that the peak ion current and the decay rate of the ion current are proportional to the pressure and arrived at a first-order approximation, as shown below, where p is pressure, I is the peak ion probe current, $\frac{dI}{dt}$ is the rate of decay of peak ion current and a_0 and a_1 are regression constants.

$$p = a_1 \frac{dI}{dt} + a_0 \tag{9.9}$$

Automotive spark plugs were modified by cutting off the ground electrode and adding steel extensions to the core to altering the area of the high voltage electrode. The above relationship between current and pressure for non-combusting air and fuel mixtures was verified, albeit with poor accuracy. There were difficulties due to EMI, which required filtering to improve the signal-to-noise ratio. In the aforementioned work, ion detector results were not compared with pressure transducer readings.

But there are many drawbacks to using ion probes for pressure detection. Ion detectors are inherently very noisy because the signals are very small, in the order of nA or $\mu\mathrm{A}$. Ionization is not a steady process. It is highly random and at low ionization levels, the signal is bound to be very erratic and noisy. A relationship between pressure and ionization current may be obtained for non-reacting fluids. As soon as reactions start, the ionization levels increase exponentially. The flame area will have relatively high ion currents, although it is low density plasma, which will saturate the probe current detector. This is because the current detector will

be set to a high sensitivity level in order to detect the low levels of currents, which as mentioned also causes increased noise. But within the flame, this high sensitivity will cause the detector to saturate. Therefore, a variable sensitivity current detector will be required. That is, a feedback is required for the detector also. But the advantages of ion probes are their good spatial and temporal resolutions and the durability of well designed detectors, such as in the shape of spark plugs. Active cooling can also be incorporated into their design, similar in concept to the pressure transducer water-cooling envelopes.

Therefore, it is recommended that ion probes be used for TOF velocity measurements along with few strategically placed pressure probes within the combustor, so as to be able to determine the detonation properties using C-J detonation relations.

9.5 Temperature Measurements

The temperature behind the detonation wave can be determined using C-J relations, making it unnecessary to measure temperature within the detonation tube. However, the air inlet temperatures and PDE exhaust or plenum chamber temperatures are required for the control of the engine. But these signals can be can be sampled at a slower rate and a time-averaged temperature may be sufficient. For the PDE combustor, the heat transfer rate can be determined from measuring the outside wall temperatures, which once again are time-averaged functions of the thermal conductivity and heat generation rate inside the combustor.

High temperature measurements are usually done with two types of sensors, resistance temperature detectors (RTDs) and thermocouples. Although modern-day optical and infra-red temperature detectors can provide fast and accurate measurements, these are not practical for application within the PDE combustor, because they would require an optical window. As mentioned earlier any optical window will gradually get tarnished by the deposition of soot and the action of the heat and the impurities will make the window opaque. Also, the window has to be made of heat and shock resistant materials. However, infra-red measurements are still possible for the inlet areas.

Thermocouples are cheap and reliable and can be built to be very robust. They can also be made into complex shapes incorporating water-cooling or other active cooling systems, such as for example, the types used in rocket motors and jet engines[168]. A list of thermocouple types, their constituent metals and their operating temperature limits are given in Table 9.2.

Table 9.2 List of standard thermocouple types.

Type	Positive	Negative	Low Temp.	High Temp	Average Sensitivity	Environment	Comments
			(℃)	(℃)	(μV/C)		
B	Pt + 30% Rh	Pt + 6% Rh	0	1700	10	Any	
C	W + 5% Rh	W + 26% Rh	0	2320	18.5	Not for Oxdizing	>400 C
D	W + 3% Rh	W + 25% Rh	0	2320	18.5		
E	Chromel	Constantan	-200	900	68	Any	
G	W	W + 26% Rh	0	2320	15		
J	Iron	Constantan	-40	750	50	Not for Oxdizing	
K	Chromel	Alumel	-200	1350	41	Any	
M	Ni + 18% M	M + 0.8% Co	0	1400	42		
N	Nicrosil	Nisil	-270	1300	39	Any	
R	Pt + 13% Rh	Pt	0	1450	10	Any	
S	Pt + 10% Rh	Pt	0	1450	10	Any	
T	Copper	Constantan	-200	350	43	Not for Oxdizing	

Name	Composition	Melting Point	Resistivity	Thermal conductivity	Density
		(℃)	(nΩ.m)	(W/m/K)	(kg/m^3)
Alumel	94% Ni, 3% Mn, 2% Al, 1% Si	1260	294	29.7	8610
Constantan	55% Cu, 45% Ni	1221-1300	520	19.5	8900
Chromel	90% Ni, 10% Cr	1420	706	19	8500
Nicrosil	14.4% Cr, 1.4 % Si, 0.1% Mg	1420	1000	13	8530
Nisil	95.6% Ni, 4.3% Si, 0.1% Mg	1420	365	27	8585

Symbol	Name	Atomic No.	Atomic Weight	Melting Point	Resistivity	Thermal conductivity	Magnetic property
				(℃)	(nΩ.m)	(W/m/K)	
Al	Aluminum	13	26.9815	660	26.5	237	para
Co	Cobalt	27	58.9332	2927	62.4	100	ferro
Cr	Chromium	24	51.9961	1907	125	93.9	anti-ferro
Cu	Copper	29	63.546	1085	16.78	401	dia
Fe	Iron	26	55.845	1538	96.1	80.4	ferro
Mg	Magnesium	12	24.305	650	43.9	156	para
Mo	Molybdenum	42	95.94	2623	53.4	138	x
Mn	Manganese	25	54.938	1246	1440	7.81	para
Ni	Nickel	28	58.6934	1455	69.3	90.9	ferro
Pt	Platinum	78	195.084	1768	105	71.6	para
Rh	Rhodium	45	102.9055	1964	43.3	150	x
Si	Silicon	14	28.0855	1414	x	149	non
W	Tungsten	74	183.84	3422	52.8	173	x

The simplest thermocouple is an open bead type, composed of just a small junction of two dissimilar metals. The bead design cannot be directly applied within a combustion or detonation environment, as it will get damaged quickly. If the bead is enclosed in a metal housing for protection, it subjects the thermocouple to a delay caused by the heat conduction rate of the metal housing. Consequently, the response time is seriously affected and it can no longer be applied in a fast changing environment, such as the combustor of a PDE. However, the enclosed thermocouples can be effectively used in the inlets or the plenum chamber and nozzle of the engine.

There is a type of high-speed thermocouples manufactured by NANMAC Corp. that has response times in the μs range, known as the eroding or self-renewing thermocouples[169]. Response times as low as 8 μs have been measured in detonation tests within shock tubes. Some of their models are rated for up to 2316 °C (4200 °F) and 680 atm (10,000 psi). Probe sizes as small as 3.175 mm (1/8 in.) and larger are available. These thermocouples are designed for use within rocket nozzles, internal combustion engines, and other situations where high pressures and temperatures are involved. The thermocouple is formed by sandwiching two thin dissimilar metal strips between a thin strip of insulation, as shown in Figure 9.14. The tips of the metal strips are made to touch to form a junction. This device is then inserted into the housing, with the end of the thermocouple junction flush with the bottom surface of the housing, which will be the sensing surface inserted into the area of interest. As the name suggests, the tip continuously wears off as it is exposed to combustion or other severe processes. Moreover, the insulator also is burnt off and a new junction forms. Thus, the junction keeps regenerating. Eventually, the sensor will be worn out and will have to be replaced. But the speed of the thermocouple response is tremendously improved as the sensing surface is directly exposed to the flame or detonation wave being measured. Nevertheless, the speed of response may not be fast enough to determine the wave speed using the TOF velocity method and, therefore, thermocouples may instead be used to determine the post-detonation wall temperatures and

heat transfer rates.

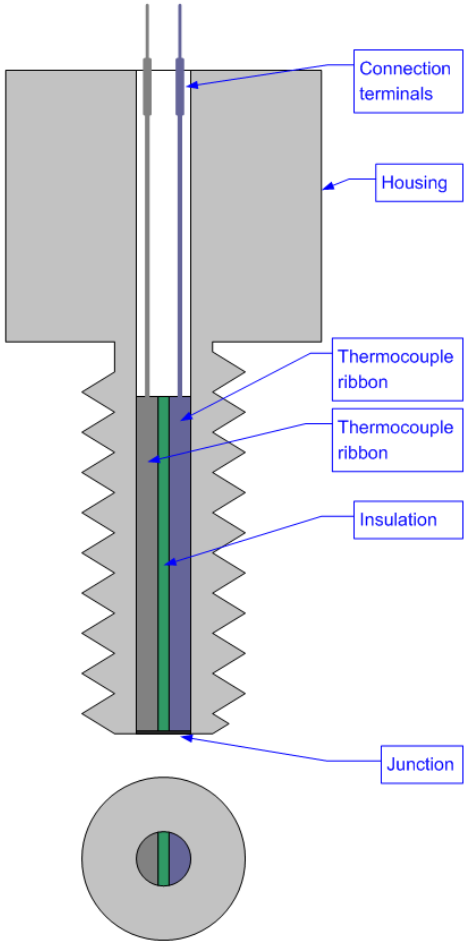

Figure 9.14 Schematic of the NANMAC eroding-junction thermocouple.

All thermocouple and RTD measurements within combustion environments have to be shielded against radiation induced errors in readings[170]. Bare thermocouples have been reported to show errors of the order of 100 ℃ when compared to suction-type pyrometers. Radiation error is proportional to the emissivity of the bead, the properties of the reactants, the convection heat transfer rate and the area of the sensing surface. The last factor plays a big role, with larger sensors having considerably larger errors. The above reference suggests a method of developing a correction factor by measuring the temperature at the same location

with two thermocouples of different sizes, so as to establish a relationship between the radiation error and the area of the sensor. This is a method that can be applied within PDEs also.

Thermocouple signals, being in the range of μV, are extremely susceptible to EMI. The effect of EMI is clearly seen in Figure 9.15 on the temperature trace which shows significant noise when a solenoid valve is energized. It is therefore recommended that thermocouple cables be shielded against EMI. If a low pass filter is used to filter out the noise, the bandwidth of the thermocouple may be restricted and limit the thermocouple being used for the measurement of high frequency phenomenon. A better approach may be to boost the signal intensity with a precise pre-amplifier with a fixed gain before transmitting the signals over long cables. At the DAQ end, the signals can be de-amplified by an equal amount before the analog-to-digital conversion (ADC) and thereby achieve a high signal-to-noise ratio. Alternatively, instead of de-amplification, the gain of the amplifier can be factored into the voltage-to-temperature correlation equation during the post processing of the signal. But the noise level may be higher in this case. Therefore, digital filters may also be required during the post processing process. If the analog-to-digital conversion is performed close to the sensor, then there are numerous choices available for transmitting the digital signals without EMI or loss of information. The digital signals can be transmitted by copper cable, fiber optic cable or by radio frequency transmission. Optical digital signals may also be sent over short distances using an infrared transmitter and receiver.

9.6 Mass Flow Rate Measurements

It is extremely important to measure mass flow rates of fuel, oxidizer and purge air in a PDE in order to control the initial conditions of the combustor, such as equivalence ratio and initial pressure and temperature. Without flow rate measurements, the final conditions cannot be calculated using C-J detonation relations, as mentioned earlier, and the required results, namely, detonation pressure, velocity, thrust, etc., cannot be achieved. Mass flow rate measurement is the hardest to perform for PDE applications because none of the typical mass

flow meters work properly for pulsed flow. Typical mass flow meters used in large flow rate conditions are based on differential pressure measurements. They include orifice meters, venturi meters and sonic flow nozzles[161]. Orifice and venturi meters may be applied within the inlet of a PDE, where the flow is relatively steady, before branching out into the various valves and combustors. In this location, a pitot tube may also be used to measure air velocity to determine the mass flow rate. But the flow of air entering into each combustor and the fuel flow are unsteady. In their standard form, these aforementioned devices are not suitable for measuring mass flow in the combustor.

The sonic flow nozzle can be used to measure mass flow rates. It is favored by many because it offers an easy to apply formula in which the flow rate is a function of the total pressure upstream of the throat[153] . The schematic of a sonic flow nozzle is shown in Figure 9.15.

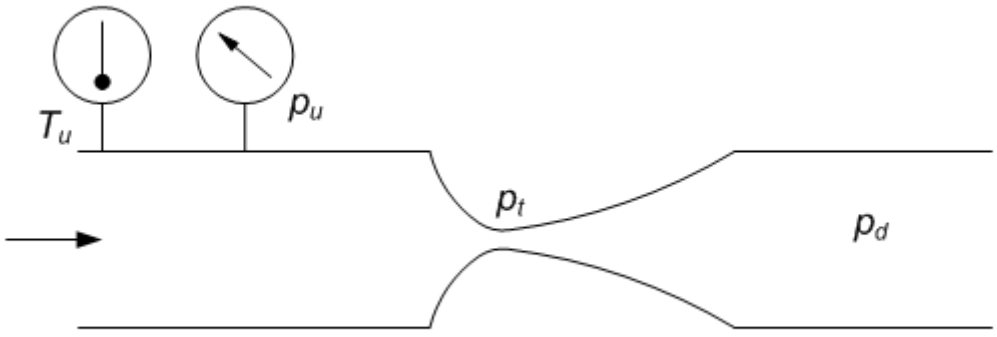

Figure 9.15 Schematic of a sonic flow nozzle mass flow meter.

The mass flow rate equations are given as below in Equations (9.10) and (9.11), where R is the universal gas constant, γ is the specific heat ratio, A is the area of the throat and c_d is a discharge coefficient obtained by calibration and is specified by the manufacturer. The pressure and temperature upstream of the throat is denoted as p_u and T_u respectively.

$$\dot{m} = c_d A \sqrt{\frac{2}{RT^*}} \sqrt{\frac{T^*}{T_u}} \sqrt{\frac{\gamma}{\gamma-1}} \cdot p_u \left[\left(\frac{p_t}{p_u} \right)^{\frac{2}{\gamma}} - \left(\frac{p_t}{p_u} \right)^{\frac{\gamma+1}{\gamma}} \right]^{\frac{1}{2}} \quad \left(\text{unchoked flow, } \frac{p_t}{p_u} > p_{cr} \right) \quad (9.10)$$

$$\dot{m} = c_d A \sqrt{\frac{2}{RT^*}} \sqrt{\frac{T^*}{T_u}} \sqrt{\frac{\gamma}{\gamma-1}} \cdot p_u \left[\left(p_{cr} \right)^{\frac{2}{\gamma}} - \left(p_{cr} \right)^{\frac{\gamma+1}{\gamma}} \right]^{\frac{1}{2}} \quad \left(\text{choked flow, } \frac{p_t}{p_u} = p_{cr} \right) \quad (9.11)$$

T^* is a reference temperature used to evaluate the coefficients so that the temperature may be entered in the form of a ratio, making the calculations simpler. The critical pressure ratio determines whether the flow is choked or not, and is given by

$$p_{cr} = \left(\frac{2}{\gamma+1} \right)^{\frac{\gamma}{\gamma-1}} \quad (9.12)$$

There are several problems with the use of sonic flow nozzles in PDE studies.

1. Sonic flow nozzles are designed for steady flows and not for pulsed flows.
2. If there are any choke points downstream of the throat, the flow at the throat of the sonic nozzle may not be choked. This is often the case due to the presence of check-valves and solenoid valves which have small orifices, smaller than the throat size of the nozzle. Therefore, in the case of pulsed flows, the pressure readings at the upstream pressure port of the sonic flow nozzle cannot be directly used in the choked-flow mass flow rate equation (Equation 9.11), without performing a detailed analysis of the pressure history. This is inconvenient for real-time monitoring of pulsed flow rates.
3. The pressure transducer is connected to a port located at the inlet of the nozzle and it measures static pressure. For larger tubes, the static pressure upstream of the throat may be considered to be the total pressure, but it does not hold for smaller tubes and if the flow is pulsed, as is the case in PDEs.
4. In the case of pulsed flow conditions, when the valves downstream of the nozzle are opened, the pressure upstream drops as the fluid flows. Even with a fast-acting pressure regulator, this pressure will drop slightly, when the valves

downstream are opened. When the valves are closed, the pressure will go back to the original higher level. This issue was discussed earlier in Section 8.7. Figure 9.15 shows the drop in the static pressures measured at the sonic flow nozzles when the valves are opened. Thus, if the static pressure is plugged into the flow rate equation, it will yield a higher mass flow reading when the valves are closed. This is further complicated by the following point.

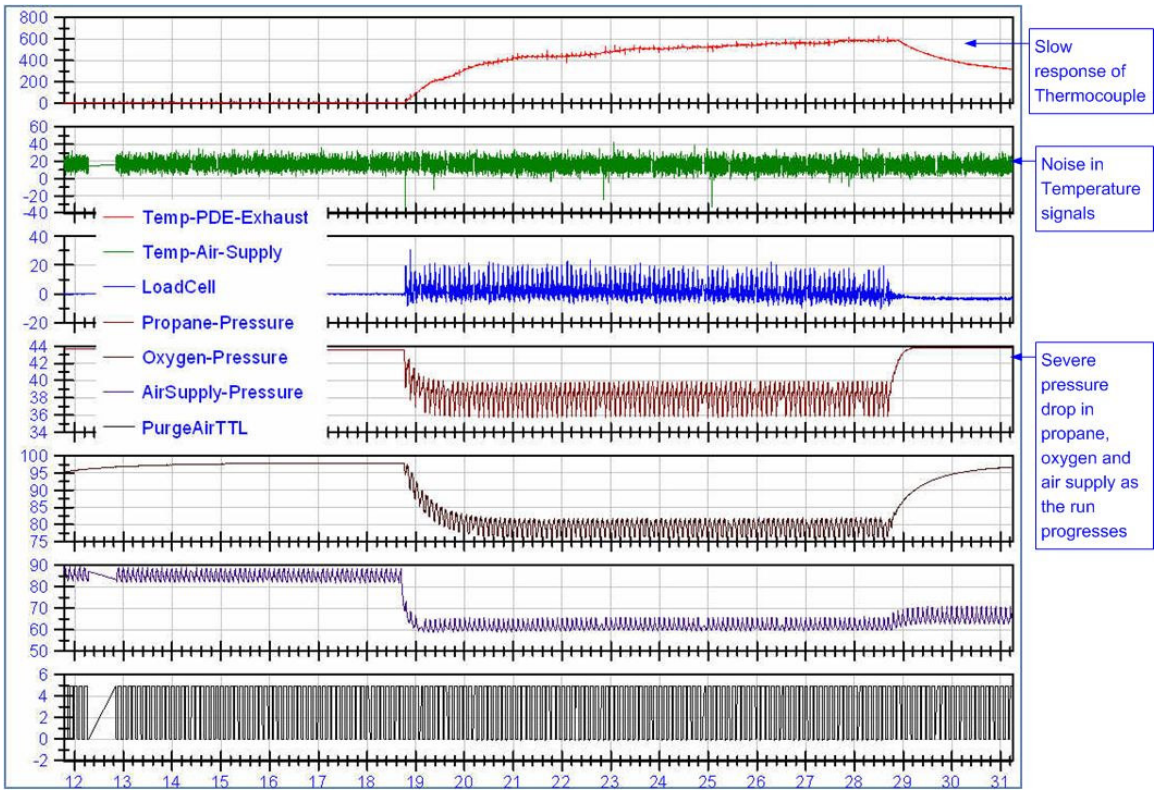

Figure 9.16 The dramatic drop in line pressures of propane, oxygen and air supply is seen during a test of the dual-stage PDE at 10 Hz. Also in evidence is the effect of the noise on the thermocouple signal as soon as the purge-air valves are turned on.

5. If the nozzle and pressure transducers are placed at a distance upstream of the valves, when the valves open and close, the pressure pulses travel back up to the transducer at the speed of sound, as the flow responds to the opening and closing of the valves, as in a water hammer. As a result, the drop in the pressure when the valve is opened is registered with a delay by the

transducer. Similarly, the rise in pressure when the valve closes is also delayed at the transducer. Thus, the pressure readings of the transducer are phase shifted with the valve's positions. At higher pulse rates, this phase shift is even more pronounced and haphazard that it is very difficult to determine flow rates from the pressure data using Equations (9.9) and (9.10). This effect is clearly visible in Figure 9.17.

From the above reasons, it is clear that sonic flow nozzles are not very practical for pulsed flow conditions.

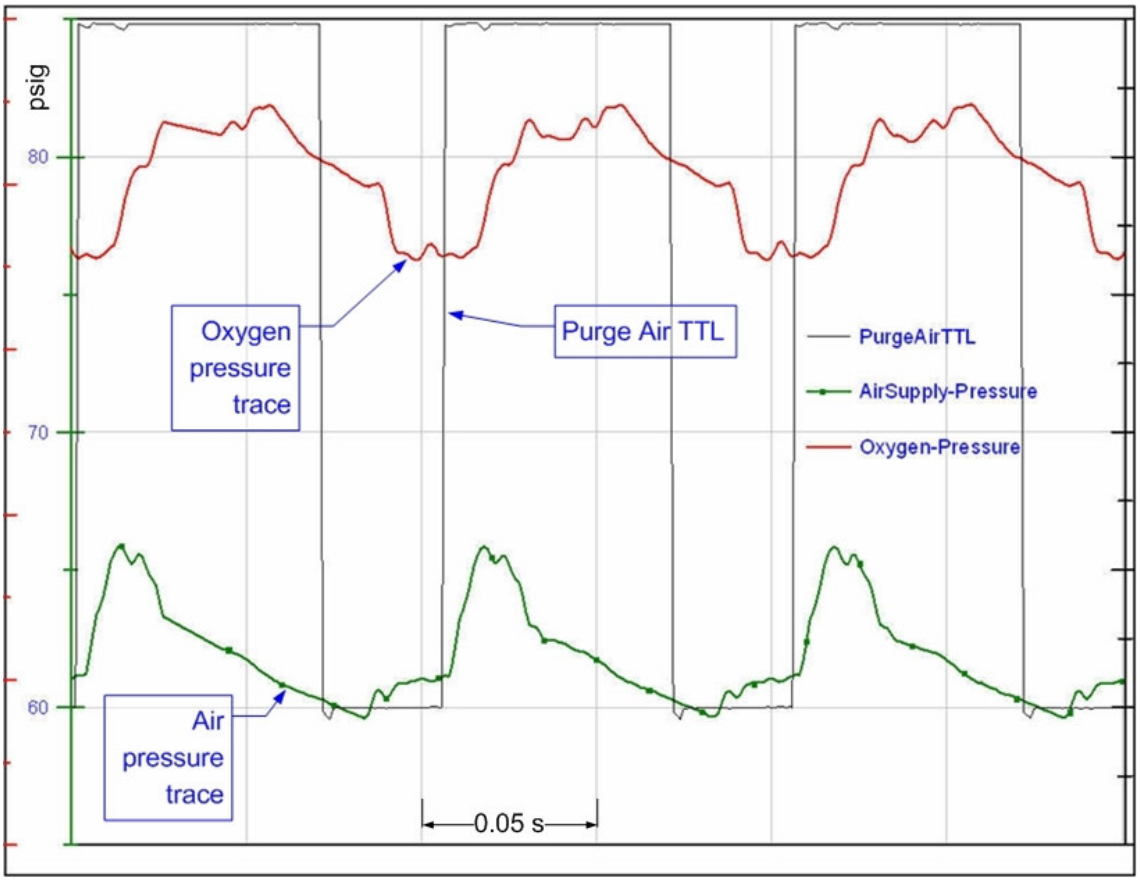

Figure 9.17 The pressures upstream of the sonic flow nozzles of oxygen and air are shown for a 10 Hz run of the dual-stage PDE. When the TTL signal is high the purge air valves are opened. When the TTL is low, both the oxygen and air supply valves are opened and the purge air valves are closed. The air supply and the purge air were supplied from a single line through one sonic nozzle. The pressures readings are not in phase with the TTL, due to the time taken by the pressure expansion wave to reach the transducer from the valve.

In the gas supply system set up for the PDE tests, sonic nozzle flow meters were originally used for flow rate measurements. A schematic of the setup for one gas line is shown in Figure 9.18, although there were three such lines, one each for air, oxygen and propane. As seen in the diagram, there were many sources for head pressure loss, namely long lengths of tubing and hoses, tube and pipe connectors, fittings, valves, etc., before the line was terminated at the PDE combustor. As mentioned earlier, the gas injection to the combustor was controlled with the help of solenoid valve injectors in the case of the PDE Mark 2, the PDE Mark 3 and the dual-stage PDE, while the Bantam PDE and the PDE Mark 1 used rotary valves. The connections from the injectors to the PDE combustor were also not straight forward. For such a complex system, it is very difficult to calculate the loss coefficients for all the various components and twists and turns in the tubing or connectors. It was found through direct measurements that even identical solenoid valves had differing mass flow rates. Also, older injectors had reduced flow rates than newer ones. Similarly, other valves and fittings experience wear and tear from continuous usage and their flow characteristics change over time. Therefore, the mass flow rate measurement would have a large uncertainty.

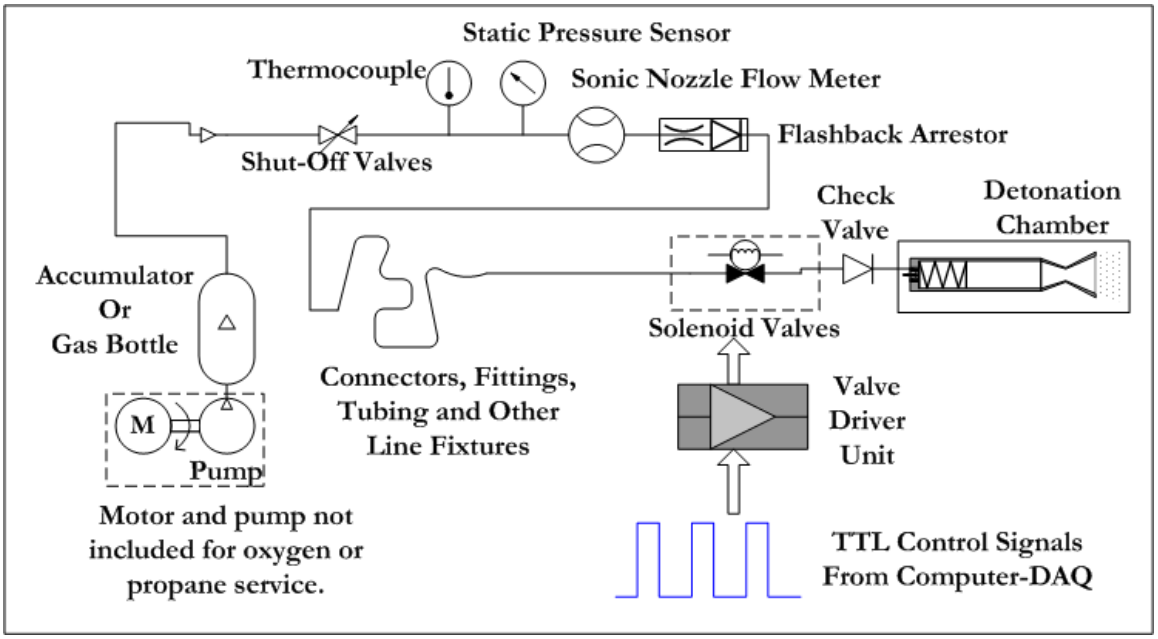

Figure 9.18 A schematic of the gas supply system for the PDE. In this figure, only one gas line is shown. Three such lines were used in the laboratory, one each for air, oxygen and propane. No pumps were used for oxygen and propane service. They were supplied from gas bottles.

One method of reducing the uncertainty in flow rate prediction is to calibrate each valve along with its associated fittings and connections and to obtain calibration curves of the flow rates in terms of supply pressure vs. mass (or volumetric) flow rate. Figure 9.19 shows a schematic of the flow rate curves that may be obtained for a valve as the frequency is varied. The diagram shows a negative trend in flow rates with increasing frequency because the mass flow is inversely proportional to frequency, since the period the valve stays open is reduced as the frequency is increased. The plots can also be obtained in terms of pulse width or duty cycle of the valve, which may be more useful for the engine controller.

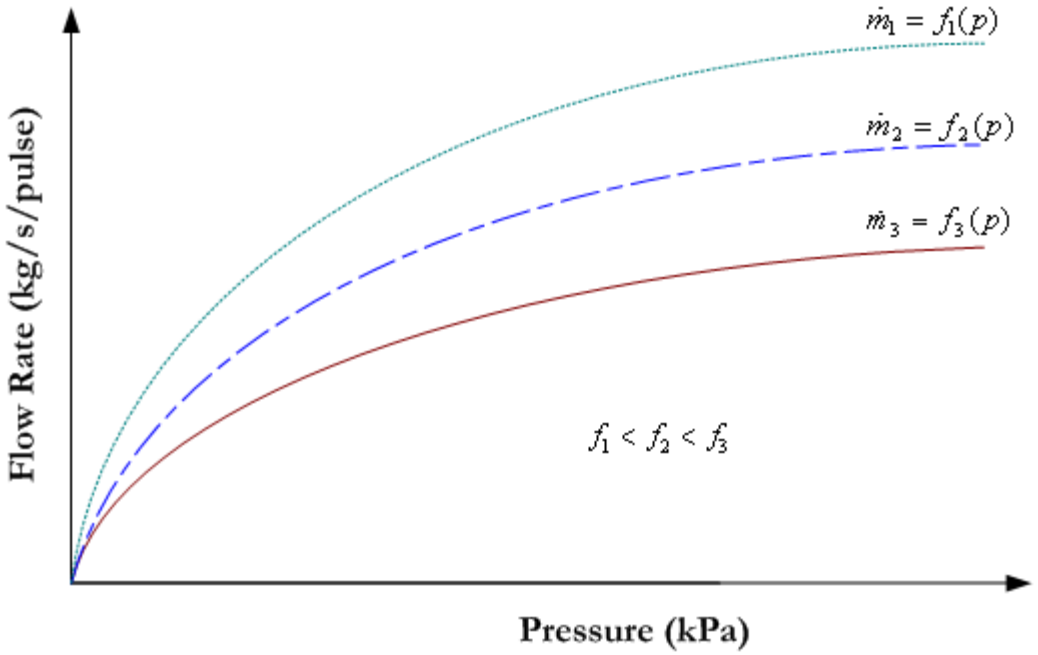

Figure 9.19 The flow rate is proportional to the square root of the pressure difference across a valve. The calibration family of curves of pressure differential vs. mass flow rate for various frequencies at 50 % duty cycle can be developed for any valve that will be used on a PDE.

Automotive valves are regularly calibrated and the data are fed into the car's computer control system to enable the engine control system to correctly regulate fuel flow rates[171]. This is a tried-and-true method and can be adapted for PDE valving systems too. The flow rates can be determined based on pressure at the inlet of the valves. Therefore, the pressure sensors should be mounted as close to the valves as possible.

Analytical solutions for mass flow rate measurements are also available. Unsal et al.[172] have developed an analytical model for calculating the flow rates from pulsed fuel injectors based on the line pressure. This method can be adapted to PDEs for liquid fuel metering provided the line pressure at the valve is known.

9.6.1 Experimental Flow Rate Calibration of DI Gasoline Injectors

Figure 9.20 shows the calibration chart of two identical Denso solenoidal direct injection (DI) gasoline injectors, labeled left and right in the figure, connected to the same fuel supply line

distributor. Table 9.3 shows the results obtained in the tests. The fluid used was kerosene which was pressurized using nitrogen with the help of the set up described in Section 4.6.5 and shown in Figure 4.16. The injectors were tested at a constant 20 Hz, 50 % duty cycle rate for different number of cycles, as shown in Table 9.3. The fuel flowing through the injectors was collected in a glass container and the mass and volume of the collected fuel was measured and recorded after each run. The calibration curves clearly show the direct relationship of flow rate with the square root of the differential pressure, as mentioned earlier. However, it is seen that even though the injectors are identical in design, their flow rates differ significantly at higher pressures. Perhaps the variations were due to uneven wear and aging of the nozzles and differences in the length of the connecting tubes, although all efforts were made to keep the connections as close to identical as possible. Thus, one way to override the difference in fluid path taken to the injectors is to mount the pressure transducer as close as possible to the injector. With the advance of newer piezoelectric injectors, the pressure sensor may even be integrated into each valve.

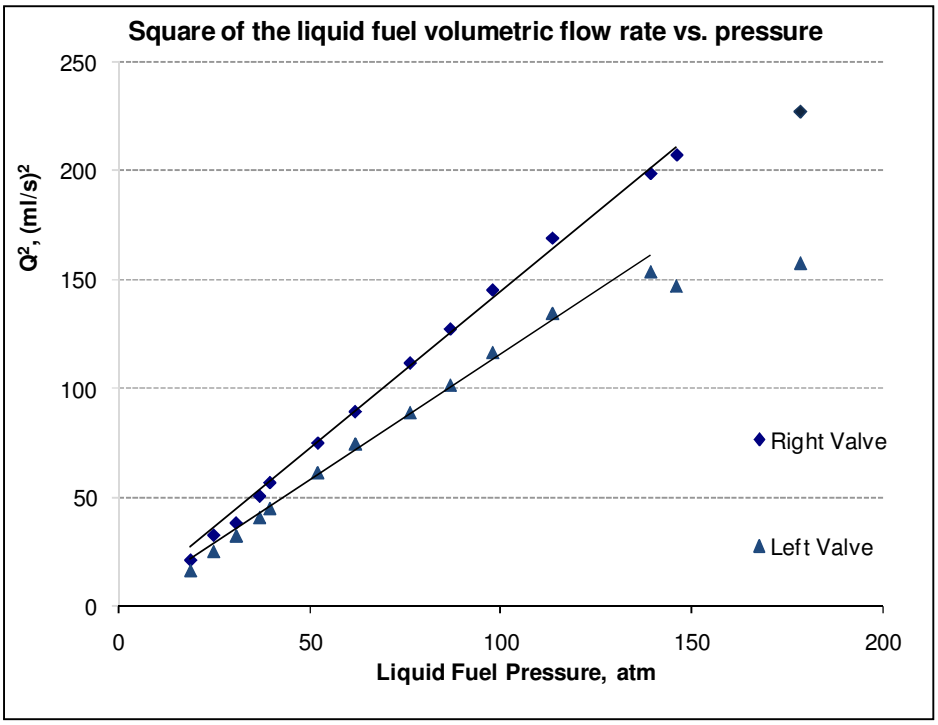

Figure 9.20 The calibration curves of two identical Denso DI gasoline injectors. Note that identical injectors produce slightly different flow rates due to wear.

Table 9.3 Calibration results of two Denso DI gasoline injectors.

No. of pulses	Frequency	Duty Cycle	Total on time	N_2 press.	Liq.Fuel press.	Liq Fuel	Vol.Flow Rt.	Q^2	Vol.Flow Rt.	Q^2
				Average	Average	Pressure	Right	Right	Left	Left
	Hz	%	s	psig	psig	atm	ml/s	$(ml/s)^2$	ml/s	$(ml/s)^2$
1000	20	50	25	265.583	262.307	18.844	4.56	20.794	4.08	16.646
1000	20	50	25	440.297	437.318	30.750	6.16	37.946	5.7	32.490
500	20	50	12.5	568.737	566.075	39.508	7.52	56.550	6.72	45.158
1000	20	50	25	354.390	350.735	24.860	5.68	32.262	5.04	25.402
500	20	50	12.5	530.191	526.881	36.842	7.08	50.126	6.4	40.960
500	20	50	12.5	753.677	749.585	51.992	8.64	74.650	7.84	61.466
500	20	50	12.5	899.760	894.186	61.829	9.44	89.114	8.64	74.650
500	20	50	12.5	1111.330	1104.597	76.143	10.56	111.514	9.44	89.114
500	20	50	12.5	1266.441	1258.662	86.623	11.28	127.238	10.08	101.606
400	20	50	10	1430.884	1421.260	97.684	12.05	145.203	10.8	116.640
400	20	50	10	1660.872	1650.845	113.302	13	169.000	11.6	134.560
400	20	50	10	2039.443	2028.017	138.960	14.1	198.810	12.4	153.760
350	20	50	8.75	2144.518	2128.475	145.794	14.4	207.360	12.114	146.756
300	20	50	7.5	2621.614	2606.064	178.283	15.067	227.004	12.533	157.084

9.6.2 Experimental Flow Rate Calibration of Gaseous Injectors

For gaseous injectors, a similar approach can be adopted for calibration, although this is a little tedious and time consuming. Nevertheless, it is easy to perform. A large balloon can

be used to collect the output flow of the injectors. The balloon and the gas within it can then be weighed and its volume can also be determined. Thus, the flow rates can be found. A whole family of curves can then be obtained for pressure vs. flow rates at different frequencies.

This technique was tried for air on an AFS Gs series valve, using a set up similar to that shown in Figure 9.21. Three-foot diameter advertising balloons were employed for the purpose of collecting the gas. The valve was run at frequencies between 1 and 10 Hz, each with 50 % duty cycle. At the lower frequencies of 1 and 2 Hz, the valve was run for about 10 to 20 cycles. At 5 and 10 Hz, the valve was run for about 25 to 50 cycles. Preliminary test results yielded a series of curves of pressure vs. volumetric flow rates for various frequencies. The curves, shown in Figure 9.22, display the inverse relationship of mass flow with frequency. Only a short study was performed using this method.

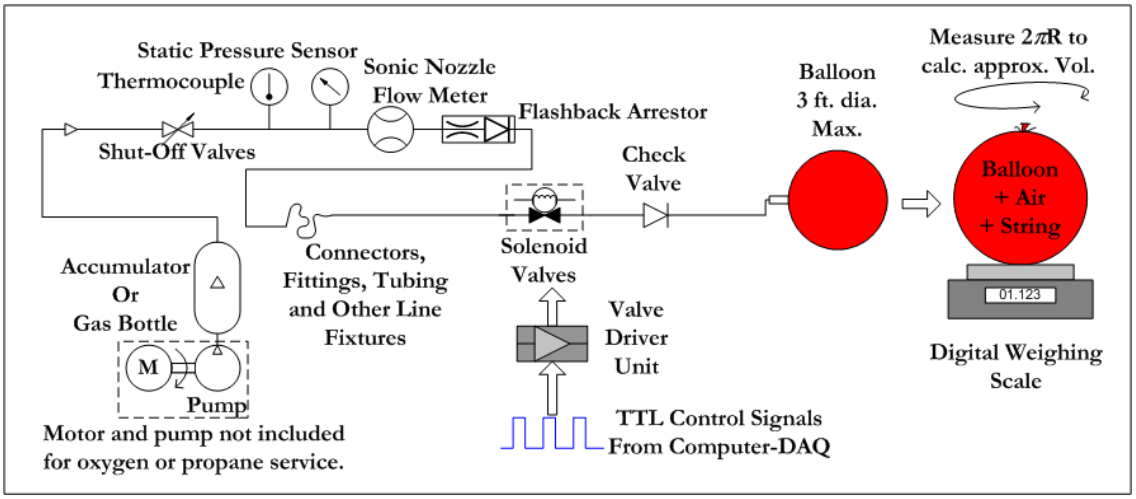

Figure 9.21 Schematic of the flow rate calibration system for gaseous valves using balloons and a sensitive weighing scale.

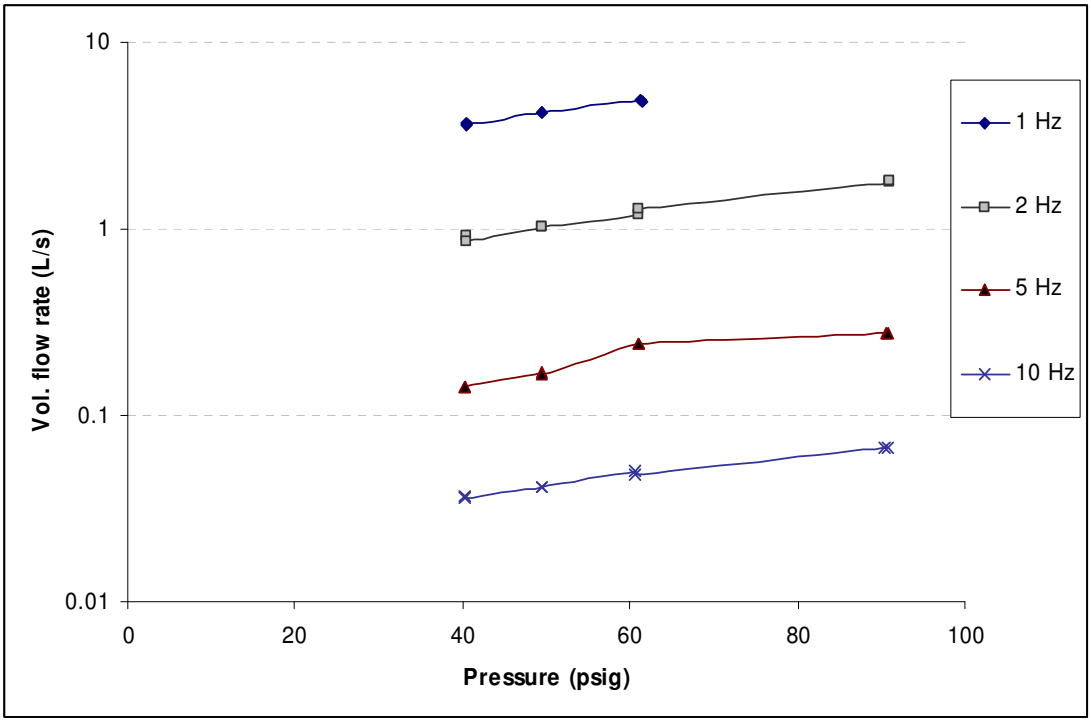

Figure 9.22 Results of volumetric flow rate tests performed on an AFS Gs series gaseous fuel valve with a three feet diameter balloon, showing an inverse relationship of flow rate with frequency.

9.7 Thrust Measurement

There are four commonly used methods for measuring thrust in PDEs. The first method is to integrate the pressure over the entire area of the closed rear end wall. This method requires a very high speed pressure sensor inside the combustor. Pressure sensors are prone to error due to high temperature causing thermal drift in their readings, as seen in Section 9.2 and Figure 9.3. Also ignition noise and other EMI affect the pressure data. Also, if a nozzle is installed, the effect of the nozzle on the thrust will be ignored. Nevertheless, this method is widely used and many studies have shown that the estimate obtained from this method gives higher thrust than direct force measurements using the following three methods[173].

The second possible method is referred to as the ballistic pendulum method, where the PDE is suspended as a pendulum and the thrust can be determined from the deflection[141,174-176]. However, this is not very practical for multi-cycle PDEs with large numbers of gas supply hoses, electrical connections, etc. Another method is to install the PDE on a movable carriage that presses against a spring that is supported against a thrust stand[148]. The deflection of the carriage is proportional to the thrust generated. This method also has drawbacks as the response at higher frequencies becomes dampened out and there will be attenuation and phase lag in the readings. However, the errors can be reduced with calibration and data reduction procedures.

The final method is to mount the PDE and associated equipment on a sliding mechanism and let the PDE push against a load cell which is balanced against a thrust stand. The PDE is prevented from moving by restraining it against the load cell. Therefore, the thrust force is measured directly by the load cell.

Strain gauge type load cells have slow responses, in the ms range. This may be adequate if only a time-averaged thrust is required. If the engine frequencies are low, in the 10 to 20 Hz range, strain gauge load cells possess sufficient bandwidth to measure the thrust adequately. While strain gauge load cells can be applied for static or low frequency dynamic

load applications piezoelectric load cells are designed for dynamic load measurements. And as such, they work well for PDE thrust measurement applications. Typical piezoelectric load cells have natural frequencies in the upper tens or low hundreds of kHz range and have the best accuracy over their output range. There are many sizes and shapes of piezoelectric load cells. The type used in this course of studies was the ring shaped load cell from PCB Piezotronics, Inc., model number 201B03, with a range of 0 to 2.224 kN (500 lbs), natural frequency of 90 kHz. It has an outer diameter of 16.51 mm (0.650 in.) and an inner diameter of 6.38 mm (0.251 in.) and a sensing area diameter of 12.7 mm (0.50 in).

There are two points that have to be considered when employing the ring shaped piezoelectric load cell. First, the load cell's sensing surface has to be perfectly parallel to the load contact surface while making maximum contact of the sensing surface. Otherwise the contact should be made at the center of the load cell, normal to the surface, as shown in Figure 9.23. Secondly, they have to be pre-loaded up to 20 % of the full range and the output has to be allowed to relax down to zero before taking measurements. That may take several minutes and no tests should be done during that time. The pre-load on the load cell used for this study is 0.89 kN (200 lbs). The load cell was mounted to a thrust stand with a threaded rod and tightened with a nut that was estimated to be close to the pre-load amount. The PDE was then allowed to push against the load cell through the threaded rod. The PDE was then restrained against the thrust stand by rubber cords.

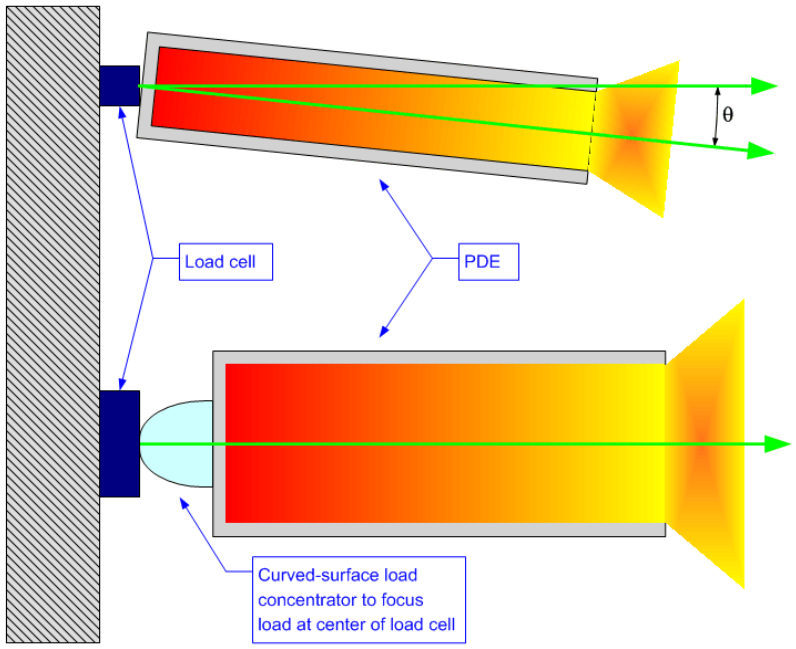

Figure 9.23 Schematic showing how to avoid edge loading of the load cell by using a curved attachment to concentrate the force at the center of the load cell. The load cell is shown enlarged for display purposes.

The PDE and its support mechanism were mounted on linear slider bearings that were balanced on dual 12mm cylindrical rails. A schematic of the slider system is shown in Figure 9.24. The rails rested on a ¾ in. (19.05 mm) thick aluminum plate. Each linear bearing was capable of bearing a weight of approximately 294 N. There were four bearings of one type and two of another, from different manufacturers, but identical in rail size. The slider bearings could move freely on the bearings, but care must be taken to prevent the buildup of dust and grime on the rails which increases friction. Also, the rails were found to have been slightly affected by corrosion due to the action of cooling water, over the course of the various studies performed with the linear slider system. Nevertheless, all the PDE apparatus, when set up on the linear bearings, were able to move freely when a tiny force was applied. One source of restraint however came from the hoses used to supply gas and fuel to the injectors and valves. Although, they were made loose enough, a small amount of damping is added. The additional

weight of the associated hardware and materials increases the inertia of the system, which affects the thrust readings.

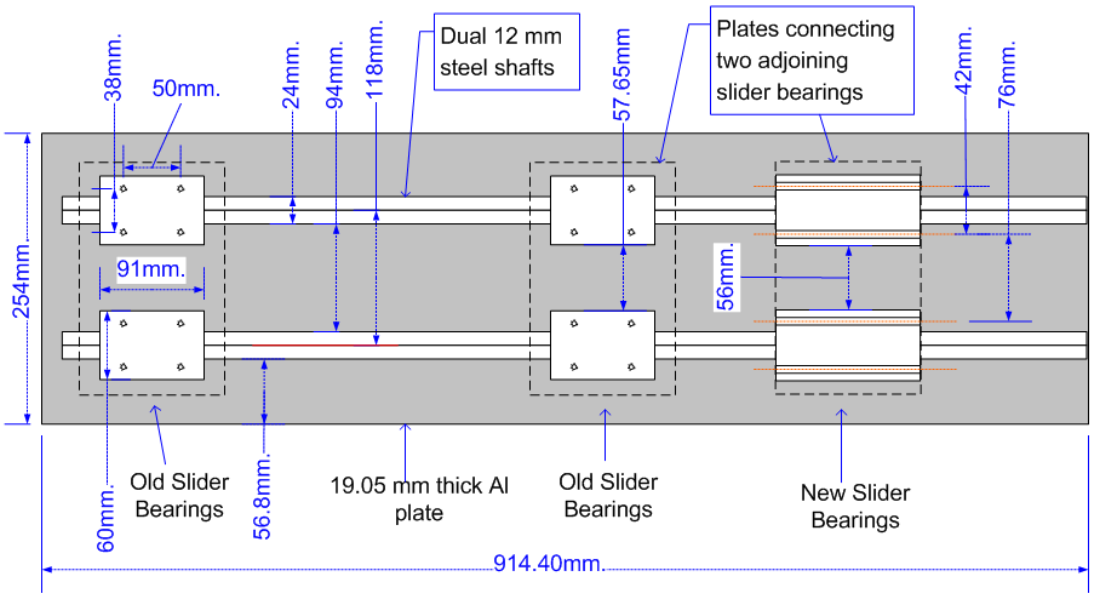

Figure 9.24 A schematic of the slider system used for the PDE thrust measurement.

The thrust measurements are very sensitive to the level of the sliding mechanism. The PDE on the sliding platform has to be horizontally and vertically level. Any mismatch in angle will result in a fraction of the resultant force being transferred to the slider platform through the bearings and misalignment at the load cell's sensing face. This can be minimized using an adapter with a curved surface that links the PDE's thrust wall to the load cell, as shown in Figure 9.23.

For thrust measurements based on a slider system and a load cell, even though the actual movement is in the order of micrometers, the starting friction of the linear bearings may still need to be overcome. In some applications, the starting friction of a static device can be overcome by adding dither to the mechanism in the form of a small vibration. It may be said that the vibration produced by the PDE can be considered to be a form of dithering.

9.7.1. Discussion on The Thrust Measurements of The Dual-Stage PDE

The dual-stage PDE, which has a 25.4 mm (1 in.) i.d. pre-detonator and a 101.6 mm (4 in.) i.d. main combustor, was put through tests at various frequencies, including 1, 2, 5 and 10 Hz. In the 1 Hz tests with near stoichiometric propane-oxygen mixtures, the reaction of the PDE set up to the detonation impulses were seen to be quite powerful, with the whole thrust stand and the PDE assembly on top of the linear slider system shaking strongly during each firing. However, the peak thrust levels measured seemed lower than expected, in the range of only 445 to 490 N (100 to 110 lbf). At 10 Hz, the thrust peak levels were seen to be much lower, at about 89 to 133.5 N (20 to 30 lbf), because the combustor could only be partially filled at higher frequencies. Thrust measurement results from a 10 Hz run are shown in Figure 9.25 and the results from a 1 Hz run are shown in Figures 9.26 and 9.27.

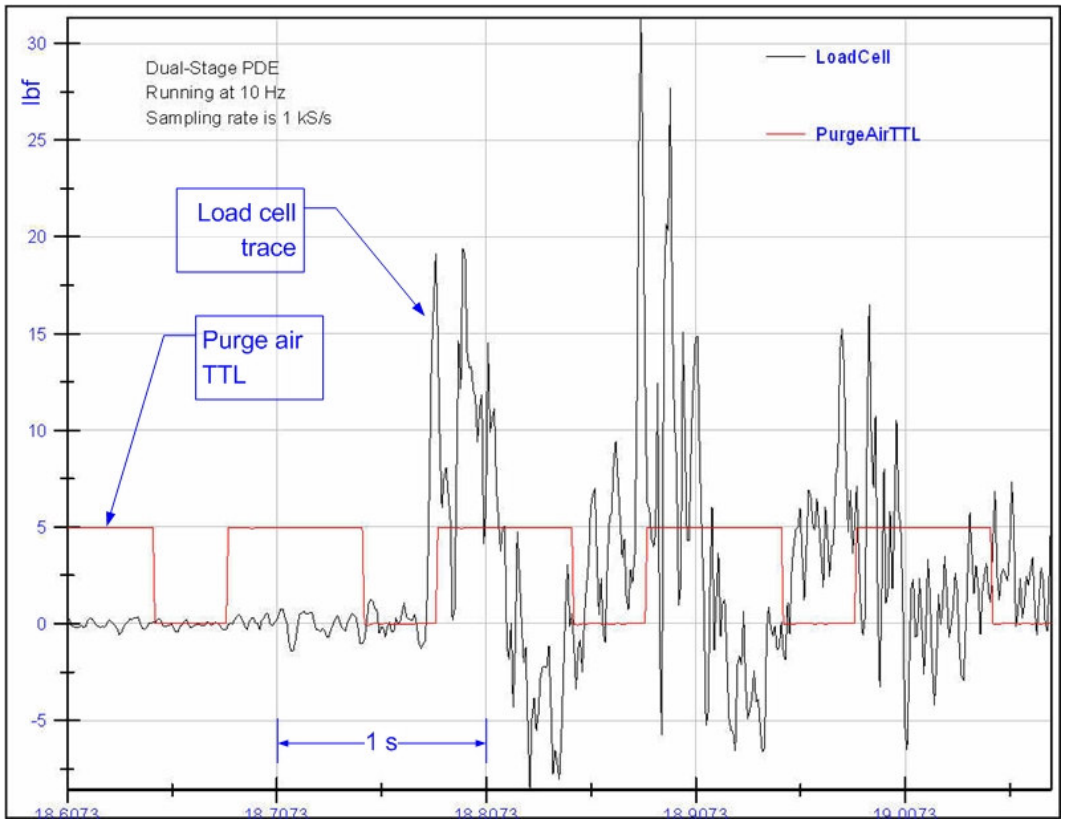

Figure 9.25 The thrust readings from a 10 Hz run of the dual-stage PDE using propane-oxygen mixtures. The ignition is fired just before the purge air TTL signal rises. The thrust pulse seems

to have occurred right at the firing time, but there are a few more repercussions following every initial thrust pulse due to the PDE chassis oscillating.

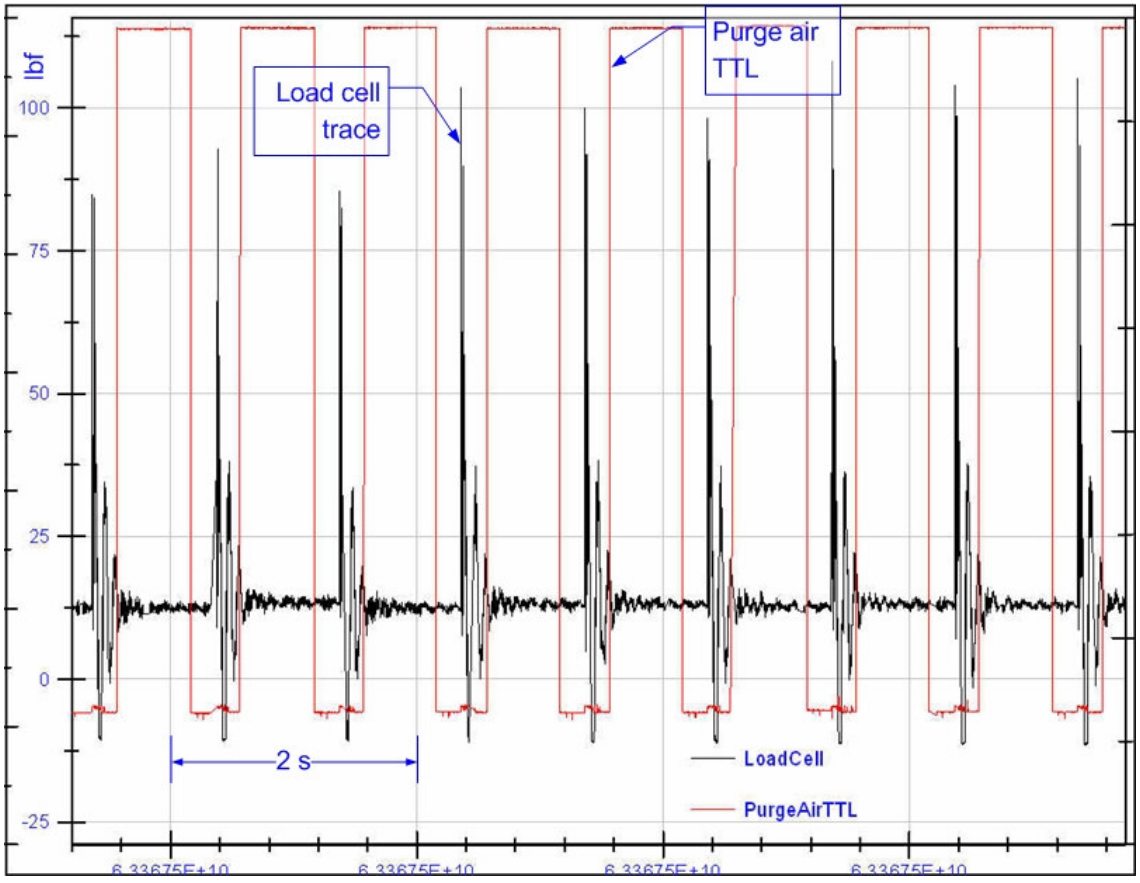

Figure 9.26 Thrust history from a 1 Hz run of the dual-stage PDE with near stoichiometric propane-oxygen mixtures. The vertical axis shows force in lbf. Sampling rate is 1 kS/s. The time period of the TTL is 1 Hz. When the TTL goes low, oxygen and propane valves are opened. The ignition is fired towards the middle of the low state of the TTL pulse.

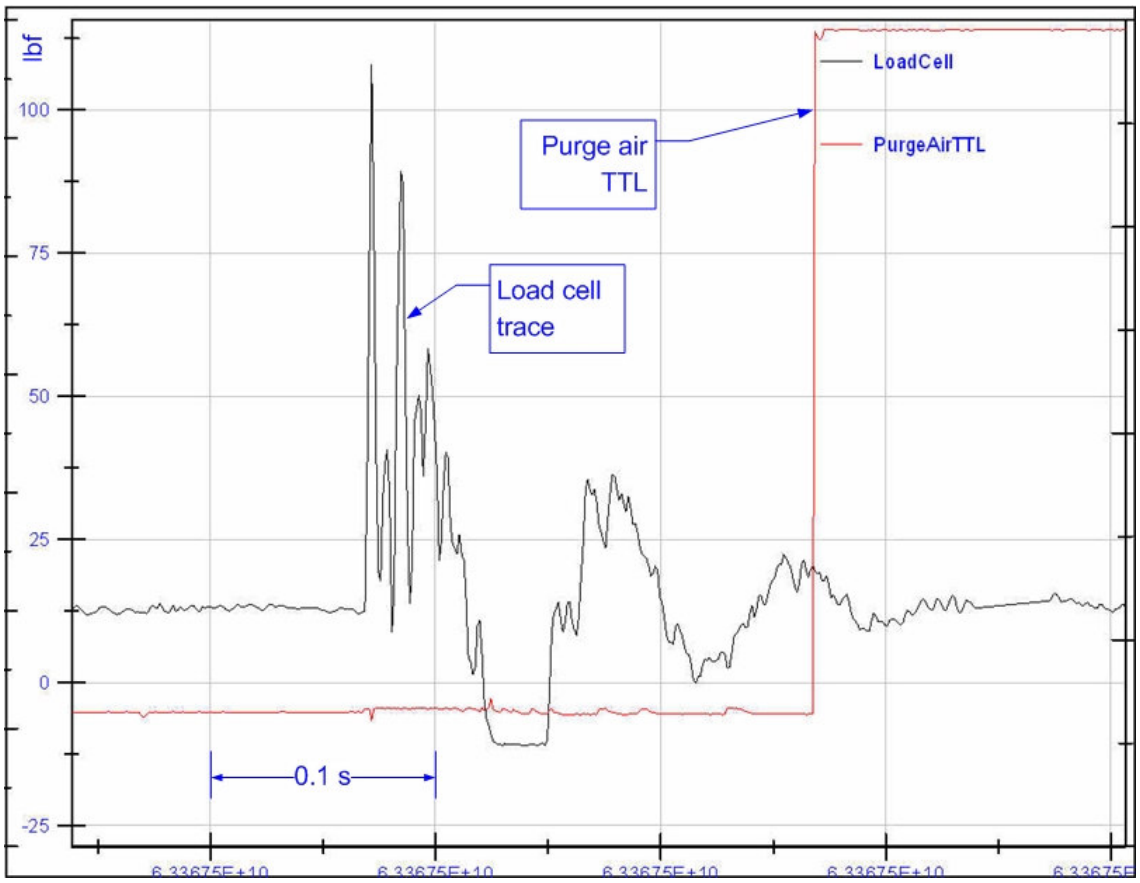

Figure 9.27 Expanded time view of a single thrust pulse from Figure 9.26. The effect of the oscillation of the PDE chassis is evident in the ringing after the first pulse. The vertical axis shows force in lbf. The sampling rate is 1 kS/s.

Since the PDE operates in a pulsed mode and the thrust produced is in the form of impulses, the force measured at the load cell is not the real impulses, but rather the reaction of the PDE apparatus to the impulses. The friction on the slider mechanism, the mass of the PDE setup, the elastic restraint due to the hoses and connectors that pull the PDE backward, as well as the pre-tensioning of the load cell and the PDE setup, all cause the PDE apparatus to behave as a linear time invariant system responding to the impulse loading. This accounts for the oscillations seen in the thrust measurements shown in Figures 9.25 through 9.27.

Quite a few studies have been performed on the measurement of impulse thrust loading by experimental and numerical studies on shock tubes, with the aim of applying the techniques

for the thrust measurement of hypersonic vehicles and PDEs[176,179,180]. Mee[176], Naumann et al.[179] and Soderling et al.[181] recommend using an accelerometer along with the load cell/force transducer so that the acceleration signals can be used to compensate for the vibrations in the thrust measurements. The reason for the accelerometer is briefly explained below. If the PDE apparatus is small, light and stiff, its natural frequency will be high and the thrust readings should follow the impulse inputs quite closely. However, if the system is heavy and large, the response of the system to the impulse will be slower. If the frequency of the impulses is of the order of the natural frequency of the system, the response to one impulse will affect the response to impulses later in time. In addition, the vibrations caused by the valve operations may also affect the thrust readings. Therefore, the accelerometer readings along with the thrust measurements from the load cell can be used to obtain the system characteristics and the true time history of the thrust using a deconvolution procedure. Mee[176] has provided a good report outlining the procedures of this technique.

9.8 Sound Measurement

The dB sound pressure level (SPL) scale is referenced at the threshold of hearing, which is 20 μPa, as shown in Equation (9.13), where p is measured in Pa.

$$\text{dB (SPL)} = 20\log_{10}\left(\frac{p}{20\times10^{-6}\,\text{Pa}}\right) \tag{9.13}$$

Dynamic microphones are the most widely used microphones for sound measurement because they are cheap, rugged and easy to maintain. They work on the principle of electromagnetic induction, whereby a moving coil attached to a diaphragm vibrates within the field of a permanent magnet, when the diaphragm is activated by sound. Thus, dynamic microphones generate their own voltage proportional to the sound pressure and do not require a power supply. However, they do need amplifiers depending on the type of application.

The three main parameters for microphone selection are their impedance, sensitivity and bandwidth. Based on the impedance, the microphones can be categorized as low

impedance (<1 k Ω), medium impedance (1 k Ω to 10 k Ω) and high impedance (>10 k Ω). The impedance rating is required to match the microphone with the input impedance of an amplifier, filter or DAQ. Most DAQs have very high input impedances and any microphone can be matched with them.

The sensitivities of some microphones are given by the manufacturer in mV/Pa. However, some manufacturers quote the sensitivity as a negative dB value along with the reference value. For example, a specification may say, "-70 dB, reference 1V/Pa." Thus, the sensitivity is calculated as follows.

$$20\log_{10}\left(\frac{x\ (\text{V/Pa})}{1\ (\text{V/Pa})}\right) = -70\ \text{dB};\ \therefore x = 10^{-3.5}\ \text{V/Pa}\ =\ 0.3162\ \text{mV/Pa} \qquad (9.14)$$

The microphone used for measuring the sound level in the dual-stage PDE study was an omni-directional dynamic moving-coil type microphone from RadioShack (model number 33-3036). Its impedance was given as 500 $\Omega \pm 30\ \%$ and its bandwidth was quoted as 60 Hz to 12 000 Hz. The sensitivity was quoted as -70 dB, 0 dB = 1 $\text{V/}\mu\text{bar}$. The sensitivity in mV/Pa is then found as follows.

$$20\log\left(\frac{x\ (\text{V/}\mu\text{bar})}{1\ (\text{V/}\mu\text{bar})}\right) = -70\ \text{dB};\quad \therefore x = 10^{-3.5}\ \text{V/}\mu\text{bar} = 3.162\ \text{mV/Pa} \qquad (9.15)$$

The microphone was connected directly into the connection box of the DAQ and sampled at rates between 1 kS/s and 10 kS/s. These low sampling rates are adequate for measuring just the RMS SPL, since the detonation sounds of interest are in the low frequency audio range. A digital SPL meter (RadioShack 33-2055) was also used to compare the results. This meter has a range of 50 to 126 dB SPL, with an accuracy of ±2 dB at 114 dB SPL. The digital SPL meter uses an electret electrostatic microphone. It has two weighting options, namely A-weighting (500 – 10 kHz, human peak audio range) and C-weighting (0 – 10 kHz, musical instruments and other sounds). The digital SPL meter was also placed at the same location as the dynamic microphone, about 2 m from the exhaust of the PDE, in a perpendicular direction to the axis of the PDE. At low sound levels, the digital readout and the corresponding

microphone signal from the DAQ were close with a difference of ±5 dB. Low levels of sound, 80 to 90 dB, were observed when the PDE was undergoing cold flow tests, that is, with just air being injected through the PDE.

When the dual-stage PDE was fired with propane-oxygen and propane-air mixtures, the digital meter soon saturated at its maximum display level of 126 dB, while the microphone output showed readings well above 140 dB. The sound intensity was higher with propane-oxygen only, going as high as 150 dB, clearly showing a difference in SPL level between detonations and deflagrations. One reason for the high sound intensity could be the reflection of the sound from the walls of the room.

The microphone used in the Dual-Stage PDE experiments did not have an amplifier and its output voltage was measured directly and converted to pressure level in dB. Since the signals were in the low mV range, and because only a single-ended channel of the DAQ was used for sound measurements, the signals were affected by EMI. Therefore, it is recommended to have an amplifier to boost the microphone signals before transmission to the DAQ. If the amplifier gain is set to G and the sensitivity of the microphone is S (V/Pa), then the SPL in dB can be expressed as

$$\text{dB (SPL)} = 20\log_{10}\left(\frac{V_{\text{microphone}}.G}{20\times10^{-6}.S.G}\right) \tag{9.16}$$

Note that G cancels out of the equation above.

9.8.2. Effect of Sound on Equipment

The high sound levels were found to be wreaking havoc with the data acquisition systems. A PC used for the slower rate acquisition of signals from the flow rate meters, thermometers, the microphone, etc., was placed in an open rack about 3 m behind the dual-stage PDE, with the exhaust of the PDE going into a collection chamber in the opposite direction. It was observed that the PC would shut down or freeze a few seconds after the firing of the PDE commenced and all data from the test would be lost. Even when the front end of the rack was shut with a wooden panel, the same effect was found. After many unsuccessful tests,

it finally became clear that the shock wave SPL emitted by the PDE were creating intense vibrations in fixtures within the room and in all the equipment, and that the high SPL was causing the connections to shake loose within the PC, making it shut down or freeze. The solution to the problem was found by moving the PC to the control room behind a concrete wall, and the transducer cables were extended and inserted through an orifice in the wall to the PC on the other side of the wall. However, the extensions in the cables made them more susceptible to EMI.

9.9 Summary

It is very important to measure the detonation wave speed so as to be able to determine the detonation properties using C-J detonation relations. The wave speed is commonly obtained by the TOF method from pressure transducer signal history. The ideal response times of transducers for the TOF wave speed measurement should be less than 1 μs to reduce the uncertainty. In this study, dynamic piezoelectric pressure transducers, ion detectors and photo-detectors were studied. Ion detectors are found to be good for TOF measurement and are simple in construction. Photo-detectors suffer from the problem of soot deposition on the optical window with progressive loss of transparency and a consequent reduction in sensitivity of the transducer. Therefore, photo-detectors have to be cleaned regularly between tests and may be useful for short duration or single shot tests. Pressure transducers suffer from thermal drift and require active cooling by means of circulating fluid, such as water. Pressure transducers are also mounted in a recessed orifice to protect the sensor. However, recessing causes the sensor to respond much more slowly and attenuates the amplitude of the pressure waves. Therefore, recessed transducers have to be calibrated so that the uncertainty may be reduced. In a PDE, pressure transducers, with active cooling, and ion detectors may be used in combination to obtain wave speed.

Flow rate measurement using sonic flow nozzles were found to be inadequate for pulsed flow rate measurement. An alternative method is to measure the static pressure at the

valve and to use an analytical relationship for the flow rate as a function of the pressure difference across the valve or to calibrate the valve's flow rate with respect to the pressure differential across it. Thermocouples were also studied for the measurement of fluid flow temperatures, surface temperatures and PDE exhaust flame temperatures. Sound measurement is also considered in this study. Thrust measurement using load cells were performed in the PDE studies. It is recommended that an accelerometer be used in conjunction with the load cell to compensate for the dynamic effects in the thrust measurements.

A possible control system for a PDE may be laid out as shown in Figure 9.28. It will have high speed sensors, such as pressure transducers and ion detectors, to measure detonation wave speed and low speed sensors to measure initial temperature, pressure, flow rates, etc. The controller will modulate the duty cycle of the fuel and air valves to meter the required mass flow rates and combustor fill rates. The controller determines if a detonation was successful from the wave speed and then adjusts the initial conditions for the subsequent cycles.

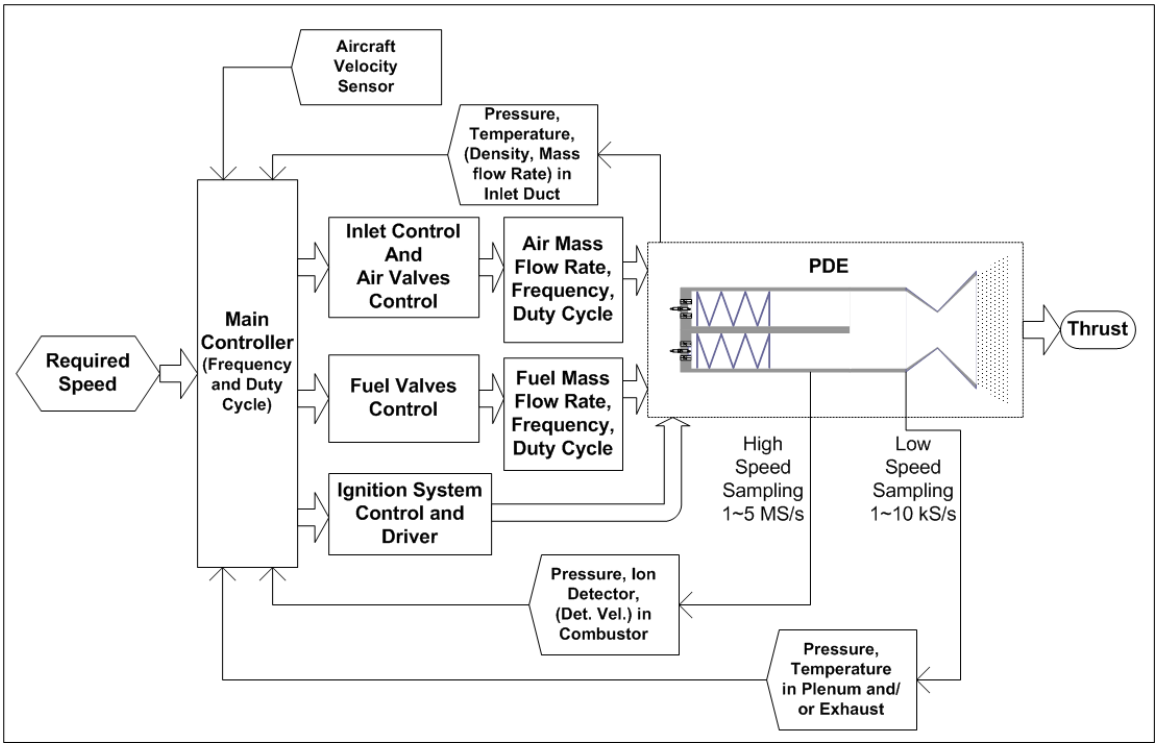

Figure 9.28 Schematic of a possible control system for a PDE.

CHAPTER 10

CONCLUSION AND RECOMMENDATIONS

The successful implementation of a PDE requires effective detonation initiation techniques, such as a pre-detonator or DDT devices, a proper ignition system, air-fuel flow and mixing control techniques including fast-acting valves, and a fast and capable, closed-loop control system. Once the geometry of the detonation chamber, including the pre-detonator or DDT devices, has been set the only variables that can be controlled are the initial temperature of the flow within the detonation chamber, the initial pressure, the fuel-oxidizer ratio and the energy and timing of the ignition. Numerical and CFD based studies are essential for designing and refining the geometry of the PDE, including inlets, internal ducting, combustors and DDT mechanisms, as well as to determine the operating window of the engine.

Numerous experimental detonation studies have demonstrated that the C-J detonation model is reliable enough to predict the properties of the detonation wave to a fairly accurate level based on the initial conditions. In addition, the post detonation flow properties can be expressed as a function of the wave Mach number, obtained from the wave speed. The C-J model can be used to control a PDE reliably by employing a fast-acting closed-loop control system to control the initial conditions within the detonation chamber. The initial temperature can be controlled with a heater or by using the heat from the engine to warm up the incoming air and the fuel, In order to study the various components and subsystems that would be required for implementation on a practical PDE, an experimental study using PDE ground demonstrators was undertaken.

- In the course of this study, five different PDE setups were designed, built and tested. The setups, which were all of single combustor design, were capable of multi-cycle

operation lasting from about 20 s to more than a minute. The size ranged from a 19.05 mm i.d. model to two 25 mm i.d. models to a dual-stage PDE with a pre-detonator. The last PDE had a 25.4 mm i.d. pre-detonator transitioning to a 101.6 mm i.d. main combustor through a 30° conical nozzle. The dual-stage PDE was water-cooled and was designed to be run for several minutes.

- The systems that were studied include various detonation chamber designs, techniques for water-cooling the detonation chambers and components, fluid delivery systems and valving, ignition systems, detonation initiation techniques such as DDT mechanisms and a pre-detonator, diagnostics and instrumentation, data acquisition and control system methodology and finally safety mechanisms in testing the engines.
- The smaller PDE setups used propane-oxygen mixtures, while the larger dual-stage PDE was tested with propane-oxygen in the pre-detonator and propane-air in the main combustor. Liquid fuel (kerosene) was also studied for use in the dual-stage PDE but the direct injection gasoline injectors were found to be inadequate for atomizing the fuel.
- Propane is recommended as a viable fuel for PDEs due to its wide availability and usage and other favorable characteristics, including high energy content in its compressed state, short ignition delay, ease of storage, ease of injection and mixing with air and the similarity of propane-air detonation cell size to that of aviation fuels and kerosene. Therefore, a detonation chamber designed for aviation fuel can also support propane-air detonations.
- A range of DDT devices were tested to determine their efficiency in achieving successful DDT with minimum drag while maintaining other favorable qualities, such as survivability and cooling. The Shchelkin spiral is found to be the best performing DDT device, but its variants such as internally grooved spirals and inter-connected rings with high blockage ratios greater than 50 % is recommended. However, the DDT section of the detonation chamber retains heat and creates hot spots that can cause pre-

ignition of the fuel-oxidizer mixture and lead to irregular firing of the engine. Also, the spirals were found to be easily destroyed. Therefore, active cooling has to be incorporated into the design of the DDT mechanisms. The Shchelkin spirals can be implemented by cutting grooves into the walls of the combustor or in the form of a replaceable spiral flanged sleeve that has spirals cut into it.

- The orifice plates are found to be a viable DDT mechanism because their design is simple and cooling features can be built into their design relatively easily. Orifice plates with BR in the range of 75 to 80 % are found in literature to produce DDT with just one or two plates.
- Both rotary valves and solenoid valves were studied. The first two PDE setups tested used a rotary valve system driven by a dc or universal motor to supply the gas to the combustor. However, rotary valves have many drawbacks. A sensor is needed to pick up the position of the valve. The frequency of the valve operation and consequently the PDE operating frequency are controlled by the speed of the motor, which could not be set precisely at low speeds. In addition, the valves were not made to tight tolerances and had large leakage and cross contamination of the gases. Since the motor turned at a steady speed, modulation of the valve timing could not be performed. Therefore, at higher frequencies, the amount of mass flowing per cycle was found to be reduced as long as the supply line pressures were maintained at the same pressure as at lower frequencies.
- Solenoid gas injectors were used in the latter three PDE setups. Solenoid valves can be precisely controlled with a TTL based timing system. Precise timing of the gas filling in conjunction with the ignition could be achieved by means of a computerized control system. The valves and the control system enabled the PDE to be tested in multi-cycle or single-shot mode without any change in geometry. The amount of mass flowing per cycle could be controlled by varying the width of the valve control pulse. However, at

higher frequencies, unless the supply line pressures are increased, the mass flow per cycle decreases.

- When the valves were opened, the line pressures were seen to drop as the gas supply lines could not maintain the flow rates required. Therefore, a closed-loop feedback pressure regulator and a high pressure pump is required to modulate the supply line pressures to enable higher mass flow rates at higher frequencies.
- Rotary valves are better for large mass flow applications, over solenoid valves, as they offer lower resistance in the flow path. Rotary valves are recommended for air flow control, with the addition of stepper motors for valve actuation. Solenoid valves are recommended for use in fuel filling. An array of high pressure injectors operating simultaneously can provide the required fuel flow rates. In addition, high pressure injectors, such as diesel injectors, are known to produce high shear on the fuel which enables the injectors to produce droplets sizes that are in the low micrometer range.
- Detonation in liquid aviation fuels are possible if they are fully vaporized and mixed with the air or if their droplet sizes are smaller than 10 μm. The atomization can be achieved by using proper injectors and preheating the fuel or air. Larger droplet sizes cause longer ignition delays.
- In addition, blending of small quantities of hydrogen to the fuel-air mixture can help in the reduction of ignition energy, ignition delays and promote DDT. The hydrogen can be produced onboard the aircraft in small quantities by means of plasmatron based fuel reformation of the hydrocarbon liquid fuels. Hydrogen can also be produced from electrolysis of water. Thus, the need for onboard hydrogen storage, which requires extreme pressurization or cryogenic cooling, is eliminated, thereby removing the associated risks of onboard hydrogen storage.
- High energy (HE) ignition systems were compared with low energy (LE) ignition systems to study their potential application in PDEs. HE ignition was found to reduce

ignition delay and also to ignite propane-air mixtures with the pre-detonator of the dual-stage PDE, which the LE ignition failed to do. However, HE ignition requires large and heavy power supplies that consume a large amount of electrical power. A large fraction of the power is wasted in the electrical components, the wires and in the electrodes of the igniters. The HE igniters suffer heavy damage and erosion of the electrodes during each firing and thus have shortened lives, which is not practical on a continuously firing PDE. LE igniters were found to work well with propane-oxygen mixtures, but not with propane-air mixtures. LE igniters also were severely damaged in the propane-oxygen detonations if they were in the line of flow. Recessing of the igniters protected them but prevented the propane-air mixtures from igniting. Therefore, a number of LE igniters (with independent power supplies) can be fired simultaneously to increase the energy transfer to the reactants.

- In addition to the LE ignition, corona discharge ionization of the air prior to fuel injection is recommended as a means to reduce the ignition delay of fuels. While corona discharge uses low amounts of power (about 500 W) it is known to produce ozone, which is a highly reactive oxidizing agent that reduces ignition delay, increases reaction rates and improves the detonation properties such as pressures and temperatures.
- Therefore, a successful PDE may use a LE ignition along with hydrogen blending, corona discharge ionization and DDT devices to produce consistent and sustained detonations.
- In this study, piezoelectric dynamic pressure transducers, ion detectors and photo-detectors were used to study the detonation waves. While dynamic pressure transducers have adequate response times, they are severely affected by the high temperatures and cannot sustain long duration runs unless they are actively cooled. An onboard refrigeration system is recommended for cooling transducers and vital components of the PDE. The pressure transducers were also recessed to protect them from the repeated detonations. However, the recessing introduces errors in the

measurements, in terms of attenuation of pressures and delayed response. Therefore, it is recommended that recessed pressure transducers be calibrated against a flush-mounted transducer to account for the errors.

- Ion transducers were found to be more reliable and durable than photo-detectors, and are recommended for the determination of wave speed in the combustor. Thus, recessed pressure transducers and ion detectors can be used in combination for detonation diagnostics.
- Other diagnostics in this study included thrust measurement with piezoelectric load cell and a linear slide mechanism, mass flow rate measurement with sonic flow nozzles and sound pressure level measurement with a microphone.
- All data acquisition and control processes were performed using LabVIEW, which enabled the real time monitoring and control of the PDEs under test. The recommended sampling rate required for detonation wave measurement is in the range of 2 to 5 MHz. However, the air and fuel flow rates, inlet and exhaust temperatures can be sampled at much lower rates, between 1 and 10 kHz, depending on the speed of the engine.
- The schematic of sample control system for a prototype PDE involving the various systems discussed here is presented. Such a system requires high speed diagnostics of the detonation wave, to measure detonation wave speed or Mach number, slow speed diagnostics to measure initial conditions within the detonation chamber, including initial temperature, pressure, fuel-air ratio, in addition to valving controls and ignition controls.

The analysis presented here of the various systems and techniques shall serve as the groundwork for the development of a fully functional PDE demonstrator that can be integrated into a vehicle.

APPENDIX A

STATION NUMBERING SCHEME FOR THE PDE

The station numbering of gas turbine and scramjets[4, 310] may also be applied for pulse detonation engines, as shown below.

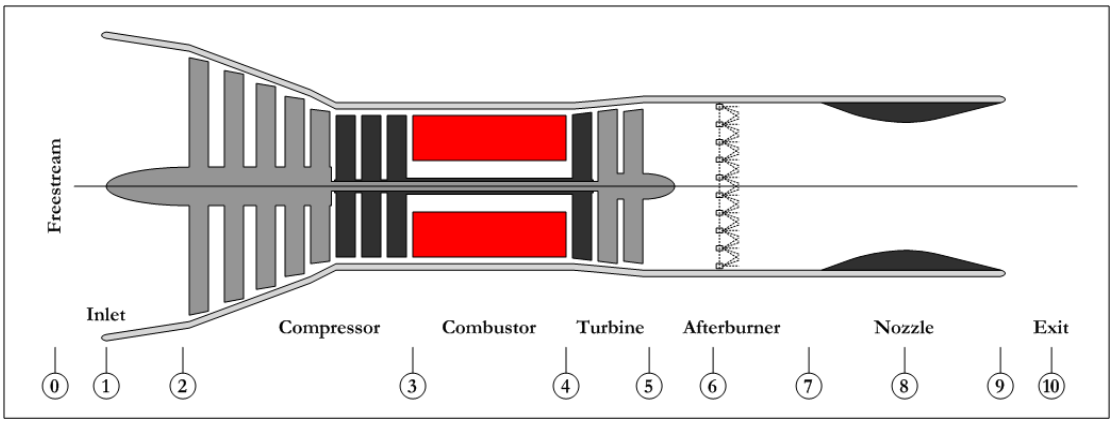

Figure A.1 Cross sectional view and station numbering scheme of a turbojet engine with afterburner.

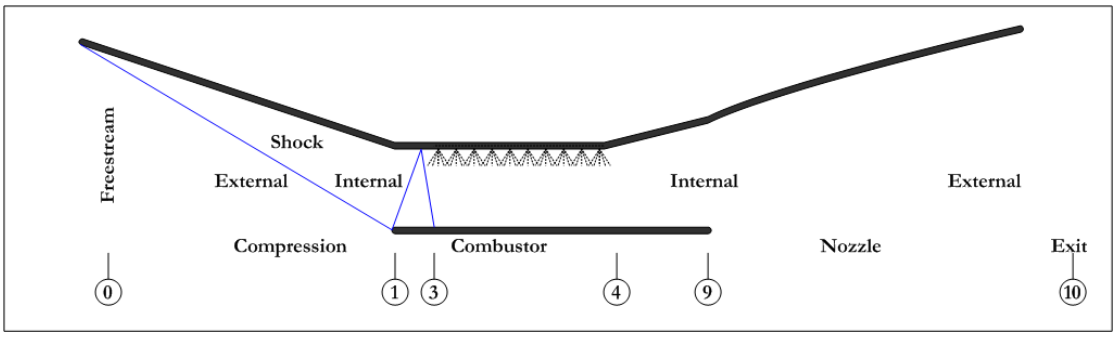

Figure A.2 Cross sectional view and station numbering scheme of a scramjet engine.

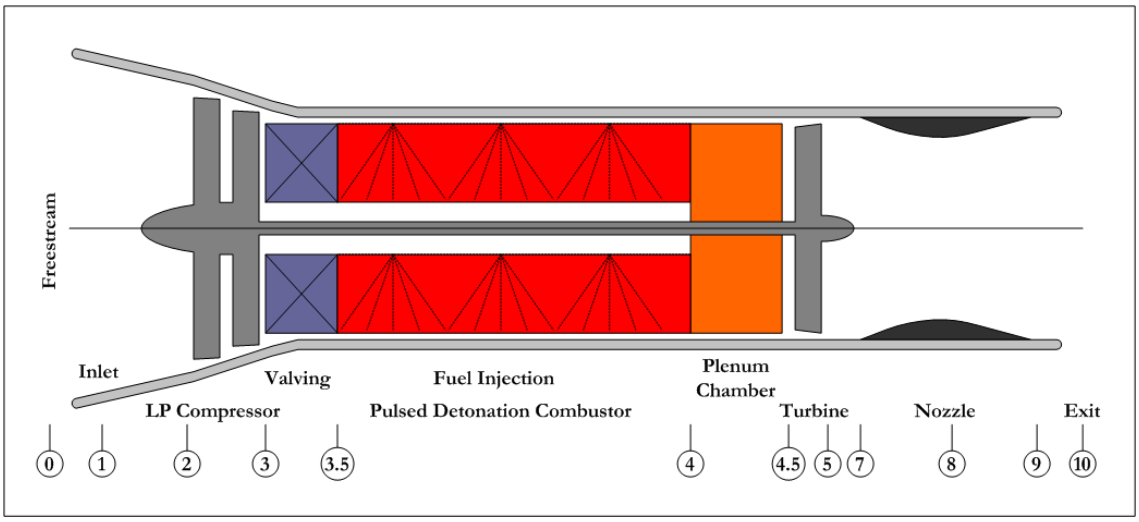

Figure A.3 Cross sectional view and station numbering scheme of a hybrid PDE.

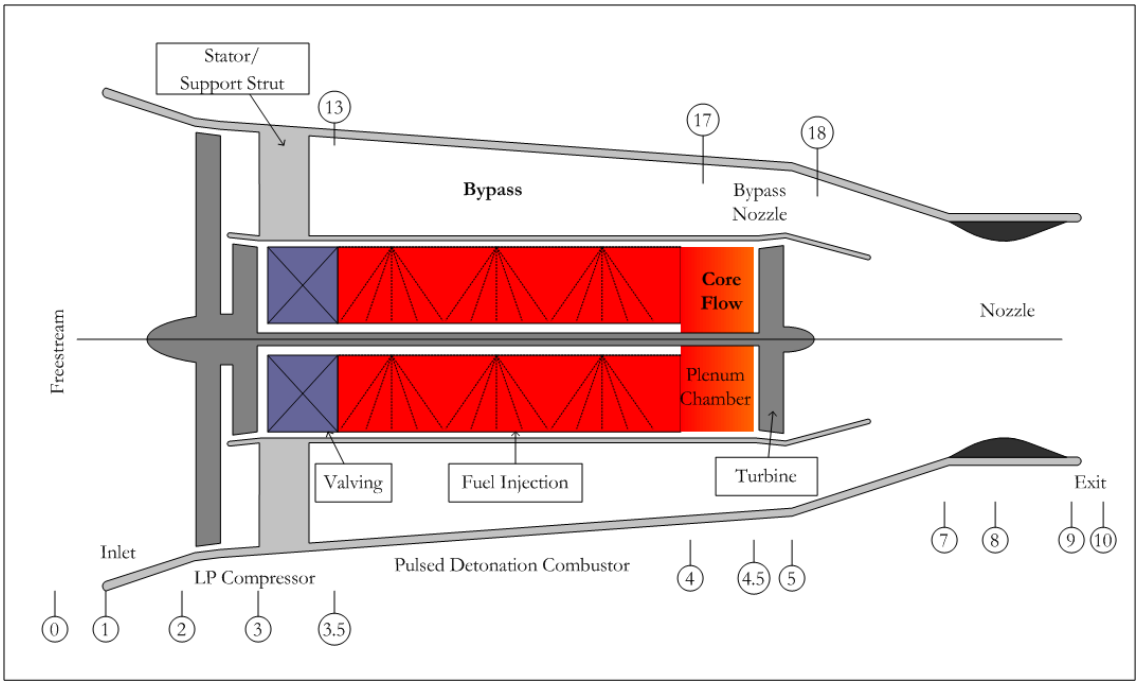

Figure A.4 Cross sectional view and station numbering scheme of a hybrid turbofan-PDE.

APPENDIX B

CIRCUIT DIAGRAMS OF THE IGNITION CIRCUIT

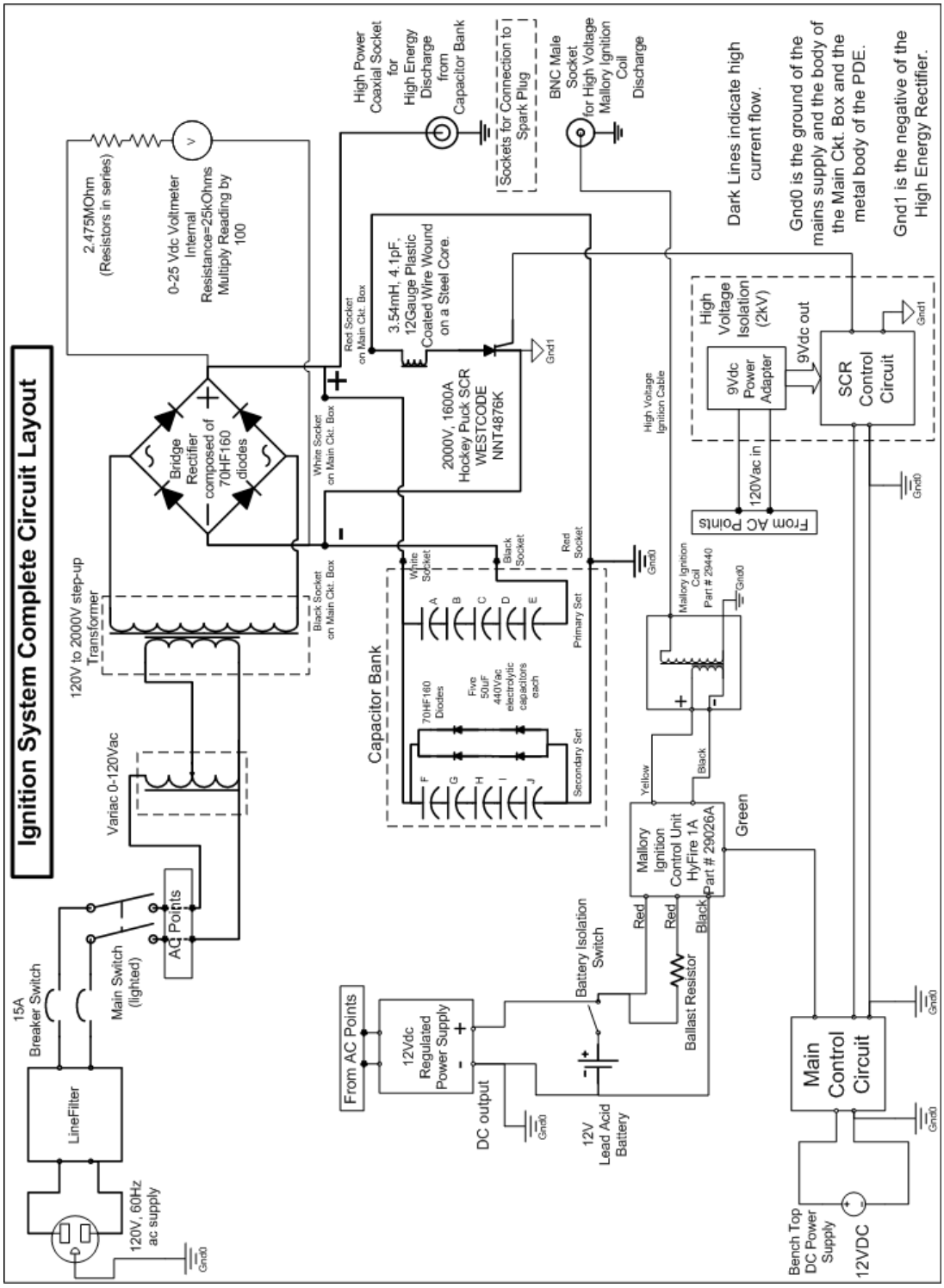

Figure B.1 Layout of the complete circuit of the dual-voltage, high energy ignition system used in the Bantam PDE and PDE Mark 1.

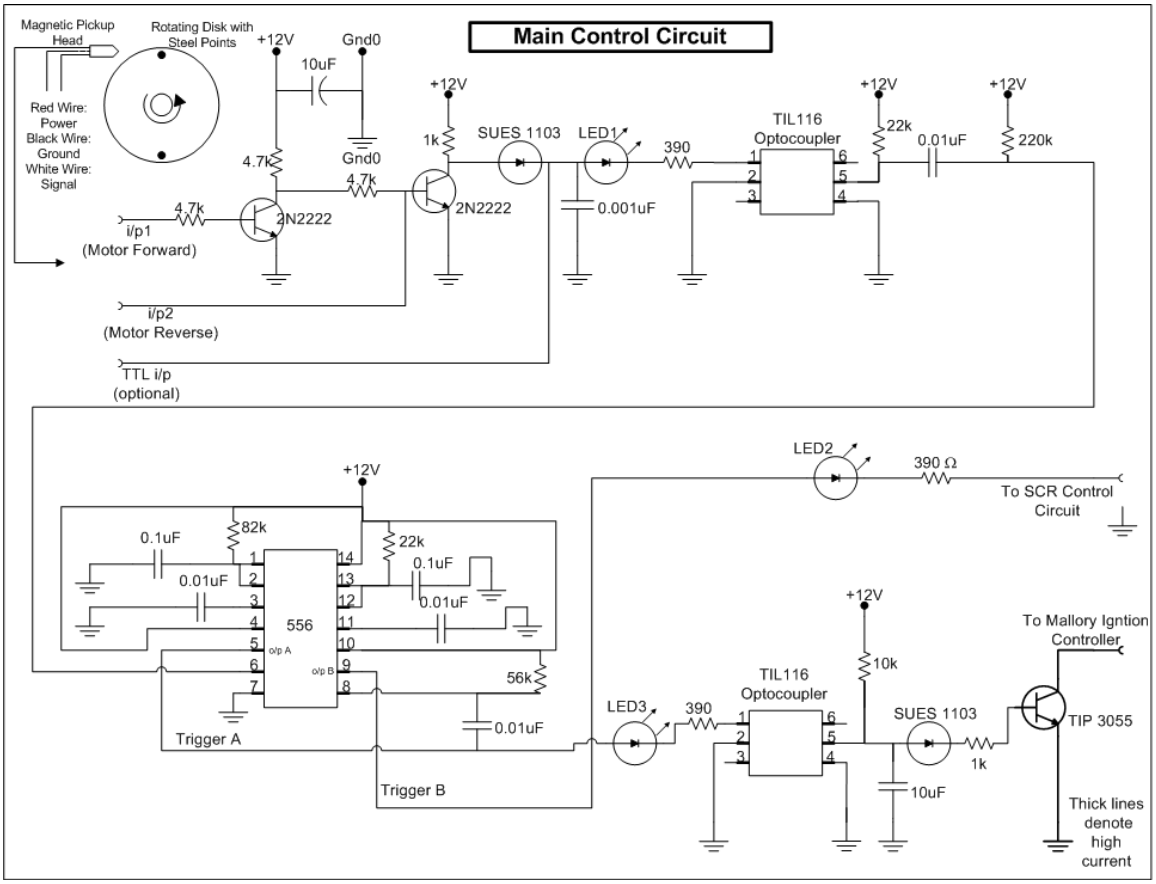

Figure B.2 Circuit diagram of the main control circuit used for the above dual-voltage, high energy ignition system.

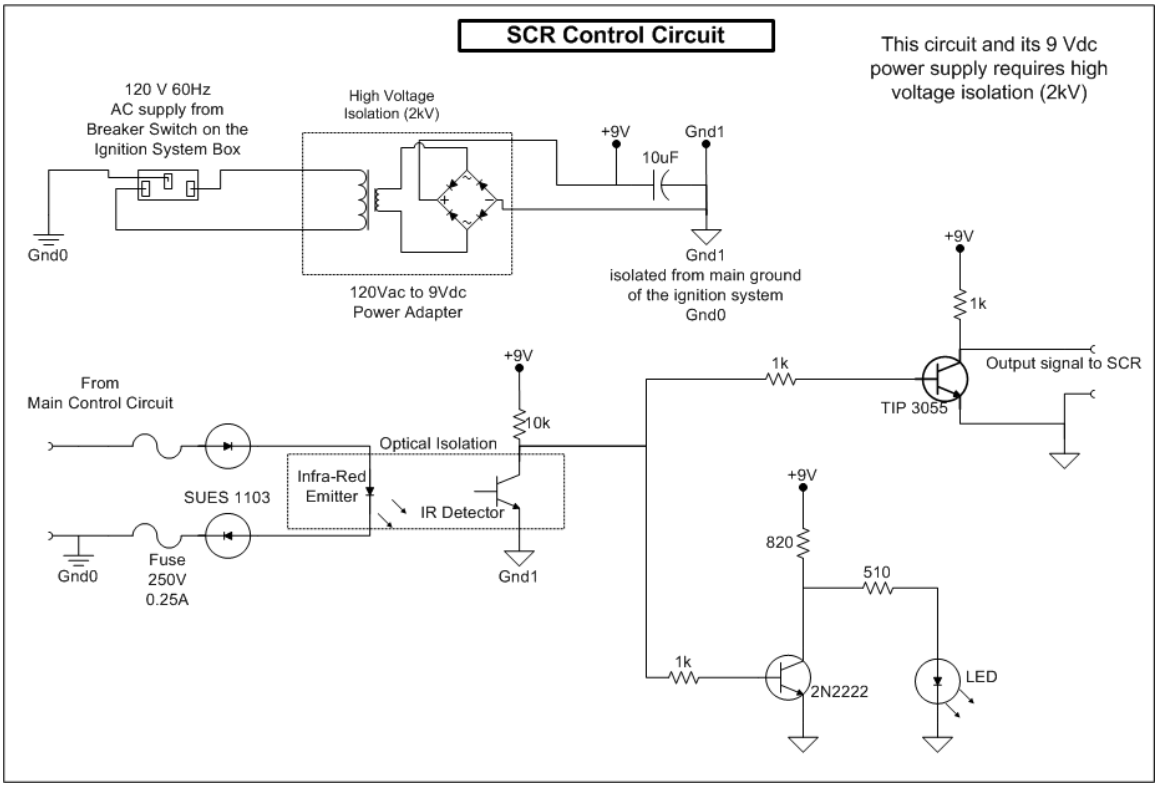

Figure B.3 Circuit diagram of the SCR control circuit used in the above dual-voltage, high energy ignition system.

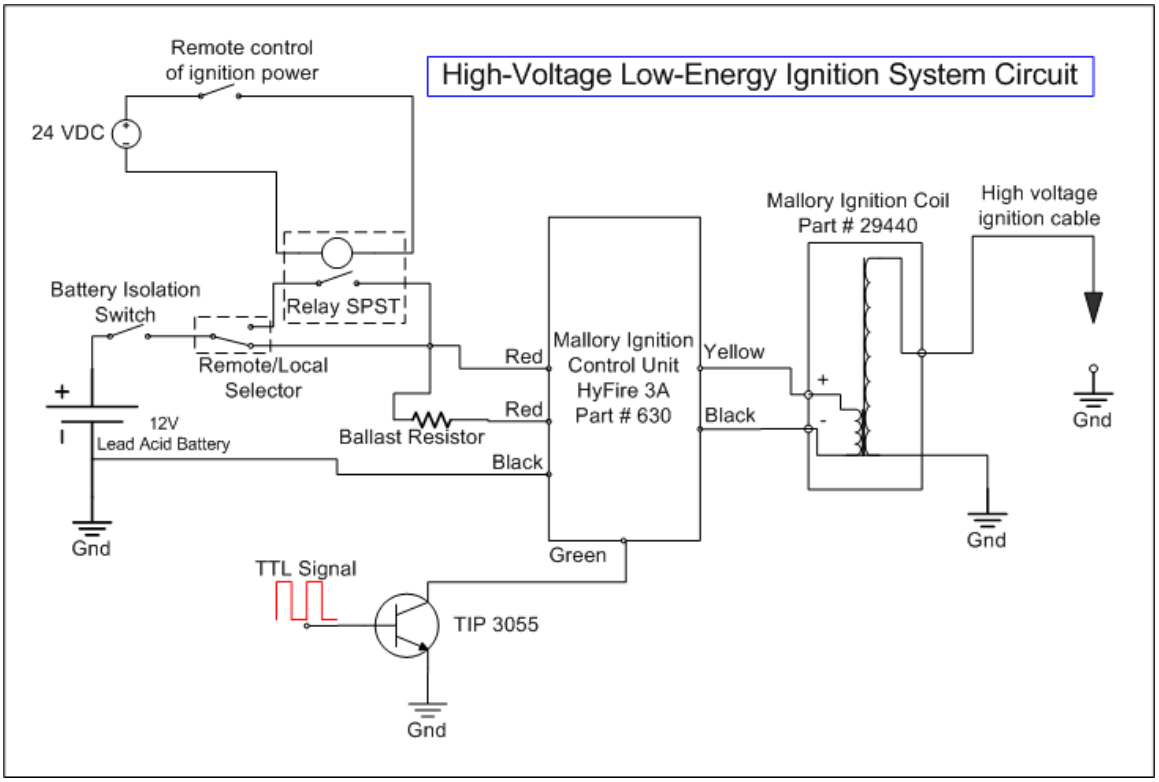

Figure B.4 Circuit diagram of the high-voltage, low energy ignition system used in PDE Mark 2, PDE Mark 3 and the dual-stage PDE.

APPENDIX C

UNCERTAINTY ANALYSIS

The true reading of a transducer R' may be expressed as the sum of the mean reading $\bar{R}$ and the uncertainty u_R at a given probability P, which is generally chosen to be the 95 % probability level[161]. Thus, the true reading may be represented as

$$R' = \bar{R} \pm u_R \quad (95\,\%) \tag{C.1}$$

The uncertainty is determined by the root-sum-squares (RSS) method by summing the squares of all the elemental errors as

$$u_R = \pm \sqrt{\sum_{k=1}^{K} e_k^2} \quad (P = 95\,\%) \tag{C.2}$$

If the property being measured by the transducer is a function of a number of independent variable $R = R\{x_1, x_2, ..., x_L\}$, then the sensitivity index due to each independent variable may be defined as

$$\theta_i = \left. \frac{\partial R}{\partial x_i} \right|_{x=\bar{x}} \tag{C.3}$$

The uncertainty in the reading due to each independent variable may then be written as

$$u_R = \pm \sqrt{\sum_{i=1}^{L} \left(\theta_i \, u_{\bar{x}_i} \right)^2} \quad (P = 95\,\%) \tag{C.4}$$

Data Acquisition Systems Used in The Study

The high speed data acquisition was performed using National Instruments (NI) PXI-6133 14-bit, 2.5 MS/s/channel simultaneous sampling DAQ cards, which were installed inside NI PXI-1042-Q chassis. The PXI-6133 cards are stated by the manufacturer's specifications to have an absolute accuracy at full scale of 2.440 $\mathrm{mV}\ (\pm 5\ \mathrm{V\ range})$ and a sensitivity of 218.4 $\mu\mathrm{V}\ (\pm 5\ \mathrm{V\ range})$. The high speed DAQ was used to acquire signals from the dynamic pressure transducers, the photo detectors and the ion transducers. The high speed DAQ, therefore, added an uncertainty of nearly 0.05 % to the reading.

The low speed data acquisition was performed using NI PCI-6024E 12-bit DAQ cards installed within a desktop computer. The PCI-6133E cards have an absolute accuracy at full

scale of 6.517 mV and a sensitivity of 0.686 mV for the $\pm 5\ \mathrm{V}$ range, while the accuracy and sensitivity were 0.119 mV and 0.009 mV respectively at the $\pm 50\ \mathrm{mV}$ range. The larger range was used for static pressure and flow rate measurements, whereas the shorter range was used for thermocouple measurements. The low speed DAQ added an uncertainty of 0.2 % on the $\pm 5\mathrm{V}$ range measurements and 0.24 % on the $\pm 50\ \mathrm{mV}$ range measurements.

For both DAQs mentioned above, the response times of the DAQ devices to the clock pulses (1 to 10 MHz) is listed as being the picoseconds (10^{-12} s). The accuracy of the clock pulses of the PXI-1042Q chassis is given as ±25 ppm with a jitter of 5 ps. Since the error due to timing of the DAQ devices is much smaller than the response times of the transducers (of the order of 1 μs), they are ignored in the uncertainty analysis. The time delays introduced by the Microsoft Windows operating system and the execution times of the LabVIEW programs vary from one program to another and from one instance to another. The delays are also in the nanoseconds and are ignored in the error analysis. The errors due to the sampling rate will be considered for the time-of-flight velocity calculations.

Uncertainties in The Output of Transducers

The uncertainties in the readings of thermocouples and static pressure transducers, calculated using the RSS method, are given below.

Table C.1 Uncertainty in temperature reading calculated using the RSS method for a variety of thermocouples.

Type	Low Temp.	High Temp	Standard error of thermocouple	Uncertainty due to DAQ	Uncertainty in temperature reading
	℃	℃	± %	± %	± %
B	0	1700	0.5	0.24	0.55
C	0	2320	1	0.24	1.03
D	0	2320	1	0.24	1.03
E	-200	900	0.5	0.24	0.55
G	0	2320	1	0.24	1.03
J	-40	750	0.75	0.24	0.79
K	-200	1350	0.75	0.24	0.79
N	-270	1300	0.75	0.24	0.79
R	0	1450	0.25	0.24	0.35
S	0	1450	0.25	0.24	0.35
T	-200	350	0.75	0.24	0.79

Table C.2 Uncertainty in the static pressure transducer readings calculated using the RSS method.

Omega static pressure transducer	200 psig
PX313-200G5V	0-5 V output
Accuracy	±0.25 %
Zero Balance	±0.4 %
Span Tolerance	±0.8 %
Long Term Stability	±0.5 %
Total Thermal Effects	±1 %
Uncertainty of Pressure Sensor	±1.45 %
Uncertainty of DAQ	±0.13 %
Total uncertainty of pressure reading	±1.46 %

Uncertainty in The Time-Of-Flight Velocity Calculations

The time-of-flight velocity of the detonation wave is given as

$$V = \frac{\Delta x}{\Delta t} \tag{C.5}$$

where Δx is the distance between the two transducers capturing the detonation wave and Δt

is the time taken for the detonation wave to traverse the distance between the two transducers. The time difference Δt and the uncertainty in the time difference $u_{\Delta t}$ are given as below.

$$\Delta t = t_2 - t_1; \quad u_{\Delta t} = \pm \frac{1}{f_{sampling}}; \tag{C.6}$$

In the above equation, the subscripts 1 and 2 denote the position of transducers, with transducer 2 being downstream of transducer 1. The uncertainty in the measurement of distance is taken as a constant value of 0.254 mm (or 0.01 in.). Errors in dimensions due to the fitting of the parts and thermal expansion are neglected. Thus, the uncertainty in the velocity is given as

$$u_{V} = \sqrt{\left(\frac{1}{\Delta t} u_{\Delta x}\right)^2 + \left(-\frac{\Delta x}{\Delta t^2} u_{\Delta t}\right)^2} \tag{C.7}$$

For example, if Δx = 50.8 mm and Δt = 20 µs, the TOF velocity is calculated to be 2540 m/s. The uncertainty for various sampling rates will be as shown in Table D.3.

Table C.3 The uncertainty calculated for various sampling rates for the case of Δx = 50.8 mm and Δt = 20 µs.

Sampling Rate, S/s	uncertainty, ± m/s
100,000	1270.063
150,000	846.762
200,000	635.127
240,000	529.319
250,000	508.159
300,000	423.524
400,000	317.754
500,000	254.317
750,000	169.809
1,000,000	127.633
1,250,000	102.391
1,500,000	85.614
2,000,000	64.758
2,500,000	52.363
3,000,000	44.197
4,000,000	34.196
5,000,000	28.398

APPENDIX D

PHOTOGRAPHS OF THE PDE APPARATUS

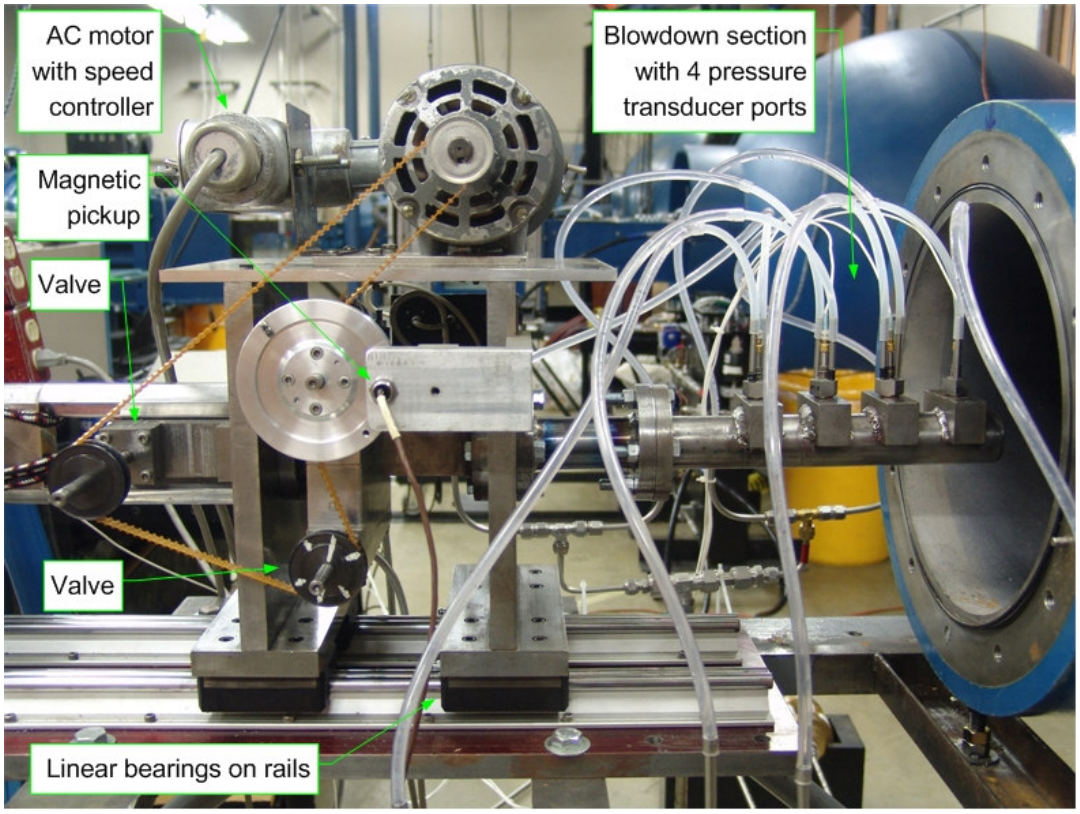

Figure D.1 Detail of the Bantam PDE.

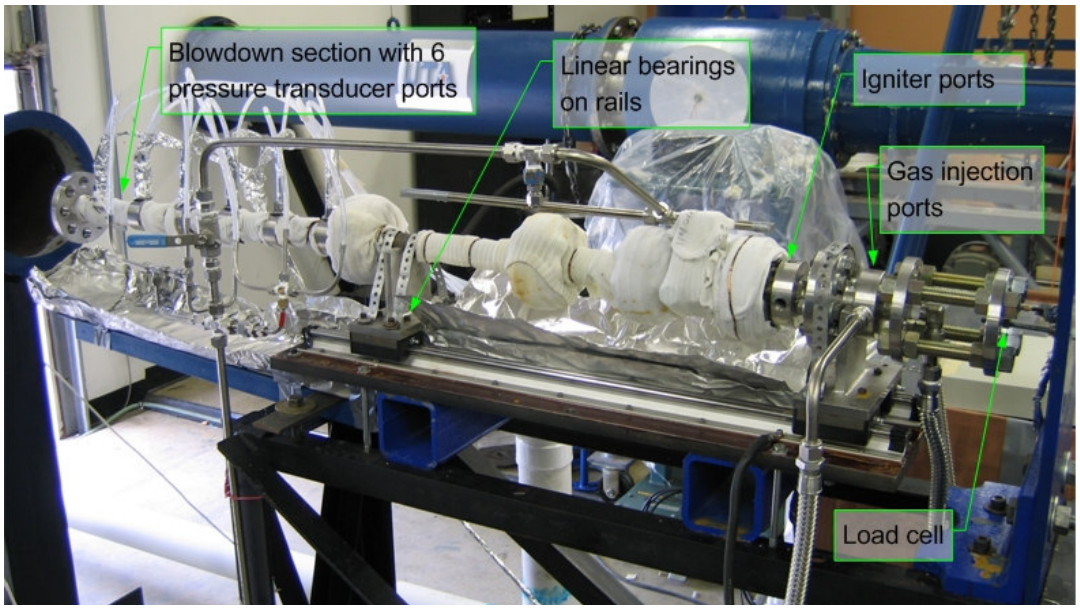

Figure D.2 Detail of the PDE Mark 1 showing the detonation tube wrapped in wetted cloth for cooling.

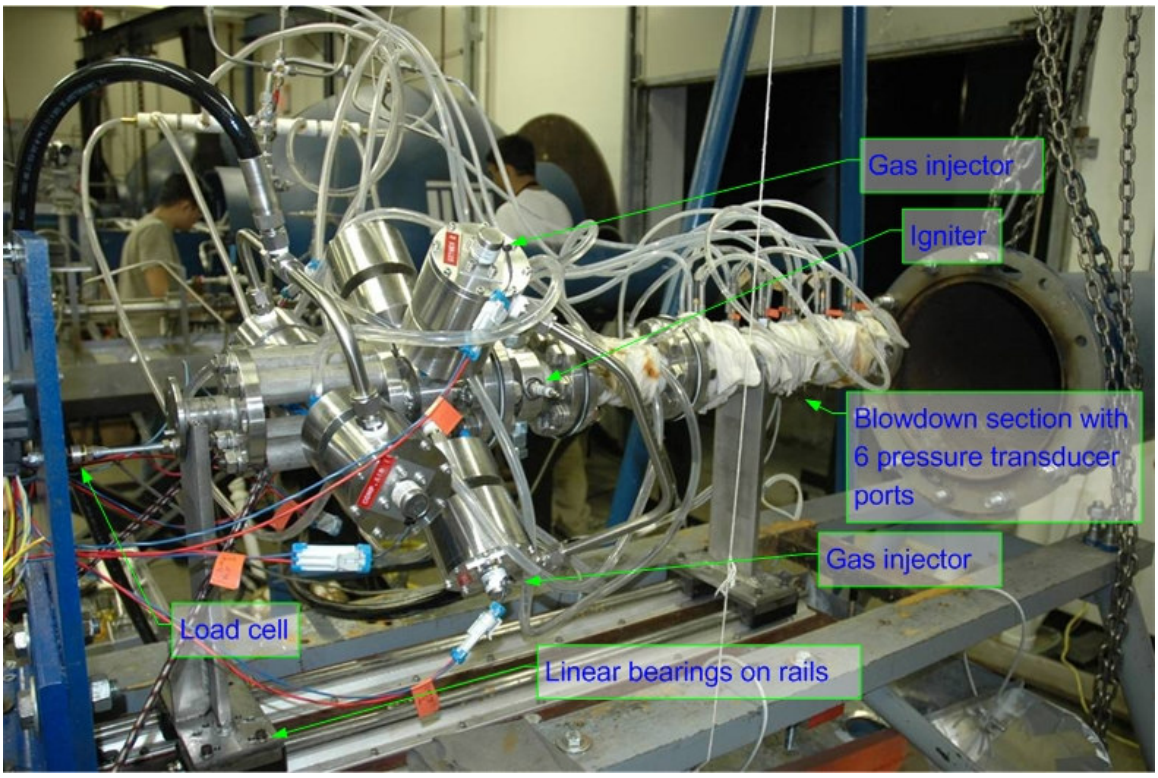

Figure D.3 Detail of the PDE Mark 2, with the transducer section wrapped with wetted cloths for cooling.

Figure D.4 Detail of a Shchelkin spiral that was tested in the PDE Mark 2 using stoichiometric propane-oxygen mixtures at 15 Hz for about 15 to 20 s. The spiral experienced significant damage.

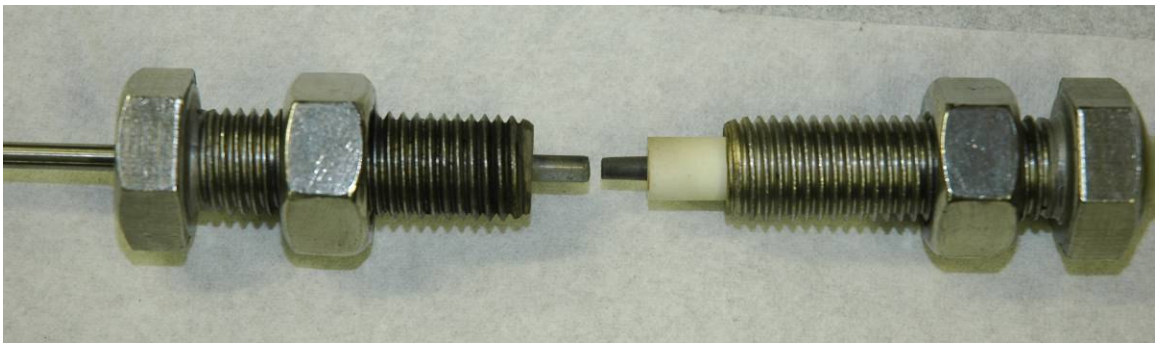

Figure D.5 Detail of the ignition plugs used in the PDE Mark 2 shown prior to testing.

Figure D.6 Detail of the ignition plug used in the PDE Mark 2 shown after testing. Significant damage was sustained in a test lasting 15 to 20 s.

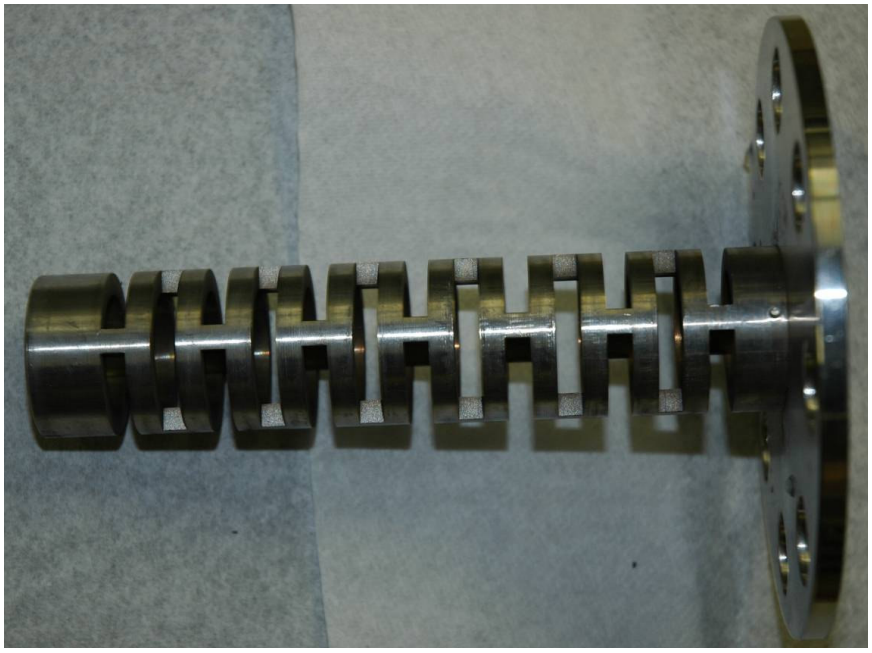

Figure D.7 Detail of the slotted-sleeve DDT device used in the PDE Mark 2.

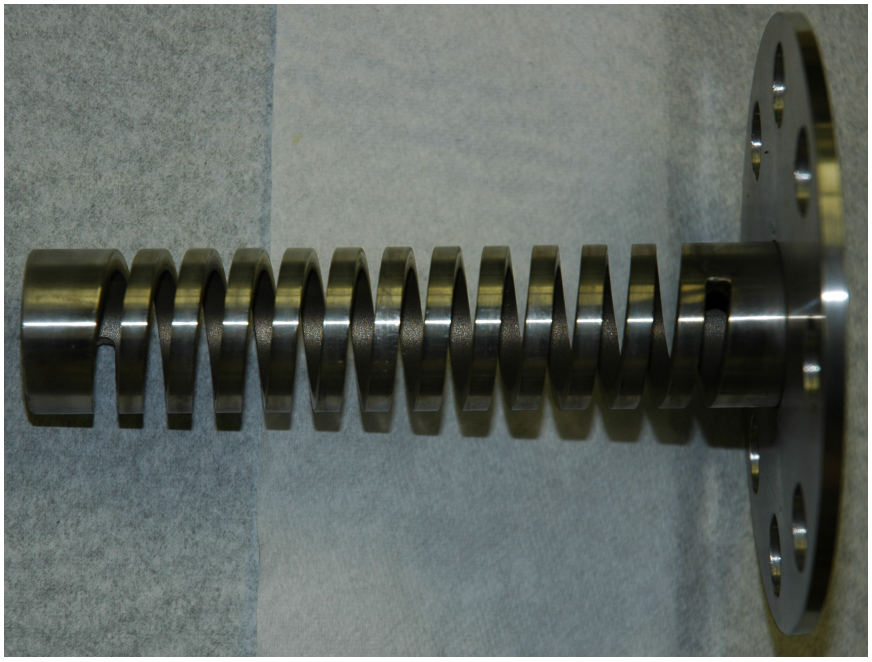

Figure D.8 Detail of the spiral-sleeve DDT device used in the PDE Mark 2.

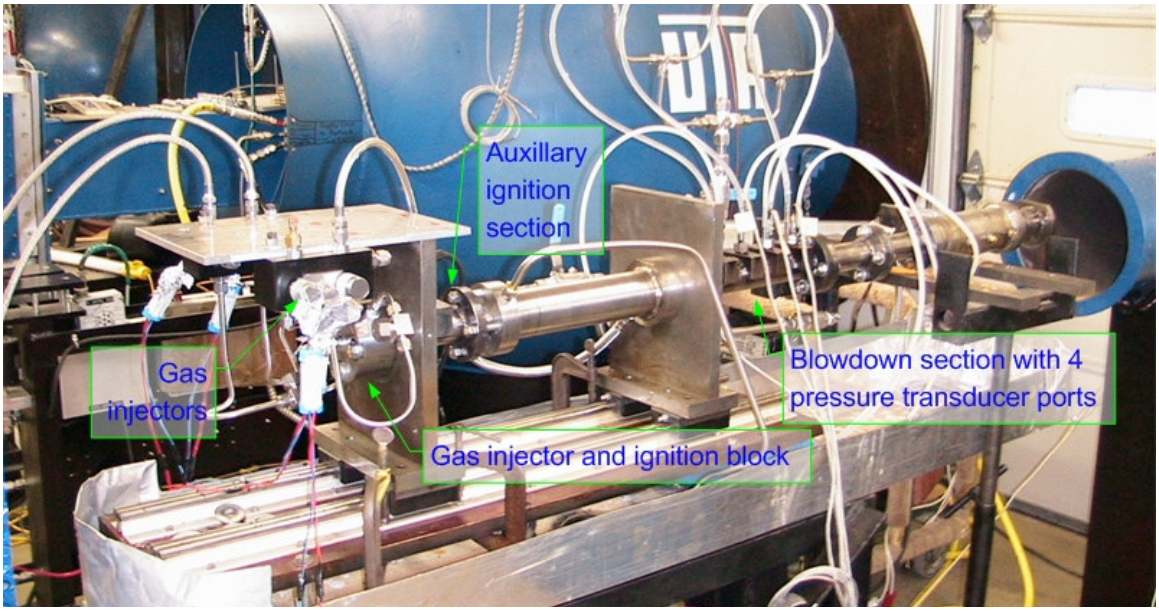

Figure D.9 Detail of the PDE Mark 3.

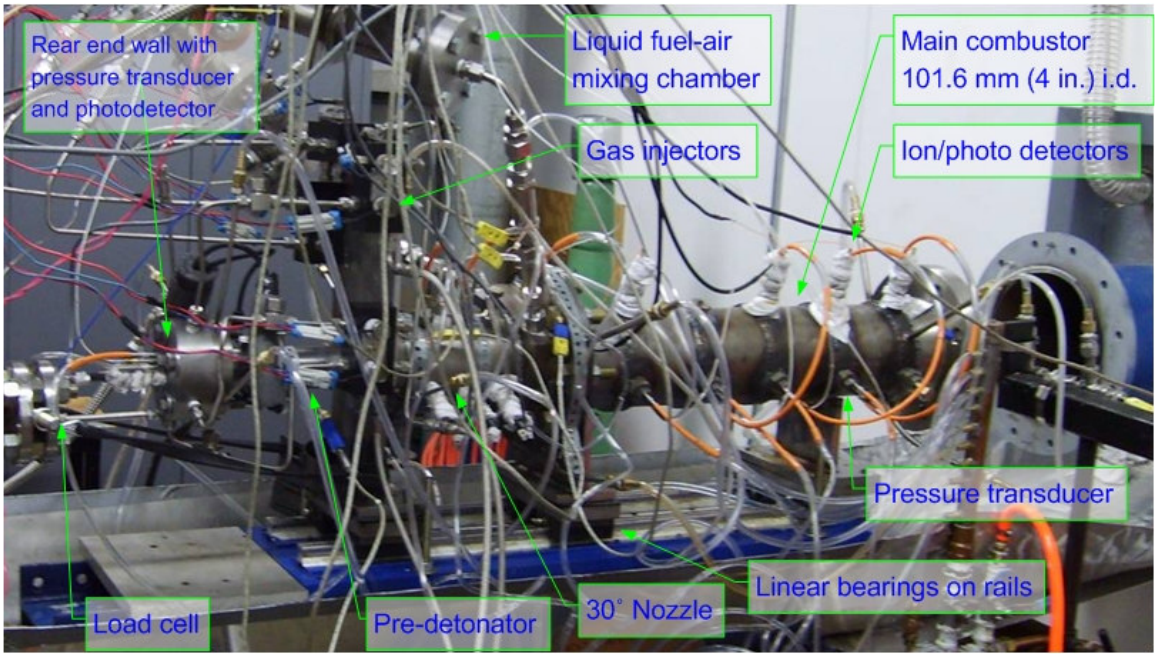

Figure D.10 Detail of the dual-stage PDE.

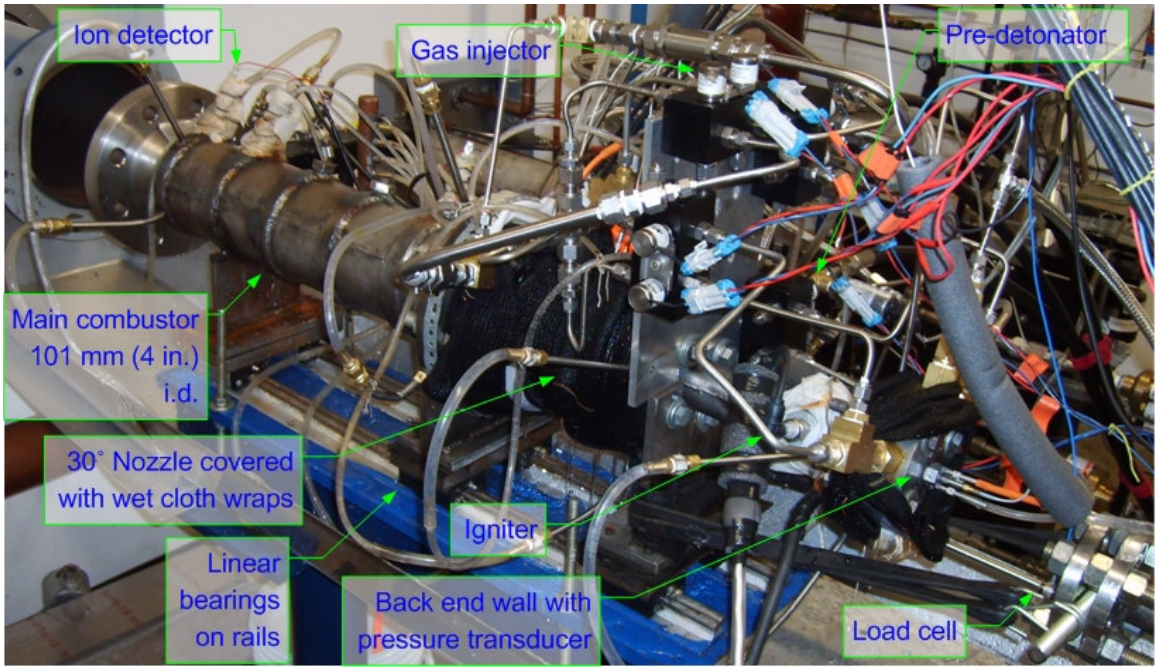

Figure D.11 Another picture of the dual-stage PDE.

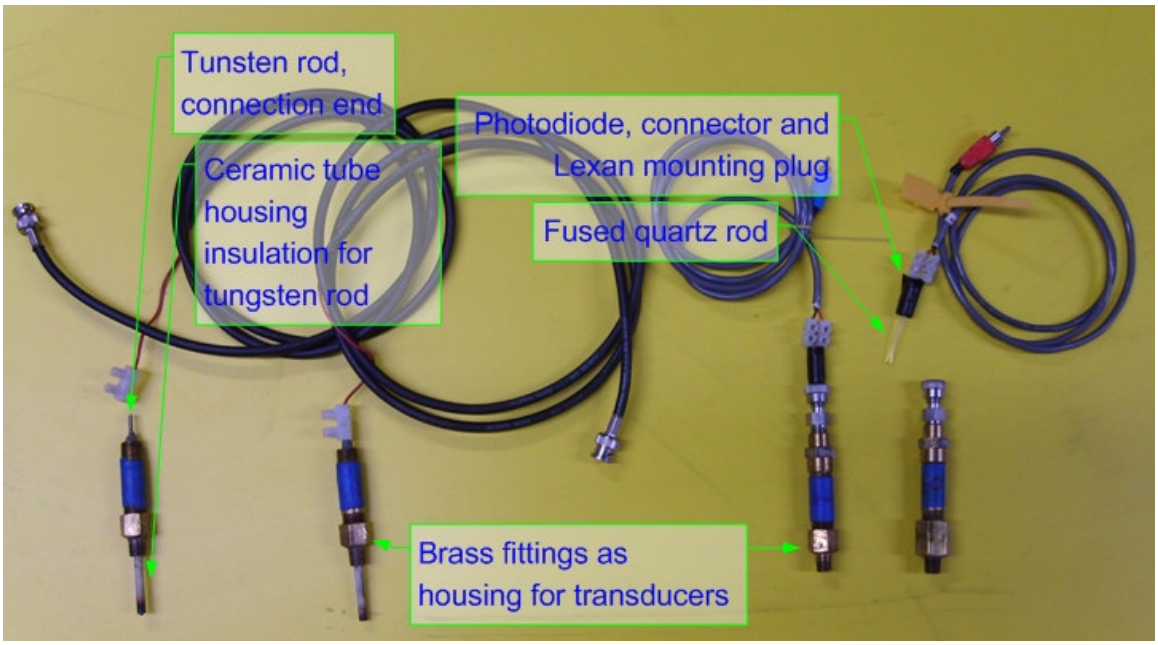

Figure D.12 Details of the ion detectors (left) and the photo detectors (right) used in the dual-stage PDE.

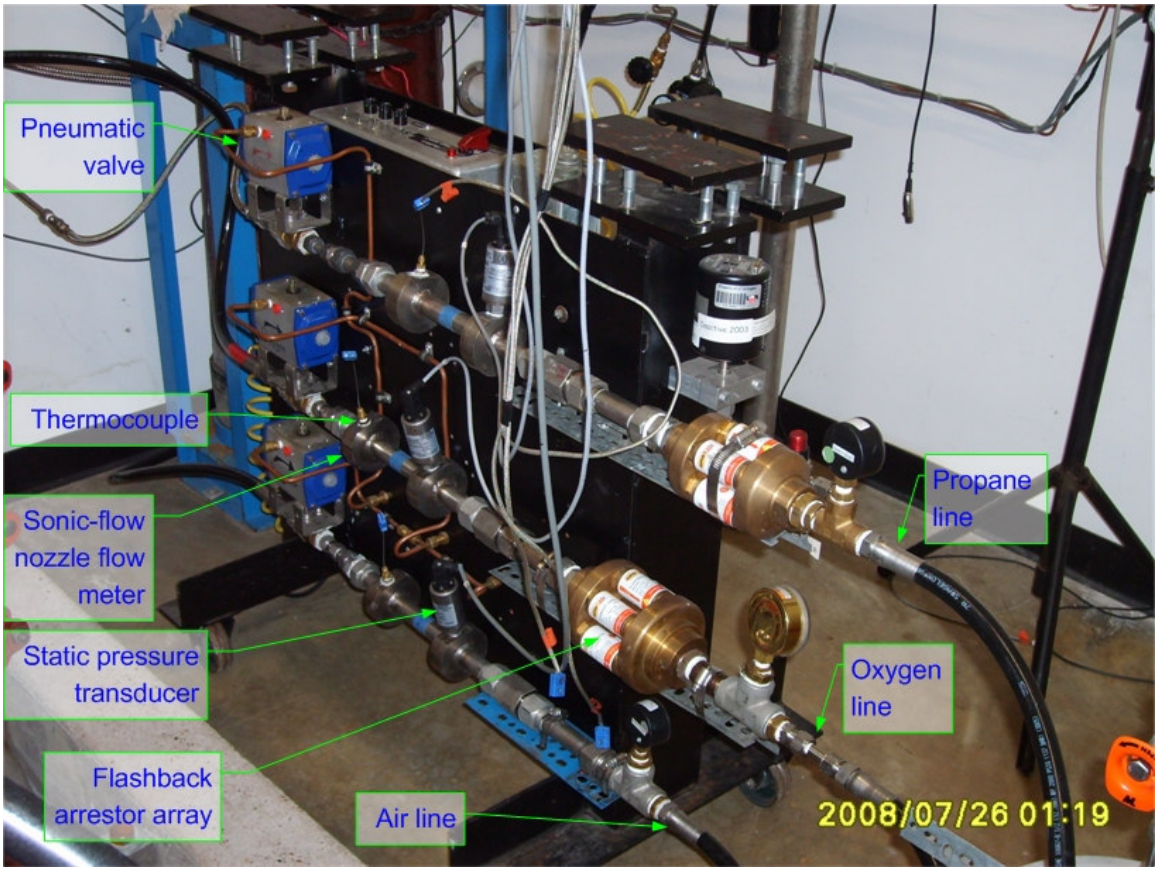

Figure D.13 Detail of the gas supply cart showing the sonic flow nozzles, flash-back arrestors and pneumatic valves.

REFERENCES

[1] *The Jet Engine*, 5th Edition, Rolls Royce PLC, Derby, England, 1996, propulsive efficiency: pg. 4-9; igniters: pg. 127-131; water injection: pp. 181-185.

[2]Riester, E., "Comparison of Turbojet, Turborocket and Ramjet as a Propulsion System for Long Range Airplanes at Mach Numbers Between 2 and 4," FTD-ID(RS)I-1653-75, 31 Jul. 1975; Edited Translation of Deutsche Luft- und Raumfahrt. Forschungsbericht (West Germany), n38, pp. 1-36, 1972.

[3]Hill, P., Peterson, C., *Mechanics and Thermodynamics of Propulsion*, 2nd Edition, Addison-Wesley Publishing Company, Inc., 1992, pp. 21, 155-164.

[4]Heiser, W.H. and Pratt, D.T., *Hypersonic Airbreathing Propulsion*, AIAA Education Series, Washington D.C., 1994, scramjet: pp. 23-26, ODWE: pp. 545-551.

[5]Kailasanath, K. "Recent Developments in the Research on Pulse Detonation Engines," AIAA Paper 2002-0470, AIAA 40th Aerospace Sciences Meeting, Reno, NV, 14–17 Jan. 2002.

[6]Bussing, T.R.A., Bratkovich, T.E. and Hinkey, J.B., "Practical Implementation of Pulse Detonation Engines," AIAA-1997-2748, 33rd AIAA/ASME/SAE/ASEE Joint Propulsion Conference and Exhibit, 6-9 Jul. 1997, Seattle, WA.

[7]Kentfield, J.A.C., "The Potential of Valveless Pulsejets For Small UAV Propulsion Applications," AIAA-1998-3879, 34th AIAA/ASME/SAE/ASEE Joint Propulsion Conference and Exhibit, Cleveland, OH, 13-15 Jul. 1998.

[8]Smith, D.E., "The Synchronous Injection Ignition Valveless Pulsejet," Doctoral Dissertation, Department of Aerospace Engineering, The University of Texas at Arlington, Arlington, TX, 1987.

[9]Oates, G.C., *Aerothermodynamics of Gas Turbine and Rocket Propulsion*, 3rd Ed., AIAA Education Series, AIAA, 1997, pp. 65.

[10]Munipalli, R., Shankar V., Wilson, D.R., and Lu F.K., "Preliminary design of a pulse detonation based combined cycle engine," ISABE Paper 2001–1213, *15th International Symposium on Airbreathing Engines*, Bangalore, India, 2–7 Sep. 2001.

[11]Frolov, S.M., "Liquid-Fueled Air Breathing Pulse Detonation Engine Demonstrator: Operation Principles and Performance," Journal of Propulsion and Power, Vol. 22, No. 6, Nov.-Dec. 2006.

[12]Rasheed, A., Furman, A. and Dean, A.J., "Experimental Investigations of an Axial Turbine Driven by a Multi-tube Pulsed Detonation Combustor System," AIAA 2005-4209, 41st AIAA/ASME/SAE/ASEE Joint Propulsion Conference, Tucson, AZ, 10-13 Jul. 2005.

[13]Kailasanath, K., "Applications of Detonations to Propulsion: A Review," AIAA 99-1067, 37th AIAA Aerospace Sciences Meeting and Exhibit, Reno, NV, 11-14 Jan. 1999.

[14]Google Patent Search, URL: www.google.com/patents, accessed May 2008.

[15]United States Patent and Trademark Office, URL: http://www.uspto.gov/patft/index.html, accessed May 2008.

[16]European Patent Office, URL: http://www.epo.org/, accessed May 2008.

[17]Nicholls, J.A., Wilkinson, H.R., Morrison, R.B., and Ong, R., "Intermittent Detonation as a Thurst-Producing Mechanism," Progress Report No. 2, Wright Aeronautical Division, Curtiss-Wright Corporation, Jul. 1954.

[18]Krzycki, L.J., "Performance Characteristics of an Intermittent Detonation Device," NAVWEPS Report 7655, Naval Ordnance Test Station, China Lake, California, Jun. 1962.

[19]Helman, D., Shreeve, R.P,, and Eidelman, S., "Detonation Pulse Engine," Naval Post Graduate School, Monterey, California, 1986.

[20]Lu, F.K. and Wilson, D.R., "Detonation Driver For Enhancing Shock Tube Performance," Shock Waves, Vol. 12, No.6, May 2003, pp. 457–468.

[21]Stanley, Steven B., "Experimental Investigation of Factors Influencing the Evolution of a Detonation Wave," Master's Thesis, Department of Mechanical and Aerospace Engineering, The University of Texas at Arlington, Arlington, TX, 1995.

[22]Stuessy, W.S. and Wilson, D.R., "Experimental Investigation Of An Annular Pulse Detonation Wave Engine," AIAA Paper 97–0808, AIAA 35th Aerospace Sciences Meeting, Reno, NV, 6–9 Jan. 1997.

[23]Burge, Karl R., "Pulse Detonation - Detonation Continuance in Fuel-Air Regions," Master Thesis, Department of Mechanical and Aerospace Engineering, The University of Texas at Arlington, Arlington, TX, 1995.

[24]Stuessy, W.S. and Wilson, D.R., "Experimental Investigation of an Annular Pulse Detonation Wave Engine," AIAA Paper 97–0808, AIAA 35th Aerospace Sciences Meeting, Reno, NV, Jan. 6–9, 1997.

[25]Meyers, J. M., "Performance Enhancements on a Pulsed Detonation Rocket," Master's Thesis, Department of Mechanical and Aerospace Engineering, The University of Texas at Arlington, Arlington, TX, 2002.

[26]Fickett, W. and Davis, W.C., *Detonation Theory and Experiment*, Dover Publications Inc., Mineola, New York, 1979; Fickett-Davis cycle: pp. 35-38.

[27]Wintenberger, E., "Application of Steady and Unsteady Detonation Waves to Propulsion," Ph.D. Thesis, California Institute of Technology, Pasadena, CA, 2004.

[28]Pulkrabek, W., *Engineering Fundamentals of the Internal Combustion Engine*, 2nd edition, Prentice Hall, New Jersey, 1997, pp. 113.

[29]Wu, Chih, *Thermodynamic Cycles: Computer-Aided Design and Optimization*, CRC Press, LLC, 2003, pp. 132.

[30]Moran, M.J. and Shapiro, H.N., *Fundamentals of Engineering Thermodynamics*, 3rd. edition, John Wiley and Sons, Inc., New York, NY, 1996, pp. 373-404.

[31]Mattingly, J.D., *Elements of Gas Turbine Propulsion*, McGraw-Hill, Inc., New York, NY, 1996, pp. 240-336.

[32]Li, J., Lai, W.H. and Chung, K., "Tube Diameter Effect on Deflagration to Detonation Transition of Propane-Oxygen Mixtures," Shock Waves, Vol. 16, No. 2, Dec. 2006, pp. 109-117.

[33]Li, J., "Experimental Study on Detonation Initiation and Transmission Across a Mixture," Ph.D. Dissertation, Department of Aeronautics and Astronautics, National Cheng Kung University, Tainan, Taiwan, ROC, Aug. 2007.

[34]Nettleton, M.A*., Gaseous Detonations: Their Nature, Effects and Control*, Chapman and Hall Ltd., New York, NY, 1987, pp. 126-129.

[35]Ciccarelli, G., Fowler, C.J., and Bardon, M., "Effect of Obstacle Size and Spacing on the Initial Stage of Flame Acceleration in a Rough Tube," Shock Waves, Vol. 14, No. 3, 2005, pp. 161-166.

[36]Bellini, R. and Lu, F.K., "Exergy Analysis of a Pulse Detonation Power Device," *10th Brazilian Congress of Thermal Engineering and Sciences*, Rio de Janeiro, Brazil, Nov. 29-Dec. 3, 2004.

[37]Heiser, W.H. and Pratt, D.T., "Thermodynamic Cycle Analysis of Pulse Detonation Engines," Journal of Propulsion and Power, Vol. 18, No. 1, Jan.-Feb. 2002.

[38]Panicker, P.K., Wilson, D.R., and Lu, F.K., "Operational Issues Affecting the Practical Implementation of Pulse Detonation Engines," AIAA-2006-7959, *14th AIAA/AHI Space Planes and Hypersonic Systems and Technologies Conference*, Canberra, Australia, 6-9 Nov. 2006.

[39]James, H., "Detonations," Health and Safety Commission of Great Britain, DIN TD5 039, Oct. 2001.

[40]Borman, G. L. and Ragland, K.W., "Combustion Engineering," McGraw Hill, 1998.

[41]Kuo, K.K., "Principles of Combustion," 2nd Ed., John Wiley and Sons, Inc., 2005.

[42]McBride, B.J. and Gordon, S., Chemical Equilibrium with Applications (CEA) code, CEA2 with CEAgui, Version 1.0, URL: http://www.grc.nasa.gov/WWW/CEAWeb/, accessed Jul. 2008.

[43] Kaneshige, M. and Shepherd, J.E., "Detonation Database. Technical Report FM97-8," GALCIT, Jul. 1997. See also the electronic hypertext version at http://www.galcit.caltech.edu/detn_db/html/, accessed May 2008.

[44]Strehlow, R.A. and Engel, C.D., "Transverse Waves in Detonations: II. Structure and Spacing in H_2-O_2, C_2H_2-O_2, C_2H_4-O_2 and CH_4-O_2 Systems," AIAA Journal, Vol. 7, No. 3, 1969, pp. 492-496.

[45]Manzhalei, V.I., Mitrofanov, V.V. and Subbotin. V.A., "Measurement of Inhomogeneities of a Detonation Front in Gas Mixtures At Elevated Pressures," Combustion Explosion Shock Waves (USSR), Vol. 10, No. 1, 1974, pp. 89-95.

[46]Denisov, Y.N. and Troshin, Y.K., "Structure of Gaseous Detonation in Tubes," Soviet. Physics – Technical Physics, Vol. 5, No. 4, 1960, pp. 419-431.

[47]Desbordes, D., "Aspects Stationnaires et Transitoires de la Detonation Dans les Gaz: Relation Avec la Structure Cellulaire du Front," Ph.D. Thesis, Universite de Poitiers, 1990.

[48]Zitoun, R., Desbordes, D, Guerraud, C. and Deshaies, B., "Direct Initiation of Detonation in Cryogenic Gaseous H_2-O_2 Mixtures," Shock Waves, Vol. 4, No. 6, 1995, pp. 331-337.

[49]Knystautas, R., Lee, J.H. and Guirao, C.M., "The Critical Tube Diameter for Detonation Failure in Hydrocarbon-Air Mixtures," Journal of Combustion and Flame, Vol. 48, No. 1, 1982, pp. 63-83.

[50]Handbook of Chemistry and Physics, 88th Edition, 2007 – 2008, CRC Press, LLC, URL: http://www.hbcpnetbase.com/; Section 2: Definitions of Scientific Terms; Section 16: Flammability of Chemical Substances; accessed Jul. 2008.

[51]McMurry, J., and Fay, R.C., *Chemistry*, 2nd Edition, Prentice Hall, NJ, 1995, pp. 942-986, Chapter 23: Organic Chemistry.

[52]*Handbook of Aviation Fuel Properties,* CRC Report No. 635, 3rd edition, Coordinating Research Council, Inc (CRC), Alpharetta, GA, 2004.

[53]Conkling, J.A., *Chemistry of Pyrotechnics: Basic Principles and Theory*, CRC Press, LLC, 1985, pp. 167-168, Chapter 8: Smoke and Sound.

[54]Morrell, J.C., (To Universal Oil Products Company, Chicago, IL), "Stabilization of Gasoline and the Like," U.S. Patent 2,354,873, 01 Aug. 1944.

[55]Vasilev, A.A., "Cell Size as the Main Geometric Parameter of a Multifront Detonation Wave," Journal of Propulsion and Power, Vol. 22, No. 6, Nov.-Dec. 2006.

[56]Kuchta, J. M., *Investigation of Fire and Explosion Accidents in the Chemical, Mining, and Fuel-Related Industries – a Manual*, Bulletin 680, U.S. Bureau of Mines, 1985, Appendix A.

[57]Bull, D.C., Elsworth, J.E., Shuff, P.J. and Metcalfe, E., "Detonation Cell Structures in Fuel/Air Mixtures," Combustion and Flame, Vol. 45, No. 1, pp. 7-22, 1982.

[58]Knystautas, R., Guirao, C., Lee, J.H. and Sulmistras, A., "Measurement of Cell Size in Hydrocarbon-Air Mixtures and Predictions of Critical Tube Diameter, Critical Initiation Energy, and Detonability Limits," Progress in Astronautics and Aeronautics, Vol. 94, pp. 23-37, 1984.

[59]*Propane, The Exceptional Energy: Policies For a 21st Century Fuel*, National Propane Gas Association, Jun. 2001, URL: http://www.npga.org/files/public/National_Energy_Policy.pdf, accessed Jun. 2008.

[60]*Key World Energy Statistics 2007*, Annual Report, International Energy Agency, URL: http://www.iea.org/textbase/nppdf/free/2007/Key_Stats_2007.pdf, accessed Jun. 2008.

[61]Ma, L, Brophy, C.M., Mattison, D.W., Hinckley, K.M., Jeffries, J.B. and Hanson, R.K., "Propane Fuel Monitoring in Pulse Detonation Engines Using a Diode-Laser Sensor," AIAA 2003-4684, 39th AIAA/ASME/SAE/ASEE Joint Propulsion Conference and Exhibit, Huntsville, AL, 20-23 Jul. 2003.

[62]DeLuchi, M.A., "Emissions of Greenhouse Gases from the Use of Transportation Fuels and Electricity," Center for Transportation Research, Argonne National Laboratory (ANL), Publication No. ANL/ESD/TM-22, Vol. 1, Publication No. UCD-ITS-RP-91-30, Nov. 1991.

[63]Material Safety Data Sheet (MSDS) for Odorized Propane, National Propane Gas Association, NPGA 210-96, issued Dec. 1996, URL: http://www.npga.org/files/public/Tech_Bulletin_NPGA_210-96.pdf, accessed Jun. 2008.

[64]NIST Standard Reference Database Number 69, Jun. 2005 Release, URL: http://webbook.nist.gov/chemistry/, accessed Jul. 2008.

[65]Ohe, S., *Computer Aided Data Book of Vapor Pressure*, 2nd Edition, Data Publishing Inc., Tokyo, Japan, 1999, URL: http://www.s-ohe.com/Propane_cal.html, accessed Jun. 2008.

[66]*Aviation Fuels Technical Review 2006*, Chevron Corporation, 2006.

[67]Day, D.A., "Aviation Fuel," U.S. Centennial of Flight Commission, Essays, URL: http://www.centennialofflight.gov/essay/Evolution_of_Technology/fuel/Tech21.htm, accessed Jun. 2008.

[68]Akbar, R., Thibault, P.A., Harris, P.G., Lussier, L.-S., Zhang, F., Murray, S.B., and Gerrard, K., "Detonation Properties of Unsensitized and Sensitized JP-10 and Jet-A Fuels in Air for Pulse Detonation Engines," AIAA-2000-3592, AIAA/ASME/SAE/ASEE 36th Joint Propulsion Conference and Exhibit, Huntsville, AL, 16-19 Jul. 2000.

[69]Mawid, M. A., Park, T. W., Sekar, B., Arana C. and Aithal, S. M. "Development of a Detailed Chemical Kinetic Mechanism for Combustion of JP-7 Fuel," AIAA 2003-4939, 39th AIAA/ASME/SAE/ASEE Joint Propulsion Conference and Exhibit, Huntsville, AL, 20-23 Jul. 2003.

[70]Helfrich, T.M., Schauer, F.R., Bradley, R.P., and Hoke, J.L., "Ignition and Detonation-Initiation Characteristics of Hydrogen and Hydrocarbon Fuels in a PDE," AIAA 2007-234, 45th AIAA Aerospace Sciences Meeting and Exhibit, Reno, NV, 8 - 11 Jan. 2007.

[71]Schauer, F. R., Miser, C. L., Tucker, K. C., Bradley, R. P., and Hoke, J. L., "Detonation Initiation of Hydrocarbon-Air Mixtures in a Pulsed Detonation Engine," AIAA 2005-1343, 43rd AIAA Aerospace Sciences Meeting and Exhibit, Reno, NV, 10-13 Jan. 2005.

[72]Lifshitz, A., "Ignition Delay Times," *Handbook of Shock Waves III*, 2001, Academic Press, Editors: Ben-Dor, G., Igra, O., and T. Elperin, Guest Editor: Lifshitz, A., pp. 211-256.

[73]Tsang, W. and Lifshitz, A., "Shock Tube Techniques in Chemical Kinetics," Annual Review of Physical Chemistry, Vol. 41, 1990, pp. 559-599.

[74]Vasu, S.S. and Davidson, D.F. and Hanson, R.K., "Shock Tube Ignition Delay Times and Modeling of Jet Fuel Mixtures," Paper AIAA-2006-4402, 42nd AIAA/ASME/SAE/ASEE Joint Propulsion Conference and Exhibit, Sacramento, CA, 9-12 Jul. 2006.

[75]Penyazkov, O.G., Ragotner, K.A., Dean, A.J. and Varatharajan, B., "Autoignition of Propane–Air Mixtures Behind Reflected Shock Waves," Proceedings of the Combustion Institute, Vol. 30, No. 2, Jan. 2005, pp. 1941-1947.

[76]Davidson, D.F., Gauthier, B.M. and Hanson, R.K., "Shock Tube Ignition Measurements of Iso-octane/Air and Toluene/Air at High Pressures," Proceedings of the Combustion Institute, Vol. 30, 2005, pp. 1175-1182.

[77]Craig, R.R., "A Shock Tube Study of the Ignition Delay of Hydrogen-Air Mixtures Near the Second Explosion Limit," Master's Thesis, Technical Report AFAPL-TR-66-74, Air Force Aero Propulsion Laboratory, Research and Technology Division, Air Force Systems Command, Wright-Patterson Air Force Base, Ohio, Nov. 1966.

[78]Steill, U., Braun-Unkhoff, M. and Aigner, M., "An Experimental and Modeling Study on the Auto-ignition of Kerosene and Surrogate Fuel Mixture," AIAA 2008-973, 46th AIAA Aerospace Sciences Meeting and Exhibit, Reno, NV, 7-10 Jan. 2008.

[79]Mikolaitis, D.W., Segal, C. and Chandy, A., "Ignition Delay for Jet Propellant-10/Air and Jet Propellant-10/High Energy Density Fuel/Air Mixtures," Journal of Propulsion and Power, Vol. 19, No. 4, Jul.-Aug. 2003, pp. 601-606.

[80]Golovichev, V. I., Dimitrov, V. I. and Soloukhin, R. I., "Numerical Analysis of Kinetic Models of Hydrogen Ignition," Combustion, Explosion, and Shock Waves, Vol. 9, No. 1, Jan. 1973.

[81]Ishii, Y., Higashino, F. and Sakurai, A., "Ignition of Spurting Hydrogen Jets Behind a Reflected Shock Wave," Bulletin of The Japan Society of Mechanical Engineers (JSME), Vo. 29, No. 256, Oct. 1986, pp. 3448-3451.

[82]Gudkovich, V.N., Granovskii, E.A.and Shtessel, E.A., "Ignition of Rich Propane-Oxygen Mixtures," Combustion, Explosion, and Shock Waves, Vol. 16, No. 6, Nov. 1980.

[83]Tanabe, M., Kono, M., Sato, J., Koenig, J., Eigenbrod, C., and Rath, H.J., "Effects of Natural Convection on Two Stage Ignition of an n-Dodecane Droplet," Symposium (International) on Combustion, Vol. 25, No. 1, 1994, pp. 455-461.

[84]Eigenbrod, C., Moriue, O., Weilmünster, P. and Rath, H.J., "Development of a Simple Model Fuel for Kerosene Droplet Ignition," 28th International Annual Conference of Fraunhofer Institut Chemische Technologie, Karlsruhe, Jun. 1997.

[85]Rocourt, X., Sochet, I., Gillard, P., Faubert, F. and Dagaut, P., "Detonability of Simple and Representative Components of Pyrolysis Products of Kerosene: Pulsed Detonation Engine Application," Shock Waves, Vol. 14, No. 4, 2005, pp. 283-291.

[86]Dabora, E.K., "Effect of Additives on the Lean Detonation Limit of Kerosene Sprays in Air," Department of Mechanical Engineering, The University of Connecticut, Final Report, Report No. A091590, U.S. Army Research Office, Grant No. DAAG 29-78-G0074, Dec. 1980.

[87]Fan, X., Yu, G., Li, J., Lu, X., Zhang, X. and Sung, C.-J., "Combustion and Ignition of Thermally Cracked Kerosene in Supersonic Model Combustors," Journal of Propulsion and Power, Vol. 23, No. 2, March-Apr. 2007, pp. 317-324.

[88]Imbert, B., Catoire, L., Chaumeix, N., Dupre, G. and Paillard, C., "Detonation Properties of Stoichiometric Gaseous n-Heptane/Oxygen/Argon Mixtures," Proceedings of the Combustion Institute, Vol. 30, No. 2, Jan. 2005, pp. 1925-1931.

[89]Austin, J.M. and Shepherd, J.E., "Detonation in Hydrocarbon Fuel Blends," Combustion and Flame, Vol. 132, No. 1-2, 2003, pp. 73-90.

[90]Cooper, M. and Shepherd, J.E., "Thermal and Catalytic Cracking of JP-10 for Pulse Detonation Engine Applications," GALCIT Report FM 2002.002, Graduate Aeronautical Labs, California Institute of Technology, Pasadena, CA, Dec. 2002.

[91]Kawanabe, H. and Shioji, M., "Effect of Hydrogen Addition to Hydrocarbon Fuels on Combustion Characteristics," Transactions of the Japan Society of Mechanical Engineers, Vol. 71, No. 704, 2005, pp. 1177-1182.

[92]Yu, G., Li, J.G., Chang, X.Y., Chen, L.H. and Sung, C.J., "Fuel Injection and Flame Stabilization in a Liquid-Kerosene-Fueled Supersonic Combustor," Journal of Propulsion and Power, Vol. 19, No. 5, 2003, pp. 885-893.

[93]Yu, G., Li, J.G., Chang, X.Y., Chen, L.H. and Sung, C.J., "Investigation of Kerosene Combustion Characteristics with Pilot Hydrogen in Model Supersonic Combustors," Journal of Propulsion and Power, 0748-4658, Vol. 17, No. 6, 2001, pp. 1263-1272.

[94]Vinogradov, V., Kobigsky, S. and Petrov, S., "Experimental Investigation of Liquid Carbon-Hydrogen Fuel Combustion in Channel at Supersonic Velocities," AIAA-1992-3429, 28th SAE, ASME, and ASEE Joint Propulsion Conference and Exhibit, Nashville, TN, 6-8 Jul. 1992.

[95]Owens, M., Segal, C. and Auslender, A.H., "Effects of Mixing Schemes on Kerosene Combustion in a Supersonic Airstream," Journal of Propulsion and Power, Vol. 13, No. 4, Jul.-Aug. 1997.

[96]Wong, Y.K. and Karim, G.A., "An Analytical Examination Of The Effects Of Hydrogen Addition On Cyclic Variations In Homogeneously Charged Compression-Ignition Engines," International Journal of Hydrogen Energy, Vol. 25, No. 12, Dec. 2000, pp. 1217-1224.

[97]Chaumeix, N., Pichon, S., Lafosse, F. and Paillard, C.-E., "Role of Chemical Kinetics on the Detonation Properties of Hydrogen/Natural Gas/Air Mixtures," International Journal of Hydrogen Energy, Vol. 32, No. 13, Sep. 2007, pp. 2216-2226.

[98]Yamada, Y., Matsuki, N., Ohmori, T., Mametsuka, H., Kondo, M., Matsuda, A. and Suzuki, E., "One Chip Photovoltaic Water Electrolysis Device," International Journal of Hydrogen Energy, Vol. 28, No. 11, Nov. 2003, pp. 1167-1169.

[99]Nagai, N., Takeuchi, M, Kimura, T. and Oka, T., "Existence of Optimum Space Between Electrodes on Hydrogen Production by Water Electrolysis," International Journal of Hydrogen Energy, Vol. 28, No. 1, Jan. 2003, pp. 35-41.

[100]Ando, Y. and Tanaka, T., "Proposal For a New System For Simultaneous Production of Hydrogen and Hydrogen Peroxide by Water Electrolysis," International Journal of Hydrogen Energy, Vol. 29, No. 13, Oct. 2004, pp. 1349-1354.

[101]Lu, F.K., Roseberry, C.M., Meyers, J.M., Wilson, D.R., Lee, Y.-M., Czysz, P., "Reformation of Methane in a Supersonic, Arc-Heated Flow," AIAA Paper 2004-1132, 42nd AIAA Aerospace Sciences Meeting and Exhibit, Reno, NV, 5-8 Jan. 2004.

[102]Zhdanok, S.A., Vasil'ev, G.M., Vasetskii, V.A. and Khavets, A.V., "Use of Plasma Reforming of Fuel for Reduction of the Toxicity of Diesel Engines," Journal of Engineering Physics and Thermophysics, Vol. 78, No. 1, 2005.

[103]Plaksin, V.Y., Lee, H.J and Riaby, V.A., "The Effect of Component Gas on Diesel Reformation by a Plasmatron," IEEE Transactions on Plasma Science, Vol. 35, No. 6, Dec. 2007.

[104]Bromberg, L., Cohn, D.R., Rabinovich, A. and Alexeev, N., "Plasma Catalytic Reforming of Methane," International Journal of Hydrogen Energy, Vol. 24, 1999, pg. 1131-1137.

[105]Bromberg, L., Cohn, D.R. and Rabinovich, A., "Hydrogen Manufacturing Using Low Current, Non-Thermal Plasma Boosted Fuel Converters," PSFC/RR-01-1, Plasma Science and Fusion Center, Massachusetts Institute of Technology, Dec. 2000, Published in the Proceedings of the Symposium on Energy For The 21st Century: Hydrogen Energy, San Diego, CA, Apr. 2001.

[106]Cohn, D.R., Rabinovich, A., Titus, C.H. and Bromberg, L., "Near-Term Possibilities For Extremely Low Emission Vehicles Using Onboard Plasmatron Generation of Hydrogen," International Journal of Hydrogen Energy, Vol. 22, No. 7, Jul. 1997, pp. 715-723.

[107]Bromberg, L, Crane, S., Rabinovich, A., Kong, Y., Cohn, D.R., Heywood, J., Alexeev, N. and Samokhin, A., "Hydrogen Generation From Plasmatron Reformers: A Promising Technology For NOx Adsorber Regenertion And Other Automotive Applications," PSFC/JA-03-27, Plasma Science and Fusion Center, Massachusetts Institute of Technology, Dec. 2003, Proceedings of the Diesel Engine Emission Reduction (DEER) Workshop, Newport, RI, 24-28 Aug. 2003.

[108]Reddy, N.K.N., "Development and Testing of a Miniature Pulse Detonation Engine," Master's Thesis, Department of Mechanical and Aerospace Engineering, The University of Texas at Arlington, Arlington, TX, 2004.

[109]New, T.H., Panicker, P.K., Lu, F.K., and Tsai, H., "Experimental Investigations on DDT Enhancements by Shchelkin Spirals in a PDE," AIAA-2006-552, 44th AIAA Aerospace Sciences Meeting and Exhibit, Reno, NV, 9-12 Jan.2006.

[110]New, T., Panicker, P.K., Chui, K., Tsai, H., and Lu, F.K., "Experimental Study on Deflagration-to-Detonation Transition Enhancement Methods in a PDE," AIAA-2006-7958, 14th AIAA/AHI Space Planes and Hypersonic Systems and Technologies Conference, Canberra, Australia, 6-9 Nov. 2006.

[111]Panicker, P.K., Li, J., Lu, F.K., and Wilson, D.R., "Application of a Pulsed Detonation Engine for Electric Power Generation," AIAA-2007-1246, 45th AIAA Aerospace Sciences Meeting and Exhibit, Reno, NV, 8-11 Jan. 2007.

[112]Panicker, P.K., Li, J., Lu, F.K., and Wilson, D.R., "Development of a Compact Liquid Fueled PDE with Pre-detonator," AIAA-2007-237, 45th AIAA Aerospace Sciences Meeting and Exhibit, Reno, NV, 8-11Jan. 2007.

[113]Roy, G.D., Frolov, S.M., Borisov, A.A., and Netzer, D.W., "Pulse Detonation Propulsion: Challenges, Current and Future Perspective," Progress in Energy and Combustion Science 30, 2004, pp. 545-672.

[114]Kawamura, K., Saito, A., Kanda, M., Kashiwagura, T. and Yamamoto, Y., "Spray Characteristics of Slit Nozzle for Direct Injection Gasoline Engines," Japan Society of Mechanical Engineers International Journal, Series B, Vol. 46, No. 1, 2003, pp. 10-16.

[115] Lee, S-Y, Watts, J., Saretto, S., Pal, S., Conrad, C., Woodward, R. and Santoro, R., "Deflagration to Detonation Transition Processes by Turbulence-Generating Obstacles in Pulse Detonation Engines," Journal of Propulsion and Power, Vol. 20, No. 6, Nov.-Dec. 2004.

[116]Zhang, F.Y., Fujiwara, T., Nakayama, E., Hattori, T. and Hanson, R.K., "Detonation Studies of High-Frequency-Operation Pulse Detonation Engine With Air/Hydrogen," AIAA 2003-1169, 41st Aerospace Sciences Meeting and Exhibit, Reno, NV, 6-9 Jan. 2003.

[117]Hayashi, A.K., Adachi, H., Mitani, T. and Sato, H., "DDT Reduction by Perforated Plates in H_2/O_2 Mixture," 21st ICDERS, Poitiers, France, 23-27 Jul. 2007.

[118]Ciccarelli, G. and deWitt, B., "Detonation Initiation by Shock Reflection From an Orifice Plate," Shock Waves, Vol. 15, No. 3-4, Jul. 2006, pp. 259-265.

[119]Glaser, A., Caldwell, N., Gutmark, E., "Experimental Investigation Into The Acoustic Performance of a Pulse Detonation Engine With Ejector," AIAA 2005-1345, 43rd AIAA Aerospace Sciences Meeting and Exhibit, Reno, NV, 10-13 Jan. 2005.

[120]Chao, J., Otsuka, T. and Lee, J.H.S., "An Experimental Investigation of The Onset of Detonation," Proceedings of the Combustion Institute, Vo. 30, 2005, pp. 1889-1897.

[121]Sorin, R., Zitoun, R. and Desbordes, D., "Optimization of The Deflagration to Detonation Transition: Reduction of Length and Time of Transition," Shock Waves, Vol. 15, No. 2, Jun. 2006, pp. 137-145.

[122]Hopper, D.R., King, P.I. and Schauer, F.R., "Propagation of Detonations Across a Step Area Change in a Pulsed Detonation Engine," AIAA 2007-446, 45th AIAA Aerospace Sciences Meeting and Exhibit, Reno, NV, 8-11 Jan. 2007.

[123]Schultz, E., "Detonation Diffraction Through an Abrupt Area Expansion," Ph.D. Dissertation, California Institute of Technology, Pasadena, CA, Apr. 2000.

[124]Levin, V.A. and Markov, V.V., "Entry of a Detonation Wave Into an Expanding Channel," Fluid Dynamics, Vol. 16, Number 3, May 1981, pages 389-392.

[125]Papalexandris, M.V., Thomas, J.F., Jacobs, C. and Deledicque, V., "Structural Characteristics of Detonation Expansion From a Small Channel to a Larger One," Proceedings of the Combustion Institute, Vol. 31, No. 2, 2006, pp. 2407-2414.

[126]Yatsufusa, T., Ohira, M., Yamamoto, S., Endo, T. and Taki, S., "Development of Liquid-Fuel Initiator For Liquid-Fuel PDE," AIAA 2004-1213, Proceedings of the 42nd AIAA Aerospace Sciences Meeting and Exhibit, Reno, NV, 5-8 Jan. 2004.

[127]Khasainov, B., Presles, H-N, Desbordes, D., Demontis, P. and Vidal, P., "Detonation Diffraction From Circular Tubes to Cones," Shock Waves, Vol. 14, No. 3, 2005, pp. 187-192.

[128]Thomas, G.O. and Williams R.L., "Detonation Interaction With Wedges and Bends," Shock Waves, Vol. 11, 2002, pp. 481-492.

[129]Frolov, S.M., Aksenov, V.S. and Shamshin, I.O., "Shock Wave and Detonation Propagation Through U-bend Tubes," Proceedings of the Combustion Institute, Vol. 31, 2007, pp. 2421-2428.

[130]Frolov, S.M., Aksenov, V.S. and Basevich, V. Y., "Initiation of Heterogeneous Detonation in Tubes With Coils and Shchelkin Spirals," High Temperature Journal, Vol. 44, No. 2, Mar. 2006, pp. 283-290.

[131]Conrad, C., Saretto, S.R., Lee, S-Y. and Santoro, R.J., "Studies of Overdriven Detonation Wave Transition in a Gradual Area Expansion for PDE Applications," AIAA 2004-3397, 40th AIAA/ASMA/SAE/ASEE Joint Propulsion Conference and Exhibit, Fort Lauderdale, FL, 11-14 Jul. 2004.

[132]*Fundamentals of Aircraft Power Plants*, Field Manual FM 1-506, Headquarters, Department of the Army, Washington, D.C., 30 Nov. 1990, URL: http://www.globalsecurity.org/military/library/policy/army/fm/1-506/index.html, accessed Jul. 2008.

[133]Maintenance of Mechanical and Electrical Equipment at Command, Control Communications, Intelligence, Surveillance, and Reconnaissance (C4ISR) Facilities: Recommended Maintenance Practices, Army TM 5-692-1, Department of the Army (CEMP), 22 Jul. 2005, Chapter 4- Gas Turbines, URL: http://www.usace.army.mil/publications/armytm/tm5-692-1/, accessed Jul. 2008.

[134]Retrofit Ignition System for Ruston TA1750 and TB5000 Gas Turbines, Patented Systems Incorporated, URL: http://www.patented-systems.com/products_ignition_sys_liquid_fuel.html, accessed Jul. 2008.

[135]Tang, K.Y, *Alternating Current Circuits*, 2nd Edition, International Textbook Company, Scranton, Pennsylvania, 1951, pp. 8-26, 223-251.

[136]Babrauskas, V., *Ignition Handbook*, Issaquah, WA, Fire Science Publishers, 2003.

[137]Borisov, A.A., Galkin, A.F., Zhivotov, V.K., Zaitsev, S.A., Konovalov, G.M., Korobtsev, S.V., Krotov, M.F., Medvedev, D.D., Potapkin, B.V. and Smirnov, R.V., "Effect of Corona Discharge on Detonation Initiation With a Weak Energy Source," High Energy Chemistry, Vol. 41, No. 5, Sep. 2007, pp. 366-369.

[138]Rodriguez, J., "Investigation of Transient Plasma Ignition For a Pulse Detonation Engine," M.S. Thesis, Naval Postgraduate School, Monterey, CA, Mar. 2005.

[139]Wang, F., Jiang, C., Kuthi, A., Gundersen, M.A., Brophy, C., Sinibaldi, J.O. and Lee, L.C., "Transient Plasma Ignition of Hydrocarbon-Air Mixture in Pulse Detonation Engine," AIAA 2004-0834, 42nd AIAA Aerospace Sciences Meeting and Exhibit, Reno, NV, 5-8 Jan. 2004.

[140]Busby, K., Corrigan, J., Yu, S., Williams, S., Carter, C., Shauer, F., Hoke, J., Cathey, C., and Gundersen, M., "Effects of Corona, Spark and Surface Discharges on Ignition Delay and

Deflagration-to-Detonation Times in Pulsed Detonation Engines," AIAA-2007-1028, 45th AIAA Aerospace Sciences Meeting and Exhibit, Reno, NV, 8-11 Jan. 2007.

[141]Lieberman, D.H., Shepherd, J.E., Wang, F., Liu, J. and Gundersen, M.A., "Characterization of a Corona Discharge Initiator Using Detonation Tube Impulse Measurements," AIAA 2005-1344, 43rd AIAA Aerospace Sciences Meeting and Exhibit, Reno, NV, 10-13 Jan. 2005.

[142]Zhukov, V.P., Rakitin, A.E., and Starikovskii, A.Y., "Effect of High-Voltage Pulsed Discharges on Deflagration to Detonation Transition," Journal of Propulsion and Power, Vol. 24, No. 1, Jan.-Feb. 2008, pp. 88-93.

[143]Zhukov, V.P., Rakitin, A.E. and Starikovskii, A.Y., "Detonation Initiation by High Voltage Pulsed Discharges, AIAA-2007-1029, 45th AIAA Aerospace Sciences Meeting and Exhibit, Reno, NV, 8-11 Jan. 2007.

[144]Lukes, P., Clupek, M., Babicky, V. and Sunka, P., "Generation of Ozone by Pulsed Corona Discharge Over Water Surface in Hybrid Gas-Liquid Electrical Discharge Reactor," Journal of Physics D: Applied Physics, Vol. 38, 2005, pp. 409-416.

[145]Nishida, H., Ishii, T., Hirashima, S. and Tachibana, T., "Effect of Ozone on Combustion of a Dual Fuel Engine," Transactions of the Japan Society of Mechanical Engineers, Vol 70, No. 695, 2004, pp. 1884-1889.

[146]Dors, M. and Mizeraczyk, J., "NOx Removal From a Flue Gas in a Corona Discharge-Catalyst Hybrid System," Catalysis Today, Vol. 89, No. 1-2, 29 Feb. 2004, pp. 127-133.

[147]Satyanand, U.S., Panicker, P.K., Lu, F.K., and Emanuel, G., "Preliminary study of ionization of supersonic air by means of corona discharge," AIAA Paper 2003–6925, 12th AIAA International Space Planes and Hypersonic Systems and Technologies, Norfolk, Virginia, 15–18 Dec. 2003.

[148]Brophy, C.M., Werner, S., Sinibaldi, J.O., "Performance Characterization of a Valve.less Pulse Detonation Engine," AIAA 2003-1344, 41st Aerospace Sciences Meeting and Exhibit, 6-9 Jan. 2003, Reno, NV.

[149]Shimo, M. and Heister, S., "Multi-cyclic Detonation Initation Studies in Valveless Pulsed Detonation Combustors," AIAA 2006-4308, 42nd AIAA/ASME/SAE/ASEE Joint Propulsion Conference and Exhibit, Sacramento, CA , 9-12 Jul. 2006.

[150]Hinkey, J.B., Henderson, S.E. and Bussing, T.R.A., "Operation of a Fight Scale Rotary Valved Multiple Combustor Pulse Detonation Engine (RVMPDE)," AIAA 98-3881, 34th AIAA/ASME/SAE/ASEE Joint Propulsion Conference and Exhibit, Cleveland, OH, 13-15 Jul. 1988.

[151]Pegg, R.J., Couch, B.D. and Hunter, L.G., "Pulse Detonation Engine Air Induction System Analysis," AIAA 96-2918, 32nd AIAA/ASME/SAE/ASEE Joint Propulsion Conference and Exhibit, 1-3 Jul. 1996, Buena Vista, FL.

[152]Schauer, F., Stutrud, J., and Bradley, R., "Detonation Initiation Studies and Performance Results for Pulse Detonation Engine Applications," AIAA Paper 2001-1129, 39th AIAA Aerospace Sciences Meeting and Exhibit, Reno, NV, 8-11 Jan, 2001.

[153]Woods, R.L., "Fluid Power Control," Reference Material for ME5306/MAE4320, University of Texas at Arlington, 2008.

[154]CVVT, URL: http://www.honda.com/vtec/, accessed Jul. 2008.

[155]"What is The Definition of a TTL Compatible Signal?," National Instruments Knowledge Base, URL: http://digital.ni.com/public.nsf/allkb/ACB4BD7550C4374C86256BFB0067A4BD, accessed Jul. 2008.

[156]Lu, F.K. and .Jensen, D.S., "Potential Viability of a Fast-Acting Micro-Solenoid Valve for Pulsed Detonation Fuel Injection," AIAA 2003–0888, 41st AIAA Aerospace Sciences Meeting, Reno, NV, 6–9 Jan. 2003.

[157]Shiraishi, N., Sakai, K., Nagasaka, S., Takano, T. and Sami, H., "Study of Direct Injection Gasoline Combustion Using Constant-Volume Combustion Vessel-Diagnostics of Stratification Degree in Relation to Major Design Factors," Japan Society of Mechanical Engineers International Journal, Series B, Vol. 45, No. 2, 2002, pp. 363-372.

[158]Ganser, M.A., "Common-Rail Injectors for 2000 Bar and Beyond," SAE 2000-02-0706, SAE 2000 World Congress Proceedings.

[159]Strakey, P.A., Talley, D.G., and Hutt, J.J., "Mixing Characteristics of Coaxial Injectors at High Gas/Liquid Momentum Ratios," Journal of Propulsion and Power, Vol. 17, No. 2, Mar.-Apr. 2001, pp. 401-410.

[160]Moon, I-M., Seo, S., Han, Y-M., Lim, B. and Choi, H-S, "Parametric Study on Combustion Characteristics of Bi-Liquid Swirl Coaxial Injectors," AIAA 2006-5201, 42nd AIAA/ASME/SAE/ASEE Joint Propulsion Conference and Exhibit, Sacramento, CA, 9-12 Jul. 2006.

[161]Figliola, R.S. and Beasley, D.E., *Theory and Design For Mechanical Measurements*, 4th Edition, John Wiley and Son, Inc., 2006., Chapter 7: Sampling; Chapter 8: Temperature Measurements.

[162]Piezoelectric Sensors For Dynamic Pressure Measurements, Pressure Catalog, PCB Piezotronics, Inc., pp. 45: Helium Bleed Sensors, pp. 13-36: High Frequency Pressure Transducers, URL: http://www.pcb.com/Linked_Documents/Pressure/PFScat.pdf, accessed Jul. 2008.

[163]Hamamatsu Silicon Photodiodes, URL: http://www.sales.hamamatsu.com/, accessed: Jul. 2008.

[164]Batani, D., Alba, S., Lombardi, P. and Galassi, A., "Use of Langmuir Probes in a Weakly Ionized, Steady-Stage Plasma With Strong Magnetic Field," Review of Scientific Instruments, Vo. 68, No. 11, Nov. 1997, pp. 4043-4050.

[165]Zdenek, J.S., "Ion Based Pressure Sensor For Pulse Detonation Engines," AFIT/GAE/ENY/04-M17, Master's Thesis, Department of the Air Force Air University, Air Force Institute of Technology, Wright-Patterson Air Force Base, Ohio, Mar. 2004.

[166]McMillan, R.J., "Shock Tube Investigation of Pressure and Ion Sensors Used in Pulse Detonation Engine Research," AFIT/GAE/ENY/04-J07, Master's Thesis, Department of the Air

Force Air University, Air Force Institute of Technology, Wright-Patterson Air Force Base, Ohio, Jun. 2004.

[167]Swain, M.R., Blanco, J.A., and Swain, M.N., "A Non-Intrusive Surface Ignition Detector," Journal of Physics E: Scientific Instruments, Vol. 22, No. 10, Oct. 1989, pp. 838-840.

[168]Warren, R.C., "Design of Thermocouple Probes For Measurement of Rocket Exhaust Plume Temperatures," DSTO-TR-0006, Technical Report, Department of Defense, Jun. 1994.

[169]Nanigian, J. and Nanigian, D., "Unique Thermocouple to Measure the Temperatures of Squibs, Igniters, Propellants and Rocket Nozzles," Proceedings of the SPIE, Vol. 6222, No. 622203, 10 May 2006.

[170]Brohez, S., Delvosalle, C. and Marlair, G., "A Two Thermocouple Probe For Radiation Corrections of Measured Temperatures in Compartment Fires," Fire Safety Journal, Vol. 39, No. 5, Jul. 2004, pp. 399-411.

[171]Hartman, J., *How to Tune And Modify Engine Management Systems*, 1st ed., MotorBooks/MBI Publishing Company, Jan. 2004.

[172]Unsal, B., Trimis, D. and Durst, F., "Instantaneous Mass Flowrate Measurements Through Fuel Injection Nozzles," International Journal of Engine Research, Vol. 7, No. 5, 2006, pp. 371-380.

[173]Aarnio, M.J., Hinkey, J.B. and Bussing, T.R.A., "Multiple Cycle Detonation Experiments During The Development of a Pulse Detonation Engine," AIAA-96-3263, Proceedings of AIAA, ASME,SAE, ASEE Joint Propulsion Conference and Exhibit, Buena Vista, FL, 1-3 Jul. 1996.

[174]Wu, Y., Ma, F. and Yang, V., "System Performance And Thermodynamic Cycle Analysis of Airbreathing Pulse Detonation Engines," Journal of Propulsion and Power, Vol. 19, No. 4, Jul.-Aug. 2003, pp. 556-567.

[175]Canteins, G., Franzetti, F., Zoclonska, E., Khasainov, B.A., Zitoun, R., and Desbordes, D., "Experimental and Numerical Investigations on PDE Performance Augmentation by Means of an Ejector," Shock Waves 2006, Vol 15, No. 2, pages 103-112.

[176]Mee, D., "Dynamic Calibration of Force Balances," Research Report No. 2002/6, The University of Queensland, Department of Mechanical Engineering, 02 Jan. 2003.

[177]Frolov, S.M., Basevich, V.Y. and Aksenov, V.S., "Combined Strategies of Detonation Initiation in a Liquid-Fueled Air-Breathing PDE," ISABE-2005-1292, 17th International Symposium on Air Breathing Engines, Munich, 2005.

[178]*Introduction to Piezoelectric Force Sensors*, PCB Piezotronics, Inc., URL: http://www.pcb.com/techsupport/tech_force.php, accessed Jul. 2009.

[179]Naumann, K.W., Ende, H. and Mathieu, G., "Technique for Aerodynamic Force Measurements Within Milliseconds in Shock Tunnel," Shock Waves, Sep. 1991, Vol.1, No. 3, pp. 223-232.

[180]Kasahara, J., Liang, Z., Browne, S.T. and Shepherd, J.E., "Impulse Generation by an Open Shock Tube," AIAA Journal, Vol. 46, No. 7, Jul. 2008, pp. 1593-1603.

[181]Soderling, S.C. and Saari, B.J., "Transducer Acceleration Compensation With Frequency Domain Amplitude and/or Phase Compensation," US Patent 7331209, Issued on 19 Feb. 2008.

[182]Marcolini, M.A., Lorber, P.F., Miller, W.T. and Covino, A.F., Frequency Response Calibration of Recess-Mounted Pressure Transducers," NASA Technical Memorandum 10431, NASA Langley Research Center, Hampton, Virginia, March 1991.

[183]Campbell, E., Galbraith, W. and Hayward, G., "A New Electrostatic Transducer Incorporating Fluidic Amplification," IEEE Ultrasonics Symposium 2006, 1-6 Oct. 2006, pp. 1445-1448.

[184]Kobayashi, H., Leger, T. and Wolff, J.M., "Experimental And Theoretical Frequency Response of Pressure Transducers For High Speed Turbomachinery," AIAA 1998-3745, 34th AIAA/ASME/ASEE Joint Propulsion Conference and Exhibit, Cleveland, OH, 13-15 Jul. 1998.

[185]*Model 112A03 Charge Output Dynamic Pressure Sensor Installation and Operating Manual*, Pressure Division, PCB Piezotronics Inc., URL: http://www.pcb.com/contentstore/docs/PCB_Corporate/Pressure/products/Manuals/112A03.pdf, accessed Jul. 2008.

[186]Kailasanath, K., "Liquid-Fueled Detonations in Tubes," Journal of Propulsion and Power, Vol. 22, No. 6, Nov.-Dec. 2006, pp. 1261-1268.

BIOGRAPHICAL INFORMATION

Philip Panicker was born on September 4th, 1973, in the small town of Mavelikara, in Kerala, India. He attended The Bishop Moore Vidhyapith School in Mavelikara up to the 3rd standard and then was enrolled in The Indian High School Dubai, Dubai, United Arab Emirates, till the 12th standard. He completed his Bachelor of Engineering in Electronics and Telecommunication in 1995 from M. S. Ramaiah Institute of Technology in Bangalore, India. After a short stint as a sales engineer in his father's air-conditioning and refrigeration retail business in Dubai, UAE, he joined The University of Texas at Arlington to pursue a Master's degree in Aerospace Engineering. He became a researcher at the Aerodynamics Research Center (ARC) on a project entitled "Ionization of Air by Corona Discharge" which was a technique intended for supersonic flows created within a shock tube. After completing his MS degree in the Fall Semester of 2004, he returned to his family in Dubai, UAE. In the fall of 2004, he re-enrolled at UT Arlington to pursue a Doctoral degree in Aerospace Engineering. He performed experimental work on the development of pulsed detonation engines (PDE) at the ARC.

During his time as a PhD candidate, he was also an instructor for a sophomore level course, MAE2381 Experimental Methods and Measurements. He has been a student member of the American Institute of Aeronautics and Astronautics since the year 2000. He presented papers at several AIAA conferences and at other seminars. He enjoys soccer, motorcycling and traveling.